

BENZOTHIADIAZOLE DERIVATIVES FOR PHOTOVOLTAIC DEVICES

A THESIS

*Submitted in partial fulfilment of the
requirements for the award of the degree
of*

DOCTOR OF PHILOSOPHY

in

CHEMISTRY

by

M N K PRASAD BOLISETTY



**DEPARTMENT OF CHEMISTRY
INDIAN INSTITUTE OF TECHNOLOGY ROORKEE
ROORKEE-247 667 (INDIA)
MAY, 2014**

©INDIAN INSTITUTE OF TECHNOLOGY ROORKEE, ROORKEE-2014
ALL RIGHTS RESERVED



INDIAN INSTITUTE OF TECHNOLOGY ROORKEE
ROORKEE
CANDIDATE'S DECLARATION

I hereby certify that the work which is being presented in the thesis entitled “**BENZOTHIADIAZOLE DERIVATIVES FOR PHOTOVOLTAIC DEVICES**” in partial fulfillment of the requirements for the award of the Degree of Doctor of Philosophy and submitted in the Department of Chemistry of the Indian Institute of Technology Roorkee, Roorkee is an authentic record of my own work carried out during a period from January, 2009 to April, 2014 under the supervision of Dr. K. R. Justin Thomas, Associate Professor and Dr. Kaushik Ghosh, Associate Professor, Department of Chemistry, Indian Institute of Technology Roorkee, Roorkee.

The matter presented in the thesis has not been submitted by me for the award of any other degree of this or any other Institute.

(M N K PRASAD BOLISETTY)

This is to certify that the above statement made by the candidate is correct to the best of my knowledge.

(Kaushik Ghosh)
Supervisor

(K. R. Justin Thomas)
Supervisor

Date:

The Ph.D. Viva-Voce examination of **Mr. M N K PRASAD BOLISETTY**, Research Scholar, has been held on

Supervisor

Chairman, SRC

External Examiner

Head of the Department/Chairman, ODC

ACKNOWLEDGEMENTS

Foremost, I humbly and politely bow my head to thyness, the *Lord Shiva* and *Goddess Saraswati* “*The Goddess of Wisdom*” who bestowed upon me an opportunity to do this work and gave me ample vision and strength to accomplish this task successfully. I thank the almighty *God* whose gracious blessings and spiritual support always help me to withstand and overcome the difficulties in my life.

I would like to convey my deepest gratitude and reverence to my supervisor Dr. K. R. Justin Thomas, Associate Professor, Department of Chemistry, IIT Roorkee for his helpful counsel, management, professionalism and continued hopefulness, which make him an outstanding advisor. I am highly thankful for his time, attempt and editing skills. His constant support, the trust he placed in my abilities, encouragement and judicious interventions made this thesis to come into picture. I humbly acknowledge a life time’s gratitude to him. No words articulate to acknowledge the didactic guidance rendered by him.

I highly appreciate my co-supervisor Dr. Kaushik Ghosh, Associate Professor, Department of Chemistry, IIT Roorkee to make me as the part of his group and potential moral support during my PhD tenure.

I am thankful to Prof. Anil Kumar, Prof. V. K. Gupta and Prof. Kamaluddin, the present and the former Heads, Department of Chemistry, IIT Roorkee, for providing me all the instrumental, necessary facilities and support to carry out these investigations.

The financial support from University Grants Commission (UGC), New Delhi to complete the present investigations is highly acknowledged. My thanks are due for the Institute Instrumentation Centre, IIT Roorkee. I am thankful to Prof. Ritu Barthwal for the NMR facility. I wish to thank all the faculty members and non-teaching staff of the Department of Chemistry, IIT Roorkee. I would also like to thank Mr. Madan Pal for all the technical assistance in the Department of Chemistry. I am grateful to Prof. Kuo-Chuan Ho and Chuan-Pei Lee of the department of Chemical Engineering, National Taiwan University, Taipei, Taiwan for their meticulous DSSC studies on my dyes.

In my lab, I express my special thanks to Payal Tyagi and Sushil Kumar for all the scientific discussions and their invaluable help to make my work more precious. Without their help it was

not possible to produce many results. My sincere appreciation goes to Mr. Venkat for her timely help during the execution of this work and moral support.

I wish to thank my other lab members Neha, Abishek, Babu, Karthik, Rajendra and Rajesh for their support in their own way. I express my special thanks to my lovely friend Subbarao who always stayed with me during all the ups and downs of my life. His amusing company with positive attitude has always been inspiring me to achieve best in the life. My sincere appreciation goes to my friends Veeranjanyulu, Mallikharjuna Rao, Venkata Babu, Naveen, Koti, Kishore, Varun, Raman Maurya. I always feel lucky to have friends like them.

This thesis is dedicated to my parents, Rushi and Leelakumari, for their unconditional love, encouragement and blessings. I also wish to express my feelings for my sister Mahathi from the bottom of my heart for which my mere expression of thanks will not suffice. At last but not the least, I wish to extend my genuine gratefulness to my wife Hima Bindu for years of affection and support.

I am extremely grateful to the people whose names have been unknowingly left. I apologize and believe that their wishes will always be with me as they were during the times of need.

M N K PRASAD BOLISSETTY

Abstract

Organic materials containing low band-gap chromophores such as benzothiadiazole, benzotriazole, diketopyrrolopyrrole, isoindigo, quinoxaline, phthalimide, thiazolo[5,4-*d*]thiazole, and benzo[1,2-*d*:4,5-*d'*]bisthiazole.etc have been attracted wide interest among academicians and industrialists owing to their potential application in dye sensitized solar cells (DSSCs), bulk hetero-junction solar cells (BHJSCs), light-emitting diodes (OLEDs) and related opto-electronic devices. Benzothiadiazole has been regarded as a promising π -conjugation unit for the construction of organic semiconductor materials due to its high electron-accepting capabilities and facile functionalization possibilities at 4,7-positions. The chemical modifications allow to tune the photophysical and electrochemical properties. Particularly, it has been recognized that conjugating the electron-donating group with benzothiadiazole helps to balance the hole and electron mobility in the molecular layer. It also modulates the highest occupied molecular orbital (HOMO) and lowest unoccupied molecular orbital (LUMO) of the molecules and ensure longer wavelength absorption. Electron-rich chromophores can be integrated with benzothiadiazole by several palladium catalyzed cross-coupling reactions leading to the formation of vinyl (Heck), acetylene (Sonogashira), C-C (Stille or Suzuki or Negishi) and C-N (Buchwald-Hartwig) linkages. Though several dipolar compounds featuring benzothiadiazole acceptor and donors such as triphenylamine, indoline, carbazole, fluorene, etc. have been known in the literature, the best of our knowledge, compounds containing amines directly attached to benzothiadiazole and benzothiadiazole functionalized with phenothiazine, pyridine or ferrocene are not yet explored. It is our intention to use phenothiazine and ferrocene as donor components in the construction of dipolar compounds suitable for application in BHJSCs. Also suitably designed molecules with cyanoacrylic acid or pyridine as end groups can be exploited as sensitizers for DSSCs. Both the vinylic and C-C linkages have been used to tether the benzothiadiazole with the functional chromophores such as phenothiazine and amine donors. This allows us to evaluate the effect of slight alternations in the structure on the electronic properties and thermal stability of the molecules.

The thesis is divided into eight chapters. First chapter presents the aim and scope of the work. Second chapter outlines the review of the available literature related to the synthesis, optical and electrochemical characterization and electronic applications of benzothiadiazole-based compounds used in DSSCs and BHJSCs.

Figure 1. Structures of the amine directly integrated benzothiadiazole sensitizers.

Chapter 3 describes the synthesis, photophysical, electrochemical and photovoltaic performance of the amine directly integrated benzothiadiazole featured sensitizers (Figure 1). The dyes were constructed by C-N, C-C bond forming reactions followed by a Knoevenagel condensation reaction. They exhibited excellent light harvesting properties as identified from their absorption spectra. All the dyes showed two prominent bands originating from the charge transfer and π - π^* transitions respectively. These assignments were confirmed by the time-dependent density functional theoretical calculations. Effects of protonation/deprotonation on the absorption profile of the sensitizers have been investigated by electronic absorption measurements in the presence of TFA/TEA. The dyes showed blue shifted absorption on addition of trifluoroacetic acid and triethyl amine, due to the protonation of the amine group and deprotonation of the cyanoacrylic acid groups, respectively. Time-dependent density functional theoretical calculations were performed to evaluate the nature of the electronic excitations occurred by the absorption of light. The torsion angles (θ) between the benzothiadiazole moiety and thiophene, bithiophene were less when compared with the phenyl spacer, allows the high electronic communication and resulted to the larger red-shift in absorption bands in former dyes. The DSCs sensitized by the dyes **6a** and **6b** obtained the η values 1.68 % ($J_{sc} = 7.54 \text{ mA cm}^{-2}$, $V_{oc} = 0.36 \text{ V}$ and $ff = 0.62$) and 3.07 % ($J_{sc} = 12.4 \text{ mA cm}^{-2}$, $V_{oc} = 0.40 \text{ V}$ and $ff = 0.63$) respectively. It is ascertained that direct attachment of donor to the BTD-unit is not jeopardized, to obtain better solar cell performance of these dyes further molecular design is needed.

We have developed four novel D-A- π -A organic dyes (Figure 2) incorporating benzothiadiazole/benzotriazole as the auxiliary acceptor units, phenothiazine as the electron donor, cyanoacrylic acid as the anchoring group and thiophene, benzene are used as the π -linker between auxiliary acceptor and cyanoacrylic acid acceptor in Chapter 4. These sensitizers were unambiguously characterized by spectroscopic and TD-DFT techniques. The photophysical and electrochemical properties of the dyes were conveniently tuned by alternating the auxiliary acceptor and the π -linker. Incorporation of a phenothiazine donor group on the benzo(thiadiazole/triazole) conjugation segment bathochromically shifted the absorption wavelength probably due to the ICT, which results in a pronounced donor-acceptor interaction. The absorption and electrochemical properties dyes reveals that the both auxiliary acceptor analogs play exactly different roles. The TDDFT calculations proved that, the photoexcited electrons could be successively transferred from the phenothiazine donor to the benzo(thiadiazole/triazole) auxiliary acceptor unit, then transferred to the cyanoacetic acid subunit, and finally to nanocrystalline TiO₂ surface. It was consistent with our proposed auxiliary acceptor cascaded role. The molecular engineering approach demonstrated in this chapter provides an important guide for choice of the auxiliary acceptors for the development of novel materials for use in dye sensitized solar cells as well as BHJ solar cells.

Figure 2. Structures of the benzothiadiazole/benzotriazole based sensitizers.

The synthesis and electro-optical properties of the organic dyes derived from benzothiadiazole and pyridine connected by a vinyl bridge featured with different donors (Figure 3) are presented in the Chapter 5. The donors piperidine, morpholine were directly attached and carbazole, phenothiazine, ferrocene were attached by vinyl linkage to benzothiadiazole, respectively. The effect of the protonation/deprotonation of the pyridine unit on absorption spectra of the dyes was studied by addition trifluoroacetic acid/triethylamine. The

addition of TFA leads to a significant red-shift in the absorption spectra, owing to the protonation occurred on nitrogen atom of the pyridine ring. And red shifted absorption spectra attained the indigene position by deprotonation of the dyes on addition of TEA. From DFT calculations it was confirmed that, when these pyridine anchoring dyes applied in DSSCs, electrons from donor part sequentially transferred to benzothiadiazole moiety, then shifted to the pyridine anchoring unit, and finally to nanocrystalline TiO₂ surface.

Figure 3. Structures of pyridine anchoring sensitizers featured with benzothiadiazole.

The synthesis and characterization of a new family of phenothiazine-benzothiadiazole vinyl hybrids (Figure 4) were described in the chapter 6. The dyes were synthesized by palladium-catalyzed Heck cross coupling reactions and isolated in good yields. The extended conjugation in the dyes **28a**, **28b** drafted to display the red shifted absorptions with high molar extension coefficients than **26a**, **26b**. All the new dyes displayed one-electron reversible oxidation, irreversible reduction peaks in cyclic voltammetry which are attributable to the oxidation of the phenothiazine and reduction of the benzothiadiazole units, respectively. The dye **27** exhibited the low band gap in the series due to the presence of two strong electron donating phenothiazine units. There is a reasonable correlation between the experimental and calculated optical data from TDDFT. The thermal decomposition temperatures of the dyes are greater than 400 °C, which is good enough to apply in any optoelectronic device. The photophysical and electrochemical properties of the dyes are highly dependent on the conjugation length and the pattern of the linkage mode between benzothiadiazole and phenothiazine. In this chapter we

have established the structure-property relationship in the new phenothiazine-benzothiadiazole conjugates extended through vinyl linkage.

Figure 4. Structures of the benzothiadiazole-phenothiazine vinyl conjugated derivatives.

Chapter 7 describes the synthesis, photophysical and electrochemical properties of the organic-inorganic hybrid materials containing benzothiadiazole-ferrocene (Figure 5). The complexes were thoroughly characterized by the routine spectroscopic techniques, the structure of complex **30a** was confirmed by single crystal X-ray diffraction analysis. The dyes were exhibited excellent light absorbing properties and non-fluorescent in nature. All these complexes exhibited one-electron reversible oxidation, irreversible reduction peaks in cyclic voltammetry which are attributable to the removal of electron from ferrocene and reduction of the benzothiadiazole units, respectively. The electronic properties of these complexes were also examined by the DFT calculations and found to be in agreement with the observed trends. All the complexes showed the high thermal stability. It was demonstrated that the optical and electrochemical properties of the complexes are tuned by modulation of electro-active group on the benzothiadiazole unit.

Figure 5. Structures of the benzothiadiazole-ferrocene complexes.

In Chapter 8, a summary of the work accomplished during the dissertation work is presented. A comparison of the optical, electrochemical and DSSC characteristics of the benzothiadiazole based dyes reported in this dissertation with that known in the literature is taken into account. The role of direct attachment of amine directly connected to benzothiadiazole for DSSC, benzothiadiazole linked with double bond to phenothiazine, pyridine and ferrocene, which are suitable in the design for organic solar cells (OSC) is unraveled. Similarly the role of auxiliary acceptors benzothiadiazole/benzotriazole, in phenothiazine donor based dyes for DSSCs is seriously analyzed.

Table of contents

<i>Candidate's Declaration</i>	i
<i>Acknowledgements</i>	iii
<i>Abstract</i>	v
<i>Table of Contents</i>	xi
<i>List of Figures</i>	xv
<i>List of Tables</i>	xxi
Chapter 1 Benzo[<i>c</i>][1,2,5]thiadiazole Based Functional Materials for Organic Photovoltaic Applications	1
1.1 References	5
Chapter 2 Benzothiadiazole Based Organic Dyes for Dye-Sensitized Solar Cells: Synthesis and Structure-Property Relations	9
2.1 Introduction	9
2.2 Benzothiadiazole (BTD) Featured Organic Sensitizers for Dye-Sensitized Solar Cells	11
2.2.1 Acceptor (anchoring) group directly attached BTD featured sensitizers	35
2.2.2 5,6-bis-alkoxy-benzo[2,1,3]thiadiazole featured sensitizers	39
2.2.3 Molecular engineering at 5, 6-position of benzothiadiazole	45
2.2.4 Molecular engineering in indoline donor featured benzothiadiazole sensitizers	51
2.2.5 Benzothiadiazole and Porphyrin complex based sensitizers	58
2.2.6 Miscellaneous benzothiadiazole featured sensitizers	60
2.3 Conclusions and Outlook	63
2.4 References	64
Chapter 3 Amino-Benzothiadiazole Based Organic Dyes For Dye-Sensitized Solar Cells: Tuning the optical properties by Donor and π-linker Modification	77
3.1 Introduction	77
3.2 Results and Discussion	82
3.2.1 Synthesis and Characterization	82

3.2.2	Structural Analysis of 5a	83
3.2.3	Optical properties	84
3.2.4	Electrochemical properties	92
3.2.5	Computational studies	94
3.2.6	Photovoltaic performance	102
3.3	Conclusions	104
3.4	Experimental section	105
3.4.1	Materials and physical methods	105
3.4.2	Computational details	105
3.4.3	Synthesis	106
3.5	References	111
Chapter 4	Phenothiazine Donor Based Organic dye for Dye-Sensitized Solar Cells: Effect of Auxiliary Acceptors on Optical and Electrochemical Properties	117
4.1	Introduction	117
4.2	Results and discussions	120
4.2.1	Design and synthesis	120
4.2.2	Absorption spectra	121
4.2.3	Emission spectra	127
4.2.4	Electrochemistry	130
4.2.5	Molecular modeling	131
4.3	Conclusions	139
4.4	Experimental section	140
4.4.1	Materials and physical methods	140
4.5	References	143
Chapter 5	Benzothiadiazole Based Pyridine Anchoring Organic Dyes for Dye-Sensitized Solar Cells: Effect of Donor on Optical and Photovoltaic Properties	153
5.1	Introduction	153
5.2	Results and Discussion	158
5.2.1	Synthesis	158

5.2.2	Single-Crystal X-ray Structural Analysis of 16	159
5.2.3	Optical Properties	160
5.2.4	Electrochemical Properties	172
5.2.5	Quantum chemical calculations	175
5.2.6	Thermal properties	183
5.2.7	Photovoltaic performances	184
5.3	Conclusions	188
5.4	Experimental section	189
5.4.1	Material and Methods	189
5.4.2	Synthesis	190
Chapter 6	Benzothiadiazole-Phenothiazine Vinyl Conjugates: Effect of Conjugation on Optical and Electrochemical properties	199
6.1	Introduction	199
6.2	Results and Discussion	203
6.2.1	Synthesis and Characterization	203
6.2.2	Photophysical Properties	204
6.2.3	Electrochemical Properties	218
6.2.4	Theoretical Calculations	221
6.2.5	Thermal Properties	228
6.3	Conclusions	229
6.4	Experimental Section	230
6.4.1	Material and Methods	230
6.4.2	Synthesis	230
6.5	References	232
Chapter 7	Benzothiadiazole-Ferrocene π-Extended Conjugates with Vinyl Linkage: Synthesis, Structure, Electrochemical and Thermal Properties	241
7.1	Introduction	241
7.2	Results and Discussion	244
7.2.1	Synthesis of Ferrocene-Benzothiadiazole Conjugates	244
7.2.2	X-ray Crystallography of 30a	246

7.2.3	Absorption spectra	247
7.2.4	Electrochemical Studies	253
7.2.5	Computational Chemistry	256
7.2.6	Thermal Properties	263
7.3	Conclusions	264
7.4	Experimental Section	265
7.5	References	266
Chapter 8	Summary	275
	Supporting Information	279

List of Figures

Figure 1.1	Resonance structures of 2,1,3-benzothiadiazole	1
Figure 1.2	Structure of benzothiadiazole and closely related analogs obtained by replacement of the sulphur atom	2
Figure 1.3	Structures obtained by modulating the benzene unit in the BTD unit	3
Figure 1.4	Structures obtained by annulating the nitrogen heterocyclic units to the benzene moiety in the BTD	3
Figure 1.5	Resonance structures (aromatic and quinoid) of BTD derivatives	3
Figure 1.6	Snapshot of the proposed ideas	4
Figure 2.1	Structures of various organic sensitizers for DSSCs.	10
Figure 2.2	Structures of organic sensitizers featuring various auxiliary acceptors for DSSCs.	11
Figure 2.3	Structure and numbering of 2,1,3-benzothiadiazole	11
Figure 2.4	Configuration of benzothiadiazole organic sensitizers featured aryl amine donor	13
Figure 2.5	Structures and trends in optical and electrochemical data for benzo(thia/selena)diazole bridged organic dyes with arylamine donors	14
Figure 2.6	Structures of the π -extended benzothiadiazole sensitizers	15
Figure 2.7	Structures of the benzothiadiazole dyes with hexyl chain on the thiophene unit of <i>n</i> -hexyl dithienylbenzothiadiazole bridge	16
Figure 2.8	Structures of the dyes containing bis-fluoreneamine based donor based benzothiadiazole dyes	18
Figure 2.9	Structures of the anthracene-based dyes	19
Figure 2.10	Structures of cyanine dyes with triphenylamine donor and carboxylic acid acceptor	20
Figure 2.11	Structures of platinum(II) bis(aryleneethynylene) featured with benzothiadiazole sensitizers	21
Figure 2.12	Structures of π -conjugated fluorene-benzothiadiazole bridged sensitizers	23
Figure 2.13	Chemical structures of sensitizers based on naphtho[2,1- <i>b</i> :3,4- <i>b'</i>]dithiophene	23
Figure 2.14	Molecular structures of the dyes based on chromophoric core of cyclopentadithiophene-benzothiadiazole	24
Figure 2.15	Molecular structures of the dyes based on chromophoric core of cyclopentadithiophene-benzothiadiazole	25
Figure 2.16	Molecular structures of the dyes based on chromophoric core of cyclopentadithiophene-benzothiadiazole	27
Figure 2.17	Molecular structures of 5-phenyl-iminostilbene based sensitizers	29
Figure 2.18	Chemical structures of the carbazole based dyes	30
Figure 2.19	Molecular structures of carbazole based sensitizers	31
Figure 2.20	Structures of rigid triarylamine-donor based sensitizers	32
Figure 2.21	Molecular structures of dyes based on dihydroindolo[2,3- <i>b</i>]carbazole donor and trends observed in optical and electrochemical data	33
Figure 2.22	Configuration of acceptor (anchoring) group directly attached BTD sensitizers	35

Figure 2.23	Structures of <i>N,N</i> -diphenyl-4-vinylaniline donor featured sensitizers	37
Figure 2.24	4-(2,2'-bithiophen-5-yl)- <i>N,N</i> -bis(4-(hexyloxy)phenyl)aniline donor based BTD sensitizers	37
Figure 2.25	Structures of acceptor directly attached to benzothiadiazole based sensitizers	38
Figure 2.26	Structures of the diarylthienylamine donor based sensitizers	38
Figure 2.27	General representation of 5,6-bis-alkoxy-benzo[2,1,3]thiadiazole based sensitizers	40
Figure 2.28	Structure of the 5,6-bis-hexyloxy-benzo[2,1,3]thiadiazole based sensitizers	41
Figure 2.29	Effect of the π -spacer between diphenylamine and 5,6- bis(octyloxy)benzo[<i>c</i>][1,2,5]thiadiazole on absorption maximum	42
Figure 2.30	5,6-Bis(octyloxy)benzo[<i>c</i>][1,2,5]thiadiazole-bridged sensitizers	43
Figure 2.31	Effect of the π -spacer between 5,6- Bis(octyloxy)benzo[<i>c</i>][1,2,5]thiadiazole and cyanoacrylic acid on absorption maximum	44
Figure 2.32	Structures and trends in absorption maxima and open circuit voltage (V_{OC}) data of dyes featured with and without alkoxy chains at the benzothiadiazole entity	45
Figure.2.33	Structures of thiadiazolo[3,4- <i>c</i>]pyridine based dyes with different arylamine donors	47
Figure.2.34	Structures of thiadiazolo[3,4- <i>c</i>]pyridine based dyes with different arylamine donors	49
Figure 2.35	Molecular structures of the benzothiadiazole dyes with 2-cyanopyridine as an electron-accepting and anchoring group	50
Figure 2.36	Structures of the sensitizers containing 5 <i>H</i> -[1,2,5]thiadiazolo [3,4- <i>f</i>]isoindole-5,7(6 <i>H</i>)-dione and 6 <i>H</i> -pyrrolo[3,4- <i>g</i>]quinoxaline-6,8(7 <i>H</i>)- dione units	50
Figure 2.37	Configuration of indoline donor featured benzothiadiazole sensitizers	51
Figure 2.38	Structures of the indoline or triphenylamine donors featured benzothiadiazole sensitizers	53
Figure 2.39	Molecular structures of indoline based sensitizers	55
Figure 2.40	Structures and trends in optical and electrochemical properties of benzothiadiazole featured indoline dyes	57
Figure 2.41	Molecular structures of porphyrin dyes featured with benzothiadiazole	58
Figure 2.42	Molecular structures of the porphyrin dyes	60
Figure 2.43	Chemical structures of coumarin dyes containing benzothiadiazole	61
Figure 2.44	Structures of branchlike organic dye containing benzothiadiazole with vinylenes unit	62
Figure 2.45	Dithienylbenzothiadiazole/dithienylthienothiadiazole based sensitizer	62
Figure 3.1	Structures of the fluorene-based triarylamine sensitizers	78
Figure 3.2	Structures of the cyclopentadithiophene bridged organic sensitizers	78

Figure 3.3	Structures of the naphtho[2,1- <i>b</i> :3,4- <i>b'</i>]dithiophene based sensitizers containing triphenylamine	79
Figure 3.4	Structures of the alkoxytriphenylamine donor and benzothiadiazole based sensitizer	79
Figure 3.5	Structures of the indoline/triphenylamine donor featured benzothiadiazole sensitizers	80
Figure 3.6	Contributions of 4,7-diamino-substituted BTB forms	80
Figure 3.7	General representation and numbering of the sensitizers possessing amine directly attached to benzothiadiazole	81
Figure 3.8	Structures of the organic sensitizers with amine directly attached to benzothiadiazole	81
Figure 3.9	The molecular structure of (5a) showing the atom-labelling scheme	83
Figure 3.10	Absorption spectra of the dyes recorded in tetrahydrofuran solutions	84
Figure 3.11	Comparison of the absorption spectra of the dyes (a) 6a , (b) 6b with intermediates recorded in THF	87
Figure 3.12	Absorption spectra of dyes (a) 4a , (b) 4b , (c) 6a and (d) 6b recorded in different solvents	88
Figure 3.13	Absorption spectra of dyes(a) 6c , (b) 6d recorded in different solvents; Changes in the absorption spectra of the dyes (c) 4a , (d) 4b in dichloromethane upon addition of TFA or TEA	89
Figure 3.14	Changes in the absorption spectra of the dyes (a) 6a , (b) 6b , (c) 6c and (d) 6d in dichloromethane upon addition of TFA or TEA	90
Figure 3.15	Emission spectra of the dyes recorded in tetrahydrofuran solutions	91
Figure 3.16	(a) Cyclic voltammograms recorded for the dyes in THF (b) Differential pulse voltammograms of the dyes recorded in THF	92
Figure 3.17	Structures and trends in absorption maxima and oxidation potential of dyes studied in this chapter	94
Figure 3.18	Isodensity surface plots of dyes 4a , 4b and 6a	98
Figure 3.19	Isodensity surface plots of dyes 6b , 6c and 6d	99
Figure 3.20	Calculated inter-planar angles ($^{\circ}$) between various aromatic segments and cyanoacrylic acid plane in the optimized geometries of the dyes	101
Figure 3.21	(a) I-V and (b) IPCE (c) Nyquist and (d) Bode phase plots for the devices measured under 100 mW cm^{-2} illumination	103
Figure 4.1	Structures and numbering scheme of BTB and BTA	118
Figure 4.2	General representation of the benzothiadiazole/benzotriazole auxiliary acceptor based sensitizers	119
Figure 4.3	Molecular structures of dyes	120
Figure 4.4	Absorption spectra of the dyes recorded in THF	121
Figure 4.5	Illustration of acid-base equilibrium in the sensitizers	123
Figure 4.6	Absorption spectra of dyes (a) 11a , (b) 11b (c) 14a (d) 14b recorded in different solvents	124
Figure 4.7	Absorption spectra of dyes (a) 11a (b) 11b (c) 14a (d) 14b in DMF recorded in the presence of TFA or TEA	125
Figure 4.8	Absorption spectra of dyes (a) 11a (b) 11b (c) 14a (d) 14b in toluene recorded in the presence of TFA or TEA	126
Figure 4.9	Emission spectra of the dyes recorded in THF	128

Figure 4.10	Emission spectra of dyes (a) 11a (b) 11b (c) 14a (d) 14b recorded in different solvents.	129
Figure 4.11	(a) Cyclic voltammograms recorded for the dyes in THF (b) Differential pulse voltammograms of the dyes recorded in THF	130
Figure 4.12	Frontier molecular orbitals of the dyes 11a (left) and 11b (right)	133
Figure 4.13	Frontier molecular orbitals of the dyes 14a (right) and 14b (left)	134
Figure 4.14	Computed dihedral angles between the different aryl groups in the dyes	138
Figure 5.1	Structures of the dyes with various anchoring groups known in the literature	154
Figure 5.2	Structures of the pyridine anchoring sensitizers known in the literature	155
Figure 5.3	Structures of pyridine anchoring sensitizers featured with benzothiadiazole	157
Figure 5.4	General representation and numbering of the pyridine featured benzothiadiazole sensitizers	158
Figure 5.5	ORTEP diagram of 16 with the atom-numbering scheme.	160
Figure 5.6	Absorption spectra of dyes recorded in dichloromethane	160
Figure 5.7	Absorption spectra of intermediates 2a , 2b and 16 recorded in dichloromethane	161
Figure 5.8	Absorption spectra of dyes recorded on thin film	161
Figure 5.9	Effect of the donor attached to benzothiadiazole unit and effect of addition of TFA on absorption maximum	163
Figure 5.10	Absorption spectra of (a) 15a (b) 15b (c) 17 (d) 19a recorded in different solvents	166
Figure 5.11	Absorption spectra of (a) 19b (b) 19c recorded in different solvents and (c) 15a (d) 15b recorded in toluene before and after addition of TFA and TEA	167
Figure 5.12	Changes in the absorption spectra of (a) 17 (b) 19a (c) 19b (d) 19c addition of TFA and TEA recorded in toluene	168
Figure 5.13	Emission spectra of the dyes recorded in toluene	169
Figure 5.14	Emission spectra of the dyes recorded in different solvents (a) 15a (b) 15b (c) 17 (d) 19a	171
Figure 5.15	(a) Emission spectra of the dye 19b recorded in different solvents. Correlation of solvent-induced Stokes shift with (b) orientation polarizability (c) $E_T(30)$ parameter for compounds 17 and 19a	171
Figure 5.16	Differential pulse voltammograms recorded for intermediates 2a , 2b and 16 in dichloromethane	173
Figure 5.17	Differential pulse voltammograms recorded for dyes in dichloromethane	173
Figure 5.18	Frontier molecular orbitals of dyes 15a , 15b and 17 computed by using TDDFT at the B3LYP level	176
Figure 5.19	Frontier molecular orbitals of dyes 19a , 19b and 19c computed by using TDDFT at the B3LYP level	177
Figure 5.20	Calculated dihedral angle angles ($^\circ$) between various aromatic segments and vinyl pyridine planes in the optimized geometries of the dyes	181
Figure 5.21	Direction of the dipole moment of the dyes	182
Figure 5.22	Thermograms of the benzothiadiazole-vinylpyridine dyes	184
Figure 5.23	(a) I-V characteristics (b) IPCE plots (c) Nyquist plots (d) Bode phase plots for the DSSCs that were fabricated by using these dyes under	185

	illumination at 100 mWcm ⁻²	
Figure 5.24	(a) Nyquist plots of the DSSCs fabricated using the dyes under dark conditions (b) Absorption spectra of the dyes anchored on nanocrystalline TiO ₂	187
Figure 6.1	Resonance structures (aromatic and quinoid) of BTD	200
Figure 6.2	Structures of the tetrathiafulvalene-benzothiadiazole based derivatives	200
Figure 6.3	Structures of triphenylamine-benzothiadiazole reported vinyl derivatives	200
Figure 6.4	Structures of the phenothiazine based vinyl derivatives known in the literature.	201
Figure 6.5	Structures of the benzothiadiazole-phenothiazine vinyl conjugated derivatives	202
Figure 6.6	Absorption spectra of the dyes recorded in dichloromethane	204
Figure 6.7	Absorption spectra of the dyes recorded on thin film	205
Figure 6.8	Absorption spectra of the dyes (a) 26a (b) 26b (c) 27 (d) 28a recorded in different solvents	206
Figure 6.9	Absorption spectra of 28b recorded in different solvents	207
Figure 6.10	Emission spectra of the dyes recorded in DCM	208
Figure 6.11	Emission spectra of the dyes recorded in toluene	208
Figure 6.12	Emission spectra of the dye (a) 26a , (b) 26b , (c) 27 and (d) 28a recorded in different solvents	211
Figure 6.13	Emission spectra of the dye (a) 28b recorded in different solvents, (b) 28a recorded at various concentrations in toluene and (c) 28b recorded at various concentrations in toluene	212
Figure 6.14	Plots for 26a in different solvents (a) Lippert-Mataga plot showing Stokes' shift vs orientation polarizability of the solvents, (b) Stokes' shift vs $E_T(30)$ parameter, (c) Emission maxima (in wavenumber unit) vs Kamlet-Taft solvent polarity	213
Figure 6.15	Plots for 26b in different solvents (a) Lippert-Mataga plot showing Stokes' shift vs orientation polarizability of the solvents, (b) Stokes' shift vs $E_T(30)$ parameter, (c) Emission maxima (in wavenumber unit) vs Kamlet-Taft solvent polarity	214
Figure 6.16	Plots for 27 in different solvents (a) Lippert-Mataga plot showing Stokes' shift vs orientation polarizability of the solvents, (b) Stokes' shift vs $E_T(30)$ parameter, (c) Emission maxima (in wavenumber unit) vs Kamlet-Taft solvent polarity parameter	215
Figure 6.17	Plots for 28a in different solvents (a) Lippert-Mataga plot showing Stokes' shift vs orientation polarizability of the solvents, (b) Stokes' shift vs $E_T(30)$ parameter, (c) Emission maxima (in wavenumber unit) vs Kamlet-Taft solvent polarity parameter	216
Figure 6.18	Plots for 28b in different solvents (a) Lippert-Mataga plot showing Stokes' shift vs orientation polarizability of the solvents, (b) Stokes' shift vs $E_T(30)$ parameter, (c) Emission maxima (in wavenumber unit) vs Kamlet-Taft solvent polarity parameter	217
Figure.6.19	(a) Cyclic voltammograms recorded for the dyes 26a-b , 27 , 28a (b) Differential pulse voltammograms of the dyes recorded in	219

	dichloromethane solution	
Figure 6.20	Energy-level diagram of the phenothiazine-benzothiadiazole hybrids	220
Figure 6.21	Snap shot of the trends in absorption and electrochemical data of the new benzothiadiazole-phenothiazine dyes	220
Figure 6.22	Electronic distribution observed for the frontier molecular orbitals of the dyes 26a , 26b and 27	222
Figure 6.23	Electronic distribution observed for the frontier molecular orbitals of the dyes 28a and 28b	223
Figure 6.24	Simulated electronic transitions for the dyes by MPW1K	227
Figure 6.25	TGA plots for the dyes	228
Figure 7.1	Structures of the known ferrocene-benzothiadiazole dyes in the literature	243
Figure 7.2	Structures of the benzothiadiazole-ferrocene hybrid complexes	244
Figure 7.3	Ferrocene-benzothiadiazole vinyl hybrid complexes general representation	244
Figure 7.4	ORTEP plot of the complex 30a	247
Figure 7.5	Absorption spectra of the complexes recorded in (a) dichloromethane (b) thin solid film	248
Figure 7.6	Absorption spectra of the complexes recorded in different solvents (a) 30a (b) 30b , (c) 30c and (d) 19c	250
Figure 7.7	Absorption spectra of the complex (a) 30d recorded in different solvents (b) 30a in toluene before and after addition of TFA or TEA	251
Figure 7.8	Absorption spectra of (a) 30b , (b) 30c , (c) 19c and (d) 30d in toluene before and after addition of TFA or TEA	252
Figure 7.9	Cyclic voltammograms of the ferrocene benzothiadiazole conjugates recorded in dichloromethane at the scan rate 100 mV/sec	254
Figure 7.10	Energy-level diagram of the ferrocene-benzothiadiazole hybrid complexes	255
Figure 7.11	Structures and trends in optical and electrochemical data of complexes studied in this chapter	255
Figure 7.12	Trends in optical and electrochemical data for the ferrocene derivatives	256
Figure 7.13	Electronic distributions in the frontier molecular orbitals of the complexes 30a-c	258
Figure 7.14	Electronic distributions in the frontier molecular orbitals of the complexes 19c , 30d	259
Figure 7.15	TGA plots for ferrocene-benzothiadiazole complexes	263

List of tables

Table 2.1	Photophysical, electrochemical and photovoltaic performances of DSSCs data based on dyes 1-17	20
Table 2.2	Photophysical, electrochemical and photovoltaic performances of DSSCs data based on dyes 18-38	27
Table 2.3	Photophysical, electrochemical and photovoltaic performances of DSSCs data based on dyes 39-61	34
Table 2.4	Photophysical, electrochemical and photovoltaic performances of DSSCs data based on dyes 62-72	39
Table 2.5	Photophysical, electrochemical and photovoltaic performances of DSSCs data based on dyes 73-83	44
Table 2.6	Photophysical, electrochemical and photovoltaic performances of DSSCs data based on dyes 84-102	51
Table 2.7	Photophysical, electrochemical and photovoltaic performances of DSSCs data based on dyes 103-116	57
Table 2.8	Photophysical, electrochemical and photovoltaic performances of DSSCs data based on dyes 117-123	60
Table 2.9	Photophysical, electrochemical and photovoltaic performances of DSSCs data based on dyes 124-128	63
Table 3.1	Optical data of dyes recorded in tetrahydrofuran	85
Table 3.2	Absorption spectral data for the dyes in different solvents	87
Table 3.3	Electrochemical properties of the benzothiadiazole based sensitizers	93
Table 3.4	Computed vertical excitation energies, dipole moments, and frontier orbital energies for dyes using B3LYP (gas)	95
Table 3.5	Computed vertical excitation energies, dipole moments, and frontier orbital energies for dyes using MPW1K (gas)	96
Table 3.6	Computed vertical excitation energies, dipole moments, and frontier orbital energies for dyes using MPW1K (THF)	97
Table 3.7	Photovoltaic-performance parameters of the dyes	102
Table 4.1	Absorption data of the dyes recorded in tetrahydrofuran	122
Table 4.2	Absorption data for the dyes in various solvents.	123
Table 4.3	Emission properties and Stokes shift observed for the dyes in the different solvents	128
Table 4.4	Electrochemical properties of the benzothiadiazole based sensitizers	131
Table 4.5	Computed vertical transition energies, oscillator strengths (<i>f</i>), and their assignment for the dyes using B3LYP (gas)	135
Table 4.6	Computed vertical transition energies, oscillator strengths (<i>f</i>), and their assignment for the dyes using MPW1K (gas)	136
Table 4.7	Computed vertical transition energies, oscillator strengths (<i>f</i>), and their assignment for the dyes ^[a] MPW1K (THF)	137
Table 5.1	Absorption properties of dyes in different solvents	164
Table 5.2	Absorption data of the dyes recorded in dichloromethane	164
Table 5.3	Optical, electrochemical and DSSC data for organic dyes having pyridine anchoring group for DSSCs	164
Table 5.4	Absorption data of the dyes recorded in toluene before and after addition of	165

	TFA or TEA	
Table 5.5	Emission properties and Stokes shift observed for the dyes in the different solvents	172
Table 5.6	Electrochemical data of complexes recorded in dichloromethane	174
Table 5.7	Predicted vertical transitions, oscillator strength, configurations, orbital energies, and dipole moments using B3LYP (gas)	178
Table 5.8	Predicted vertical transitions, oscillator strength, configurations, orbital energies, and dipole moments using MPW1K (gas)	179
Table 5.9	Predicted vertical transitions, oscillator strength, configurations, orbital energies and dipole moments using MPW1K (THF)	180
Table 5.10	Thermal properties of the benzothiadiazole-pyridine anchoring sensitizers	184
Table 5.11	Photovoltaic-performance parameters of the dyes.	187
Table 6.1	Absorption data of the dyes recorded in different solvents	207
Table 6.2	Emission properties and Stokes shift observed for the dyes in different solvents	209
Table 6.3	Electrochemical properties of the dyes in dichloromethane solution	219
Table 6.4	Predicted vertical transitions and their assignments by B3LYP (gas)	224
Table 6.5	Predicted vertical transitions and their assignments by MPW1K (gas)	225
Table 6.6	Predicted vertical transitions and their assignments by MPW1K (THF)	226
Table 6.7	Thermal properties of the benzothiadiazole-phenothiazine conjugates	229
Table 7.1	¹ H Spectral data of the complexes recorded in CDCl ₃	246
Table 7.2	¹³ C Spectral data the complexes recorded in CDCl ₃	246
Table 7.3	Absorption spectral data of the hybrid complexes recorded in different solvents	249
Table 7.4	Absorption data of the complexes recorded in toluene before and after addition of TFA/TEA	251
Table 7.5	Electrochemical data of complexes recorded in dichloromethane	253
Table 7.6	Computed vertical transition energies, oscillator strengths (<i>f</i>), and their assignment for the complexes ^[a] using B3LYP (gas)	260
Table 7.7	Computed vertical transition energies, oscillator strengths (<i>f</i>), and their assignment for the complexes ^[a] using PBE1PBE (THF)	261
Table 7.8	Direction and size of dipole moment of the complexes	262
Table 7.9	Thermal properties of the benzothiadiazole-ferrocene complexes	264

Chapter 1

Benzo[*c*][1,2,5]thiadiazole Based Functional Materials for Organic Photovoltaic Applications

Recently, small molecule based low band gap organic materials have attracted immense attention owing to their potential application in a wide variety of electronic and optoelectronic devices, such as organic light-emitting diodes (OLEDs) [1-4], organic field-effect transistors (OFETs) [5-7], organic solar cells (OSC) [8-11], liquid crystals [12-13], sensors [14-16] etc. These low molecular weight low band gap organic π -conjugated materials have several advantages over the polymer counter parts due to the well-defined structures, high purity and these materials can be processable by either vacuum sublimation or solution casting [17-18]. In the class of low band gap small molecule based dyes, benzothiadiazole derivatives have become popular and are still in the focus of intensive research. 2,1,3-benzothiadiazole (BTD) is a bicyclic compound that contains an unsaturated 6-membered ring fused to a five-membered ring with two nitrogen atoms at 1,3 position and one sulphur atom at 2 position. It bears a thiadiazole chromophore (-N=S=N-) which make it electron deficient, the structure and resonance forms were shown in Figure 1.1.

Figure 1.1 Resonance structures of 2,1,3-benzothiadiazole

BTD unit has a well conjugated structure. Due to its low energy gap between the highest occupied molecular orbital (HOMO) and lowest unoccupied molecular orbital (LUMO), BTD derivatives are recognized as promising candidates for application in dye-sensitized, bulk heterojunction solar cells. BTD can be easily functionalized at 4 and 7 positions by versatile synthetic strategies. Due to high electron affinity of BTD, both small molecules and polymers

containing electron-rich (donor) units in conjugation established to have low band gap. Owing to the strong intermolecular interactions across heteroatom contacts and/or π - π interactions, benzothiadiazole derivatives exhibited well-ordered crystal structures [19]. In small molecules, as compared to polymers, precise control is possible to place and position the electron releasing/donating chromophores and they also enjoy the advantage of post structural modifications via simple chemical reactions while retaining high purity, long life and thermal stability [20-21]. Distinct synthetic design in small molecule based systems allows the tailoring of the energy gap between the HOMO and the LUMO. Extension of conjugation with amine, BTD core renders to exhibit low band gap and intense red emission. Due to this they have attracted considerable interest and widely employed as electron transport materials in organic light emitting diodes, as sensitizers in dye-sensitized solar cells, as a donor material in bulk heterojunction solar cells and as semiconductors in organic field effect transistors (OFETs). BTD and its derivatives have played a pivotal role in the development of organic semiconducting materials. The success of BTD in constructing highly efficient organic photovoltaic materials inspired chemists to exploit its analogues as building blocks for new photovoltaic materials. If the sulphur atom of the BTD is replaced with the oxygen, selenium, nitrogen and carbon atoms, their emerged new acceptor units benzooxadiazole, benzoselenadiazole, benzotriazole, dialkyl-2*H*-benzimidazole, respectively [22] (Figure 1.2).

Figure 1.2 Structure of benzothiadiazole and closely related analogs obtained by replacement of the sulphur atom

BTB and related derivations have already become popular and are still in the focus of intensive research, due to the great potential to generate an effective photocurrent in organic solar cells, when appropriate donor-acceptor units are present in their backbone. The optical and electronic properties of the materials can also be fine-tuned by the replacement of the benzene ring in the BTB unit with more electron-deficient heterocycle such as pyridine [17-18] and the

replacement of the hydrogen atoms in the 5,6-positions of BTD with fluorine atoms [23-24] and alkyloxyl chains [25] (Figure 1.3). By annulating another nitrogen heterocyclic to the benzene unit in the BTD unit several new derivatives were obtained and structures are shown in Figure 1.4.

Figure 1.3 Structures obtained by modulating the benzene unit in the BTD unit

Figure 1.4 Structures obtained by annulating the nitrogen heterocyclic units to the benzene moiety in the BTD

In most cases, the quinoid form has a smaller band gap (HOMO/LUMO energy difference) than the aromatic mesomeric form. Generally, the molecules which contains BTD chromophore show smaller band gaps, this may be due to the π -conjugated system adopts a quinoid geometry seems to be the case of these molecules [19, 26] (Figure 1.5).

Figure 1.5 Resonance structures (aromatic and quinoid) of BTD derivatives

The combination of donor and acceptor units within a same conjugated molecule constructs the bipolar materials which have been used in photovoltaic devices. Organic dyes have many advantages such as high light harvesting property and easier structural-modifications which regulate the photophysical properties along with good charge transport properties, solubility, morphological stability and cost effectively. Owing to the strong electron withdrawing character of benzothiadiazole, it normally strengthens the donor-acceptor interaction in the bipolar

materials and benefits the absorption properties. It is interesting to examine the effect of structural differences arising due to the functionalization of benzothiadiazole with different donors, acceptors and π -linkers. We wish to study how the modulation of these chromophores plays a significant role in tuning the photophysical, electro chemical properties of the benzothiadiazole dyes.

Figure 1.6 Snapshot of the proposed ideas

In this thesis we have developed benzothiadiazole-based organic materials which possess absorption in the low energy region and these materials can be used as opto-electronic materials in suitable electronic devices. Most of the materials developed in this thesis work are interesting due to their structural simplicity and diverse photophysical properties. It was expected that the dyes which contain carboxylic acid can function as efficient sensitizers in dye-sensitized solar cells. Second chapter outlines the review of the available literature related to the synthesis and structure-property relations of the benzothiadiazole-based sensitizers used in DSSCs. Chapter 3 describes the synthesis, photophysical, electrochemical and photovoltaic performance of the amine directly integrated benzothiadiazole sensitizers. In Chapter 4, we have synthesized four new phenothiazine donor based sensitizers comprising benzothiadiazole/benzotriazole auxiliary acceptors and the cyanoacrylic acid unit as an electron acceptor. We have analyzed the consequences on the photophysical and electrochemical properties of the sensitizers by replacing of benzothiadiazole with benzotriazole. We have designed and synthesized a series of benzothiadiazole sensitizers with pyridine terminal anchoring group, endowed with different electron donating segments by palladium catalyzed Heck-cross coupling reactions in chapter 5. The modulation of donor segment successfully led to structure-dependent optical, electronic,

and redox properties. Chapter 6 describes the synthesis and characterization of a new family of phenothiazine-benzothiadiazole vinyl hybrids. The optical and electrochemical properties of the dyes are highly dependent on the donor strength and conjugation. In chapter 7, we have described the synthesis, photophysical and electrochemical properties of the organic-inorganic hybrid materials containing benzothiadiazole-ferrocene. It was demonstrated that the optical and electro chemical properties of the complexes can be tuned by modulation of electro-active group on the benzothiadiazole unit. In Chapter 8, a summary of the work accomplished during the dissertation work is presented.

1.1 References

- (1) K. R. J. Thomas, J. T. Lin, M. Velusamy, Y. T. Tao and C. H. Chuen, Color Tuning in Benzo[1,2,5]thiadiazole-Based Small Molecules by Amino Conjugation/Deconjugation: Bright Red-Light-Emitting Diodes. *Adv. Funct. Mater.* **2004**, *14*, 83-90.”
- (2) Y. Qiu, P. Wei, D. Q. Zhang, J. Qiao, L. Duan, Y. K. Li, Y. D. Gao and L. D. Wang, Novel Naphtho[2,3-*c*][1,2,5]thiadiazole Derivative for Non-doped Small Molecular Organic Red-Light-Emitting Diodes. *Adv. Mater.* **2006**, *18*, 1607-11.
- (3) T. Khanasa, N. Prachumrak, R. Rattanawan, S. Jungsuttiwong, T. Keawin, T. Sudyoadsuk, T. Tuntulani and V. Promarak, An efficient solution processed non-doped red emitter based on carbazole-triphenylamine end-capped di(thiophen-2-yl)benzothiadiazole for pure red organic light-emitting diodes. *Chem Commun* **2013**, *49*, 3401-3.
- (4) J. L. Wang, Y. Zhou, Y. Li and J. Pei, Solution-processable gradient red-emitting pi-conjugated dendrimers based on benzothiadiazole as core: synthesis, characterization, and device performances. *J. Org. Chem.* **2009**, *74*, 7449-56.
- (5) T. Kono, D. Kumaki, J. Nishida, S. Tokito and Y. Yamashita, Dithienylbenzobis(thiadiazole) based organic semiconductors with low LUMO levels and narrow energy gaps. *Chem Commun* **2010**, *46*, 3265-7.
- (6) X. Zhao and X. Zhan, Electron transporting semiconducting polymers in organic electronics. *Chem. Soc. Rev.* **2011**, *40*, 3728-43.
- (7) S. Kato, T. Furuya, A. Kobayashi, M. Nitani, Y. Ie, Y. Aso, T. Yoshihara, S. Tobita and Y. Nakamura, pi-Extended thiadiazoles fused with thienopyrrole or indole moieties: synthesis, structures, and properties. *J. Org. Chem.* **2012**, *77*, 7595-606.

- (8) B. Walker, X. Han, C. Kim, A. Sellinger and T. Q. Nguyen, Solution-processed organic solar cells from dye molecules: an investigation of diketopyrrolopyrrole:vinazene heterojunctions. *ACS Appl. Mater. Interfaces* **2012**, *4*, 244-50.
- (9) A. Mishra and P. Bauerle, Small molecule organic semiconductors on the move: promises for future solar energy technology. *Angew. Chem., Int. Ed.* **2012**, *51*, 2020-67.
- (10) Q. Liu, H. Zhan, C. L. Ho, F. R. Dai, Y. Fu, Z. Xie, L. Wang, J. H. Li, F. Yan, S. P. Huang and W. Y. Wong, Oligothiophene-Bridged Bis(arylene ethynylene) Small Molecules for Solution-Processible Organic Solar Cells with High Open-Circuit Voltage. *Chem. Asian J.* **2013**, *8*, 1892-900.
- (11) Y. Lin, Y. Li and X. Zhan, Small molecule semiconductors for high-efficiency organic photovoltaics. *Chem. Soc. Rev.* **2012**, *41*, 4245-72.
- (12) M. P. Aldred, M. Carrasco-Orozco, A. E. A. Contoret, D. Dong, S. R. Farrar, S. M. Kelly, S. P. Kitney, D. Mathieson, M. O'Neill, W. C. Tsoi and P. Vlachos, Organic electroluminescence using polymer networks from smectic liquid crystals. *Liq. Cryst.* **2006**, *33*, 459-67.
- (13) H. Gallardo, G. Conte, P. A. Tuzimoto, B. Behramand, F. Molin, J. Eccher and I. H. Bechtold, New Luminescent Liquid Crystals Based on 2,1,3-Benzothiadiazole and Bent Five-membered N-Heterocyclic Cores. *Liq. Cryst.* **2012**, *39*, 1099-111.
- (14) H.-B. Sun, S.-J. Liu, T.-C. Ma, N.-N. Song, Q. Zhao and W. Huang, An excellent BODIPY dye containing a benzo[2,1,3]thiadiazole bridge as a highly selective colorimetric and fluorescent probe for Hg²⁺ with naked-eye detection. *New J. Chem.* **2011**, *35*, 1194.
- (15) X. Wu, Z. Guo, Y. Wu, S. Zhu, T. D. James and W. Zhu, Near-Infrared Colorimetric and Fluorescent Cu²⁺ Sensors Based on Indoline-Benzothiadiazole Derivatives via Formation of Radical Cations. *ACS Appl. Mater. Interfaces* **2013**, *5*, 12215-20.
- (16) C. Saravanan, S. Easwaramoorthi, C.-Y. Hsiow, K. Wang, M. Hayashi and L. Wang, Benzoselenadiazole Fluorescent Probes – Near-IR Optical and Ratiometric Fluorescence Sensor for Fluoride Ion. *Org. Lett.* **2013**, *16*, 354-7.
- (17) Y. Sun, G. C. Welch, W. L. Leong, C. J. Takacs, G. C. Bazan and A. J. Heeger, Solution-processed small-molecule solar cells with 6.7% efficiency. *Nat. Mater.* **2012**, *11*, 44-8.
- (18) X. Liu, Y. Sun, L. A. Perez, W. Wen, M. F. Toney, A. J. Heeger and G. C. Bazan,

- Narrow-band-gap conjugated chromophores with extended molecular lengths. *J. Am. Chem. Soc.* **2012**, *134*, 20609-12.
- (19) B. A. D. Neto, A. A. M. Lapis, E. N. da Silva Júnior and J. Dupont, 2,1,3-Benzothiadiazole and Derivatives: Synthesis, Properties, Reactions, and Applications in Light Technology of Small Molecules. *Eur. J. Org. Chem.* **2013**, *2013*, 228-55.
- (20) Y.-H. Chen, L.-Y. Lin, C.-W. Lu, F. Lin, Z.-Y. Huang, H.-W. Lin, P.-H. Wang, Y.-H. Liu, K.-T. Wong, J. Wen, D. J. Miller and S. B. Darling, Vacuum-Deposited Small-Molecule Organic Solar Cells with High Power Conversion Efficiencies by Judicious Molecular Design and Device Optimization. *J. Am. Chem. Soc.* **2012**, *134*, 13616-23.
- (21) L.-Y. Lin, Y.-H. Chen, Z.-Y. Huang, H.-W. Lin, S.-H. Chou, F. Lin, C.-W. Chen, Y.-H. Liu and K.-T. Wong, A Low-Energy-Gap Organic Dye for High-Performance Small-Molecule Organic Solar Cells. *J. Am. Chem. Soc.* **2011**, *133*, 15822-5.
- (22) C. Duan, F. Huang and Y. Cao, Recent development of push-pull conjugated polymers for bulk-heterojunction photovoltaics: rational design and fine tailoring of molecular structures. *J. Mater. Chem.* **2012**, *22*, 10416-34.
- (23) S. Paek, N. Cho, K. Song, M.-J. Jun, J. K. Lee and J. Ko, Efficient Organic Semiconductors Containing Fluorine-Substituted Benzothiadiazole for Solution-Processed Small Molecule Organic Solar Cells. *J. Phys. Chem. C* **2012**, *116*, 23205-13.
- (24) N. Cho, J. Han, K. Song, M.-S. Kang, M.-J. Jun, Y. Kang and J. Ko, Substituent effect of fluorine atom on benzothiadiazole bridging unit in dye sensitized solar cells. *Tetrahedron* **2014**, *70*, 427-33.
- (25) H.-H. Chou, Y.-C. Chen, H.-J. Huang, T.-H. Lee, J. T. Lin, C. Tsai and K. Chen, High-performance dye-sensitized solar cells based on 5,6-bis-hexyloxy-benzo[2,1,3]thiadiazole. *J. Mater. Chem.* **2012**, *22*, 10929.
- (26) R. Mondal, S. Ko and Z. Bao, Fused aromatic thienopyrazines: structure, properties and function. *J. Mater. Chem.* **2010**, *20*, 10568-76.

Chapter 2

Benzothiadiazole Based Organic Dyes for Dye-Sensitized Solar Cells: Synthesis and Structure-Property Relationship

2.1 Introduction

Metal free organic sensitizers used in dye-sensitized solar cells (DSSCs) usually consist of donor- π -acceptor architecture [1-2]. The photophysical, electrochemical and photovoltaic performance of the sensitizer can be tuned either by altering the nature of donor, acceptor and π -linker. Electron rich system like dialkylaminophenyl group [3], triarylamine [1, 4-7], phenothiazine [8-11], carbazole [12-14], indoline [15-19], coumarin [20-22] etc. based moieties generally serve as donors. Cyanoacrylic acid [4, 23-25], rhodanine-3-acetic acid [10, 26], carboxylic acid [27], pyridine ring [28] etc. which can effectively bind with nanocrystalline TiO₂ can act as electron-accepting/anchoring group. Any conjugated moiety which allows the transfer of electrons from donor to acceptor can act as π -linker. Phenyl, thiophene, furan, pyrrole, double, triple bond etc. are commonly employed spacers [1, 29-31].

The structures of the organic dyes having different donor- π -acceptor systems are shown in Figure 2.1. Generally, the sensitizers based on the donor- π -acceptor (D- π -A) framework show absorption in the shorter wavelength region and fail to absorb light from visible region and near IR region. The light harvesting property of the sensitizer can be improved by increasing the conjugation length, but long π -conjugated dye molecules easily form unfavourable π -stacks and are not stable when irradiated with high-energy photons [14]. Indeed, to improve photocurrent and spectral response auxiliary acceptor was introduced to remodel the molecular design of organic sensitizers. The structures of organic sensitizers featuring various auxiliary acceptors were shown Figure 2.2. By the introduction of electron withdrawing moiety in the backbone of the organic dye, we can reduce the energy gap and increase the photo stability of the sensitizer. The efficiency of amine free sensitizers is < 7% [32]. This is due to lack of effective photoinduced intramolecular charge transfer. So strong donor-acceptor interactions are

mandatory to have an effective photoinduced intramolecular charge transfer and it is beneficial for the enhancement of light-harvesting response.

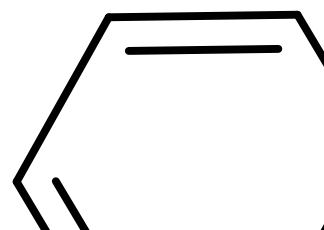


Figure 2.1 Structures of various organic sensitizers for DSSCs.

In this context Lin and co-workers introduced a new D- π -A- π -A configuration containing low bandgap chromophores as auxiliary acceptors [33]. Later, several electron withdrawing moieties such as cyano [34], benzotriazole [35-36], imidazole [32], quinoxaline [24, 37-38], diketopyrrolopyrrole [16, 39], thiazole [40], bithiazole [41], triazine [42-43], and isoindigo [4, 44] etc. were introduced in an attempt to enhance the spectral response. Among all the auxiliary acceptors, BTD unit containing sensitizers showing better results in DSSCs due to the well-aligned energy levels. In this respect, various dyes with BTD have been prepared and used as sensitizers in DSSCs. The auxiliary acceptor may be in different configurations like D- π -A- π -A or D-A- π -A or D- π -A-A. By the introduction of auxiliary acceptor in the sensitizers, the donor-acceptor interactions may be enhanced and their by photoinduced intramolecular charge transfer, light harvesting response greatly improved. The introduction of auxiliary acceptor in the sensitizers has distinguished merits such as: (I) the HOMO and LUMO energy levels will be well separated and the HOMO-LUMO energy gap reduced. (II) photo-stability of synthetic intermediates and final sensitizers will be enhanced [45]. (III) the auxiliary acceptor can facilitate the electron transfer from the donor to the acceptor. (IV) the introduction of nitrogen containing heterocyclic moieties can improve the V_{oc} by uplifting the conduction band edge of TiO_2 [46]. (V) the photocurrent and light harvesting properties of the sensitizer will be greatly enhanced.

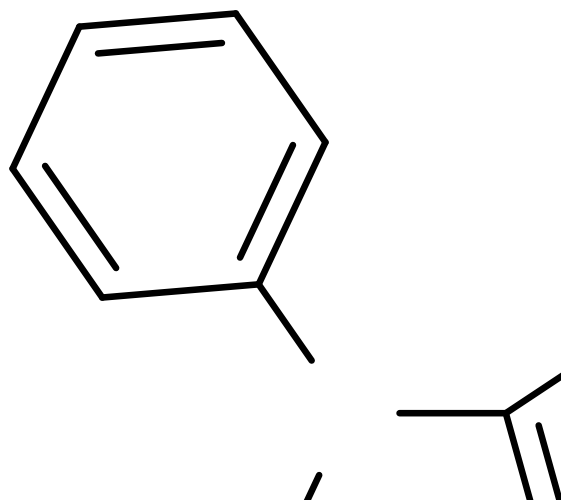


Figure 2.2 Structures of organic sensitizers featuring various auxiliary acceptors for DSSCs.

2.2 Benzothiadiazole (BTD) Featured Organic Sensitizers for Dye-Sensitized Solar Cells

Figure 2.3 Structure and numbering of 2,1,3-benzothiadiazole.

Benzothiadiazole (BTD) structure and numbering is shown in Figure 2.3. The most commonly used intermediate for the synthesis of benzothiadiazole-containing π -extended sensitizers is 4,7-dibromo-2,1,3-benzothiadiazole. From commercially available ortho-

phenylenediamine, the intermediate 4,7-dibromo-2,1,3-benzothiadiazole can be easily prepared in two steps with high yields on a multigram scale (Scheme 2.1) [47].

Scheme 2.1 Synthesis of 4,7-dibromo-2,1,3-benzothiadiazole.

Recently, the synthesis, properties and reactions of BTD have been reviewed [48]. Indeed, BTD derivatives have proved as promising candidates for numerous opto-electronic applications like organic light-emitting diodes (OLEDs) [49-51], organic thin-film transistors (OFETs) [52], dye-sensitized solar cells (DSSCs) [27, 53-55], bulk-heterojunction solar cells (BHJs) [56-58], two-photon absorption [59-60], chemosensors [61-62], and so on. In this chapter, we mainly focused on the dyes composed with benzothiadiazole and applied in dye sensitized solar. Organic dyes with configuration of D- π -A have absorption maxima in the shorter wavelength region and suffer from the lack of absorption in near IR regime. To enhance the photocurrent response in the longer wavelength region by lowering the HOMO-LUMO energy gap electron deficient benzothiadiazole was introduced in the organic dye backbone. Indeed, the HOMO/LUMO levels of π -extended conjugated sensitizers are determined by their electron affinity and ionization potential, which is directly correlated with electrochemical reduction and oxidation potentials. Compounds bearing this BTD ring are good candidates as electron carriers due to their relatively high reduction potential and electron affinity. Molecular design of the organic sensitizer plays a pivotal role in the performance of the DSSCs. The position of donor, acceptor and spacers in the dye design play major role in the photovoltaic performance of the dye. So in this context we discuss the influence of donor, acceptor and spacers on photophysical, electrochemical properties and DSSCs performance of the benzothiadiazole dyes.

Benzothiadiazole based organic dyes with different molecular architectures for dye-sensitized solar cells have received great attention in the last decade because of their great potential to absorbing lower energy radiations, achieved low band gaps by lowering the LUMO energy level and so on. In the ahead of time, the efficiency of DSSCs with benzothiadiazole organic dyes was far behind that of DSSCs with ruthenium(II) complexes partly due to the lack

of information about the structure-property relationship between the chemical structures and the photovoltaic performance of the dyes. However energizing progress has been recently made and power conversion efficiencies over 9% were obtained for DSSCs with benzothiadiazole organic dyes. The light absorption capabilities, donor and acceptor strength with different π -spacers and the efficiency of the solar cell are equated, providing a comprehensive overview of benzothiadiazole organic dyes. The general configuration of benzothiadiazole organic sensitizers featured with aryl amine donor is shown in Figure 2.4. The optical, electrochemical and DSSC data of the dyes **1-17** were presented in Table 2.1.

Figure 2.4 Configuration of benzothiadiazole organic sensitizers featured aryl amine donor

Although benzothiadiazole was known in polymers, from the report of Lin and co-workers [33] benzothiadiazole based dyes was recognized as promising candidates for DSSCs. In this article authors have developed benzothiadiazole and benzoselenadiazole chromophore based dyes (Figure 2.5) which perform efficiently in DSSC. The synthesis of low band gap benzo(thia/selena)diazole featuring sensitizers was achieved in three steps and is shown in Scheme 2.2. The first step involves the integration of BTD core with donor by Stille or Suzuki coupling reactions. In the next step, the mono bromo derivatives were exposed to Stille coupling reaction with (5-(1,3-dioxolan-2-yl)thiophen-2-yl)tributyl stannane, followed by the cleavage of the 1,3-dioxalane protecting group to produce aldehyde derivatives. Finally the aldehyde intermediates were converted to required dyes by Knoevenagel condensation on reaction with cyanoacetic acid. In these dyes triarylamine derivatives were used as donors, thiophene as linker between BTD and cyanoarylic acid. *N,N*-diphenylthiophen-2-amine donor based derivatives **3-4** were showing red-shifted absorption profiles than triphenyl amine based dyes **1-2**, this is due to the more electron donating ability and coplanarity of the donor segment. Benzothiadiazole dyes showing promising results than benzoselanadiazole dyes, because of higher optical density for the charge transfer transition. In the benzothiadiazole dyes, phenylene conjugated derivative (**1**) showing enhanced efficiency due to a twisted non-planar geometry, which will decelerate the recombination of charges in the charge separated state when compared to the thiophene analogue.

Scheme 2.2 Synthesis of the low band gap benzo(thia/selena)diazole chromophore featuring dyes.

Figure 2.5 Structures and trends in optical and electrochemical data for benzo(thia/selena)diazole bridged organic dyes with arylamine donors.

Kim and co-workers [63] synthesised series of dyes in which triphenyl amine acts as donor, benzothiadiazole as spacer and cyano acrylic acid as acceptor (Figure 2.6). In this piece of work

Benzothiadiazole-Based Sensitizers for DSSCs: A Review

authors have examined the effect of mode of linkage between triphenyl amine and benzothiadiazole from single, double, triple bonds on photophysical, electrochemical, photovoltaic performance. Dye **6** showed red shifted absorption, low oxidation potential due to the relatively longer conjugation by alkene bridging unit. Introduction of bulky alkoxy group onto triphenylamine unit in **8**, bathochromically shifted the absorption maxima and cathodically shifted oxidation potential when compared with the dye **5**. Owing to the higher charge separation, C-C bond bridged dye **5** exhibit better photovoltaic performance than double and triple bond linked dyes. By the introduction of bulky alkoxy group on triphenyl amine donor in **8**, by red shifting the absorption profile and reducing the aggregation, achieved 7.30% efficiency with $J_{SC} = 17.9 \text{ mA cm}^{-2}$, $V_{OC} = 0.62 \text{ V}$, $ff = 0.66$ under standard global AM 1.5G illumination.

Figure 2.6 Structures of the π -extended benzothiadiazole sensitizers.

Pei and co-workers [64] developed two novel benzothiadiazole dyes **9** and **10** (Figure 2.7) showing 6.04%, 4.68% efficiency which contains triphenyl amine and methoxytriphenyl amine derivative as donors, respectively. The dye **10** showed 17 nm red shifted absorption and low oxidation potential due to the electron richness of the donor. The electrochemical properties of the dyes in thin films were probed by cyclic voltammetry (CV). The HOMO and LUMO energy levels of the dyes determined from electrochemical measurements in thin films were 0.83 V, 0.67 V and -1.03 V, -0.88 V respectively. Even though dye **10** having low band gap than the dye **9** showing less efficiency due to the weaker driving force of dye regeneration and electron injection process of the dye.

Figure 2.7 Structures of the benzothiadiazole dyes with hexyl chain on the thiophene unit of *n*-hexyl dithienylbenzothiadiazole bridge.

Ko and co-workers [65-66] demonstrated the nonplanar bis-dimethyl-fluorenylamino moiety as donor and a cyanoacrylic acid acceptor (Figure 2.8). The synthesis of sensitizers was achieved in several steps and is shown in Scheme 2.3. They have investigated the substitution effect of hexyl and fluorine atom at 5-and/or 6-position of 2,1,3-benzothiadiazole bridging unit on photovoltaic performance. The sensitizers were prepared by synthetic protocols shown in Scheme. The introduction of hexyl groups on dithienyl benzothiadiazole blue shifted the absorption by 66 nm, due to the twist between thienyl and benzothiadiazole units in **12**. The dihedral angle of the thienyl and benzothiadiazole units in **11** is 5.8°, where as in **12** the dihedral angle is 44.4° (Figure 2.11). The dyes **11**, **12** showing conversion efficiency of 4.66% ($J_{SC} = 9.58 \text{ mA cm}^{-2}$, $V_{OC} = 643 \text{ mV}$) and 6.61% ($J_{SC} = 12.03 \text{ mA cm}^{-2}$, $V_{OC} = 720 \text{ mV}$), respectively using a polymer gel electrolyte comprising 0.6 M 1,2-dimethylpropylimidazolium iodide, 0.1 M I_2 , poly(vinylidene fluoride-co-hexafluoro)propylene (5% PVDF-HFP) and 0.5 M NMBI in 3-methoxypropionitrile (MPN). Enhanced V_{OC} is due to the increased electron life time by preventing the dark current and high J_{SC} is due to the reduced reorganization energy by the introduction of hexyl groups on thiophene units in dye **12**, which assisted to increase the efficiency. The DSSCs based on **11** and **12** achieved efficiencies of 7.51% and 8.19% respectively, using an acetonitrile electrolyte comprising 0.6 M DMPIImI, 0.05 M I_2 , 0.1 M LiI and 0.5 M *tert*-butylpyridine. The dyes **13** and **14** showed higher J_{SC} and V_{OC} compared to the dye **11** which have no fluorine atom substitution. The dye **14** achieved efficiency of 5.91% which is higher than the dye **11** (4.11%) under similar conditions due to the less molecular aggregation.

Scheme 2.3 Synthetic Strategy used for the formation of dye **11-14**.

Figure 2.8 Structures of the dyes containing bis-fluoreneamine based donor based benzothiadiazole dyes.

Thomas and co-workers [67] developed new metal free 9,10-difunctionalized anthracene-based dyes (Figure 2.9) for DSSCs. The synthesis of the 9,10-difunctionalized anthracene integrated BTD sensitizer **17** was achieved by multi step protocol, which was shown in the Scheme 2.4. The first step involves the synthesis of mono thiophene derivative from dibromoanthracene by treating with thienylmagnesiumbromide in the presence of $\text{Pd}(\text{PPh}_3)_2\text{Cl}_2$ in tetrahydrofuran. The donor was attached to anthracene by palladium catalyzed ($\text{Pd}(\text{dba})_2/(\text{t-Bu})_3\text{P}$) C-N cross coupling with N-phenylnaphthalen-1-amine. The aldehyde derivative was accessed by condensing the stannylene derivative of 2,6-di-tert-butyl-N-(naphthalen-1-yl)-N-phenyl-9-(thiophen-2-yl)anthracen-10-amine with 5-(7-bromobenzo[*c*][1,2,5]thiadiazol-4-yl)thiophene-2-carbaldehyde by following the Stille coupling protocol and $\text{Pd}(\text{PPh}_3)_2\text{Cl}_2/\text{DMF}$ reagent system. In the final step, the aldehyde precursor was successfully converted to the desired dye **17** on treatment with cyanoacetic acid in the presence of ammonium acetate catalyst in acetic acid. By the inclusion of the benzothiadiazole in the conjugation path improved the optical properties, interestingly oxidation potential was cathodically shifted due to the lack strong interaction between donor and acceptor unit, and helped to localize the unoccupied molecular orbital (LUMO) on the acceptor segment which is useful for the facile charge transfer

Benzothiadiazole-Based Sensitizers for DSSCs: A Review

transition. Finally hike in efficiency for dye **17** (3.23%) was observed with $J_{SC} = 9.80 \text{ mA cm}^{-2}$, $V_{OC} = 520 \text{ mV}$ and $ff = 0.63$ by the adoption of benzothiadiazole unit than the dye **16** (2.91%).

Scheme 2.4 Synthetic Strategy used for the formation of dye **17**

Figure 2.9 Structures of the anthracene-based dyes

Benzothiadiazole-Based Sensitizers for DSSCs: A Review

Table 2.1 Photophysical, electrochemical and photovoltaic performances of DSSCs data based on dyes **1-17**

Dye	$\lambda_{\text{abs}}/\text{nm}$	$E_{\text{OX}}/\text{V}(\text{NHE})$	$E^*_{\text{OX}}/\text{V}(\text{NHE})$	V_{OC}/mV	$J_{\text{SC}}/\text{mA cm}^{-2}$	ff	$\eta/\%$	Ref
1	491 ^a	1.35	-0.77	546	10.44	0.66	3.77	33
2	502 ^a	1.33	-0.69	524	8.35	0.67	2.91	33
3	541 ^a	1.09	-0.77	517	3.21	0.69	1.15	33
4	544 ^a	1.03	-0.74	474	3.57	0.66	1.11	33
5	533 ^a	1.05	-0.92	580	15.0	0.65	5.72	63
6	546 ^a	0.93	-1.01	540	10.6	0.59	3.37	63
7	515 ^a	1.19	-0.92	560	13.0	0.63	4.55	63
8	542 ^a	0.98	-0.95	620	17.9	0.66	7.30	63
9	557 ^a	0.83	-1.03	545	16.46	0.67	6.04	64
10	574 ^a	0.67	-0.88	555	11.94	0.71	4.68	64
11	534 ^b	0.98	-0.95	643	9.58	0.76	4.66	65
12	468 ^b	1.08	-0.99	720	12.03	0.76	6.61	65
13	538 ^a	0.83	-1.10	0.65	11.96	0.68	5.32	66
14	461 ^a	0.80	-1.41	0.67	12.57	0.69	5.91	66
15	434 ^a	1.37	-1.08	565	6.00	0.65	2.20	67
16	436 ^a	1.27	-1.12	535	8.28	0.66	2.91	67
17	486 ^a	1.22	-0.88	520	9.80	0.63	3.23	67

^a In THF ^b In EtOH

Figure 2.10 Structures of cyanine dyes with triphenylamine donor and carboxylic acid acceptor.

A series of cyanine dyes were synthesized and applied as sensitizer for DSSCs by Hua and co-workers [68-69] containing triphenylamine donor and carboxylic acid acceptor bridged by a low-band-gap benzothiadiazole as a conjugating fragment. For the purpose of comparison authors synthesized the corresponding cyanine dye without benzothiadiazole (Figure 2.10). The dye **19** containing benzothiadiazole achieved better performance due to broader absorption and higher molar extinction coefficient in visible region with an overall conversion efficiency of 7.62% ($J_{\text{SC}} = 22.10 \text{ mA cm}^{-2}$, $V_{\text{OC}} = 540 \text{ mV}$, $ff = 0.48$) under irradiation with 75 mW cm^{-2}

white light from a Xe lamp. Whilst under irradiation of AM1.5G simulated solar light (100 mW cm^{-2}), after addition of CDCA the dyes **19** and **20** achieved PCE of 2.59% ($J_{SC} = 8.51 \text{ mA cm}^{-2}$, $V_{OC} = 504 \text{ mV}$, $ff = 0.60$), 3.28% ($J_{SC} = 11.00 \text{ mA cm}^{-2}$, $V_{OC} = 504 \text{ mV}$, $ff = 0.59$).

Wong and co-workers [70] designed and synthesized four unsymmetric platinum(II) bis(aryleneethynylene) complexes containing 2-cyano-3-(5-ethynylthiophen-2-yl)acrylic acid as the electron acceptor and anchoring group, and the benzothiadiazole unit with triphenylamine moiety as the electron donor (Figure 2.11). Among these platinum(II) compounds, **23** exhibited red shifted ICT transition at 547 nm, which could be explained by the stronger electron-donating ability of the donor group and longer π -conjugation length. Sensitizers **21** and **22** achieved power conversion efficiency of 1.56% ($J_{SC} = 3.60 \text{ mA cm}^{-2}$, $V_{OC} = 620 \text{ mV}$, $ff = 0.70$) and 1.57% ($J_{SC} = 3.63 \text{ mA cm}^{-2}$, $V_{OC} = 590 \text{ mV}$, $ff = 0.73$) respectively. The partial charge trapping at the benzothiadiazole moiety limits the J_{SC} of the complexes and jeopardizes the electron injection from sensitizers to TiO_2 surface.

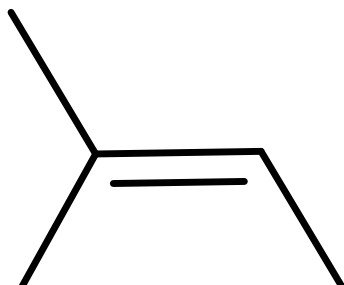


Figure 2.11 Structures of platinum(II) bis(aryleneethynylene) featured with benzothiadiazole sensitizers.

A series of organic dyes **25-27** (Figure 2.12) were prepared containing fluorene-benzothiadiazole unit as a π -conjugated bridge for the first time by Kimura and co-workers to apply as sensitizers in DSSCs [71]. The synthetic pathways for the preparation of the fluorine-benzothiadiazole bridged organic sensitizers through several steps are illustrated in Scheme 2.5. The starting precursor 4-bromo-7-(7-(7-bromobenzo[*c*][1,2,5]thiadiazol-4-yl)-9,9-dihexyl-9*H*-fluoren-2-yl)benzo[*c*][1,2,5]thiadiazole was yielded by the Suzuki coupling reaction of 9,9-dihexylfluorene-2,7-diboronic acid with three equivalents of 4,7-dibromo-2,1,3-benzothiadiazole (scheme 2.5). The dye **27**, in which the bis(4-methoxyphenyl)amine unit was directly attached to the fluorene-benzothiadiazole bridge, showed a red-shifted absorption

Benzothiadiazole-Based Sensitizers for DSSCs: A Review

maxima by 55 nm and lower oxidation potential by (90 mv) compared with **25**, **26** which confirms the stronger electron-donating nature of the bis(4-methoxyphenyl)amine unit. The DSSCs based on the dye **27** reached a PCE of 4.0%, which is 55% of the Ru dye N719 cell fabricated under the same conditions with a short-circuit photocurrent density $J_{SC} = 7.8 \text{ mA cm}^{-2}$, an open-circuit photovoltage $V_{OC} = 680 \text{ mV}$, and a fill factor $ff = 0.77$.

Scheme 2.5 Synthetic pathways for the preparation of the fluorene-benzothiadiazole bridged organic sensitizers

Figure 2.12 Structures of π -conjugated fluorene-benzothiadiazole bridged sensitizers

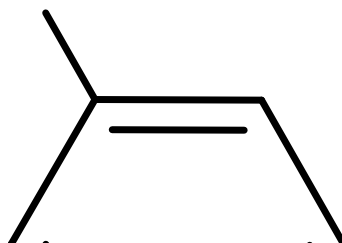


Figure 2.13 Chemical structures of sensitizers based on naphtho[2,1-*b*:3,4-*b'*]dithiophene

Wang and co-workers [54] embedded auxiliary donor (3,4-ethylenedioxythiophene) and auxiliary acceptor (benzothiadiazole) into naphtho[2,1-*b*:3,4-*b'*]dithiophene (NDT) based organic sensitizers (Figure 2.13). In this report authors have emphasized that the incorporation auxiliary acceptor benzothiadiazole is helpful for broadening of the absorption spectrum and improvement of the DSSC performance. The incorporation of 3,4-ethylenedioxythiophene, benzothiadiazole in between the electron donor and NDT moiety the absorption maximum was bathochromically shifted by 24 nm and 55 nm, respectively and which is beneficial to light-harvesting and short-circuit current enhancement. However, due to the presence of the BTD unit in **30**, the HOMO-LUMO gap was decreased by 0.2 eV. The DSSCs performance of the dyes evaluated by using a liquid electrolyte containing 0.6 M 1,2-dimethyl-3-n-propylimidazolium

Benzothiadiazole-Based Sensitizers for DSSCs: A Review

iodide (DMPIImI), 0.1 M LiI, 0.05 M I₂, and 0.5 M *tert*-butylpyridine (TBP) in acetonitrile with co-adsorbent deoxycholic acid. The dye **30** generated an impressive efficiency of 8.2% ($J_{SC} = 16.36 \text{ mA cm}^{-2}$, $V_{OC} = 694 \text{ mV}$, $ff = 0.72$), under the same conditions the device fabricated from **28** achieved only 5.2% ($J_{SC} = 10.59 \text{ mA cm}^{-2}$, $V_{OC} = 726 \text{ mV}$, $ff = 0.68$), which revealed that the inclusion of a benzothiadiazole moiety is helped for broadening the absorption spectrum of the sensitizer as well as efficiency.

Wang and co-workers [27] synthesized a series of dyes comprising chromophoric core of cyclopentadithiophene-benzothiadiazole bearing benzoic acid anchoring group as sensitizers in DSSCs (Figure 2.14). The TDDFT results reveal that the linking the triphenylamine unit to the cyclopentadithiophene raised the HOMO energy level than linking to the benzothiadiazole unit. Further attaching the benzoic acid to the benzothiadiazole segment lowered the LUMO, than attaching to the cyclopentadithiophene unit. The DSSCs was fabricated by using Co-bpy cells as the electrolyte. The dye **32** achieved a conversion efficiency of 10.4% ($J_{SC} = 7.82 \text{ mA cm}^{-2}$, $V_{OC} = 871 \text{ mV}$ and $ff = 0.766$) measured at an irradiance of 50 mW cm^{-2} , simulated AM 1.5 sunlight. The dye **34** exhibited even higher efficiencies in the range from 11.5% to 12.8% by co-grafting with the dye **31**, which is a benchmark for organic dye-sensitized solar cells. The optical, electrochemical and DSSC data of the dyes **18-38** were displayed in Table 2.2.



Figure 2.14 Molecular structures of the dyes based on chromophoric core of cyclopentadithiophene-benzothiadiazole

Benzothiadiazole-Based Sensitizers for DSSCs: A Review

Wang and co-workers synthesized two dyes (Figure 2.15) containing cyclopentathiophene π -spacer (CPDT) for broad light harvesting character and utilized for DSSC using $[\text{Co}(\text{bpy})]^{2+/3+}$ as electrolyte [72]. The synthesis of the dyes by standard protocols of Stille, Vilsmeier, Suzuki and Knoevenagel condensation reactions, synthetic scheme was shown in Scheme and structures of the dyes shown in Scheme 2.6. The introduction of BTDA as auxiliary acceptor the dye **36** showed a red shifted absorption of 44 nm compared to reference dye **35**. The broader absorption and enhanced molar extinction coefficient in the visible region for the dye **36** helped to achieve high J_{SC} and showed higher efficiency. The experimental studies reveal that the dye **36** has ultrafast charge injection in TiO_2 upon photoinduced excitation in cobalt complex electrolyte system. The dye **36** has achieved higher efficiency of 7.99% and it was improved to 9.01% by optimizing the photo anode of mesoporous TiO_2 layers (4.8 μm transparent + 2 μm scattering layers).

Scheme 2.6 Synthesis of CPDT and benzothiadiazole conjugated linker based dyes.

Figure 2.15 Molecular structures of the dyes based on chromophoric core of cyclopentadithiophene-benzothiadiazole

Benzothiadiazole-Based Sensitizers for DSSCs: A Review

Grätzel co-workers synthesized two dyes (Figure 2.16) containing a benzothiadiazole unit in a π -spacer and a cyanoacrylic acid as an acceptor and tested as sensitizers in dye-sensitized solar cells [73]. The synthetic protocol used to accomplish the dyes is shown in Scheme 2.7. The dyes mainly differ in donor group attached to the benzothiadiazole unit. The introduction of dibutoxy phenyl as peripheral group on donor part gave the dye **38**. The extension of the π -conjugation on the electron donating diphenylamine moiety does not lead to a significant change in the position of the absorption bands. But the introduction of dibutoxy phenyl in the dye **38** helped to improve the excited state lifetime by 3-fold when compared with the dye **37**. The introduction of dibutoxy phenyl helped to improve the photovoltaic conversion efficiency due to an increase in J_{SC} and V_{OC} values. The dye **38** achieved higher efficiency of 8.0% ($J_{SC} = 16.0 \text{ mA cm}^{-2}$, $V_{OC} = 678 \text{ mV}$, and $ff = 0.73$) when compared to the dye **37** ($\eta = 7.01\%$) due to extension of the π -system on the donor moiety. The optical, electrochemical and DSSC data of the dyes **18-38** were presented in Table 2.2.

Scheme 2.7 Synthesis of CPDT and benzothiadiazole conjugated linker based dyes.

Figure 2.16 Molecular structures of the dyes based on chromophoric core of cyclopentadithiophene-benzothiadiazole

Table 2.2 Photophysical, electrochemical and photovoltaic performances of DSSCs data based on dyes **18-38**

Dye	λ_{abs}	$E_{\text{OX}}/\text{V}(\text{NHE})$	$E^*_{\text{OX}}/\text{V}(\text{NHE})$	V_{OC}/mV	$J_{\text{SC}}/\text{mA cm}^{-2}$	ff	$\eta/\%$	Ref
18	588 ^a	-	-	570	15.79	0.55	6.58	68
19	590 ^b	1.02	-0.83	504	8.51	0.60	2.59	69
20	590 ^b	-	-	540	22.10	0.48	7.62	68
		1.07	-0.78	504	11.00	0.59	3.28	69
21	496 ^c	0.73	-1.07	620	3.60	0.70	1.56	70
22	493 ^c	0.66	-0.83	590	3.63	0.73	1.57	70
23	547 ^c	0.58	-0.89	580	3.35	0.73	1.42	70
24	484 ^c	0.50	-0.95	570	2.14	0.66	0.80	70
25	445 ^c	1.16	-1.16	650	3.90	0.71	1.80	71
26	445 ^c	1.16	-1.19	670	7.10	0.76	3.70	71
27	427, 500(s) ^c	0.97	-1.17	680	7.80	0.77	4.00	71
28	471 ^d	0.87	-1.24	726	10.59	0.68	5.20	54
29	495 ^d	0.79	-1.16	615	13.84	0.65	5.50	54
30	526 ^d	0.92	-1.00	694	16.36	0.72	8.20	54
31	538 ^d	-	-	871	7.82	0.766	10.00	27
32	545 ^d	-	-	813	15.58	0.706	9.90	27
33	-	-	-	840	9.56	0.759	12.2	27
34	-	-	-	880	9.47	0.767	12.8	27
35	512 ^c	1.02	-1.01	768	11.8	0.72	6.53	72
36	556 ^c	1.09	-0.86	786	15.2	0.67	7.99	72
37	600 ^c	0.95	-0.90	653	14.5	0.742	7.1	73
38	598 ^c	1.02	-0.83	678	16.0	0.732	8.0	73

^a In CH₃CN/C₂H₅OH (1:1) ^b In CH₃CN ^c In CH₂Cl₂ ^d In THF

Li and co-workers synthesized four dyes **39-43** containing 5-phenyl-iminostilbene as donor (Figure 2.17) [74]. The dye **43** was also synthesized without BTD for comparison. The synthetic protocols were shown in the scheme 2.8.

Scheme 2.8 Synthesis of benzothiadiazole sensitizers with indoline and triphenyl amine units as donor

The dyes showed broad absorption in the visible region (350-600 nm), which is attributed to the intramolecular charge transfer (ICT) from the 5-phenyl-iminostilbene donor to the anchoring group. The introduction of BTD extended the absorption onset by 165 nm, which is beneficial to enhance the light harvesting property and PCE. The presence of triple bond in between the BTD and donor induced a blue-shift and molar extension coefficients were decreased. This is attributed to the fact that in the alkyne bridged chromophores, the carbon atoms are in both sp and sp^2 hybridized which results in poorer π -orbital overlap and mismatch in energy of the π -orbitals. The introduction of BTD increased the V_{OC} compared to **43** due to negative shift of the conduction band. The dye **40** showed power conversion efficiency of 5.38% and raised to 6.71% by optimization of device after addition of 10 mM CDCA addition. The dyes **41-42** showed inferior efficiency compared to **39-40** due to acetylene linkage. The dye **40** showed long term stability over 1000 h with ionic liquid electrolyte under light soaking experiments.

Figure 2.17 Molecular structures of 5-phenyl-iminostilbene based sensitizers

Valiyaveetil and co-workers reported a set of dyes **44-49** based on BTD with carbazole as donor [12]. By linking carbazole's 2nd or 3rd positions to the benzothiadiazole group and changing the functional groups on the N-atom of carbazole, authors investigated subtle change in photophysical and energy conversion efficiencies. The synthetic procedure of the dyes was shown in Scheme 2.9 and structures shown in Figure 2.18.

Scheme 2.9 Synthesis of the carbazole based sensitizers

The dyes showed broad light harvesting capability due to the introduction of BTD unit. The LUMO levels of all dye molecules were found to be similar due to the same acceptor and anchoring groups. The chemical nature of substituents and position of the substituents played an important role in the performance of the DSSCs. The dyes (**45** and **46**) carbazole attached at 3-position showed higher conversion efficiency of 3.3% and 3.8% due to strong donating capability. However the dyes with carbazole as donor connected at 2-position and N9 position showed lower conversion efficiency due less donating strength of carbazole led to lower J_{SC} values.

Figure 2.18 Chemical structures of the carbazole based dyes.

In order to increase the donating strength of the carbazole unit, Hong and co-workers synthesized three dyes (**50-52**) based on carbazole as donor with substitution at 3 and 6 positions with triphenylamine as auxiliary donor (Figure 2.19) [75]. The synthetic scheme of the dyes involves various protocols such as Ullman coupling reaction, Suzuki coupling and shown in Scheme 2.10. The introduction of auxiliary donors increased the molar extinction coefficient with red shifted absorption and inhibited the aggregation of the dye on the surface of TiO₂. The introduction of hexyl chain on thiophene units induced significant blue shift in the absorption spectra, due to the twisted structure of the π -bridge. The injected electron lifetimes of the dyes were 0.1 ns (**50**), 0.1 ns (**51**), and 16.5 ns (**52**), and these results were correlated with the higher V_{OC} value of **52**. Thus, the alkyl chains on the π -bridge of **52** enhanced the photocurrent and suppressed the charge recombination process. The dye **52** showed an efficiency of 5.11% which is double the conversion efficiency compared to previous dyes (**44-49**). The addition of CDCA increases the efficiency up to 6.33% for the dye **52**.

Scheme 2.10 synthesis of the carbazole containing dyes

Figure 2.19 Molecular structures of carbazole based sensitizers

Tian and co-workers [76-77] reported a novel class of organic sensitizers based on a rigid triarylamine amine electron donor with a two-locking structure (Figure 2.20). The synthesis of new rigid triarylamine donor based benzothiadiazole dye was shown in Scheme 2.11. The bromo derivative of the new rigid triarylamine donor was prepared from the starting materials carbazole and methyl 2-iodobenzoate via Ullmann condensation, bromination, Grignard reaction and ring closure reactions sequentially. The bromo derivative was converted to boronic acid and reacted with 5-(7-bromobenzo[*c*][1,2,5]thiadiazol-4-yl)thiophene-2-carbaldehyde by Suzuki coupling protocol to get terminal aldehyde precursor. The sensitizer **55** was obtained by

Benzothiadiazole-Based Sensitizers for DSSCs: A Review

Knoevenagel condensation of aldehyde with cyanoacetic acid in the presence of a catalytic amount of piperidine in THF.

Scheme 2.11 Synthetic route to benzothiadiazole dye containing rigid triarylamine donor

The dye **55** showed red shifted absorption by 43 nm and 19 nm than the dyes **31** and **32**, respectively. The inclusion of BTD in the dye **55** reduced the LUMO level and showed smaller bandgap. The introduction of an *n*-hexyl chain on thienyl unit instead of the bare thienyl in the dye **56** induced 5 nm blue shift and the introduction of another *n*-hexyl thiophene unit in between indoline donor and BTD in the dye **57** red shifted the absorption by 32 nm. Due to the fast charge recombination and low electron lifetime, although the dye **55** has very broad absorption spectra contributed to low efficiency 4.61% ($J_{SC} = 10.0 \text{ mA cm}^{-2}$, $V_{OC} = 640 \text{ mV}$, and $ff = 0.72$), while the dye **54** exhibited a η value 6.50% ($J_{SC} = 13.7 \text{ mA cm}^{-2}$, $V_{OC} = 690 \text{ mV}$ and $ff = 0.69$) fabricated under the same conditions under standard global AM 1.5 solar light condition.

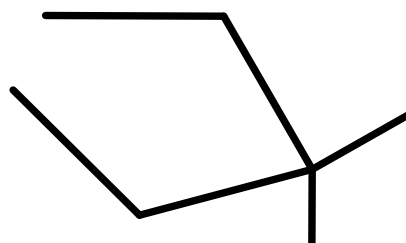


Figure 2.20 Structures of rigid triarylamine-donor based sensitizers

Benzothiadiazole-Based Sensitizers for DSSCs: A Review

Tian and co-workers [78] designed and synthesised a series of sensitizers with high molar extinction coefficients ($5.6\text{-}6.3 \times 10^4 \text{ M}^{-1}\text{cm}^{-1}$) comprising substituted dihydroindolo[2,3-*b*]carbazole (Figure 2.21) as donor. The synthesis of the sensitizers **59** comprising benzothiadiazole and dihydroindolo[2,3-*b*]carbazole as donor was shown in the Scheme 2.12.

Scheme 2.12 Synthesis of dihydroindolo[2,3-*b*]carbazole donors based benzothiadiazole sensitizer **59**

Figure 2.21 Molecular structures of dyes based on dihydroindolo[2,3-*b*]carbazole donor and trends observed in optical and electrochemical data

The dyes exhibited broad absorption band in the region 440-650 nm with the maximum absorptions at 453, 522, 464 and 522 nm, **58-61** respectively. The HOMO level energies decreased in the order of **59** (0.91 V) > **60** (0.86 V) > **58** (0.85 V) \approx **61** (0.85 V). The introduction of benzothiadiazole in the π -conjugation altered the LUMO level of the dyes

Benzothiadiazole-Based Sensitizers for DSSCs: A Review

relative to thiophene substituted dyes, which resulted in a red shifted absorption due to the smaller band gap. By permutation of the thiophene unit in **58** ($\eta = 4.11\%$) by benzothiadiazole unit in **59** ($\eta = 6.40\%$) improved the efficiency. Using the dye baths of CHCl_3 -EtOH (v/v 1 : 3), the photovoltaic performance of the dye **61** device was further enhanced to 7.03% ($J_{\text{SC}} = 14.81 \text{ mA cm}^{-2}$, $V_{\text{OC}} = 690 \text{ mV}$ and the $ff = 0.69$). The optical, electrochemical and DSSC data of the dyes **39-61** were presented in Table 2.3.

Table 2.3 Photophysical, electrochemical and photovoltaic performances of DSSCs data based on dyes **39-61**

Dye	λ_{abs}	$E_{\text{OX}}/\text{V}(\text{NHE})$	$E^*_{\text{OX}}/\text{V}(\text{NHE})$	V_{OC}/mV	$J_{\text{SC}}/\text{mA cm}^{-2}$	ff	$\eta/\%$	Ref
39	494 ^a	1.09	-0.88	657	11.94	0.66	5.16	74
40	450 ^a	1.20	-0.95	673	12.11	0.66	5.38	74
41	474 ^a	1.11	-0.89	545	3.60	0.71	1.39	74
42	455 ^a	1.14	-0.94	636	7.37	0.61	2.86	74
43	470 ^a	1.19	-0.86	665	11.04	0.72	5.27	74
44	445 ^a	1.11	-0.70	0.59	3.90	0.68	1.56	12
45	474 ^a	1.12	-0.71	0.65	7.37	0.69	3.29	12
46	484 ^a	1.07	-0.63	0.64	8.30	0.74	3.80	12
47	476 ^a	1.30	-0.72	0.65	4.85	0.74	2.36	12
48	459 ^a	1.13	-0.70	0.64	3.22	0.73	1.53	12
49	461 ^a	1.24	-0.73	0.67	2.43	0.71	1.20	12
50	488 ^b	0.90	-1.46	0.54	9.14	0.67	3.32	75
51	498 ^b	0.90	-1.41	0.55	10.01	0.68	3.70	75
52	376 ^b	0.94	-1.57	0.70	11.11	0.66	5.11	75
53	440 ^c	1.36	-1.12	740	10.40	0.74	5.43	76
54	464 ^c	1.28	-1.01	690	13.70	0.69	6.50	76
55	483 ^c	1.35	-0.88	640	10.00	0.72	4.61	76
56	478 ^c	1.15	-0.93	712	9.71	0.75	5.20	77
57	510 ^c	1.10	-0.83	682	11.82	0.72	5.82	77
58	453 ^b	0.85	-1.16	768	11.95	0.66	6.09	78
59	522 ^b	0.91	-1.00	707	11.57	0.68	5.55	78
60	464 ^b	0.86	-1.16	644	9.40	0.68	4.11	78
61	522 ^b	0.85	-1.09	674	13.96	0.68	6.40	78

^a In CH_2Cl_2 ^b In DMF ^c In THF

2.2.1 Acceptor (anchoring) group directly attached BTD featured sensitizers

Figure 2.22 Configuration of acceptor (anchoring) group directly attached BTD sensitizers

The general representation of acceptor (anchoring) group directly attached BTD sensitizers is as shown in the Figure 2.22. To achieve good overlap with the solar emission spectrum and to produce large photocurrent response benzothiadiazole entity was implanted in the conjugated spacer. On the other hand, the DSSCs based on benzothiadiazole sensitizers exhibited lower efficiencies. The root cause for the low efficiencies of the BTD dyes was revealed from the density functional theory calculation and Mulliken charges calculated from the TDDFT results. The electron density in the lowest unoccupied molecular orbital (LUMO) on the anchoring group is less dense than benzothiadiazole. The electron density on the lowest unoccupied molecular orbital (LUMO) and negative Mulliken charge around the electron-withdrawing benzothiadiazole appears to be relatively strengthened than the acceptor, indicating that the electron can be confined to the benzothiadiazole unit, by which the excited electrons facing larger obstacles to dissociate and inject into TiO_2 . However by tethering two electron-donating alkoxy chains at the BTD entity, charge trapping was not eased. So to use this negative charge fruitfully, based on the above considerations researchers decided to synthesize sensitizers with the BTD entity directly connected to 2-cyanoacrylic acid. Now the negative charge accumulated at the BTD entity may have better opportunity to inject into semiconductor due to a shorter distance between BTD and the anchoring group. Now the challenge is to synthesis, the precursor used for the synthesis of cyanoacrylic acid directly attached to BTD unit is 7-bromobenzo[*c*][1,2,5]thiadiazole-4-carbaldehyde. The synthesis of this intermediate precursor is achieved by the different synthetic protocols shown in the Scheme.2.13.

Scheme 2.13 Different protocols used for synthesis of the benzo[*c*][1,2,5]thiadiazole-4-carbaldehyde derivatives

Significant progress in the use of organic dyes containing anchoring group cyanoacrylic acid directly connected to the BTD core in DSSCs was first made by park and co-workers [79]. As shown in Figure 2.23, the anchoring group cyanoacrylic acid is directly or indirectly attached to the BTD core. The dye **62** showed 91 nm blue shifted absorption maximum and insertion of phenylenevinylene constituent in **64** as a bridging unit between BTD and cyanoacrylic acid acceptor groups blue-shifted the absorption maxima by 4 nm, with respect to anchoring group directly attached BTD dye **63**. The dye **64** with $J_{SC} = 12.24 \text{ mA cm}^{-2}$, $V_{OC} = 549 \text{ mV}$ and $ff = 0.56$ resulted an overall conversion efficiency of 3.80%, which is higher than that of **62** and **63**. The dye **64** is showing superior performance than **63**, due to the three fold highness in the electron injection efficiency and slower recombination of injected electrons with oxidized dyes.

Figure 2.23 Structures of *N,N*-diphenyl-4-vinylaniline donor featured sensitizers

Bäuerle and co-workers [80] by doing small structural modification in benzothiadiazole dyes achieved high performance in DSSCs. The two dyes (Figure 2.24) mainly differ in the position of cyanoacrylic acid acceptor. Former dye contains cyanoacrylic acid acceptor directly attached to BTD unit where as in later dye cyanoacrylic acid acceptor is separated from BTD unit by phenyl spacer. The dye **65** exhibited 55 nm red shifted absorption maximum due to the strong donor-acceptor interaction, when compared to the dye **66**. The insertion of the phenyl ring blocks the back electron transfer of the charge separated state and slowing down recombination processes by over 5 times, thus efficiency of dye **66** (8.21%) was raised by a factor of 6.5 compared to dye **65** (1.24%). From this adroit molecular design and punctilious research found that, the placement of the acceptor (anchoring group) in the BTD dyes play major role in the electron injection efficiency and power conversion efficiency. By placing the anchoring on the BTD unit achieved ample injection efficiencies, but unfortunately resulting low PCEs due to the fast electron recombination between electrons from TiO₂ and the dye radical cation.



Figure 2.24 4-(2,2'-bithiophen-5-yl)-*N,N*-bis(4-(hexyloxy)phenyl)aniline donor based BTB sensitizers

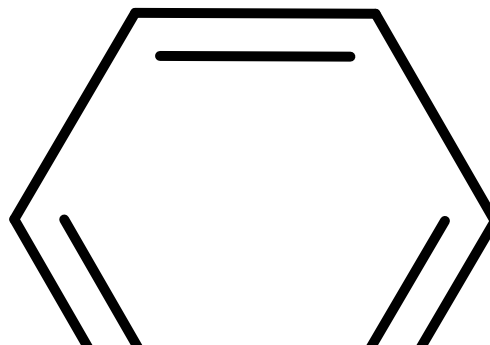


Figure 2.25 Structures of acceptor directly attached to benzothiadiazole based sensitizers

Lin and co-workers [81] designed and synthesised three sensitizers (Figure 2.25) which have BTD entity directly connected to 2-cyanoacrylic acid (also as the anchoring group) for DSSCs using ZnO as the photoanode. The λ_{abs} values are in the order of **69** (540 nm) > **68** (513 nm) > **67** (486 nm). DSSCs using benzothiadiazole-based dyes with a ZnO photoanode exhibited high conversion efficiencies (4.02% to 5.18%), one of the best efficiencies using 2-cyanoacrylic acid directly connected to BTD unit class sensitizers. Among all, the efficiency of DSSCs made from the dye **67** dramatically increased to 5.82% ($J_{\text{SC}} = 14.70 \text{ mAcm}^{-2}$, $V_{\text{OC}} = 0.61 \text{ V}$, and $ff = 0.65$), when a novel hierarchical ZnO light back scattering layer was used.

Figure 2.26 Structures of the diarylthienylamine donor based sensitizers

Wong and co-workers [82] have developed three dyes containing cyanoacrylic acid directly attached to benzothiadiazole unit (Figure 2.26). The incorporation of dialkoxy substituents on the donor moieties endowed the dyes **71** and **72** with narrower bandgap and higher HOMO level than **70**. The dye **72** showed better photophysical properties which reflected the efficiency. The preliminary results showed that the DSSCs exhibit extremely low PCEs (< 0.06%) using 0.6 M

Benzothiadiazole-Based Sensitizers for DSSCs: A Review

1-butyl-3-methylimidazolium iodide (BMII), 0.05 M LiI, 0.03 M I₂, 0.5 M 4-*tert*-butylpyridine (TBP), and 0.1 M guanidiniumthiocyanate in a mixture of acetonitrile-valeronitrile (85:15, v/v) as the redox electrolyte. The improved photovoltaic performance the DSSCs was achieved in a TBP-free condition by merely using 0.6 M 1,2-dimethyl-3-propylimidazolium iodide (DMPII), 0.05 M LiI, 0.03 M I₂ in acetonitrile as the redox electrolyte, and the best cell based on the sensitizer **72** reached a PCE of 3.16% under simulated AM 1.5G irradiation (100 mW cm⁻²). The optical, electrochemical and DSSC data of the dyes **62-72** were presented in Table 2.4.

Table 2.4 Photophysical, electrochemical and photovoltaic performances of DSSCs data based on dyes **62-72**

Dye	λ_{abs}	$E_{\text{OX}}/\text{V}(\text{NHE})$	$E^*_{\text{OX}}/\text{V}(\text{NHE})$	V_{OC}/mV	$J_{\text{SC}}/\text{mA cm}^{-2}$	ff	$\eta\%$	REF
62	407 ^a	1.11	-0.73	519	10.29	0.62	3.30	79
63	498 ^a	1.15	-0.77	470	8.13	0.65	2.49	79
64	494 ^a	1.11	-0.74	549	12.24	0.57	3.80	79
65	570 ^b	0.97	-0.63	489	3.40	0.74	1.24	80
66	515 ^b	0.88	-0.79	640	18.47	0.69	8.21	80
67	486 ^c	1.25	-0.98	590	13.50	0.65	5.18	81
68	513 ^c	1.03	-1.09	540	13.09	0.61	4.29	81
69	540 ^c	0.97	-1.09	510	12.03	0.66	4.02	81
70	613 ^b	1.02	-0.72	410	9.12	0.62	2.30	82
71	650 ^b	0.87	-0.78	390	13.06	0.62	3.13	82
72	654 ^b	0.87	-0.77	450	11.10	0.63	3.16	82

^a In EtOH ^b In CH₂Cl₂ ^c In THF

2.2.2 5,6-bis-alkoxy-benzo[2,1,3]thiadiazole featured sensitizers

The general representation and features endowed were shown in Figure 2.27. In the BTD class sensitizers, some charge trapping at the electron deficient moiety (BTD) hampering efficient electron injection from the sensitizer to the TiO₂ nanoparticles. To improve the cell performance by easing the charge trapping Lin and co-workers tethered two electron donating long alkoxy chains at the benzothiadiazole entity. The incorporation of the two long alkoxy chains at the benzothiadiazole entity can realize several merits such as: (i) improve their solubility and form a tightly packed insulating monolayer preventing I³⁻ or cations approaching the TiO₂ and help to suppress dark currents. (ii) the cell performance can be improved by counteracting the electron-deficient character of benzothiadiazole, which help to suppress the charge trapping effect (iii) suppresses the dark current, hence increases the electron lifetime and open circuit voltage (V_{oc}).

Benzothiadiazole-Based Sensitizers for DSSCs: A Review

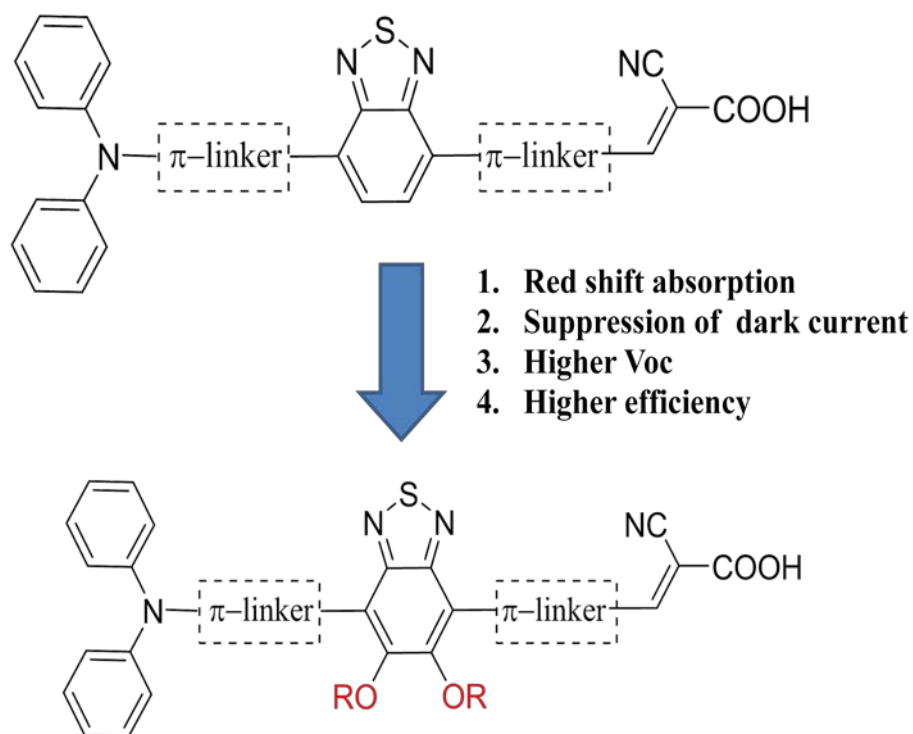


Figure 2.27 General representation of 5,6-bis-alkoxy-benzo[2,1,3]thiadiazole based sensitizers

The synthetic intermediate for the synthesis of these sensitizers is 4,7-dibromo-5,6-alkoxybenzo[*c*][1,2,5]thiadiazole, which was obtained by a five-step synthetic protocol from catechol as shown in Scheme 2.14. The diamine which is precursor for the preparation of thiadiazole core was prepared from catechol by alkylation, nitration and reduction respectively. The diamine was successfully converted to thiadiazole core by treating with SOCl_2 and triethyl amine, subsequently brominated with molecular bromine to give 4,7-dibromo-5,6-alkoxybenzo[*c*][1,2,5]thiadiazole in excellent yield.

Scheme 2.14 Synthetic routes to the 4,7-dibromo-5,6-alkoxybenzo[*c*][1,2,5]thiadiazole

Benzothiadiazole-Based Sensitizers for DSSCs: A Review

In this report the Lin and co-workers [83] introduced 5,6-bis-hexyloxy-benzo[2,1,3]thiadiazole spaced materials (Figure 2.28) for efficient dye sensitized solar cells and compared to the congeners without the hexyloxy chains. The presence of hexyloxy groups effectively suppress the dark currents and significantly improve the cell performance. High conversion efficiencies have been achieved with these dyes, and the best performance of the cells reaches > 90% of the N719-based cell fabricated and measured under similar conditions. DSSCs based on dye **76** produced a short-circuit current density (J_{SC}) of 15.2 mA cm^{-2} , with a maximum photon-to-electron conversion efficiency (η) of 6.72 %.

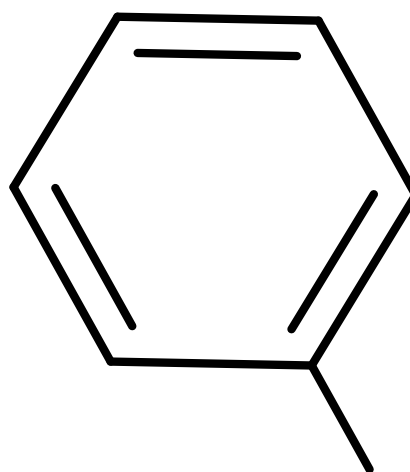


Figure 2.28 Structure of the 5,6-bis-hexyloxy-benzo[2,1,3]thiadiazole based sensitizers

Here, an interesting comparison could be carried out between these sensitizers to study the effect of different π -linkers between diphenylamine and dialkoxy BTD on absorption bands as well as J_{SC} of the devices (Figure 2.29). All the three dyes have the similar structure except the π -linker between diphenylamine and dialkoxy BTD. Their Charge transfer transition bands in THF solution and J_{SC} are in the order of **74** < **73** < **75** < **76**. Sensitizer **76** with a longer π -conjugation length (combination of phenyl and thienyl units) showed red shifted charge transfer band than others in series. In **74**, the fluorene unit make high dihedral angle with 5,6-bis-hexyloxy-benzo[2,1,3]thiadiazole when compared to the phenyl analogue (**73**), which is unfavorable for effective conjugation. Generally, the insertion of an ethynyl entity usually shows a large blue shift in the absorption due to the poorer orbital overlap of energetically mismatched SP and SP² orbitals. In contrast, the dye **75** showed 12 nm bathochromic shift,

which can be rationalized by the reason that the insertion of an ethynyl entity bridging between alkoxy benzothiadiazole and phenyl groups helped to alleviate the steric congestion and elongated the conjugation length of the molecule. With the high absorption coverage in the series, DSSCs based on sensitizer **76** showed a J_{SC} of 15.2 mA cm^{-2} and an efficiency of 6.72%.

Figure 2.29 Effect of the π -spacer between diphenylamine and 5,6-bis(octyloxy)benzo[*c*][1,2,5]thiadiazole on absorption maximum

Hua and co-workers designed and synthesised a series of 5,6-bis(octyloxy)benzo[*c*][1,2,5]thiadiazole-bridged sensitizers (Figure 2.30) and compared to the congeners without the octyloxy chains [84-85]. These dyes featured with a triphenyl moiety as the electron donor, cyanoacrylic acid as the anchoring group. Phenyl, furan and thiophene are used as linkers between alkoxy BTD and cyanoacrylic acid. The introduction of two long alkoxy chains into the benzothiadiazole ring successfully inhibited the charge recombination and the open-circuit voltage was higher for these dyes than the congener without alkoxy groups. The power conversion efficiency was sensitive to the linker unit in between alkoxy benzothiadiazole and cyanoacrylic acid anchoring moiety. Among these dyes, DSSCs based on dye **80** exhibited the best overall light-to-electricity conversion efficiency of 7.29% ($J_{SC} = 12.74 \text{ mA cm}^{-2}$, $V_{OC} = 784 \text{ mV}$, $ff = 0.73$) under AM 1.5 irradiation (100 mWcm^{-2}).

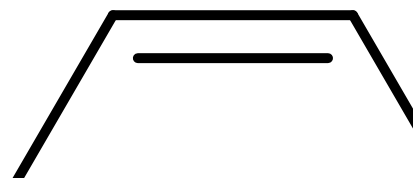


Figure 2.30 5,6-Bis(octyloxy)benzo[*c*][1,2,5]thiadiazole-bridged sensitizers

It is interesting to compare the optical properties of the dyes to study impact of the different π -linkers between dialkoxy BTD and cyanoacrylic acid (Figure 2.31). The permutation of phenyl, with furan and thiophene greatly enhances the light-harvesting nature by 40-45 nm in the long wavelength region (bathochromically shifted) and this can be rationalised by the factor that the replacement of the benzene moiety by furan or thiophene leads to a strong enhancement in the coplanarity between the 5,6-bis(octyloxy)benzo[*c*][1,2,5]thiadiazole unit and the cyanoacetic anchoring moiety. However, the phenyl π -linker between donor and dialkoxy BTD as well as dialkoxy BTD and cyanoacrylic acid seems jeopardise, because it leads to severe blue-shift in absorption and limits the light-harvesting range. The substitute to phenyl π -linker can be thiophene or oligothiophene units which have smaller resonance energies when compared with benzenoid moieties, provide more effective conjugation and facilitates charge transfer from the donor to the cyanoacrylic acid anchoring moiety. The optical, electrochemical and DSSC data of the dyes **73-83** were presented in Table 2.5.

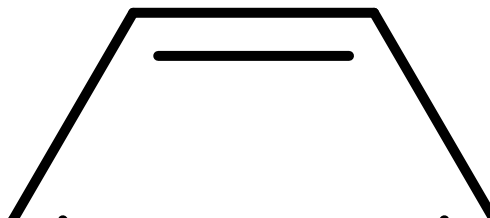


Figure 2.31 Effect of the π -spacer between 5,6-Bis(octyloxy)benzo[*c*][1,2,5]thiadiazole and cyanoacrylic acid on absorption maximum

Table 2.5 Photophysical, electrochemical and photovoltaic performances of DSSCs data based on dyes **73-83**

Dye	$\lambda_{\text{abs}}/\text{nm}$	E_{OX}/V	$E^*_{\text{OX}}/\text{V}(\text{NHE})$	V_{OC}/mV	$J_{\text{SC}}/\text{mA cm}^{-2}$	ff	$\eta\%$	REF
73	466 ^a	1.31	-0.98	0.68	12.0	0.68	5.57	83
74	454 ^a	1.19	-1.14	0.68	11.3	0.69	5.34	83
75	478 ^a	1.33	-0.98	0.70	12.7	0.70	6.22	83
76	501 ^a	1.16	-1.01	0.67	15.2	0.66	6.72	83
77	536 ^a	0.98	-1.00	0.67	11.9	0.68	5.36	83
78	423 ^b	0.99	-1.50	829	7.86	0.74	4.82	84
79	463 ^b	1.00	-1.22	818	12.10	0.73	7.19	84
80	468 ^b	1.01	-1.22	784	12.74	0.73	7.29	84
81	483 ^b	0.71	-1.40	0.686	15.05	64.53	6.66	85
82	525 ^b	0.72	-1.18	0.662	16.88	64.03	7.16	85
83	531 ^b	0.71	-1.21	0.629	15.37	64.02	6.19	85

^a In THF ^b In CH_2Cl_2

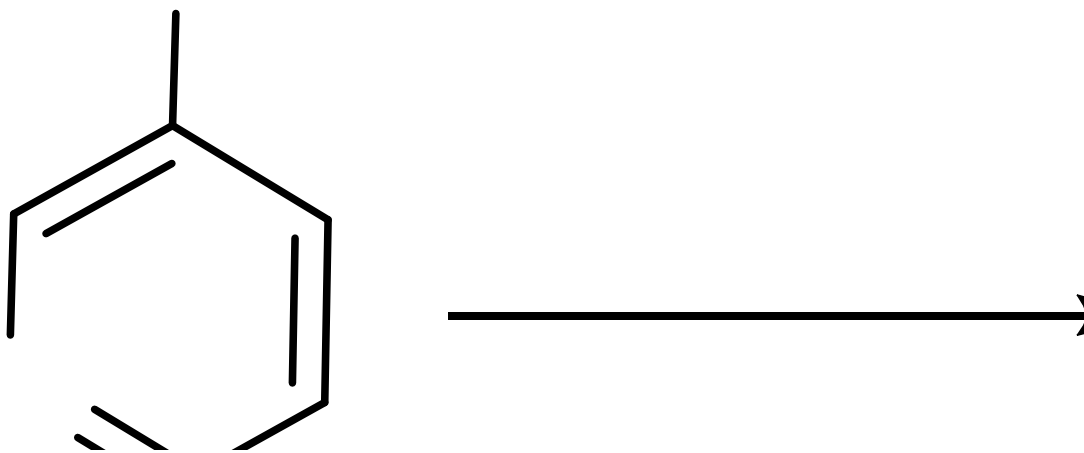
Here an interesting comparison could be carried out to reveal, the impact of tethering two long alkoxy chains at the benzothiadiazole entity, which could be monitored nicely by difference in absorption maxima and open circuit voltage (V_{OC}) of the sensitizers (Figure 2.32). Sensitizers featured with two long alkoxy chains at the benzothiadiazole entity owns steric congestion with the neighboring π -spacers, leads in twisting and jeopardizes charge transfer from the donor to the acceptor. Evidently, dyes featured with alkoxy BTD exhibits hypsochromic shift in absorption compared with its alkoxy-free congeners. Upon incorporation

of the alkoxy chains on BTD, the sensitizers successfully suppressed dark current and exhibited higher open-circuit voltages and high conversion efficiencies compared with its alkoxy-free congeners.

Figure 2.32 Structures and trends in absorption maxima and open circuit voltage (V_{OC}) data of dyes featured with and without alkoxy chains at the benzothiadiazole entity.

2.2.3 Molecular engineering at 5, 6-position of benzothiadiazole

Wong and co-workers [86] designed and synthesised three panchromatic sensitizers (Figure 2.33) based on thiadiazolo[3,4-*c*]pyridine hetero cyclic, which is obtained by permutation of the benzene ring in the BTD unit with more electron-deficient pyridine. The key intermediate for the preparation of these sensitizers was 4,7-dibromo-[1,2,5]thiadiazolo[3,4-*c*]pyridine, the synthesis of thiadiazolo[3,4-*c*]pyridine and 4,7-dibromo-[1,2,5]thiadiazolo[3,4-*c*]pyridine via different pathways were shown in Scheme 2.15.

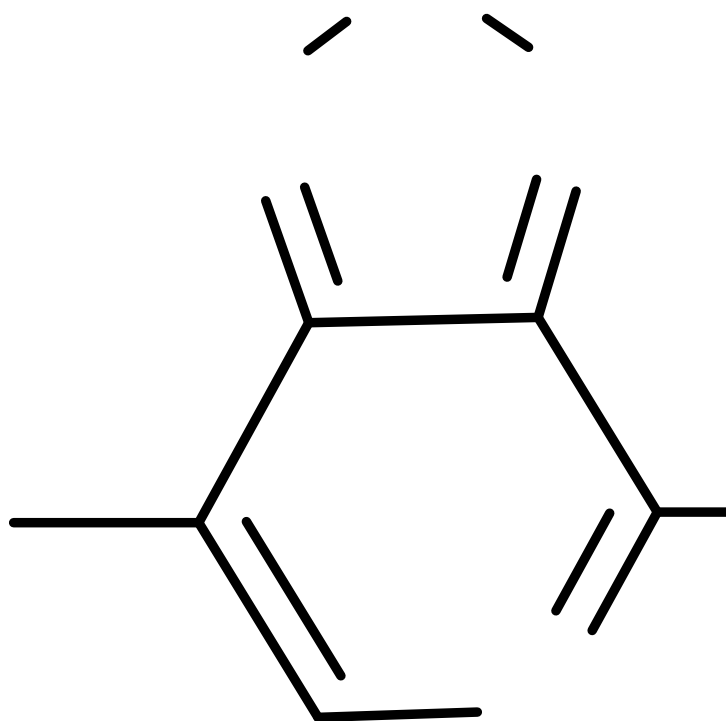


Scheme 2.15 Synthesis of thiadiazolo[3,4-*c*]pyridine and 4,7-dibromo-[1,2,5]thiadiazolo[3,4-*c*]pyridine

The sensitizers were displaying strong and broad absorption covering the spectral range of 300-750 nm. A bathochromic shift of 39 nm and 29 nm was observed by replacing triphenyl amine unit with 4-(hexyloxy)-*N*-(4-(hexyloxy)phenyl)-*N*-phenylaniline and *N,N*-bis(9,9-dimethylfluoren-2-yl)aniline donor moieties, respectively. Adsorption of the dyes on transparent thin TiO₂ film induced hypsochromic shift, which is ascertained to the deprotonation, H-aggregation of the dyes and the introduction of hexyloxy chains on the donor segment effectively inhibited the H-aggregation in the dye **85**. Cyclic voltammetry measurements revealed that the HOMO energy level raised by enhancing the donor strength, while the LUMO energy level remains essentially constant because of the same acceptor segments. The HOMO energy levels of the dyes determined by the electrochemical studies are in the **84** (0.86 V) > **85** (0.64 V) > **86** (0.57 V). The estimated optical band gap $E_{0,0}$ are **84** (1.99 eV), **85** (1.78 eV) and **86** (1.72 eV), respectively. The optical and electrochemical properties of the sensitizers were in accordance with electron-donating capability of the donor segment. DFT results revealed the HOMO orbitals were delocalized on the donor and LUMO orbitals were present from thiadiazolo[3,4-*c*]pyridine to cyanoacetic acid subunit. The IPCE spectrum of the three dyes covers the spectral range from 300-650 nm, reaching a highest value 65 % at 570 nm for the dye **85**. The higher efficiency of **85** ($\eta = 4.02\%$) than **84** ($\eta = 2.63\%$) manifests the beneficial influence of alkoxy groups on the donor segment on the photocurrent and open-circuit voltage.

Figure.2.33 Structures of thiadiazolo[3,4-*c*]pyridine based dyes with different arylamine donors

Lin and co-worker designed and synthesized a series of the dyes based on the thiadiazolo[3,4-*c*]pyridine by different linkers in the conjugation and discussed about the position of N atom in thiadiazolo[3,4-*c*]pyridine system [87]. The synthetic scheme of the dyes is shown in Scheme 2.16 and structures were shown in Figure 2.34. The charge transfer band of the dyes exhibited red shift absorption when compared to the congeners containing benzo[2,1,3]thiadiazole. The dyes with phenyl linker claimed higher J_{SC} compared to congener linkers (thiophene and furan) and achieved higher efficiency. The range of dyes as J_{SC} (0.68-9.47 mA/cm²) and V_{OC} (0.43–0.61 V) and achieved poor conversion efficiency due to the dye aggregation and charge trapping nature of the dyes. Finally the dye **94** claimed higher power conversion efficiency of 4.24%.



Scheme 2.16 Synthesis of thiazolo[3,4-*c*]pyridine containing sensitizers

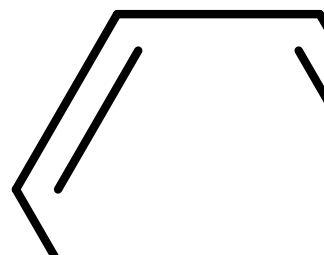


Figure.2.34 Structures of thiadiazolo[3,4-*c*]pyridine based dyes with different arylamine donors

Mao and co-workers [88] developed a series of sensitizers (Figure 2.35) comprising 2-cyanopyridine as an anchoring group by modulating the electron-deficient unit (auxiliary acceptor) in the π -conjugation with quinoxaline, benzo[1,2,5]thiadiazole and [1,2,5]thiadiazolo[3,4-*c*]pyridine units. The FT-IR results reveal the existence of characteristic stretching bands for C=N or C=C at around 1595, 1505, and 1465 cm^{-1} for all the dyes. The absorption maximum was bathochromically shifted by increasing the electron withdrawing nature of the auxiliary acceptor. The optical band gap of the dyes follows the order **99** (2.41 eV) > **100** (2.25 eV) > **97** (2.21 eV) > **98** (1.96 eV). DFT calculations have depicted that the HOMO of dyes were located on the triphenylamine donor, LUMO of the dyes were located on auxiliary acceptor and acceptor (2-cyanopyridine). DSSCs with the benzothiadiazole dye **97** produced a

higher photocurrent ($J_{SC} = 9.45 \text{ mA cm}^{-2}$), thus resulting in a higher efficiency of 4.02 % compared to that of remaining dyes in the series.

Figure 2.35 Molecular structures of the benzothiadiazole dyes with 2-cyanopyridine as an electron-accepting and anchoring group

Grimsdale and co-workers [55] annulated a new electron withdrawing pyrrolidine-2,5-dione heterocyclic moiety with benzo[*c*][1,2,5]thiadiazole to form 5*H*-[1,2,5]thiadiazolo[3,4-*f*]isoindole-5,7(6*H*)-dione to enhance the intramolecular charge transfer of the BTD sensitizers. The new sensitizer compared with 6*H*-pyrrolo[3,4-*g*]quinoxaline-6,8(7*H*)-dione analog **102** (Figure 2.36). The former dye exhibited 65 nm red-shifted absorption maxima when compared to that of later dye due to the stronger quinoid character of the core structure. Despite the broader absorption window, due to high exciton binding energy and larger recombination rate the dye **101** showed a relatively lower PCE of 4.14% with a J_{SC} of 8.86 mA cm^{-2} and a V_{OC} of 630 mV. While the dye **102** showed a promising PCE of 6.2% with a J_{SC} of 12.0 mA cm^{-2} and a V_{OC} of 730 mV. The optical, electrochemical and DSSC data of the dyes **84-102** were presented in Table 2.6.

Figure 2.36 Structures of the sensitizers containing 5*H*-[1,2,5]thiadiazolo [3,4-*f*]isoindole-5,7(6*H*)-dione and 6*H*-pyrrolo[3,4-*g*]quinoxaline-6,8(7*H*)-dione units

Table 2.6 Photophysical, electrochemical and photovoltaic performances of DSSCs data based on dyes **84-102**

Dye	λ_{abs}	$E_{\text{OX}}/\text{V}(\text{NHE})$	$E^*_{\text{OX}}/\text{V}(\text{NHE})$	V_{OC}/mV	$J_{\text{SC}}/\text{mA cm}^{-2}$	ff	$\eta/\%$	Ref
84	546 ^a	0.86	-1.13	367	11.23	0.64	2.63	86
85	585 ^a	0.57	-1.15	462	14.19	0.64	4.20	86
86	575 ^a	0.64	-1.14	432	12.00	0.69	3.58	86
87	522 ^b	1.26	-0.64	0.45	0.72	0.59	0.19	87
88	548 ^b	1.26	-0.65	0.48	2.67	0.61	0.78	87
89	498 ^b	1.26	-0.84	0.57	7.06	0.72	2.88	87
90	526 ^b	1.12	-0.77	0.56	2.89	0.65	1.06	87
91	536 ^b	1.28	-0.75	0.52	2.41	0.65	0.82	87
92	546 ^b	1.33	-0.63	0.52	3.35	0.67	1.16	87
93	497 ^b	1.29	-0.84	0.60	9.47	0.68	3.87	87
94	518 ^b	1.17	-0.83	0.61	7.15	0.70	3.06	87
95	525 ^b	0.98	-0.90	0.55	3.18	0.72	1.26	87
96	580 ^b	0.81	-0.92	0.51	2.18	0.62	0.69	87
97	473 ^a	1.01	-1.20	600	9.45	0.70	4.02	88
98	519 ^a	1.00	-0.96	450	0.62	0.60	0.17	88
99	419 ^a	0.97	-1.44	520	1.00	0.69	0.36	88
100	461 ^a	1.03	-1.22	570	5.24	0.70	2.10	88
101	542 ^a	0.94	-0.83	630	8.86	0.73	4.14	55
102	477 ^a	0.87	-1.05	730	12.00	0.70	6.20	55

^a In CH₂Cl₂ ^b In THF

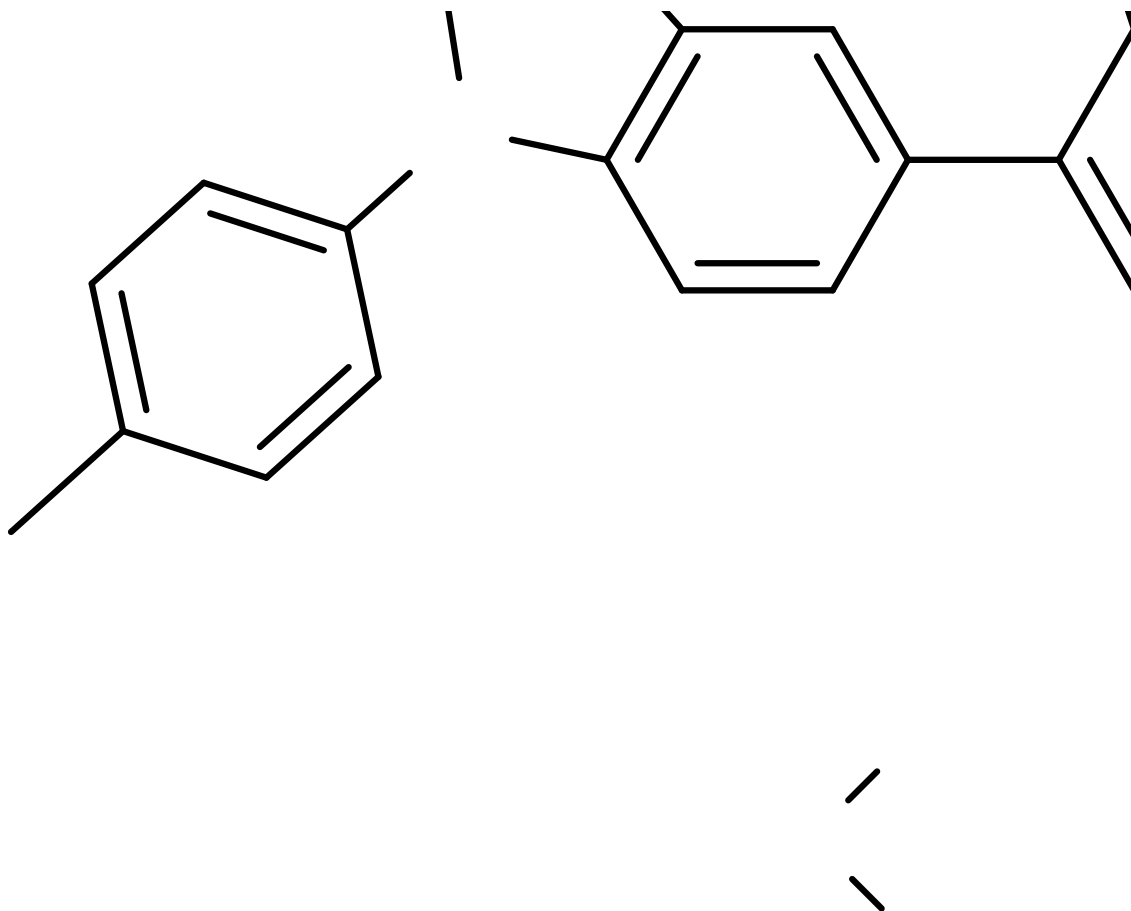
2.2.4 Molecular engineering in indoline donor featured benzothiadiazole sensitizers

Figure 2.37 Configuration of indoline donor featured benzothiadiazole sensitizers

The general Configuration of indoline donor featured benzothiadiazole sensitizers is as shown in Figure 2.37. Tian and co-workers [45] blossomed hope to make the high efficiency DSSCs with benzothiadiazole class of organic dyes by introducing indoline donor unit. In this report, authors studied a series of benzothiadiazole dyes (Figure 2.38) with different donors and

Benzothiadiazole-Based Sensitizers for DSSCs: A Review

spacer moieties in between benzothiadiazole and cyanoacrylic acid and found that the conversion efficiency increased with increasing the donor, spacers electron richness. Synthesis of benzothiadiazole sensitizers (**103-106**) with indoline and triphenyl amine donor units was shown in Scheme 2.17.



Scheme 2.17 Synthesis of benzothiadiazole sensitizers with indoline and triphenyl amine units as donor

Two steps of Suzuki coupling reactions on 4,7-dibromobenzothiadiazole with triphenyl amine/indoline boronic and 5-formylthiophen-2-ylboronic acid/ 4-formylphenylboronic acid respectively, resulted in the corresponding aldehyde precursors. On treatment of aldehyde precursors with cyanoacetic acid under typical Knoevenagel condensation reaction obtained the targeted indoline-benzothiadiazole sensitizers. Due to the endowed electron donating ability of

indoline, the dyes **105** and **106** were showing red shifted absorption profiles and lower oxidation potentials, when compared with triphenyl amine counter parts. Indoline dye **106** was achieved the high J_{SC} (17.7 mA cm^{-2}) upon co-adsorption with 20 mM deoxycholic acid (DCA), DSSCs gave η of 8.7% owing to the broad characteristics of IPCE spectrum. Finally, the photo-stability and redox stability of the indoline sensitizers were greatly enhanced by integrating BTD with indoline segment.



Figure 2.38 Structures of the indoline or triphenylamine donors featured benzothiadiazole sensitizers

Later Zhu and co workers [15] investigated the impact of hexylthiophene unit on the performance of the DSSCs in indoline-BTD sensitizers. The authors designed new sensitizer **107**, by introduction of an *n*-hexyl alkyl chain on thienyl unit instead of the bare thienyl in **106**. The *n*-hexyl chain in **107** reduced the intermolecular aggregation and improved electron injection efficiency without altering the absorption profile and energy levels. Without DCA co-adsorption, the dye **107** achieved the η of 7.76% ($V_{OC} = 672 \text{ mV}$) on $16 \mu\text{m}$ -thick TiO_2 film, which is 45% higher than that of **106** ($\eta = 5.31\%$, $V_{OC} = 600 \text{ mV}$) under the same conditions. These results indicate that dye aggregation is efficiently prohibited by the alkyl chain and DCA is not necessary to improve the efficiency of the dye **107** on thick TiO_2 films. The additional *n*-hexyl thiophene unit in between BTD and indoline in the dye **112** leads to a significant red shift in the charge transfer band and photocurrent response by extending the conjugation, but causes a low incident photon-to-current conversion efficiency. These results show that the attachment of *n*-hexyl chains in the sensitizers can effectively suppress charge recombination, resulting in a decreased dark current and enhanced V_{OC} , which influences the performance of the DSSCs.

Benzothiadiazole-Based Sensitizers for DSSCs: A Review

By the introduction of *n*-hexyl thiophene unit in between BTD and thiophene in the dye **106** resulted a new dye **111** and successfully inherited the aggregation and increased the injected electron lifetime and charge recombination resistance resulting in a high V_{OC} (696 mV) and a promising high power conversion efficiency of 9.04% for the **111** dye (Figure 2.38) [89]. This is the record efficiency achieved by the benzothiadiazole dye and one of the best efficiency achieved by metal free sensitizers in dye sensitized solar cell. These results override the argument that the some charge trapping at the electron deficient BTD moiety, hampered the efficient electron injection from the sensitizer to the semiconductor surface. The replacement of benzothiadiazole unit in the dye **106** with more electron deficient thiadiazolo[3,4-*c*]pyridine [90], induced 43 nm red shift for the dye **108**. Further extension of π -conjugation with cyclopentadithiophene in the dye **109**, red shifted the absorption spectrum and also suppressed the charge recombination rate. The panchromatic absorption of the dye **109** resulted in larger J_{SC} values of 11.20 mA cm⁻² with higher conversion efficiency of 6.7% compared to the dye **108** (3.6%). Later Zhu and co-workers [91] extended the conjugation from thiophene to bithiophene in between BTD and acrylic acid in the dye **106** resulted new a dye **110**. They also constructed a dye without benzothiadiazole (BTB) in molecular skeleton to get insight into the effect BTB on photophysical and photovoltaic performances. The introduction of BTB in the dye **110** resulted in panchromatic absorption which helps to increase the J_{SC} from 13.77 to 16.91 mA cm⁻². The dye **110** showed power conversion efficiency of 8.15% with increment of V_{OC} (57 mV) due to uplift of conduction band of TiO₂. The introduction of BTB in the dye **110** (8.15%) increased the efficiency by 36.5%, when compared to the dye **113** (5.97%). Table 2.7 shows the optical, electrochemical and DSSC data of the dyes **103-116**. Synthetic scheme for the dyes **108-110** are shown in the Schemes 2.18 & 2.19.

Scheme 2.18 Molecular structures of indoline based sensitizers

Scheme 2.19 Synthesis of benzothiadiazole sensitizers with indoline donor

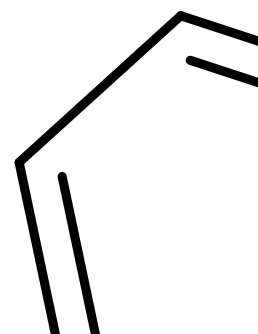


Figure 2.39 Molecular structures of indoline based sensitizers

Later Xue and co-workers [92] evaluated the feasibility of Co(II/III)tris(1,10-phenanthroline)-based redox electrolyte in the indoline sensitizers (Figure 2.39), to further improve the open-circuit voltages (V_{OC}). The inclusion of BTD in the dye **115** bathochromically shifted the charge transfer transition by 42 nm relative to the reference dye **114**. The modulation of *tert*-butylbenzene by dipropylfluorene induced 15 nm red shifted absorption maximum with higher molar absorption. Due to the deprotonation and formation of H-aggregation, blue shift in

Benzothiadiazole-Based Sensitizers for DSSCs: A Review

the absorption spectra was noticed on TiO₂. The deprotonation effect was weakened on introduction of benzothiadiazole unit and dipropylfluorene on the indoline is more efficient than *tert*-butylbenzene to diminish the tendency of dyes to form aggregates. The HOMO energy levels of sensitizers are **114** (0.82V), **115** (0.90V) and **116** (0.92V), which are more positive than the [Co(II/III)(phen)₃]ⁿ⁺ redox couple. Even though cobalt cells achieved high open circuit voltages than iodine cells, due to the lesser driving forces for dye regeneration in cobalt cells achieved low short circuit photocurrent density (J_{SC}). The dye **115** with cobalt DSC with 6 mm film showed a power conversion efficiency of 7.06% ($J_{SC} = 13.6 \text{ mA cm}^{-2}$, $V_{OC} = 775 \text{ mV}$ and $ff = 0.67$) under simulated AM1.5G solar light.

The trends in the photophysical and first oxidation potential of the indoline-benzothiadiazole sensitizers were compared for the purpose to understand the dependence of charge transfer transition on the device performance (Figure 2.40). Red shift in absorption maxima for the charge transfer transition by 47 nm was observed for the dye **106** relative to **LS-1**, when BTD is introduced. Interestingly the red shifting and broadening of the charge transfer band was achieved by the inclusion BTD via decreasing HOMO–LUMO gap by 0.36 eV. Triphenyl amine donor based dyes of the BTD were blue shift when compared with indoline analogs, which conforms the superior electron-donating capability of the indoline unit than that of triphenylamine. The aggregation of the dye **106** was solved by incorporation of a hexyl thiophene unit on the π -bridge in dyes **107** and **111**. The incorporation of *n*-hexylthiophene unit in the dye **106** effectively red shifted the absorption maxima by 10 nm in the dye **111** and resulted a higher V_{OC} and a promising high power conversion efficiency of 9.04%. The studies with BTD-indoline sensitizers revealed that, novel ‘‘D-A- π -A’’ concept proposed by Tian and co-workers, in which electron-withdrawing BTD unit is incorporated into the π bridge tailored molecular structures and optimized energy levels. The incorporation of electron-withdrawing BTD as the additional acceptor to the indoline dyes showing several distinguished merits such as: (I) the photo-stability of the sensitizers as well as intermediates were improved (II) redox stability which is a key factor for the solar cell device lifetime was greatly enhanced (III) beneficial to enhance the sensitizer light harvesting in the long wavelength region, as well as optimizing the match in energy levels to get the maximum photon-to-electricity conversion. (IV) the presence of BTD in the backbone of the sensitizer manifested the weakening the deprotonation effect on a TiO₂ film of the indoline dyes. (V) the stability and lifetime of DSSCs based on indoline sensitizers were greatly enhanced by the inclusion of BTD.

Figure 2.40 Structures and trends in optical and electrochemical properties of benzothiadiazole featured indoline dyes.

Table 2.6 Photophysical, electrochemical and photovoltaic performances of DSSCs data based on dyes **103-116**

Dye	$\lambda_{\text{abs}}/\text{nm}$	E_{OX}/mV	$E^*_{\text{OX}}/\text{V(NHE)}$	V_{OC}/mV	$J_{\text{SC}}/\text{mA cm}^{-2}$	ff	$\eta\%$	REF
103	455 ^a	0.95	-1.32	690	9.50	0.75	4.90	45
104	497 ^a	0.95	-1.16	600	11.20	0.75	5.00	45
105	496 ^a	0.67	-1.39	650	11.90	0.68	5.30	45
106	533 ^a	0.67	-1.23	650	17.70	0.76	8.70 ^c	45
	546 ^b	0.67	-1.33	633	14.28	0.75	6.70 ^c	
107	547 ^b	0.67	-1.39	672	15.00	0.77	7.76	15
108	576 ^c	0.89	-0.93	543	9.2	0.72	3.6	90
109	593 ^c	0.88	-0.95	612	15.1	0.72	6.7	90
110	545 ^b	0.81	-1.06	672	16.91	0.717	8.15	91
111	536 ^b	0.66	-1.39	696	18.00	0.72	9.04	89
112	557 ^b	0.57	-1.28	629	10.40	0.71	4.64	15
113	518 ^b	0.76	-1.25	615	13.77	0.705	5.97	91
114	508 ^b	0.82	-1.32	676	13.50	0.68	6.20	92
				770	11.50	0.67	5.93	
115	550 ^b	0.90	-1.05	686	14.80	0.68	6.90	92
				800	13.00	0.66	6.86	
116	535 ^b	0.92	-1.04	640	13.30	0.69	5.87	92
				750	11.40	0.66	5.64	

^a In CHCl₃/CH₃OH = 4/1 ^b In CH₂Cl₂ ^c In CHCl₃

2.2.5 Benzothiadiazole and Porphyrin complex based sensitizers

Figure 2.41 Molecular structures of porphyrin dyes featured with benzothiadiazole

Tan and co-workers [93] designed two novel porphyrin sensitizers (Figure 2.41) in combination with dithienylbenzothiadiazole linker for DSSCs. The solar cells based on sensitizers **117** and **118** achieved the short circuit photocurrent densities (J_{SC}) of 14.11 and 10.86 mA cm⁻², open circuit voltages (V_{OC}) of 0.59 and 0.61 V and the fill factors (ff) of 0.66 and 0.71, corresponding to overall conversion efficiencies of 5.46% and 4.67%, respectively. The methyl groups on the thienyls in **117** are more effective in reducing the charge recombination of the injected electrons with triiodide ions than hexyls on thienyls, which reflected the efficiency. Incorporation of low-band-gap chromophore benzothiadiazole unit at meso-position of the porphyrin dyes narrowed the energy gap and boosted the photo current response by improving the light-harvesting ability of the dyes.

Grätzel and co-workers developed highly efficient zinc porphyrin dyes (Figure 2.42) in conjunction with Co(II/III)tris(bipyridyl)-based redox electrolyte [94-96]. The synthesis of benzothiadiazole-zinc porphyrin sensitizers was displayed in Scheme 2.20. Arylamine groups attached to the porphyrin ring acts as an electron donor, and carboxylic acid moiety serves as an acceptor/anchoring group. The role of π -linker segment on mediating the electronic communication between donor and acceptor has been thoroughly investigated.

Scheme 2.20 Synthesis of zinc-porphrin based benzothiadiazole sensitizers

Absorption measurements indicated that the insertion of BTD linker in between porphyrin and phenyl segments beneficial for broadening and redshifting of the Soret and Q-bands, improved light harvesting property. Even though J_{SC} was enhanced by the insertion of BTD,

Benzothiadiazole-Based Sensitizers for DSSCs: A Review

V_{OC} was reduced due to the electron recapturing nature of the BTD unit at the TiO_2 -electrolyte interface. However, the loss in the V_{OC} was counterbalanced by gain in J_{SC} , resulting in the superior performance. The extension of the π -conjugation on electron donating moiety does not lead to a significant change in the position of the absorption bands. The direct attachment of anchoring group to BTD in **120** red shifted the Soret band, but enhanced the recombination and chemical capacitance when compared with **121**. Over all, the dye **123** gave a high J_{sc} of 18.1 $mA\ cm^{-2}$, a V_{oc} of 0.91 V and η of 13.0% under standard AM1.5G conditions. Table 2.8 shows the optical, electrochemical and DSSC data of the dyes **117-123**.

Figure 2.42 Molecular structures of the porphyrin dyes.

Table 2.8 Photophysical, electrochemical and photovoltaic performances of DSSCs data based on dyes **117-123**

Dye	λ_{abs}/nm	E_{OX}/V	$E^*_{OX}/V(NHE)$	V_{OC}/mV	$J_{SC}/mA\ cm^{-2}$	ff	$\eta\%$	REF
117	571 ^a	1.11	-0.98	590	14.11	0.66	5.46	93
118	552 ^a	1.15	-1.00	610	10.86	0.71	4.67	93
119	645 ^b	+0.82	-1.29	965	17.3	0.71	11.9	94
120	669 ^b	+ 0.83	-1.21	615	5.03	0.798	2.52	95
121	665 ^b	+0.79	-1.14	885	18.53	0.773	12.75	95
122	646 ^b	+0.89	-1.21	0.96	15.9	0.79	12.0	96
123	668 ^b	+0.88	-0.99	0.91	18.1	0.78	13.0	96

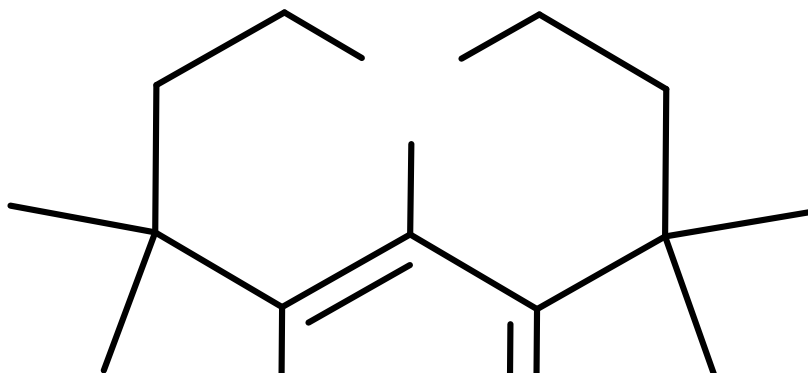
^aIn $CHCl_3$ ^bIn THF

2.2.6 Miscellaneous benzothiadiazole featured sensitizers

Kim and co-workers [97] introduced coumarin donor to benzothiadiazole based sensitizers. Authors have altered the spacers between benzothiadiazole and cyanoarylic acid acceptor (Figure 2.43). The synthetic protocol for coumarin featuring benzothiadiazole dyes is depicted

Benzothiadiazole-Based Sensitizers for DSSCs: A Review

in Scheme 2.21. The coumarin featured monobromo benzothiadiazole derivative was converted to aldehyde derivative by Stille coupling reaction, subsequently the aldehyde derivatives on reaction with cyanoacetic acid in the presence of a piperidine catalyst, produced the coumarin dyes containing benzothiadiazole. The optical, electrochemical and DSSC data of the dyes from **124-128** were displayed in Table 2.9.



Scheme 2.21 Synthesis of coumarin dyes containing benzothiadiazole for DSSCs.

The dye **125** showed better planarity, hence better conjugation which lead to 13 nm red shifted absorption than **124**. Thiophene spaced dye **124** exhibited better performance than 3,4-ethylenedioxythiophene (EDOT) spaced dye **125**, due to less efficient strong π - π^* interactions. The dye **124** achieved a J_{SC} of 14.3 mA cm^{-2} , a V_{OC} of 580 mV, and an ff of 0.72, corresponding to an overall conversion efficiency of 5.97% under standard AM 1.5G irradiation.

Figure 2.43 Chemical structures of coumarin dyes containing benzothiadiazole

Figure 2.44 Structures of branchlike organic dye containing benzothiadiazole with vinylenes unit

Tan and co-workers [98] reported a novel branchlike organic dyes **126** (Figure 2.44) based on 4,7-bis-(4-hexylthiophen-2-yl)benzo[1,2,5]thiadiazole (DTBT). The dye exhibited broad absorption profile in the range of 350-600 nm and achieved moderate η value of 2.18% ($J_{SC} = 5.83 \text{ mA cm}^{-2}$, $V_{OC} = 520 \text{ mV}$, $ff = 0.72$), may be due to lack of donor segment in the sensitizer. These results reveal that the photovoltaic performance can be significantly depend on the donor strength and the photovoltaic performance of the benzothiadiazole dye can improved by introducing a strong donor group in the molecule.

Sharma and co-workers [99-100] have developed a dye **127** (Figure 2.45) featuring dithienylbenzothiadiazole core as π -conjugated bridge with two cyanoacrylic acid anchoring groups, applied as a sensitizer in DSSCs. Improvement in efficiency was observed 2.42% to 3.6% by using composite zinc titanium oxide (ZTO) and 2.42% to 4.38% by using nanoporous TiO_2 electrode modified with an insulating material - BaCO_3 respectively, instead of bare TiO_2 electrode. Enhancement in the electron lifetime and reduction in recombination rate are main causes for increment of efficiency.

Figure 2.45 Dithienylbenzothiadiazole based sensitizer

Later Sharma and co-workers [101] designed and synthesised an organic dye **128** (Figure 2.45) featuring dithienylthienothiadiazole segment as central core and two cyanoacrylic acid anchoring side groups with a broad absorption band extended up to approximately 750 nm. The enhancement in light to power conversion efficiency from 2.75 to 4.22% was found by

increasing the thickness of the TiO₂ film from 8 to 12 nm, further increase in the TiO₂ film thickness was found to deteriorate the efficiency which was explained by aggregation of the dye. In an optimized cell, with CDCA as a coadsorbant, yielded an overall efficiency of 5.46% with $J_{SC} = 11.52 \text{ mA cm}^{-2}$, $V_{OC} = 660 \text{ mV}$ and $ff = 0.72$.

Table 2.9 Photophysical, electrochemical and photovoltaic performances of DSSCs data based on dyes **124-128**

Dye	λ_{abs}	E_{OX}, V	$E^*_{OX}/V(NHE)$	V_{OC}/mV	$J_{SC}/mA \text{ cm}^{-2}$	ff	$\eta\%$	REF
124	507 ^a	1.06	-1.06	580	14.30	0.72	5.97	97
125	520 ^a	1.03	-1.02	560	13.30	0.68	5.03	97
126	492 ^b	1.19	-1.04	520	5.83	0.72	2.18	98
127	455 ^c	-	-	720	11.50	0.53	4.38	99
		-	-	710	10.34	0.51	3.60	99
128	611 ^d	1.06	-1.00	660	11.52	0.72	5.46	100

^a CHCl₃/MeOH (3:1) ^b CHCl₃ ^c THF ^d DMSO

2.3 Conclusions and Outlook

The introduction of the auxiliary acceptor is extremely beneficial for the enhancement of photophysical properties, photo-stability, photo current and finally for light harvesting properties. Since the first report on benzothiadiazole based DSSCs in 2005, these materials have emerged as one important class of organic sensitizers. As demonstrated in this account a wide range of benzothiadiazole-based sensitizers can be made by efficient chemical synthetic routes, electronic properties can be tuned in different ways and able to produce moderate to good efficiencies in dye-sensitized solar cells. Some basic design rationales of benzothiadiazole organic dyes and information about the relationship between the chemical structures and photovoltaic performance of DSSCs have also been presented. In particular, indoline-benzothiadiazole and cyclopentadithiophene-benzothiadiazole based sensitizers seems to exhibit an excellent performances and are regarded as the most promising classes of organic sensitizers for DSSCs. It should be noted that it is still challenging for benzothiadiazole based organic dyes to achieve higher efficiency. Already 9.04%, > 13% power conversion efficiencies have been demonstrated in iodine and cobalt redox electrolytes, respectively and there are good grounds for believing that benzothiadiazole materials can be designed and made with efficiencies being required for commercial application. Benzothiadiazole-based materials can produce good light harvesting properties with high charge injection, suitable bandgaps and orbital energies which are necessary for obtaining high performance in solar cells.

One possible problem that still remains with 2,1,3-benzothiadiazole based sensitizers is the residing of negative charge on the thiadiazole moiety, by which the excited electrons facing larger obstacles to dissociate and inject into TiO_2 and the light-to-electric energy-conversion behavior significantly deteriorates. Positioning of more electron deficient anchoring group, which can take away the negative charge from thiadiazole fragment can relieve the detrimental electron injection of the BTD sensitizers and greatly alleviate light-to-electric energy-conversion efficiency. The challenge remains to design and produce a material with benzothiadiazole that possesses all these properties simultaneously. The further investigations include: (1) as already we have seen benzothiadiazole dyes covered the whole visible region, now the design and synthesis of new of panchromatic benzothiadiazole organic dyes possessing broad absorption characteristics extended to NIR regions with high molar extension coefficients, suitable electronic levels and steric properties based on fundamental insights into the interface processes. (2) the attachment of strong donor moieties directly to BTD unit without any π -linker may produce some fruitful results by derogating the charge trapping effect (3) functionalization and utilization of 5,6-position of BTD systems are still unexplored and many opportunities and discoveries remain to be made to explore new possibilities (4) the exploration of benzothiadiazole organic dyes to match suitable new metal-complexes based redox couple other than the I^-/I_3^- redox couples in DSSCs. Despite all these recent contributions, many aspects of benzothiadiazole chemistry still unexplored, many opportunities and discoveries remain to be made. A bright future is anticipated for benzothiadiazole based sensitizers for high efficient DSSCs.

2.4 References

- (1) M. Liang and J. Chen, Arylamine organic dyes for dye-sensitized solar cells. *Chem. Soc. Rev.* **2013**, *42*, 3453-88.
- (2) Y. Wu and W. Zhu, Organic sensitizers from D- π -A to D-A- π -A: effect of the internal electron-withdrawing units on molecular absorption, energy levels and photovoltaic performances. *Chem. Soc. Rev.* **2013**, *42*, 2039-58.
- (3) S. W. Park, K.-I. Son, M. J. Ko, K. Kim and N.-G. Park, Effect of donor moiety in organic sensitizer on spectral response, electrochemical and photovoltaic properties. *Synth. Met.* **2009**, *159*, 2571-7.
- (4) W. Ying, F. Guo, J. Li, Q. Zhang, W. Wu, H. Tian and J. Hua, Series of new D-A- π -A

- organic broadly absorbing sensitizers containing isoindigo unit for highly efficient dye-sensitized solar cells. *ACS Appl. Mater. Interfaces* **2012**, *4*, 4215-24.
- (5) A. Leliege, J. Grolleau, M. Allain, P. Blanchard, D. Demeter, T. Rousseau and J. Roncali, Small D- π -A systems with o-phenylene-bridged accepting units as active materials for organic photovoltaics. *Chem. Eur. J.* **2013**, *19*, 9948-60.
- (6) P. Singh, A. Baheti and K. R. J. Thomas, Synthesis and optical properties of acidochromic amine-substituted benzo[a]phenazines. *J. Org. Chem.* **2011**, *76*, 6134-45.
- (7) A. Baheti, P. Tyagi, K. R. J. Thomas, Y.-C. Hsu and J. T. s. Lin, Simple Triarylamine-Based Dyes Containing Fluorene and Biphenyl Linkers for Efficient Dye-Sensitized Solar Cells. *J. Phys. Chem. C* **2009**, *113*, 8541-7.
- (8) W. Wu, J. Yang, J. Hua, J. Tang, L. Zhang, Y. Long and H. Tian, Efficient and stable dye-sensitized solar cells based on phenothiazine sensitizers with thiophene units. *J. Mater. Chem.* **2010**, *20*, 1772-9.
- (9) J. Zhao, X. Yang, M. Cheng, S. Li and L. Sun, Molecular design and performance of hydroxylpyridium sensitizers for dye-sensitized solar cells. *ACS Appl. Mater. Interfaces* **2013**, *5*, 5227-31.
- (10) H. Tian, X. Yang, R. Chen, Y. Pan, L. Li, A. Hagfeldt and L. Sun, Phenothiazine derivatives for efficient organic dye-sensitized solar cells. *Chem. Commun.* **2007**, 3741-3.
- (11) Y. Hua, S. Chang, D. Huang, X. Zhou, X. Zhu, J. Zhao, T. Chen, W.-Y. Wong and W.-K. Wong, Significant Improvement of Dye-Sensitized Solar Cell Performance Using Simple Phenothiazine-Based Dyes. *Chem. Mater.* **2013**, *25*, 2146-53.
- (12) A. Keerthi, D. Sriramulu, Y. Liu, C. T. Yuan Timothy, Q. Wang and S. Valiyaveetil, Architectural influence of carbazole push-pull-pull dyes on dye sensitized solar cells. *Dyes Pigm.* **2013**, *99*, 787-97.
- (13) S. Ramkumar and S. Anandan, Synthesis of bianchored metal free organic dyes for dye sensitized solar cells. *Dyes Pigm.* **2013**, *97*, 397-404.
- (14) T. Sudyoadsuk, S. Pansay, S. Morada, R. Rattanawan, S. Namuangruk, T. Kaewin, S. Jungsuttiwong and V. Promarak, Synthesis and Characterization of D-D- π -A-Type Organic Dyes Bearing Carbazole-Carbazole as a Donor Moiety (D-D) for Efficient Dye-Sensitized Solar Cells. *Eur. J. Org. Chem.* **2013**, *2013*, 5051-63.

Benzothiadiazole-Based Sensitizers for DSSCs: A Review

- (15) Y. Wu, X. Zhang, W. Li, Z.-S. Wang, H. Tian and W. Zhu, Hexylthiophene-Featured D–A– π –A Structural Indoline Chromophores for Coadsorbent-Free and Panchromatic Dye-Sensitized Solar Cells. *Advanced Energy Materials* **2012**, *2*, 149-56.
- (16) S. Qu, C. Qin, A. Islam, J. Hua, H. Chen, H. Tian and L. Han, Tuning the electrical and optical properties of diketopyrrolopyrrole complexes for panchromatic dye-sensitized solar cells. *Chem.-Asian J.* **2012**, *7*, 2895-903.
- (17) B. Liu, Q. Liu, D. You, X. Li, Y. Naruta and W. Zhu, Molecular engineering of indoline based organic sensitizers for highly efficient dye-sensitized solar cells. *J. Mater. Chem.* **2012**, *22*, 13348.
- (18) W.-L. Ding, D.-M. Wang, Z.-Y. Geng, X.-L. Zhao and Y.-F. Yan, Molecular Engineering of Indoline-Based D–A– π –A Organic Sensitizers toward High Efficiency Performance from First-Principles Calculations. *J. Phys. Chem. C* **2013**, *117*, 17382-98.
- (19) B. Liu, W. Wu, X. Li, L. Li, S. Guo, X. Wei, W. Zhu and Q. Liu, Molecular engineering and theoretical investigation of organic sensitizers based on indoline dyes for quasi-solid state dye-sensitized solar cells. *Phys. Chem. Chem. Phys.* **2011**, *13*, 8985-92.
- (20) K. D. Seo, H. M. Song, M. J. Lee, M. Pastore, C. Anselmi, F. De Angelis, M. K. Nazeeruddin, M. Grätzel and H. K. Kim, Coumarin dyes containing low-band-gap chromophores for dye-sensitised solar cells. *Dyes Pigm.* **2011**, *90*, 304-10.
- (21) K. Hara, M. Kurashige, Y. Dan-oh, C. Kasada, A. Shinpo, S. Suga, K. Sayama and H. Arakawa, Design of new coumarin dyes having thiophene moieties for highly efficient organic-dye-sensitized solar cells. *New J. Chem.* **2003**, *27*, 783-5.
- (22) R. Sanchez-de-Armas, M. A. San Miguel, J. Oviedo and J. F. Sanz, Coumarin derivatives for dye sensitized solar cells: a TD-DFT study. *Phys. Chem. Chem. Phys.* **2012**, *14*, 225-33.
- (23) K. R. J. Thomas, N. Kapoor, C. P. Lee and K. C. Ho, Organic dyes containing pyrenylamine-based cascade donor systems with different aromatic pi linkers for dye-sensitized solar cells: optical, electrochemical, and device characteristics. *Chem.-Asian J.* **2012**, *7*, 738-50.
- (24) S. R. Li, C. P. Lee, H. T. Kuo, K. C. Ho and S. S. Sun, High-performance dipolar organic dyes with an electron-deficient diphenylquinoxaline moiety in the π -conjugation framework for dye-sensitized solar cells. *Chem. Eur. J.* **2012**, *18*, 12085-95.

Benzothiadiazole-Based Sensitizers for DSSCs: A Review

- (25) A. Baheti, P. Singh, C. P. Lee, K. R. J. Thomas and K. C. Ho, 2,7-Diaminofluorene-based organic dyes for dye-sensitized solar cells: effect of auxiliary donor on optical and electrochemical properties. *J. Org. Chem.* **2011**, *76*, 4910-20.
- (26) Q.-P. Wu, L. Zhang, M. Liang, Z. Sun and S. Xue, Sensitizers containing donor cascade and rhodanine-3-acetic acid moieties for dye-sensitized solar cells. *Solar Energy* **2011**, *85*, 1-6.
- (27) M. Zhang, Y. Wang, M. Xu, W. Ma, R. Li and P. Wang, Design of high-efficiency organic dyes for titania solar cells based on the chromophoric core of cyclopentadithiophene-benzothiadiazole. *Energy & Environmental Science* **2013**, *6*, 2944-9.
- (28) Y. Ooyama, S. Inoue, T. Nagano, K. Kushimoto, J. Ohshita, I. Imae, K. Komaguchi and Y. Harima, Dye-sensitized solar cells based on donor-acceptor pi-conjugated fluorescent dyes with a pyridine ring as an electron-withdrawing anchoring group. *Angew. Chem. Int. Ed.* **2011**, *50*, 7429-33.
- (29) A. Baheti, K. R. J. Thomas, C.-P. Lee and K.-C. Ho, Fine Tuning the Performance of DSSCs by Variation of the π -Spacers in Organic Dyes that Contain a 2,7-Diaminofluorene Donor. *Chemistry – An Asian Journal* **2012**, *7*, 2942-54.
- (30) A. Baheti, C. P. Lee, K. R. J. Thomas and K. C. Ho, Pyrene-based organic dyes with thiophene containing pi-linkers for dye-sensitized solar cells: optical, electrochemical and theoretical investigations. *Phys. Chem. Chem. Phys.* **2011**, *13*, 17210-21.
- (31) P. Singh, A. Baheti, K. R. J. Thomas, C.-P. Lee and K.-C. Ho, Fluorene-based organic dyes containing acetylene linkage for dye-sensitized solar cells. *Dyes Pigm.* **2012**, *95*, 523-33.
- (32) D. Kumar, K. R. J. Thomas, C.-P. Lee and K.-C. Ho, Novel Pyrenoimidazole-Based Organic Dyes for Dye-Sensitized Solar Cells. *Org. Lett.* **2011**, *13*, 2622-5.
- (33) M. Velusamy, K. R. J. Thomas, J. T. Lin, Y.-C. Hsu and K.-C. Ho, Organic Dyes Incorporating Low-Band-Gap Chromophores for Dye-Sensitized Solar Cells. *Org. Lett.* **2005**, *7*, 1899-902.
- (34) S.-T. Huang, Y.-C. Hsu, Y.-S. Yen, H. H. Chou, J. T. Lin, C.-W. Chang, C.-P. Hsu, C. Tsai and D.-J. Yin, Organic Dyes Containing a Cyanovinyl Entity in the Spacer for Solar Cells Applications. *J. Phys. Chem. C* **2008**, *112*, 19739-47.

Benzothiadiazole-Based Sensitizers for DSSCs: A Review

- (35) J. Mao, F. Guo, W. Ying, W. Wu, J. Li and J. Hua, Benzotriazole-bridged sensitizers containing a furan moiety for dye-sensitized solar cells with high open-circuit voltage performance. *Chem.-Asian J.* **2012**, *7*, 982-91.
- (36) Y. S. Yen, C. T. Lee, C. Y. Hsu, H. H. Chou, Y. C. Chen and J. T. Lin, Benzotriazole-containing D-pi-A conjugated organic dyes for dye-sensitized solar cells. *Chem.-Asian J.* **2013**, *8*, 809-16.
- (37) K. Pei, Y. Wu, W. Wu, Q. Zhang, B. Chen, H. Tian and W. Zhu, Constructing organic D-A-p-A-featured sensitizers with a quinoxaline unit for high-efficiency solar cells: the effect of an auxiliary acceptor on the absorption and the energy level alignment. *Chem. Eur. J.* **2012**, *18*, 8190-200.
- (38) S.-R. Li, C.-P. Lee, H.-T. Kuo, K.-C. Ho and S.-S. Sun, High-Performance Dipolar Organic Dyes with an Electron-Deficient Diphenylquinoxaline Moiety in the π -Conjugation Framework for Dye-Sensitized Solar Cells. *Chem. Eur. J.* **2012**, *18*, 12085-95.
- (39) T. W. Holcombe, J. H. Yum, J. Yoon, P. Gao, M. Marszalek, D. Di Censo, K. Rakstys, M. K. Nazeeruddin and M. Graetzel, A structural study of DPP-based sensitizers for DSC applications. *Chem. Commun.* **2012**, *48*, 10724-6.
- (40) J. Zeng, T. Zhang, X. Zang, D. Kuang, H. Meier and D. Cao, D-A- π -A organic sensitizers containing a benzothiazole moiety as an additional acceptor for use in solar cells. *Science China Chemistry* **2012**, *56*, 505-13.
- (41) J. He, W. Wu, J. Hua, Y. Jiang, S. Qu, J. Li, Y. Long and H. Tian, Bithiazole-bridged dyes for dye-sensitized solar cells with high open circuit voltage performance. *J. Mater. Chem.* **2011**, *21*, 6054.
- (42) J. Liu, K. Wang, X. Zhang, C. Li and X. You, Triazine dyes as photosensitizers for dye-sensitized solar cells. *Tetrahedron* **2013**, *69*, 190-200.
- (43) J. Liu, K. Wang, F. Xu, Z. Tang, W. Zheng, J. Zhang, C. Li, T. Yu and X. You, Synthesis and photovoltaic performances of donor- π -acceptor dyes utilizing 1,3,5-triazine as π spacers. *Tetrahedron Lett.* **2011**, *52*, 6492-6.
- (44) W. Gang, T. Haijun, Z. Yiping, W. Yingying, H. Zhubin, Y. Guipeng and P. Chunyue, Series of D- π -A system based on isoindigo dyes for DSSC: Synthesis, electrochemical and photovoltaic properties. *Synth. Met.* **2014**, *187*, 17-23.

Benzothiadiazole-Based Sensitizers for DSSCs: A Review

- (45) W. Zhu, Y. Wu, S. Wang, W. Li, X. Li, J. Chen, Z.-s. Wang and H. Tian, Organic D-A- π -A Solar Cell Sensitizers with Improved Stability and Spectral Response. *Adv. Funct. Mater.* **2011**, *21*, 756-63.
- (46) Y. Cui, Y. Wu, X. Lu, X. Zhang, G. Zhou, F. B. Miapéh, W. Zhu and Z.-S. Wang, Incorporating Benzotriazole Moiety to Construct D-A- π -A Organic Sensitizers for Solar Cells: Significant Enhancement of Open-Circuit Photovoltage with Long Alkyl Group. *Chem. Mater.* **2011**, *23*, 4394-401.
- (47) K. Pilgram, M. Zupan and R. Skiles, Bromination of 2,1,3-benzothiadiazoles. *J. Heterocycl. Chem.* **1970**, *7*, 629-33.
- (48) B. A. D. Neto, A. A. M. Lapis, E. N. da Silva Júnior and J. Dupont, 2,1,3-Benzothiadiazole and Derivatives: Synthesis, Properties, Reactions, and Applications in Light Technology of Small Molecules. *Eur. J. Org. Chem.* **2013**, *2013*, 228-55.
- (49) T. Khanasa, N. Prachumrak, R. Rattanawan, S. Jungsuttiwong, T. Keawin, T. Sudyoasuk, T. Tuntulani and V. Promarak, An efficient solution processed non-doped red emitter based on carbazole-triphenylamine end-capped di(thiophen-2-yl)benzothiadiazole for pure red organic light-emitting diodes. *Chem Commun* **2013**, *49*, 3401-3.
- (50) Z. Zhao, C. Deng, S. Chen, J. W. Lam, W. Qin, P. Lu, Z. Wang, H. S. Kwok, Y. Ma, H. Qiu and B. Z. Tang, Full emission color tuning in luminogens constructed from tetraphenylethene, benzo-2,1,3-thiadiazole and thiophene building blocks. *Chem Commun* **2011**, *47*, 8847-9.
- (51) S.-Y. Ku, L.-C. Chi, W.-Y. Hung, S.-W. Yang, T.-C. Tsai, K.-T. Wong, Y.-H. Chen and C.-I. Wu, High-luminescence non-doped green OLEDs based on a 9,9-diarylfuorene-terminated 2,1,3-benzothiadiazole derivative. *J. Mater. Chem.* **2009**, *19*, 773-80
- (52) T. Kono, D. Kumaki, J. Nishida, S. Tokito and Y. Yamashita, Dithienylbenzobis(thiadiazole) based organic semiconductors with low LUMO levels and narrow energy gaps. *Chem Commun* **2010**, *46*, 3265-7.
- (53) C. P. Yau, Z. Fei, R. S. Ashraf, M. Shahid, S. E. Watkins, P. Pattanasattayavong, T. D. Anthopoulos, V. G. Gregoriou, C. L. Chochos and M. Heeney, Influence of the Electron Deficient Co-Monomer on the Optoelectronic Properties and Photovoltaic Performance of Dithienogermole-based Co-Polymers. *Adv. Funct. Mater.* **2014**, *24*, 678-87.

Benzothiadiazole-Based Sensitizers for DSSCs: A Review

- (54) Q. Feng, X. Jia, G. Zhou and Z.-S. Wang, Embedding an electron donor or acceptor into naphtho[2,1-b:3,4-b']dithiophene based organic sensitizers for dye-sensitized solar cells. *Chem. Commun.* **2013**, 49, 7445-7.
- (55) H. Li, T. M. Koh, A. Hagfeldt, M. Gratzel, S. G. Mhaisalkar and A. C. Grimsdale, New donor- π -acceptor sensitizers containing 5*H*-[1,2,5]thiadiazolo [3,4-*f*]isoindole-5,7(6*H*)-dione and 6*H*-pyrrolo[3,4-*g*]quinoxaline-6,8(7*H*)-dione units. *Chem. Commun.* **2013**, 49, 2409-11.
- (56) J. J. Chen, T. L. Chen, B. Kim, D. A. Poulsen, J. L. Mynar, J. M. Frechet and B. Ma, Quinacridone-based molecular donors for solution processed bulk-heterojunction organic solar cells. *ACS Appl. Mater. Interfaces* **2010**, 2, 2679-86.
- (57) Q. Liu, H. Zhan, C. L. Ho, F. R. Dai, Y. Fu, Z. Xie, L. Wang, J. H. Li, F. Yan, S. P. Huang and W. Y. Wong, Oligothiophene-Bridged Bis(arylene ethynylene) Small Molecules for Solution-Processible Organic Solar Cells with High Open-Circuit Voltage. *Chem.-Asian J.* **2013**, 8, 1892-900.
- (58) F. R. Dai, H. M. Zhan, Q. Liu, Y. Y. Fu, J. H. Li, Q. W. Wang, Z. Xie, L. Wang, F. Yan and W. Y. Wong, Platinum(II)-bis(aryleneethynylene) complexes for solution-processible molecular bulk heterojunction solar cells. *Chem. Eur. J.* **2012**, 18, 1502-11.
- (59) T. He, Z. B. Lim, L. Ma, H. Li, D. Rajwar, Y. Ying, Z. Di, A. C. Grimsdale and H. Sun, Large two-photon absorption of terpyridine-based quadrupolar derivatives: towards their applications in optical limiting and biological imaging. *Chem.-Asian J.* **2013**, 8, 564-71.
- (60) S. Kato, T. Matsumoto, M. Shigeiwa, H. Gorohmaru, S. Maeda, T. Ishi-i and S. Mataka, Novel 2,1,3-benzothiadiazole-based red-fluorescent dyes with enhanced two-photon absorption cross-sections. *Chem. Eur. J.* **2006**, 12, 2303-17.
- (61) G. Yang, C.-a. Di, G. Zhang, J. Zhang, J. Xiang, D. Zhang and D. Zhu, Highly Sensitive Chemical-Vapor Sensor Based on Thin-Film Organic Field-Effect Transistors with Benzothiadiazole-Fused-Tetrathiafulvalene. *Adv. Funct. Mater.* **2013**, 23, 1671-6.
- (62) H.-B. Sun, S.-J. Liu, T.-C. Ma, N.-N. Song, Q. Zhao and W. Huang, An excellent BODIPY dye containing a benzo[2,1,3]thiadiazole bridge as a highly selective colorimetric and fluorescent probe for Hg²⁺ with naked-eye detection. *New J. Chem.* **2011**, 35, 1194.

Benzothiadiazole-Based Sensitizers for DSSCs: A Review

- (63) D. H. Lee, M. J. Lee, H. M. Song, B. J. Song, K. D. Seo, M. Pastore, C. Anselmi, S. Fantacci, F. De Angelis, M. K. Nazeeruddin, M. Grätzel and H. K. Kim, Organic dyes incorporating low-band-gap chromophores based on π -extended benzothiadiazole for dye-sensitized solar cells. *Dyes Pigm.* **2011**, *91*, 192-8.
- (64) Z. M. Tang, T. Lei, K. J. Jiang, Y. L. Song and J. Pei, Benzothiadiazole containing D- π -A conjugated compounds for dye-sensitized solar cells: synthesis, properties, and photovoltaic performances. *Chem.-Asian J.* **2010**, *5*, 1911-7.
- (65) J.-J. Kim, H. Choi, J.-W. Lee, M.-S. Kang, K. Song, S. O. Kang and J. Ko, A polymer gel electrolyte to achieve $\geq 6\%$ power conversion efficiency with a novel organic dye incorporating a low-band-gap chromophore. *J. Mater. Chem.* **2008**, *18*, 5223.
- (66) N. Cho, J. Han, K. Song, M.-S. Kang, M.-J. Jun, Y. Kang and J. Ko, Substituent effect of fluorine atom on benzothiadiazole bridging unit in dye sensitized solar cells. *Tetrahedron* **2014**, *70*, 427-33.
- (67) K. R. J. Thomas, P. Singh, A. Baheti, Y.-C. Hsu, K.-C. Ho and J. T. s. Lin, Electro-optical properties of new anthracene based organic dyes for dye-sensitized solar cells. *Dyes Pigm.* **2011**, *91*, 33-43.
- (68) X. Ma, J. Hua, W. Wu, Y. Jin, F. Meng, W. Zhan and H. Tian, A high-efficiency cyanine dye for dye-sensitized solar cells. *Tetrahedron* **2008**, *64*, 345-50.
- (69) L. Jing, W. Wenjun, H. Jinxiang, H. Jianli, Synthesis and Photovoltaic Properties of Benzothiadiazole Based Cyanine Dyes for Dye-sensitized Solar Cells. *ACTA CHIM SINICA* **2010**, *68*, 2551-58.
- (70) F. R. Dai, Y. C. Chen, L. F. Lai, W. J. Wu, C. H. Cui, G. P. Tan, X. Z. Wang, J. T. Lin, H. Tian and W. Y. Wong, Unsymmetric platinum(II) bis(aryleneethynylene) complexes as photosensitizers for dye-sensitized solar cells. *Chem.-Asian J.* **2012**, *7*, 1426-34.
- (71) M. Kimura, M. Karasawa, N. Sasagawa, K. Takemoto, R. Goto and S. Mori, Organic Sensitizers Including π -Conjugated Fluorene-Benzothiadiazole Bridge for Dye-sensitized Solar Cells. *Chem. Lett.* **2012**, *41*, 1613-5.
- (72) X. Wang, J. Yang, H. Yu, F. Li, L. Fan, W. Sun, Y. Liu, Z. Y. Koh, J. Pan, W.-L. Yim, L. Yan and Q. Wang, A benzothiazole-cyclopentadithiophene bridged D-A- π -A sensitizer with enhanced light absorption for high efficiency dye-sensitized solar cells. *Chem. Commun.* **2014**, *50*, 3965-8.

Benzothiadiazole-Based Sensitizers for DSSCs: A Review

- (73) M. Katono, M. Wielopolski, M. Marszalek, T. Bessho, J.-E. Moser, R. Humphry-Baker, S. M. Zakeeruddin and M. Grätzel, Effect of Extended π -Conjugation of the Donor Structure of Organic D-A- π -A Dyes on the Photovoltaic Performance of Dye-Sensitized Solar Cells. *J. Phys. Chem. C* **2014**.
- (74) C. Wang, M. Wu, Y. Hu, W. Wu, J. Su and J. Li, 5-Phenyl-iminostilbene based organic dyes for efficient dye-sensitized solar cells. *Tetrahedron* **2014**, <http://dx.doi.org/10.1016/j.tet.2014.02.074>.
- (75) W. Lee, J. y. Seng and J.-I. Hong, Metal-free organic dyes with benzothiadiazole as an internal acceptor for dye-sensitized solar cells. *Tetrahedron* **2013**, *69*, 9175-82.
- (76) S. Cai, X. Hu, Z. Zhang, J. Su, X. Li, A. Islam, L. Han and H. Tian, Rigid triarylamine-based efficient DSSC sensitizers with high molar extinction coefficients. *J. Mater. Chem. A* **2013**, *1*, 4763-72.
- (77) X. Hu, S. Cai, G. Tian, X. Li, J. Su and J. Li, Rigid triarylamine-based D-A- π -A structural organic sensitizers for solar cells: the significant enhancement of open-circuit photovoltage with a long alkyl group. *RSC Advances* **2013**, *3*, 22544-53.
- (78) S. Cai, G. Tian, X. Li, J. Su and H. Tian, Efficient and stable DSSC sensitizers based on substituted dihydroindolo[2,3-*b*]carbazole donors with high molar extinction coefficients. *J. Mater. Chem. A* **2013**, *1*, 11295-305.
- (79) K. Sukwon, L. Hunbae, K. Kwanghyun, K. Chulhee, K. Tae Yeon, K. Min Jae, K. Kyungkon and P. Nam-Gyu, Synthetic Strategy of Low-Bandgap Organic Sensitizers and Their Photoelectron Injection Characteristics. *Selected Topics in Quantum Electronics, IEEE Journal of* **2010**, *16*, 1627-34.
- (80) S. Haid, M. Marszalek, A. Mishra, M. Wielopolski, J. Teuscher, J.-E. Moser, R. Humphry-Baker, S. M. Zakeeruddin, M. Grätzel and P. Bäuerle, Significant Improvement of Dye-Sensitized Solar Cell Performance by Small Structural Modification in π -Conjugated Donor-Acceptor Dyes. *Adv. Funct. Mater.* **2012**, *22*, 1291-302.
- (81) R. Y. Lin, C. P. Lee, Y. C. Chen, J. D. Peng, T. C. Chu, H. H. Chou, H. M. Yang, J. T. Lin and K. C. Ho, Benzothiadiazole-containing donor-acceptor-acceptor type organic sensitizers for solar cells with ZnO photoanodes. *Chem Commun* **2012**, *48*, 12071-3.
- (82) L.-Y. Lin, C.-H. Tsai, F. Lin, T.-W. Huang, S.-H. Chou, C.-C. Wu and K.-T. Wong,

- 2,1,3-Benzothiadiazole-containing donor–acceptor–acceptor dyes for dye-sensitized solar cells. *Tetrahedron* **2012**, *68*, 7509-16.
- (83) H.-H. Chou, Y.-C. Chen, H.-J. Huang, T.-H. Lee, J. T. Lin, C. Tsai and K. Chen, High-performance dye-sensitized solar cells based on 5,6-bis-hexyloxybenzo[2,1,3]thiadiazole. *J. Mater. Chem.* **2012**, *22*, 10929.
- (84) L. Chen, X. Li, W. Ying, X. Zhang, F. Guo, J. Li and J. Hua, 5,6-Bis(octyloxy)benzo[*c*][1,2,5]thiadiazole-Bridged Dyes for Dye-Sensitized Solar Cells with High Open-Circuit Voltage Performance. *Eur. J. Org. Chem.* **2013**, *2013*, 1770-80.
- (85) X. Zhang, L. Chen, X. Li, J. Mao, W. Wu, H. Agren and J. Hua, Photovoltaic properties of bis(octyloxy)benzo-*c*[1,2,5]thiadiazole sensitizers based on an N,N-diphenylthiophen-2-amine donor. *J. Mater. Chem. C* **2014**, *2*, 4063-72.
- (86) Y. Hua, H. Wang, X. Zhu, A. Islam, L. Han, C. Qin, W.-Y. Wong and W.-K. Wong, New simple panchromatic dyes based on thiadiazolo[3,4-*c*]pyridine unit for dye-sensitized solar cells. *Dyes Pigm.* **2014**, *102*, 196-203.
- (87) S. Chaurasia, C.-Y. Hsu, H.-H. Chou and J. T. Lin, Synthesis, optical and electrochemical properties of pyridal[2,1,3]thiadiazole based organic dyes for dye sensitized solar cells. *Organic Electronics* **2014**, *15*, 378-90.
- (88) J. Mao, D. Wang, S.-H. Liu, Y. Hang, Y. Xu, Q. Zhang, W. Wu, P.-T. Chou and J. Hua, Dye-Sensitized Solar Cells Based on Functionally Separated D- π -A Dyes with 2-Cyanopyridine as an Electron-Accepting and Anchoring Group. *Asian Journal of Organic Chemistry* **2014**, *3*, 153-60.
- (89) Y. Wu, M. Marszalek, S. M. Zakeeruddin, Q. Zhang, H. Tian, M. Grätzel and W. Zhu, High-conversion-efficiency organic dye-sensitized solar cells: molecular engineering on D–A– π -A featured organic indoline dyes. *Energy & Environmental Science* **2012**, *5*, 8261-72.
- (90) J. Mao, J. Yang, J. Teuscher, T. Moehl, C. Yi, R. Humphry-Baker, P. Comte, C. Graetzel, J. Hua, S. M. Zakeeruddin, H. Tian and M. Grätzel, Thiadiazolo[3,4-*c*]pyridine Acceptor Based Blue Sensitizers for High Efficiency Dye-Sensitized Solar Cells. *J. Phys. Chem. C* **2014**. DOI/10.1021/jp501173b.
- (91) H. Zhu, W. Li, Y. Wu, B. Liu, S. Zhu, X. Li, H. Ågren and W. Zhu, Insight into Benzothiadiazole Acceptor in D–A– π -A Configuration on Photovoltaic Performances

Benzothiadiazole-Based Sensitizers for DSSCs: A Review

- of Dye-Sensitized Solar Cells. *ACS Sustainable Chemistry & Engineering* **2014**, *2*, 1026-34.
- (92) L. Wang, M. Liang, Y. Zhang, F. Cheng, X. Wang, Z. Sun and S. Xue, Influence of donor and bridge structure in D–A– π –A indoline dyes on the photovoltaic properties of dye-sensitized solar cells employing iodine/cobalt electrolyte. *Dyes Pigm.* **2014**, *101*, 270-9.
- (93) W. Zhou, Z. Cao, S. Jiang, H. Huang, L. Deng, Y. Liu, P. Shen, B. Zhao, S. Tan and X. Zhang, Porphyrins modified with a low-band-gap chromophore for dye-sensitized solar cells. *Organic Electronics* **2012**, *13*, 560-9.
- (94) A. Yella, H.-W. Lee, H. N. Tsao, C. Yi, A. K. Chandiran, M. K. Nazeeruddin, E. W.-G. Diau, C.-Y. Yeh, S. M. Zakeeruddin and M. Grätzel, Porphyrin-Sensitized Solar Cells with Cobalt (II/III)–Based Redox Electrolyte Exceed 12 Percent Efficiency. *Science* **2011**, *334*, 629-34.
- (95) A. Yella, C.-L. Mai, S. M. Zakeeruddin, S.-N. Chang, C.-H. Hsieh, C.-Y. Yeh and M. Grätzel, Molecular Engineering of Push–Pull Porphyrin Dyes for Highly Efficient Dye-Sensitized Solar Cells: The Role of Benzene Spacers. *Angew. Chem. Int. Ed.* **2014**, *53*, 2973-7.
- (96) S. Mathew, A. Yella, P. Gao, R. Humphry-Baker, F. E. Curchod, N. Ashari-Astani, I. Tavernelli, U. Rothlisberger, K. Nazeeruddin and M. Grätzel, Dye-sensitized solar cells with 13% efficiency achieved through the molecular engineering of porphyrin sensitizers. *Nat Chem* **2014**, *6*, 242-7.
- (97) K. D. Seo, I. T. Choi, Y. G. Park, S. Kang, J. Y. Lee and H. K. Kim, Novel D–A– π –A coumarin dyes containing low band-gap chromophores for dye-sensitized solar cells. *Dyes Pigm.* **2012**, *94*, 469-74.
- (98) C. Wang, Y. Fang, Z. Cao, H. Huang, B. Zhao, H. Li, Y. Liu and S. Tan, Synthesis and photovoltaic properties of new branchlike organic dyes containing benzothiadiazole or triphenylamine-linked consecutive vinylene units. *Dyes Pigm.* **2013**, *97*, 405-11.
- (99) J. A. Mikroyannidis, P. Suresh, M. S. Roy and G. D. Sharma, Triphenylamine- and benzothiadiazole-based dyes with multiple acceptors for application in dye-sensitized solar cells. *J. Power Sources* **2010**, *195*, 3002-10.

Benzothiadiazole-Based Sensitizers for DSSCs: A Review

- (100) G. D. Sharma, P. Suresh, M. S. Roy and J. A. Mikroyannidis, Effect of surface modification of TiO₂ on the photovoltaic performance of the quasi solid state dye sensitized solar cells using a benzothiadiazole-based dye. *J. Power Sources* **2010**, *195*, 3011-6.
- (101) G. D. Sharma, J. A. Mikroyannidis, M. S. Roy, K. R. J. Thomas, R. J. Ball and R. Kurchania, Dithienylthienothiadiazole-based organic dye containing two cyanoacrylic acid anchoring units for dye-sensitized solar cells. *RSC Advances* **2012**, *2*, 11457-64.

Chapter 3

Amino-Benzothiadiazole Based Organic Dyes For Dye-Sensitized Solar Cells: Tuning the optical properties by Donor and π -linker Modification

3.1 Introduction

The production of electricity from renewable energies will avoid burning of millions tons of coal around the world [1]. In the renewable energy sources, sun light is diffuse and intermittent [2]. The conversion of sun light in to electricity by dye-sensitized solar cells (DSSCs) have captured intense attention over the conventional photovoltaic devices due to the significant economic and environmental advantages [3]. Recently, DSSCs achieved over 12% photoelectric conversion efficiencies using a liquid electrolyte from a porphyrin dye drawn a great interest [4]. However, device efficiencies of the organic dyes are still considerably lower than those of inorganic dyes, due to their relatively narrow absorption spectrum [5]. Enormous efforts have been made to broaden and intensify the absorption spectra by introducing long π -conjugated spacers between the donor and acceptor [6-8]. This strategy is fruitful for light harvesting due to the facile charge migration from the donor to the acceptor *via* π -space. Despite this advantage, the inclusion of long π -conjugated moieties constitutes rod-like sensitizers, and have propensity to form π -aggregates and not very stable when irradiated with high-energy photons [9-11]. To overcome these drawbacks, auxiliary donor and acceptors in the vicinity of the donor and acceptor ends, respectively was used and found to improve the efficiency of the DSSC [5, 11-13]. Thomas and co-workers found that the introduction of auxiliary donor onto fluorene-based triarylamine (Figure 3.1) helped to improve the photocurrent generation as well as efficiency of their corresponding dye [13].

Figure 3.1 Structures of the fluorene-based triarylamine sensitizers

The introduction of additional acceptor (auxiliary acceptor) has been widely utilized in the design of organic sensitizers for DSSCs [14-16]. Wang co-workers [17] demonstrate that the presence of a strong electron-withdrawing benzothiadiazole auxiliary acceptor unit (Figure 3.2) in the π -bridge enhances the absorption in the low energy region. As a result, the dye **C4** achieved superior power conversion efficiency under similar conditions than **C3**.

Figure 3.2 Structures of the cyclopentadithiophene bridged organic sensitizers

Wang and co-workers proved that the incorporation of an auxiliary acceptor (Figure 3.3) is superior to that of an auxiliary donor for improvement of light-harvesting property and DSSC performance [18]. The incorporation of 3,4-ethylenedioxythiophene, benzothiadiazole in between the electron donor and NDT moiety the absorption maximum was bathochromically shifted by 24 nm and 55 nm, respectively. However, due to the presence of the BTD unit in **C7**, the HOMO-LUMO gap was decreased by 0.2 eV. The dye **C7** generated an impressive efficiency of 8.2% ($J_{SC} = 16.36 \text{ mA cm}^{-2}$, $V_{OC} = 694 \text{ mV}$, $ff = 0.72$), under the same conditions the device fabricated from **C5** achieved only 5.2% ($J_{SC} = 10.59 \text{ mA cm}^{-2}$, $V_{OC} = 726 \text{ mV}$, $ff = 0.68$), which revealed that the inclusion of a benzothiadiazole moiety is helped for broadening the absorption spectrum of the sensitizer as well as efficiency.

Figure 3.3 Structures of the naphtho[2,1-*b*:3,4-*b'*]dithiophene based sensitizers containing triphenylamine

Bäuerle and co-workers by their judicious molecular design with benzothiadiazole (Figure 3.4) achieved a high efficiency ($\eta = 8.21\%$) and ascertained that the location of the BTD unit played a crucial role in the device performance [5]. The placement of BTD unit at the proximity of the anchoring moiety led to unwanted back-electron transfer reaction and deteriorated the electron-injection efficiency into nanocrystalline TiO₂ from the excited state of the dye (PCE 1.24%). The insertion of an additional phenyl ring between the BTD and cyanoarlic acid segments found to be a remedy for this issue and dramatically improved the light-to-electric-energy conversion efficiency by 6.5 times (PCE 8.21%).



Figure 3.4 Structures of the alkoxytriphenylamine donor and benzothiadiazole based sensitizer

Recently, Tian and co-workers [19-20] have reported a series of benzothiadiazole based organic dyes with triphenylamine/indoline as electron donors (Figure 3.5), tailored the molecular structures and optimized the energy levels. Due to the stronger electron donating ability of indoline, the dyes **C10** and **C11** were showing red shifted absorption profiles and lower oxidation potentials, when compared with triphenyl amine counter parts. Indoline dye **C11** achieved the high J_{SC} (17.7 mA cm⁻²) upon co-adsorption with 20 mM deoxycholic acid

Amine Directly Attached Benzothiadiazole Sensitizers

(DCA), DSSCs gave η of 8.7% owing to the broad characteristics of IPCE spectrum. By the introduction of *n*-hexylthiophene unit in between BTD and thiophene in the dye **C11** successfully inherited the aggregation and increased the injected electron lifetime and charge recombination resistance resulting in a high V_{OC} (696 mV) and a promising high power conversion efficiency of 9.04% for the dye **C14**.

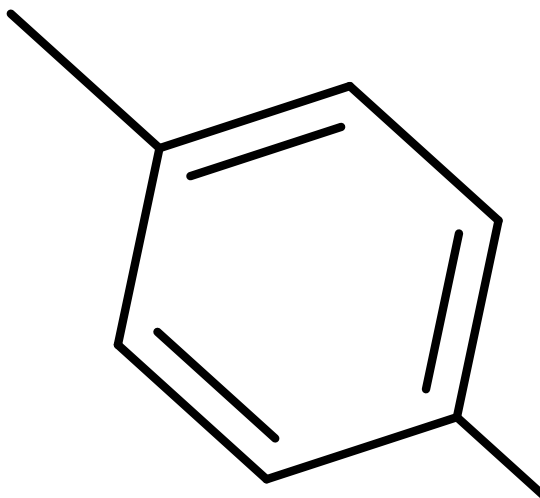


Figure 3.5 Structures of the indoline/triphenylamine donor featured benzothiadiazole sensitizers

Figure 3.6 Contributions of 4,7-diamino-substituted BTD forms.

4,7-diamino-substituted BTD systems can exist in three different forms (Figure 3.6). Interestingly, Suzuki and co-workers discovered that 4,7-diamino-substituted BTD systems mainly exist in quinoid conformation and it was confirmed by X-ray analysis [21]. Hence sensitizers with amine directly attached to 4th position of BTD segment may adapt quinoid conformation and display red-shifted absorption profiles. Already numerous attempts have been devoted to achieve high-performance in the benzothiadiazole dyes by locating the π -conjugated

Amine Directly Attached Benzothiadiazole Sensitizers

spacer in between the donor and BTD segments [14, 21-27]. However judicious chemical modification of the sensitizers by varying the location of the BTD, donor and acceptor segments is desirable to fine tune the optical, redox properties and light harvesting efficiency of the dyes. Bearing all these points in mind, we have designed and synthesized a series of organic sensitizers in which donor's piperidine and morpholine were directly attached to the BTD unit. The amines were directly attached to 4-position of BTD and acceptor (cyanoacrylic acid) with different π -conjugation length (phenyl/thiophene/bithiophene) were attached to the 7-position of BTD. Although the diphenyl amino group have been usually used as the donor, we introduced piperidine/morpholine groups to induce the red-shifted absorption due to the stronger electron donating ability, which may benefit the light-harvesting efficiency. These dyes have an architecture D-A- π -A, the general representation and structures of the dyes are shown in the Figures 3.7 and 3.8, respectively. We anticipated that the direct attachment of amine unit to BTD will induce subtle changes in optical and electrochemical properties

Figure 3.7 General representation and numbering of the sensitizers possessing amine directly attached to benzothiadiazole

Figure 3.8 Structures of the organic sensitizers with amine directly attached to benzothiadiazole

3.2 Results and Discussion

3.2.1 Synthesis and Characterization

The synthetic protocols used to obtain the amine directly integrated benzothiadiazole based dyes are shown in Scheme 3.1. The starting material 4,7-dibromobenzo[*c*][1,2,5]thiadiazole (**1**) was prepared according to the reported procedure [28]. The first step involves the introduction of piperidine (or) morpholine on 4th position of BTD. The introduction of piperidine unit was done by procedure reported in the literature [29]. Morpholine also introduced by adopting the same procedure as piperidine. In the second step by Stille coupling protocol with (5-(1,3-dioxolan-2-yl)thiophen-2-yl)tributylstannane and (5'-(1,3-dioxolan-2-yl)-2,2'-bithiophen-5-yl)tributylstannane, thiophene and bithiophene aldehydes were introduced. The phenyl spacer was introduced by the Suzuki coupling protocol with 4-formylphenylboronic acid. In the final step, by the Knoevenagel condensation the aldehyde precursors were successfully converted to the desired dyes on treatment with cyanoacetic acid in presence of ammonium acetate as a catalyst in acetic acid. The dyes **7a**, **7b** was also synthesized from **2a**, **2b** by Stille coupling protocol with tributyl(thiophen-2-yl)stannane to study the impact of the conjugation on optical properties.

Scheme 3.1 Synthesis of amine directly integrated to benzothiadiazole sensitizers

The newly synthesised phenyl spaced dyes are red in colour where as thiophene and bithiophene dyes are black in colour. The dyes are thoroughly characterized by IR, NMR (^1H and ^{13}C) and mass spectral methods. In addition to these characterizations, the structure of the intermediate **5a** was confirmed by single crystal X-ray diffraction analysis. All six dipolar dyes are air stable and possess fairly good solubility in THF, DMF and moderately soluble in CH_2Cl_2 , CHCl_3 , acetonitrile and toluene.

3.2.2 Structural Analysis of **5a**

Single crystals of **5a** suitable for X-ray crystallographic analysis were grown by slow evaporation from its solution in a dichloromethane/hexanes mixture. The ORTEP plot of **5a** is shown in Figure 3.9. The single crystal X-ray structure determination of intermediate **5a** confirms the presence of the newly introduced C-C bonding between benzothiadiazole unit and thiophene unit by Stille coupling protocol. The intermediate **5a** crystallizes in the monoclinic space group $P2_1/c$. The benzothiadiazole ring is nearly coplanar with the neighboring thiophene segment with an inter-planar angle 1.10° . The dihedral angles between the planes containing the piperidine-benzothiadiazole, benzothiadiazole-thiophene and thiophene-carbaldehyde were found to 28.21° , 1.10° and 4.73° , respectively. The bond length of C9-C12 (1.46 \AA) was shorter than the C-C (1.54 \AA) bond length. The C6-N1 (1.40 \AA) bond distances in between the piperidine nucleus and benzothiadiazole moiety is shorter than the aromatic C-N bond distance (C-N single bond 1.47 \AA ; double bond 1.34 \AA), which indicates that the lone pair on the piperidine nitrogen is delocalized into the benzothiadiazole segment probably due to the electron-deficient nature of the thiadiazole nucleus and cyanoacrylic acid. This also confirms the quinoid conformation of the intermediate **5a**.

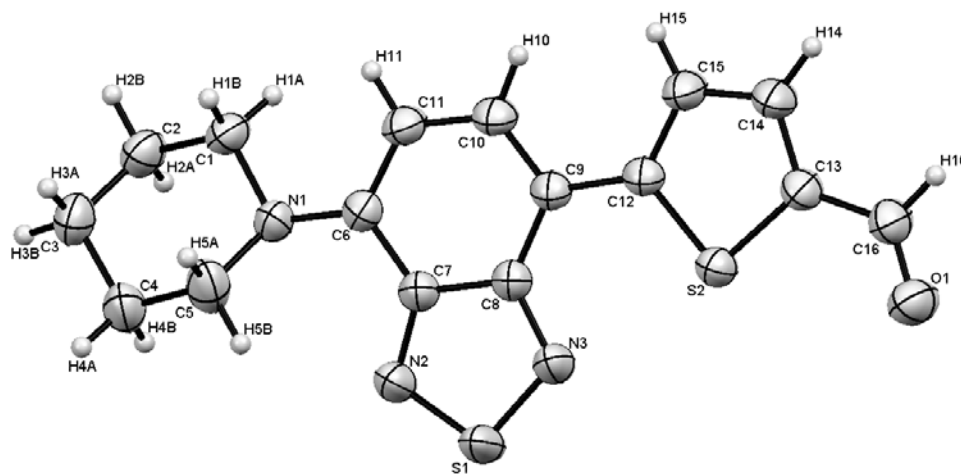


Figure 3.9 The molecular structure of (**5a**) showing the atom-labelling scheme

3.2.3 Optical properties

The light-harvesting properties of the sensitizers were investigated by measuring the absorption spectra in tetrahydrofuran solution (2×10^{-5} M) and shown in Figure 3.10. The corresponding optical data are compiled in Table 3.1. All the dyes showed two main absorption bands. The absorption bands below 400 nm is probably due to a localized $\pi-\pi^*$ transition and the longer wavelength region absorption (400-650 nm) is ascribed to the intramolecular charge transfer transition with slight contribution from the $\pi-\pi^*$ transition character. The sensitizers mainly differ in their donor attached to benzothiadiazole and spacer entity in between the benzothiadiazole and cyanoacrylic acid. As well known in literature, the absorption profile originating from intramolecular charge transfer (ICT) is readily influenced by the electron-donating ability of the donor part and the conjugation length of the π -bridge. A closer inspection of the absorption profiles of the sensitizers reveals the impact of donor strength and conjugation length of the π -bridge on the absorption.

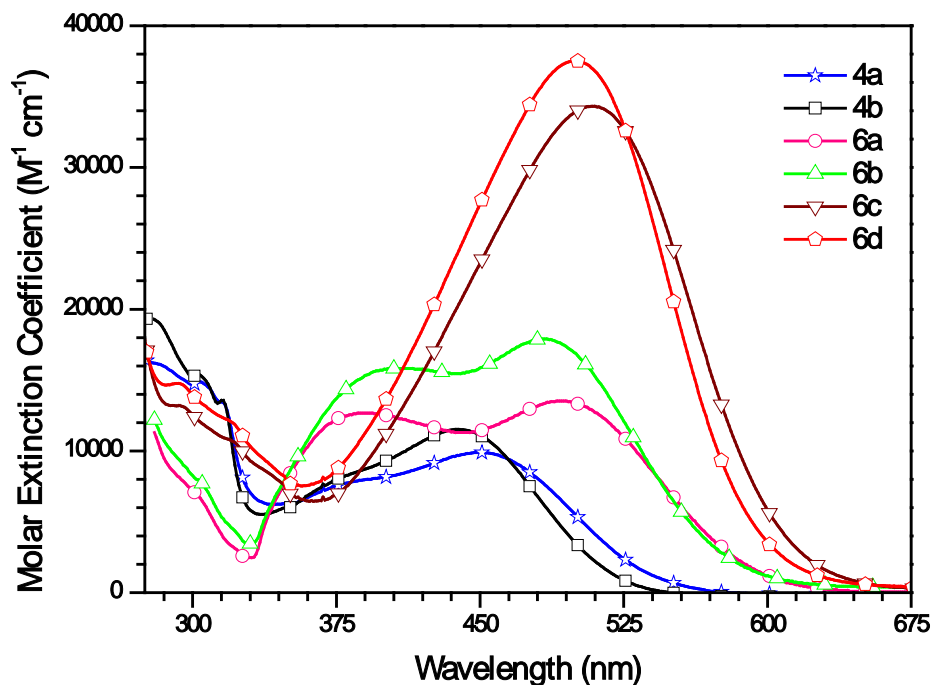


Figure 3.10 Absorption spectra of the dyes recorded in tetrahydrofuran solutions

The donor strength of the amines can be estimated on the basis of their pK_b . The amines piperidine, morpholine are arranged in the decreasing order of donor strength as: piperidine ($pK_b = 2.8$) > morpholine ($pK_b = 5.6$) [30]. The absorption maximum of the piperidine based donor derivatives was red shifted by (9-13 nm) than the morpholine derivative for a fixed spacer system. Thus, the absorption maxima of **4a**, **6a** and **6c** were red shifted than **4b**, **6b** and **6d**

respectively. This is in agreement with the donor strength. It is indicative that the introduction of piperidine unit as electron donor beneficially favours the light-harvesting of the sensitizer with a red-shifted absorption. The molar extinction coefficients of the morpholine derivatives were high when compared to the piperidine based derivatives. The steady-state results clearly hint to a reduction of the overall π -conjugation in piperidine derivatives by (2-3°) than morpholine derivatives. Hence the increase in the extinction coefficient for the morpholine dyes may be attributed to the increase in the coplanarity between the electron donor and the electron acceptor BTD moiety, which would eventually hike the magnitude of the transition probability.

The optical absorption and charge transfer properties of the organic sensitizers mainly depend on the linker group between the electron donor and the acceptor. It was also anticipated that the dye with extended π -conjugation network display lower energy absorption profiles and more extended spectral coverage. So to fine tune the light harvesting properties of the sensitizers, we perturbed the linker with different aromatic groups such as a benzene, thiophene, and bithiophene. The longer wavelength absorption occurring in the visible region is sensitive to the nature of the conjugation pathway and red-shifted on progressive increment of electron richness of the π -bridging unit between BTD and cyanoacrylic acid. The bithiophene bridged sensitizers **6c** and **6d** inherit the most bathochromically shifted absorption profile while the phenyl linked derivatives **4a** and **4b** displayed the mediocre intense peak in the series suggesting the role attributed to the electron donation ability and planarity of the π -linker. The dyes **6c** and **6d** were showing red shifted absorption and high molar extension coefficient in series with λ_{abs} at 509 ($34300 \text{ M}^{-1} \text{ cm}^{-1}$) and 500 ($37500 \text{ M}^{-1} \text{ cm}^{-1}$), respectively. These two dyes possess high molar extinction coefficient and a strong absorption within a relatively narrow spectrum range (400–600 nm), make them good candidates for co-sensitization, which have complementary absorption properties in the near infrared (NIR) region and shorter wavelength region.

Table 3.1 Optical data of dyes recorded in tetrahydrofuran

Dye	λ_{abs} , nm ($\epsilon \times 10^3 \text{ M}^{-1} \text{ cm}^{-1}$)	λ_{em} , nm	Stokes' shift, cm^{-1}
4a	257 (19.8), 304 (14.9) 449 (9.9)	619	6117
4b	254 (23.4), 278 (19.3) 303 (15.4) 438 (11.5)	615	6571
6a	390 (12.7), 493 (13.5)	639	4635
6b	409 (15.8), 484 (17.9)	633	4863
6c	264 (24.1), 509 (34.3)	-	-
6d	261 (26.9), 500 (37.5)	-	-

Amine Directly Attached Benzothiadiazole Sensitizers

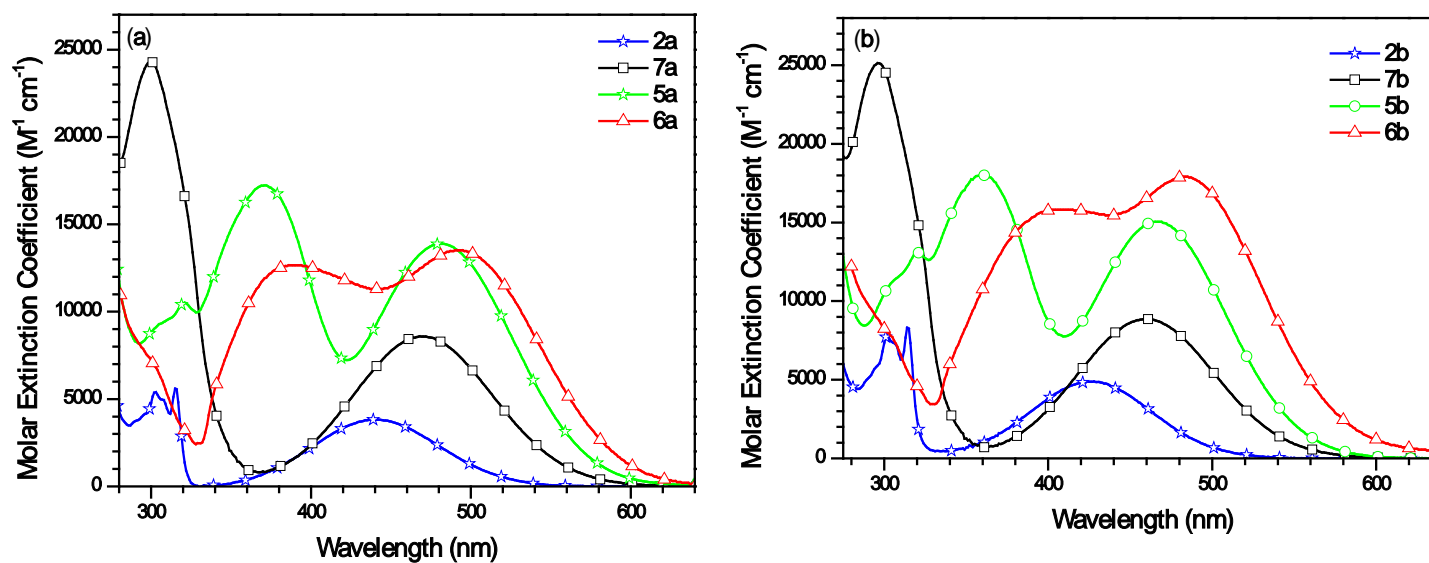
For the similar structural configuration derivatives, the absorption maxima and molar extension coefficients were in order phenyl < thiophene < bithiophene. This can be rationalized on the basis that extension of conjugation by the electron rich spacer from phenyl to bithiophene, enhances the density of electron delocalization over the whole molecule, results in better conjugated system and intensifies the ICT interactions between the electron-donating amine group and electron-withdrawing cyanoacrylic acid group. The extension of the conjugation by bithiophene, resulted in a broader responsive wavelength region and higher light-harvesting property. The absorption shifted towards longer wavelength as the electron donation ability of the π -linker unit increased. In view of the above facts, absorption of sensitizers is assigned as a charge-transfer transition with contribution from the π - π^* transition. Thus, by changing the conjugation of π -linker, electro-optical properties can be tuned. This result reveals that in fine tuning the optical properties of the dyes electron-donating ability of the π -bridge plays a major role.

To get more information about the absorption spectra of the dyes, we have recorded the absorption spectra of the bromo, thiophene and aldehyde precursors along with the cyanoacrylic acid derivatives **6a** and **6b**. To have fair comparison, we have synthesised the thiophene derivatives. This reveals the origin of the transitions and helped to understand the impact of the electron-accepting group. From the Figure 3.11, it is evident that the introduction of the thiophene improves the π - π^* and ICT transitions. Further addition of carbaldehyde on thiophene shifted the π - π^* transition towards the ICT transition and reduced the gap between them. Finally, the presence of more electron deficient acrylic acid in **6a** and **6b** leads to the merging of the π - π^* and ICT transitions. The maximum absorption wavelength and molar extension coefficient increases as the conjugation increases and the acceptor strength becomes stronger. (Accepting strength: Br < CHO < CH = C(CN)(COOH)).

To probe the effect of solvent polarity on the ground state of the sensitizers, the solvatochromism studies were performed by measuring the absorption spectra in different solvents such as toluene (TOL), tetrahydrofuran (THF), dichloromethane (DCM), acetonitrile (ACN), dimethylformamide (DMF) and methanol (MeOH). The changes in the absorption properties of the dyes with the solvent polarity were shown in Figures 3.12, 3.13 (a), (b) and data compiled in Table 3.2.

Table 3.2 Absorption spectral data for the dyes in different solvents

Dye	λ_{abs} , nm						
	TOL	DCM	DCM+TFA	DCM+TEA	ACN	DMF	MeOH
5a	286, 317, 452	257, 304, 449	314, 363	304, 315, 444	256, 302, 442	305, 448	254, 303, 437
5b	304, 317, 440	254, 278, 303, 316, 433	314, 361	303, 430	315, 253, 275, 302, 314, 430	304, 316, 437	303, 315, 340, 427
6a	378, 490	396, 489	314, 430	395, 486	374, 484	380, 489	378, 484
6b	372, 483	381, 485	315, 430	384.5, 475	481	377, 482	392, 472
6c	305, 511	266, 517	297, 479	316, 487	263, 498	418, 485	260, 315, 476
6d	362, 483	263, 504	297, 481	476	261, 495	414, 477	259, 473


Figure 3.11 Comparison of the absorption spectra of the dyes (a) **6a**, (b) **6b** with intermediates recorded in THF

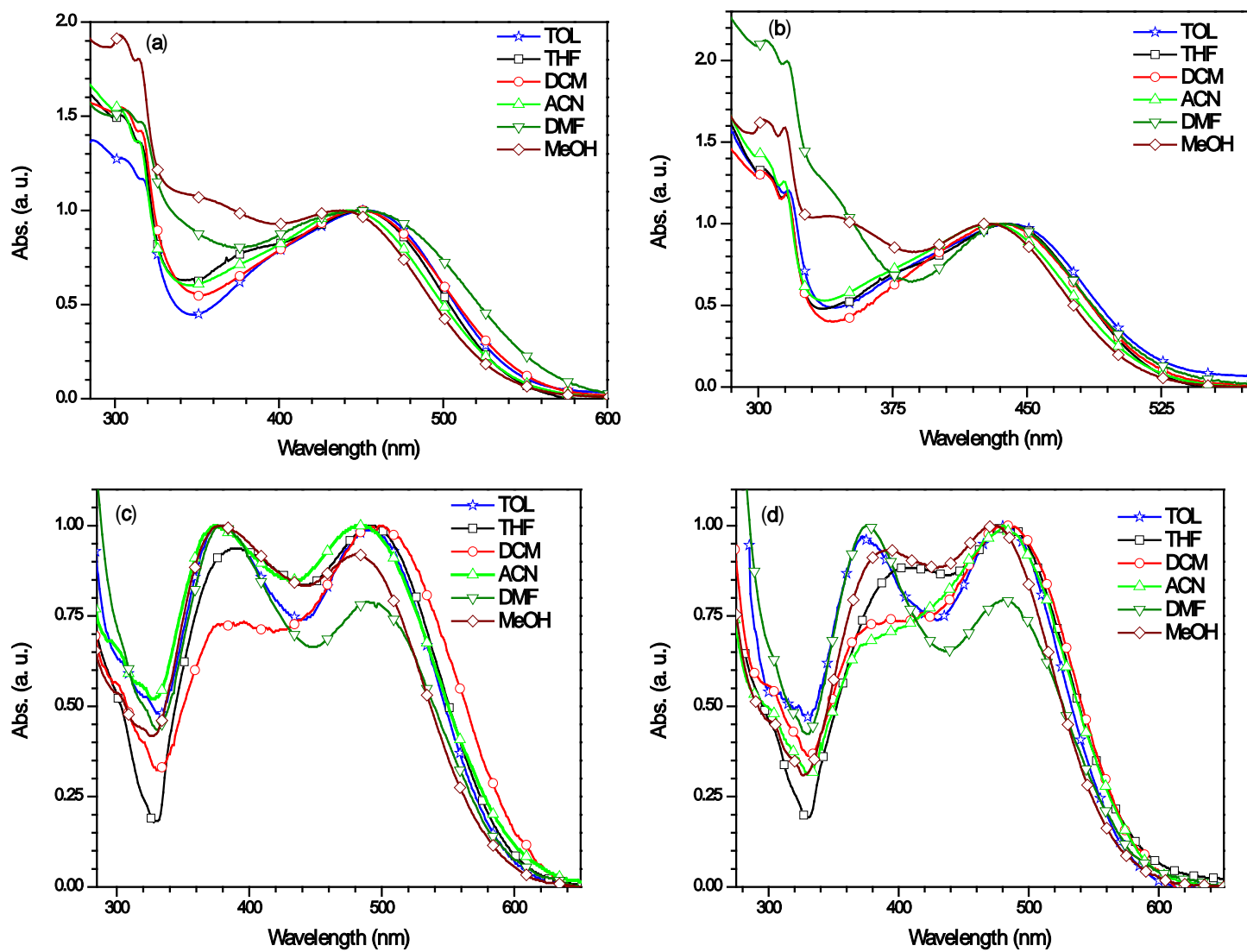


Figure 3.12 Absorption spectra of dyes (a) **4a**, (b) **4b**, (c) **6a** and (d) **6b** recorded in different solvents

Amine Directly Attached Benzothiadiazole Sensitizers

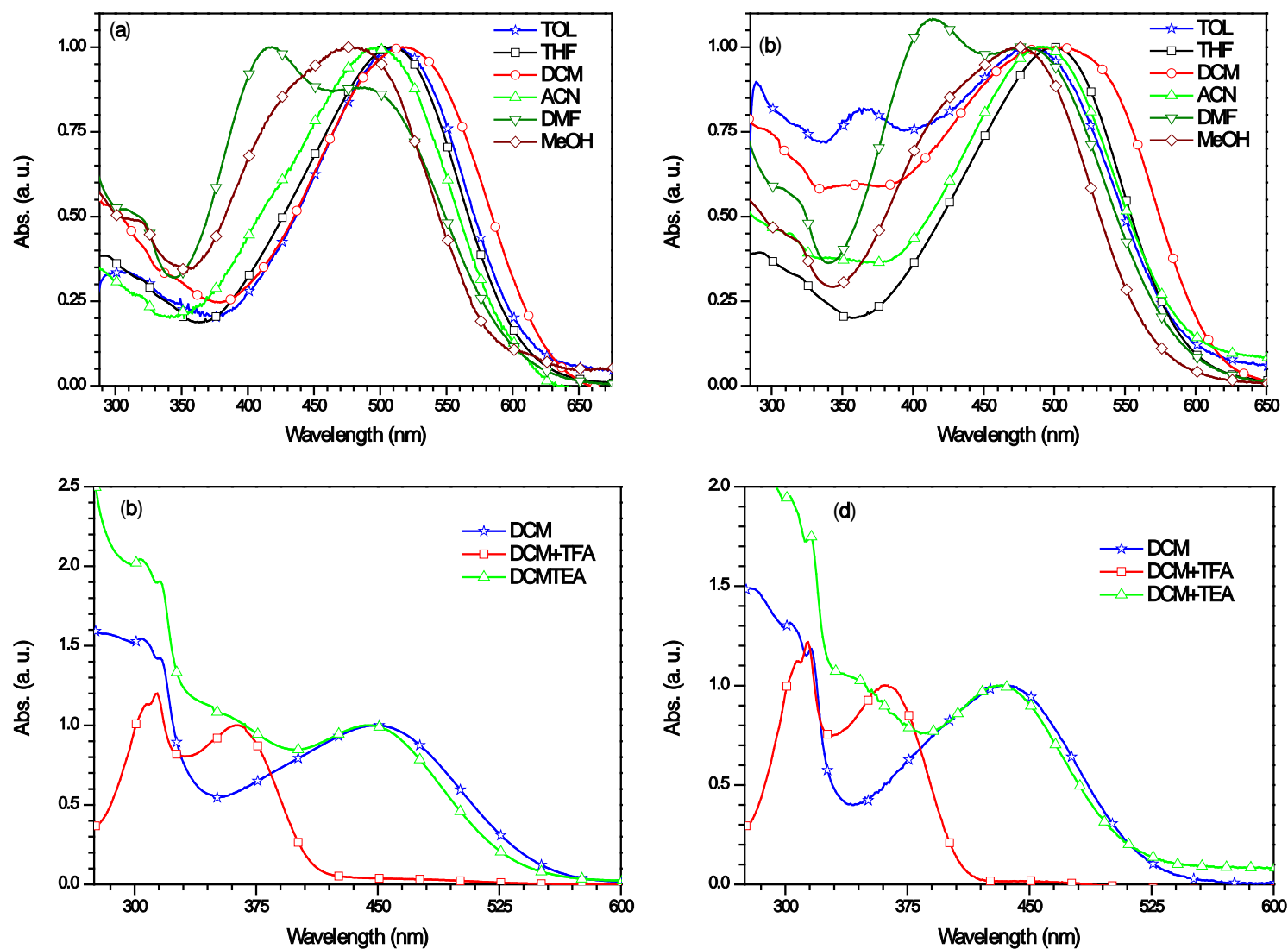


Figure 3.13 Absorption spectra of dyes (a) **6c**, (b) **6d** recorded in different solvents; Changes in the absorption spectra of the dyes (c) **4a**, (d) **4b** in dichloromethane upon addition of TFA or TEA

Amine Directly Attached Benzothiadiazole Sensitizers

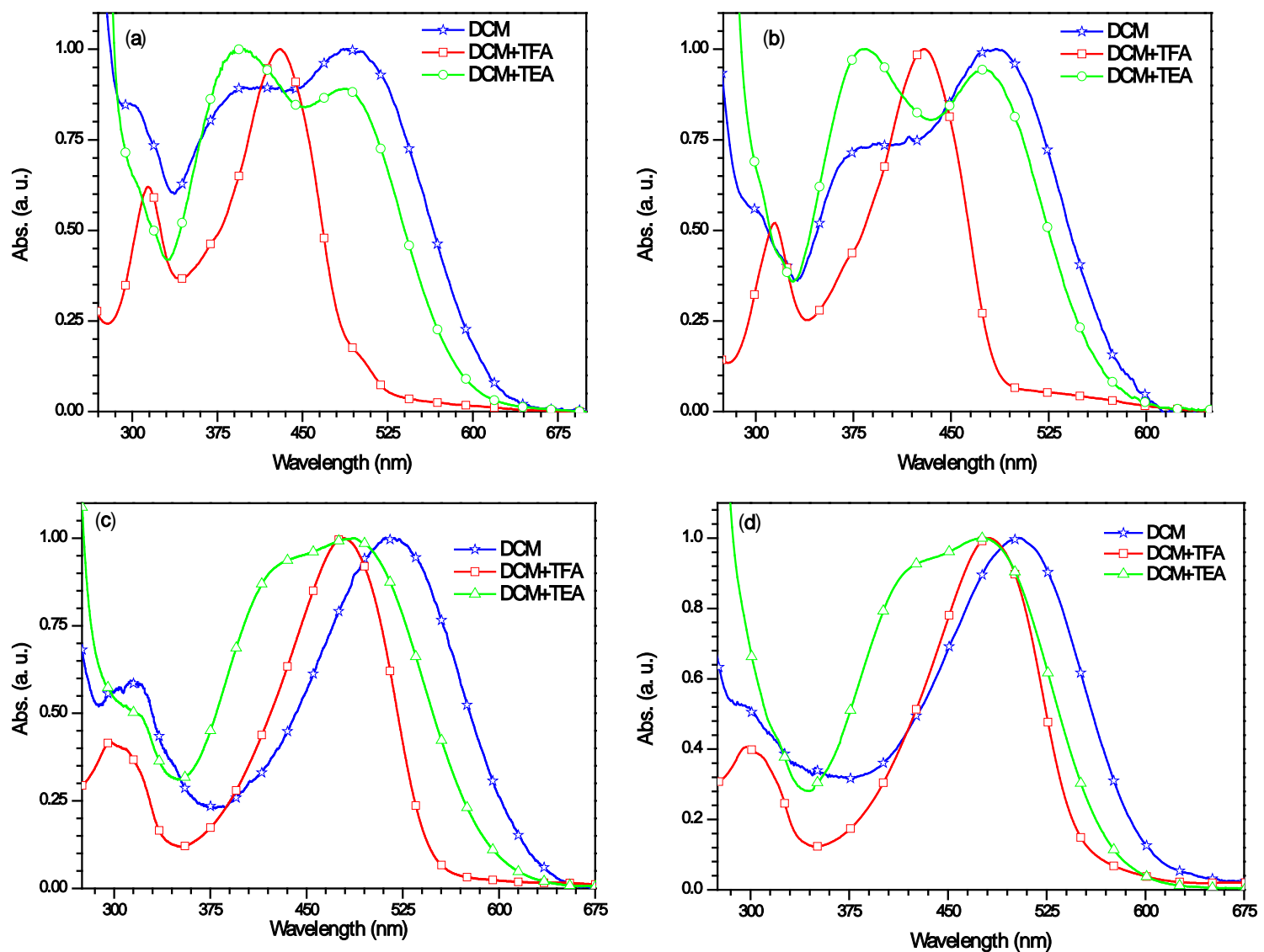


Figure 3.14 Changes in the absorption spectra of the dyes (a) **6a**, (b) **6b**, (c) **6c** and (d) **6d** in dichloromethane upon addition of TFA or TEA

Amine Directly Attached Benzothiadiazole Sensitizers

The absorption spectra of the dyes showed significant difference by changing the solvent from non-polar to polar. Absorption spectra of the dyes in DMF and methanol displayed considerable blue-shift in the absorption spectra than that of the other solvents. This clearly indicates that the dyes are partially in the deprotonated form in these solutions. Deprotonation would diminish the electron accepting ability of acceptor, results the less donor-acceptor interactions. This blue shift in the absorption spectrum was consistent with the basicity of the solvents. The protonation-deprotonation studies of the dyes were performed by recording absorption spectra of the dyes in dichloromethane solutions (Table 3.2 and Figure 3.13 (c), (d) & 3.14) by the addition of trifluoroacetic acid (TFA) and triethylamine (TEA). The absorption spectra of the dyes were drastically blue shifted by the addition of TFA due to the protonation of the alkyl amines piperidine/morpholine. The absorption profile in the presence of TFA is the characteristic of the π - π^* transition and the intermolecular charge transfer transition vanished. Interestingly, the addition of TEA yielded slight blue shift in the absorption spectra due to the deprotonation of the carboxylic acid group by which the electron-accepting strength of the cyanoacrylic acid moiety diminishes. Similar type of behaviour is quite observed in organic dyes containing carboxylic acid in the literature [12, 31-33]. Since, the ICT transition from amine to cyanoacrylic acid is not significant in phenyl spaced dyes **4a** and **4b**, the effect of TEA addition is less pronounced when compared to the thiophene and bithiophene dyes.

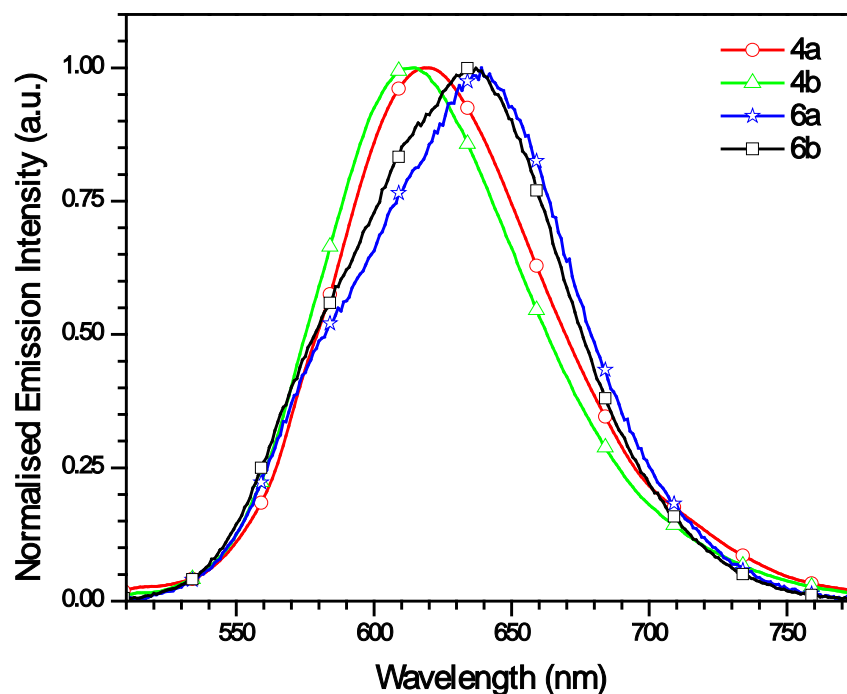


Figure 3.15 Emission spectra of the dyes recorded in tetrahydrofuran solutions

Amine Directly Attached Benzothiadiazole Sensitizers

The emission spectra recorded for the dyes in THF are displayed Figure 3.15. All the dyes except **6c** and **6d** displayed weak red emission. The emission spectra of the dyes follow the same trend as the absorption spectra. The longer wave length emission observed for **6a** and **6b** is attributed to the thiophene unit. Though the emission maxima for **4a** and **4b** were blue shifted than the **6a** and **6b**, the former dyes exhibited larger Stokes shifts. Larger Stokes shifts observed for the phenyl derivatives indicates a structural reorganization on photoexcitation.

3.2.4 Electrochemical properties

Electrochemical measurements were performed for the dyes to evaluate the viability of the photogenerated electron injection from the excited-state of the dyes to the TiO₂ conduction band and the dye regeneration by the iodine/iodide redox couple. Cyclic voltammetry (CV) and differential pulse voltammetric (DPV) measurements were carried out by conventional three electrode system. The electrochemical analysis were performed in THF solutions (2×10^{-4} M) using tetrabutylammonium perchlorate as a supporting electrolyte with a scan rate of 100 mV S^{-1} . The reference electrode was Ag/AgNO₃, and the potentials were calibrated using ferrocene as an internal standard. The excited-state oxidation potential (E_{OX}^*) can be obtained by subtracting the zero-zero transition energy (E_{0-0}) from E_{OX} , where the E_{0-0} value derived from the absorption edge. The cyclic voltammograms and differential pulse voltammograms recorded for the dyes in the presence of ferrocene are shown in Figure 3.16 and the corresponding data are compiled in Table 3.3.

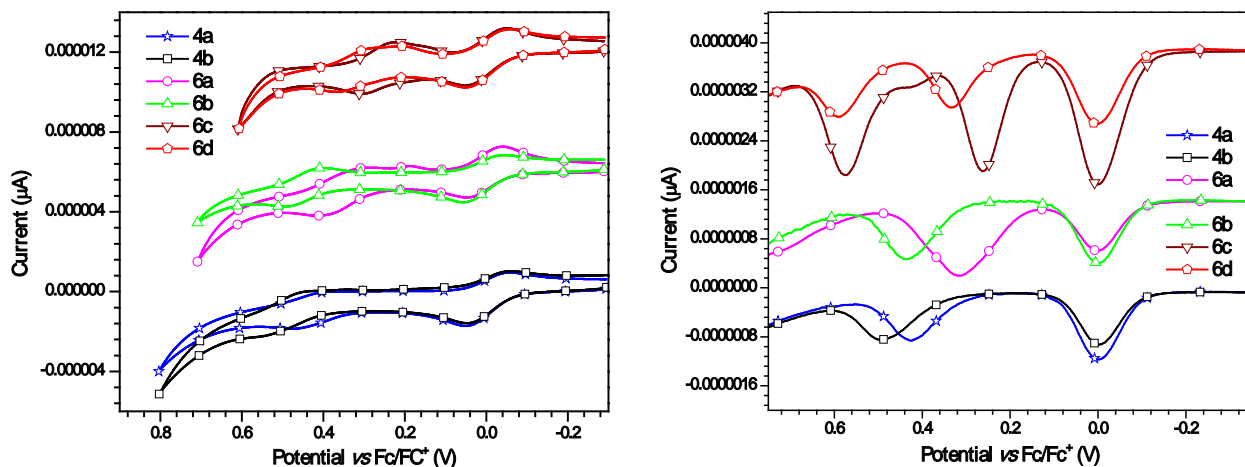


Figure 3.16 (a) Cyclic voltammograms recorded for the dyes in THF (b) Differential pulse voltammograms of the dyes recorded in THF

The dyes displayed a quasi-reversible one-electron oxidation couple in the range 269-447 mV *versus* ferrocene, which was attributed to the removal of electron from amine and aromatic

Amine Directly Attached Benzothiadiazole Sensitizers

π -system. Consequently, the magnitude of the oxidation potential for the dyes was dictated by the nature of the donor and π -bridge which connects the benzothiadiazole and cyanoacrylic acid units. piperidine based dyes (**4a**, **6a** and **6c**) displayed cathodically shifted oxidation potential when compared to the corresponding morpholine analogs (**4b**, **6b** and **6d**) due to the stronger electron-donating nature of piperidine. Reduced donor strength observed for the morpholine sensitizers in the absorption spectra is also corroborated by the electrochemical studies. However, within a series the oxidation potential is also dependent on the π -linker and follow the order phenyl > thiophene > bithiophene. Insertion of the more electron-rich π -spacer segment in between the benzothiadiazole and cyanoacrylic acid facilitates the oxidation propensity of the amine unit, which clearly indicates the presence of an electronic communication from the amine donor and the cyanoacrylic acid acceptor. From the orbital energies it was evident that, incorporation of electron rich donor and π -spacer segments in the dyes raised the HOMO energy level.

Table 3.3 Electrochemical properties of the benzothiadiazole based sensitizers

Dye	E_{OX} , mV (ΔE_p , mV) ^a	E_{OX} , mV ^b	E_{OX} vs NHE, V ^c	HOMO, eV ^d	LUMO, eV ^e	E_{0-0} , eV ^f	E_{OX}^* , V ^g
4a	438 (85)	426	1.196	5.226	3.016	2.21	-1.014
4b	511 (109)	494	1.264	5.294	2.994	2.30	-1.036
6a	345 (128)	316	1.086	5.116	3.146	1.97	-0.884
6b	442 (94)	440	1.210	5.24	3.24	2.00	-0.79
6c	264 (83)	264, 574	1.034	5.064	3.124	1.94	-0.906
6d	290 (157)	334, 590	1.104	5.134	3.164	1.97	-0.866

^a potentials with reference to ferrocene internal standard from CV; ^b potentials with reference to ferrocene internal standard from DPV; ^c Ground-state oxidation potential versus NHE ^d Deduced from the equation HOMO = $E_{OX} + 4.8$; ^e Deduced from the equation LUMO = HOMO - E_{0-0} ; ^f Derived from optical edge; ^g Deduced from formula $E_{OX}^* = E_{OX} - E_{0-0}$

The ground-state oxidation potentials of the dyes fall in the range 1.04-1.22 V *versus* the normal hydrogen electrode (NHE), which guarantees the efficient regeneration of the dye from the iodide/triiodide redox couple (0.42 V *vs* NHE) [34]. The excited-state oxidation potential (E_{OX}^*) values are in the range of -0.83 to -1.00 V *versus* NHE, which are more negative than the conduction band of TiO₂ (-0.5 V *vs* NHE) [35-36]. Thus, this downhill energy offset in the dyes ensures the thermodynamic driving force for the electron injection. The trends in absorption maximum and oxidation potential of dyes studied in this chapter were displayed in the Figure 3.17.

Figure 3.17 Structures and trends in absorption maxima and oxidation potential of dyes studied in this chapter

3.2.5 Computational studies

To understand the nature of absorption and electronic excitation on photoexcitation in the sensitizers, DFT [37] calculations were performed by using the Gaussian 09 program package [31]. The ground-state geometries of dyes were optimized in the gas phase by DFT by using the hybrid B3LYP [38-39] functional and the standard 6-31g(d,p) basis set. The TD-DFT calculations were performed on the B3LYP-optimized ground-state geometries by using the hybrid B3LYP or MPW1K [40] /6-31g(d,p)functional basis set and outcomes were listed in Table 3.4, 3.5 & 3.6. The isodensity surface plots of the dyes are shown in the Figures 3.18 & 3.19. Electron distribution is almost similar in all the dyes. Where the HOMO and HOMO-1 are delocalized over the π -conjugated system from amine to spacer attached to cyanoacrylic acid, while the LUMO and LUMO+1 is a π^* orbital delocalized across from benzothiadiazole unit and up to the anchoring group. Since HOMO is distributed over the amine, benzothiadiazole and π -linker, the removal of electron is assigned to the oxidation of the conjugated backbone.

Table 3.4 Computed vertical excitation energies, dipole moments, and frontier orbital energies for dyes using B3LYP (gas)

Dye	λ_{\max}/nm	f	Configuration	HOMO, eV	LUMO, eV	μ_g , Debye
4a	489.5	0.4679	HOMO→LUMO (87%), HOMO→LUMO+1 (12%)	-5.50	-2.63	9.85
	432.6	0.2736	HOMO→LUMO+1 (86%), HOMO→LUMO (12%)			
	334.3	0.1370	HOMO-1→LUMO (84%), HOMO-1→LUMO+1(13%)			
	298.9	0.3862	HOMO-1→LUMO+1(81%), HOMO-1→LUMO (11%)			
	258.7	0.1306	HOMO→LUMO+3 (59%), HOMO-3→LUMO+1(13%)			
4b	484.6	0.4333	HOMO→LUMO (88%), HOMO→LUMO+1 (11%)	-5.63	-2.71	8.36
	424.7	0.2966	HOMO →LUMO+1 (87%), HOMO→LUMO (11%)			
	337.1	0.1178	HOMO-1→LUMO (86%), HOMO-1→LUMO+1 (11%)			
	298.4	0.3907	HOMO-1→LUMO+1 (75%), HOMO-1→LUMO (10%)			
6a	541.5	0.3908	HOMO→ LUMO (88%), HOMO→ LUMO+1 (11%)	-5.39	-2.80	7.94
	441.2	0.5107	HOMO→ LUMO+1 (84%), HOMO→ LUMO (11%)			
	363.4	0.1057	HOMO-1→ LUMO (88%)			
	309.9	0.1693	HOMO-1→LUMO+1(79%)			
	265.6	0.1193	HOMO→LUMO+2 (45%), HOMO→LUMO+3 (27%)			
6b	538.8	0.3744	HOMO→LUMO (89%), HOMO→LUMO+1(10%)	-5.50	-2.90	6.89
	435.7	0.5080	HOMO→LUMO+1 (85%), HOMO→ LUMO (10%)			
	365.4	0.1044	HOMO-1→ LUMO (88%)			
	308.9	0.1629	HOMO-1→LUMO+1(66%), HOMO-3→ LUMO (16%)			
6c	576.3	0.7978	HOMO→LUMO (86%), HOMO→LUMO+1 (14%)	-5.19	-2.79	11.12
	508.1	0.3422	HOMO→LUMO+1 (82%), HOMO→LUMO (14%)			
	403.7	0.1572	HOMO-1→LUMO (84%), HOMO-1→LUMO+1 (10%)			
	365.7	0.2668	HOMO-1→LUMO+1(80%), HOMO→LUMO+2 (12%)			
6d	574.9	0.7299	HOMO→LUMO (86%), HOMO→LUMO+1 (14%)	-5.28	-2.86	9.23
	501.6	0.4122	HOMO→LUMO+1 (82%), HOMO→LUMO (14%)			
	403.9	0.1310	HOMO-1→LUMO (84%), HOMO-1→LUMO+1 (10%)			
	363.7	0.2693	HOMO-1→LUMO+1 (80%), HOMO→LUMO+2 (12%)			

Table 3.5 Computed vertical excitation energies, dipole moments, and frontier orbital energies for dyes using MPW1K (gas)

Dye	λ_{\max}/nm	f	Configuration	HOMO, eV	LUMO, eV	μ_g , Debye
4a	404.0	0.6285	HOMO→LUMO (82%), HOMO→LUMO+1 (16%)	-6.46	-2.04	9.39
	339.1	0.4179	HOMO→LUMO+1 (80%), HOMO→LUMO (15%)			
	276.4	0.1664	HOMO-1→LUMO (90%)			
	258.1	0.1448	HOMO-3→LUMO (58%), HOMO-3→LUMO+1 (17%) HOMO→LUMO+4(13%)			
4b	399.2	0.6014	HOMO→LUMO (84%), HOMO→LUMO+1 (14%)	-6.59	-2.12	8.04
	334.1	0.4462	HOMO→LUMO+1(82%), HOMO→LUMO (13%)			
	275.7	0.1410	HOMO-1→LUMO (90%)			
	257.6	0.1424	HOMO-3→LUMO (57%), HOMO-3→LUMO+1 (15%) HOMO→LUMO+4(13%)			
6a	447.0	0.6793	HOMO→LUMO (93%)	-6.30	-2.24	7.31
	360.2	0.4084	HOMO→LUMO+1(92%)			
	251.9	0.1299	HOMO-1→LUMO+1(72%), HOMO-3→LUMO (10%)			
6b	443.3	0.6548	HOMO→LUMO (94%)	-6.42	-2.33	6.50
	356.5	0.4183	HOMO→LUMO+1(92%)			
	251.1	0.1311	HOMO-1→LUMO+1 (74%), HOMO-3→LUMO (13%)			
6c	469.0	1.1866	HOMO→LUMO (87%)	-6.08	-2.25	10.30
	397.4	0.2401	HOMO→LUMO+1 (84%)			
	282.7	0.1470	HOMO→LUMO+2 (70%), HOMO-1→LUMO+1 (17%)			
6d	462.7	1.1399	HOMO→LUMO (87%)	-6.18	-2.30	8.51
	393.2	0.2763	HOMO→LUMO+1 (84%)			
	280.8	0.1448	HOMO→LUMO+2 (71%), HOMO-1→LUMO+1 (15%)			

Table 3.6 Computed vertical excitation energies, dipole moments, and frontier orbital energies for dyes using MPW1K (THF)

Dye	λ_{\max}/nm	f	Configuration	HOMO, eV	LUMO, eV	μ_g , Debye
4a	420.6	0.8504	HOMO→LUMO (81%), HOMO→LUMO+1 (17%)	-6.40	-2.12	11.76
	356.8	0.2920	HOMO→LUMO+1 (80%), HOMO→LUMO (15%)			
	281.7	0.2422	HOMO-1→LUMO (90%)			
	262.9	0.2046	HOMO-2→LUMO (43%), HOMO-2→LUMO+1 (27%) HOMO-3→LUMO (10%), HOMO→LUMO+4 (10%)			
4b	412.8	0.8311	HOMO→LUMO (82%), HOMO→LUMO+1 (16%)	-6.50	-2.15	10.24
	350.4	0.3102	HOMO→LUMO+1 (81%), HOMO→LUMO (14%)			
	280.1	0.2198	HOMO-1→LUMO (89%)			
	262.4	0.2063	HOMO-2→LUMO (28%), HOMO-3→LUMO (26%) HOMO-2→LUMO+1(19%)			
6a	469.2	0.9658	HOMO→LUMO (94%)	-6.26	-2.31	9.66
	375.7	0.2759	HOMO→LUMO+1 (93%)			
	300.3	0.1173	HOMO-1→LUMO (93%)			
	254.2	0.1407	HOMO-1→LUMO+1 (72%), HOMO-3→LUMO (12%)			
6b	462.0	0.9436	HOMO→LUMO (95%)	-6.35	-2.34	8.66
	369.9	0.2791	HOMO→LUMO+1 (93%)			
	298.9	0.1053	HOMO-1→LUMO (92%)			
	253.3	0.1451	HOMO-1→LUMO+1 (72%), HOMO-3→LUMO (11%)			
6c	493.6	1.4716	HOMO→LUMO (88%)	-6.07	-2.35	13.24
	285.4	0.1608	HOMO→LUMO+2 (55%), HOMO-1→LUMO+1 (32%)			
	263.2	0.1256	HOMO-4→LUMO (36%), HOMO-4→LUMO+1 (27%) HOMO-5→LUMO (12%)			
6d	483.5	1.4670	HOMO→LUMO (88%)	-6.15	-2.36	11.16
	283.0	0.1532	HOMO→LUMO+2 (60%), HOMO-1→LUMO+1 (27%)			
	262.7	0.1284	HOMO-4→LUMO (35%), HOMO-4→LUMO+1(31%)			

Amine Directly Attached Benzothiadiazole Sensitizers

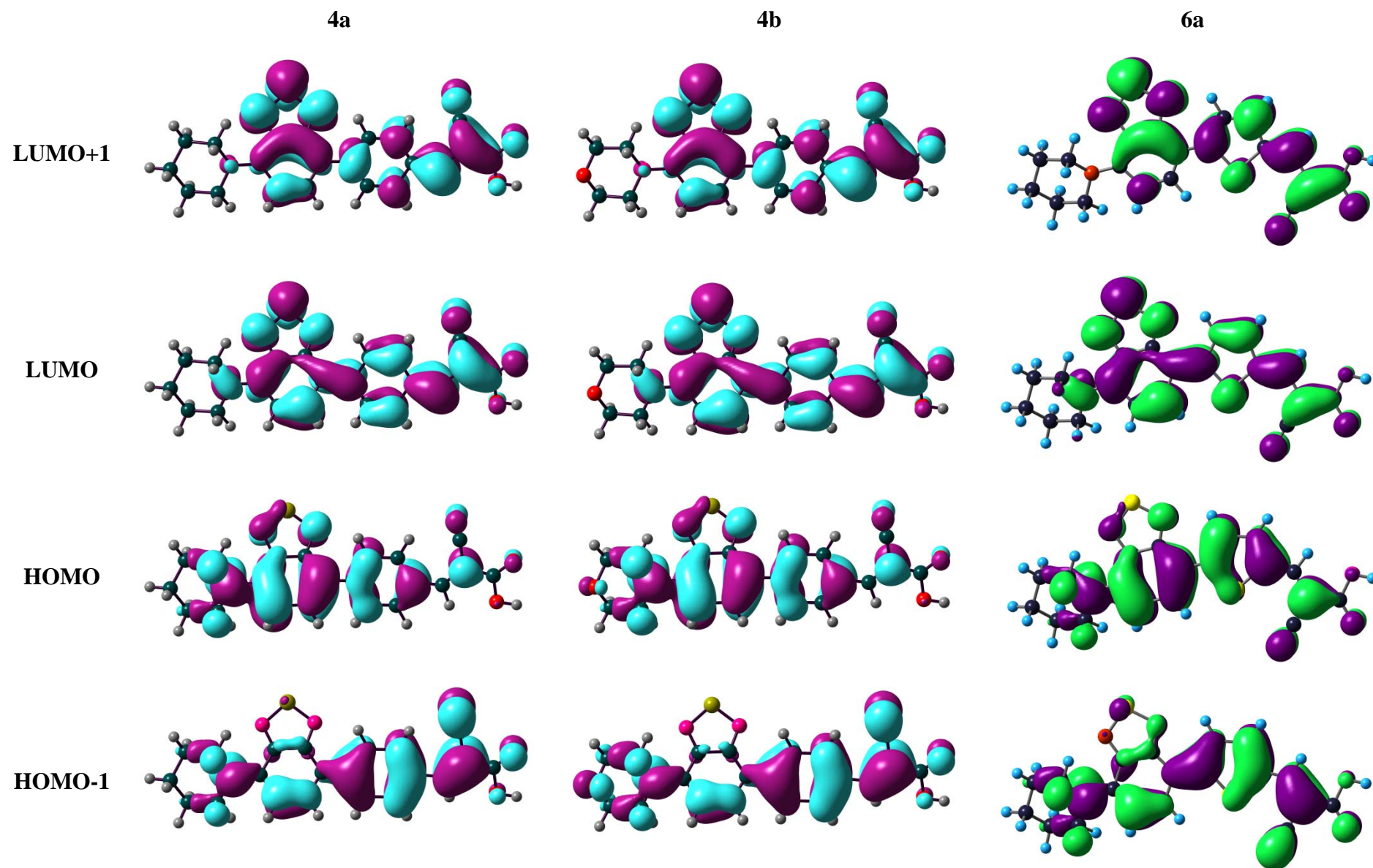


Figure 3.18 Isodensity surface plots of dyes 4a, 4b and 6a

Amine Directly Attached Benzothiadiazole Sensitizers

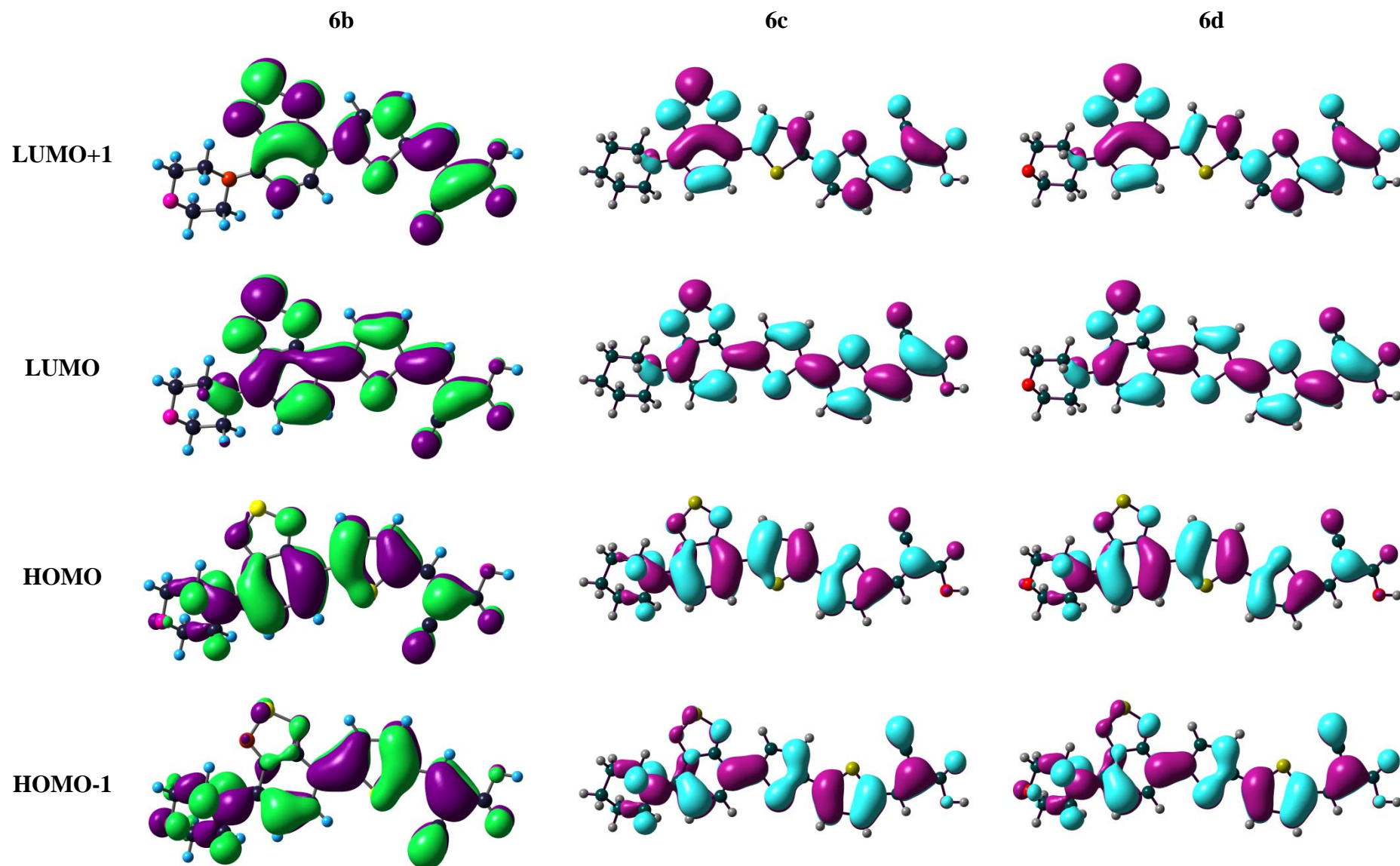


Figure 3.19 Isodensity surface plots of dyes 6b, 6c and 6d

Amine Directly Attached Benzothiadiazole Sensitizers

The contribution of cyanoacetic acid to the LUMO is expected to make certain that there is an effective electronic coupling between the TiO₂ conduction band and dye excited state. The electronic transitions from the HOMO/HOMO-1 to LUMO/LUMO+1 may generate effective photon-to-electron conversion. From the electronic distributions in the frontier molecular orbitals of the dyes, the longer wavelength electronic excitation for the dyes is predicted to contain charge transfer transition with contribution from the π - π^* transition character. Also the absorption wavelength increases with π -linker electron richness and length, in agreement with experimental absorption spectra. However, the computed wavelengths by B3LYP are overestimated, and the overestimation is more pronounced for the longer dyes. This mismatch is attributed to the incorrect asymptotic behavior of B3LYP functional for systems containing intramolecular charge transfer and error increases with the distance between donor and acceptor [41].

We presume that the composition of the transitions predicted by the MPKW1K is more reliable and the vertical excitations calculated by MPW1K show close resemblance to the experimentally observed values in tetrahydrofuran. The lower energy absorption predicted is originating from the HOMO/LUMO and HOMO/LUMO+1 transitions for these dyes. This clearly suggests that the longer wavelength absorption present in the dyes is due to the charge transfer transition with contribution from the π - π^* transition as well. As the HOMO is located all over molecule, these two electronic transitions HOMO \rightarrow LUMO and HOMO \rightarrow LUMO+1 expected to contribute positively to the electron injection, since both the transitions lead to the electron injection from the whole molecule to the acceptor cyanoacrylic group. The overlapping distribution of the HOMO and LUMO orbitals on the benzothiadiazole segment implies that this unit could facilitate the electron transfer to the anchoring/acceptor group from the donor.

It is worth noting that the dihedral angle between the benzothiadiazole and neighbored spacer units in the sensitizers correlate well with the photophysical properties. Figure 3.20 shows the ground-state geometries of the dyes with dihedral angles between two neighboring conjugated segments indicated. The dihedral angles between benzothiadiazole and phenyl (Ph) planes in **5a** and **5b** are as large as 33.37°-33.68° and possesses a twisted non-planar structures. This interrupted the conjugation system resulted to blue shift in the absorption maxima, which is consistent with the experimental observation in the absorption spectra of the sensitizers in comparison to those for thiophene and bithiophene sensitizers. Alternatively, the relative small torsion angle between benzothiadiazole-thiophene (3.62°-4.07°) and benzothiadiazole-

Amine Directly Attached Benzothiadiazole Sensitizers

bithiophene (2.69° - 1.12°) bridges ensures a good molecular coplanarity to facilitate good electronic communication with respect to phenylene-bridged and results in the above-mentioned larger red-shift in absorption band by 60-62 nm in solution.

In all the dyes, the cyanoacrylic acid moiety is found to be coplanar with the adjacent π -spacer unit (phenyl/thiophene/bithiophene), indicating a facile extension of conjugation between the π -linker and cyanoacrylic acid groups. This suggests that π -electrons can delocalise effectively from the donor moiety to acceptor unit, which can subsequently transfer to the conduction band of TiO_2 . From molecular modelling results, we can conclude that in the amine directly integrated with BTD sensitizers, phenyl π -linker between BTD and cyanoacrylic acid looks not beneficial and a thienyl or oligothieryl π -linker seems to be beneficial for charge transfer as it tends to assume planar arrangement which can guarantee a good electronic conjugation and light harvesting response.

Figure 3.20 Calculated inter-planar angles ($^\circ$) between various aromatic segments and cyanoacrylic acid plane in the optimized geometries of the dyes

3.2.6 Photovoltaic performance

The dye-sensitized solar cells were constructed by using the selected dyes **6a** and **6b** as the sensitizer for nanocrystalline anatase TiO₂. Typical solar cells, with an effective area of 0.25 cm², were fabricated with an electrolyte composed of 0.05 M I₂/0.5 M LiI/0.5 M tertbutylpyridine in acetonitrile solution. The device performance statistics was done under AM 1.5 illumination solar irradiation. The I-V curve and the IPCE spectra of the DSCs sensitized by the dyes **6a** and **6b** are shown in Figure 3.21 (a) and (b). The detailed photovoltaic parameters are summarized in Table 3.7. The dye **6b** exhibits maximum IPCE (>70%) between 400 and 550 nm with broader IPCE spectra which extends to 700 nm. The DSSCs sensitized by the dyes **6a** and **6b** obtained the η values 1.68% ($J_{SC} = 7.54 \text{ mA cm}^{-2}$, $V_{OC} = 359 \text{ mV}$, $ff = 0.62$) and 3.07% ($J_{SC} = 12.40 \text{ mA cm}^{-2}$, $V_{OC} = 396 \text{ mV}$, $ff = 0.63$) respectively. Electrochemical impedance spectroscopy (EIS) analysis was performed to study the interfacial charge transfer processes in DSSC sensitized by these dyes. The Nyquist plot displayed in Figure 3.21 (c) shows two semicircles which correspond to the charge-transfer resistances at the counter electrode and TiO₂/dye/electrolyte interface, respectively.

Table 3.7 Photovoltaic-performance parameters of the dyes

Dyes	η (%)	V_{OC} (mV)	J_{SC} (mA cm ⁻²)	ff	R_{ct2} (ohm)	f_{max} (Hz)	τ_e (ms)	R_{rec} (ohm)
6a	1.68	359	7.54	0.62	18.17	205.11	0.78	4.34
6b	3.07	396	12.40	0.63	16.33	92.68	1.72	4.73
D149	6.03	510	20.20	0.59	12.17	8.55	18.6	13.55
N719	7.69	556	21.90	0.63	9.83	7.01	22.69	8.94

For the dye **6a**, the radius of the bigger semicircle is significantly larger than the other dye **6b**. The dye morpholine derivative **6b** is exhibiting comparatively higher device efficiency than the piperidine derivative **6a**. This may probably stem from the higher molar extinction coefficient of the morpholine derivative, which can generate more excited electrons under the same wavelength light irradiation than the piperidine-based dye. The charge-transfer resistance assumes the order of **6b** < **6a**. The V_{OC} for the devices increases in the order of **6a** < **6b**, which was in good agreement with the trend of the cell performance. The electron lifetime can be extracted from the angular frequency (ω_{min}) at the mid frequency peak in the Bode phase plot (Figure 3.21 d) using $\tau_e = 1/\omega_{min}$. The electron lifetime measured for the dyes **6a** and **6b** are 0.78, 1.72 ms respectively, and follows the trend **6a** < **6b**.

Amine Directly Attached Benzothiadiazole Sensitizers

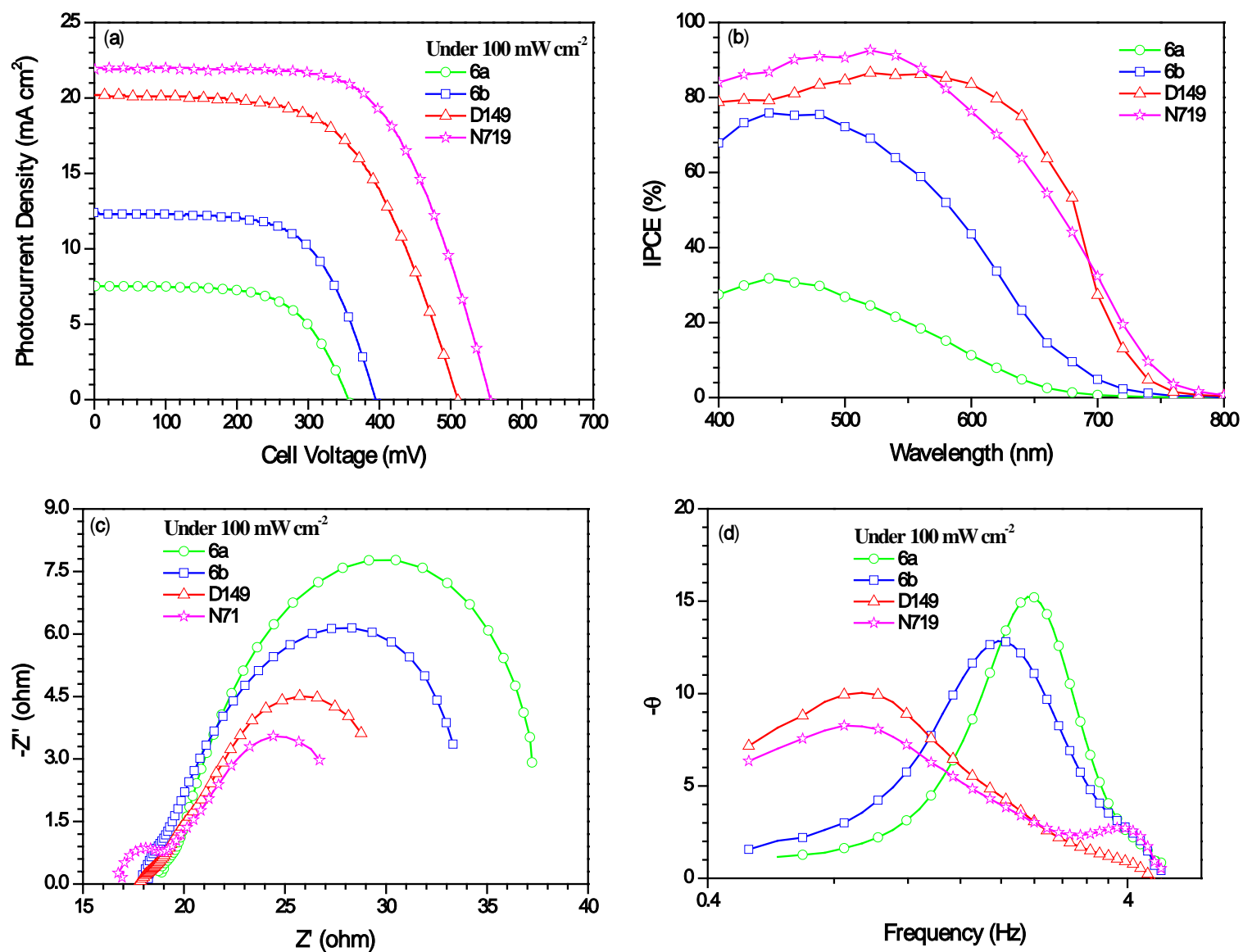


Figure 3.21 (a) I-V and (b) IPCE (c) Nyquist and (d) Bode phase plots for the devices measured under 100 mW cm⁻² illumination.

The increased electron lifetime reduces of the chance of back reaction of the injected electrons with the I^{3-} in the electrolyte by alternation of HOMO of the sensitizer, which leads to the improvement in the photocurrent, photovoltage and device efficiency. Since the electron lifetime was found higher for the dye **6b**, it displayed the higher V_{OC} and device efficiency

3.3 Conclusions

In summary, six new metal-free organic dyes containing piperidine/morpholine donor, benzothiadiazole and phenyl/thiophene/bithiophene units as a conjugated spacer are prepared and their optical, electrochemical properties and theoretical studies as well as photovoltaic performance of some of the dyes were studied. These dyes have low band gap benzothiadiazole as an auxiliary acceptor, cyanoacrylic acid units as the acceptors. All these new sensitizers displaying excellent light absorbing properties and the absorption profile of the dyes are red shifted and broader as compared to their corresponding bromo and aldehydes due to the extension of conjugation and origin of charge transfer transition from amine donor to cyanoacrylic acid acceptor. A blue shift in the absorption profile of the dyes observed by the protonation of amine unit by addition of TFA and deprotonation of carboxylic acid moiety by addition of TEA. Time-dependent density functional theoretical calculations were unravelled the nature of the electronic excitations induced by the absorption of light. The low energy absorption peaks observed for the dyes were attributed to π - π^* transition with a contribution from the charge transfer transition which becomes prominent for the bithiophene bridged derivatives. The torsion angles (θ) between the benzothiadiazole moiety and phenyl spacer **4a** and **4b** were more twisted than that of the thiophene and bithiophene spacers, precluding efficient intermolecular charge transfer. The best photovoltaic performance was achieved by the morpholine based dye **6b**, resulting in an efficiency of 3.07% with $J_{SC} = 12.40 \text{ mA cm}^{-2}$, $V_{OC} = 0.396 \text{ V}$, $ff = 0.63$. The dyes introduced in this work may function as efficient co-adsorbents, due to small molecular size for high efficiency solar cells and especially the dyes **6c** and **6d** can be used in co-sensitization in combination with the dyes containing complementary absorption. The strategy presented here for the construction of amine directly attached benzothiadiazole dyes could be extended to design the new dyes with infrared absorption for more efficient DSSC. Further structural modification of these dyes with arylamines is anticipated to improve the light absorption in the near-IR ranges for higher DSSCs performance.

3.4 Experimental section

3.4.1 Materials and physical methods

All commercial chemicals were used as received. Most of the chemicals were purchased from Sigma Aldrich. Column chromatography was performed by using silica gel (Rankem, 100-200 mesh) as stationary phase. All solvents used in synthesis and spectroscopic measurements were distilled over appropriate drying and/or degassing reagents. ^1H and ^{13}C NMR spectra were recorded on Bruker AV500 O FT-NMR spectrometer operating at 500 and 125 MHz respectively in CDCl_3 (chemical shifts (δ) in ppm and coupling constants (J) in Hz). Me_4Si (0.00 ppm) served as internal standard. The ^1H and ^{13}C spectra were referenced to the solvent signals: $[\text{D}_1]$ chloroform at ^1H NMR, $\delta = 7.26$ ppm; ^{13}C NMR $\delta = 77.00$ ppm and $[\text{D}_6]$ DMSO (^1H NMR, $\delta = 2.5$ ppm; ^{13}C NMR $\delta = 40.45$ ppm). All chromatographic separations were carried out on silica gel (100–200 mesh). The IR spectra were recorded on THERMO NICOLET NEXUS FT-IR spectrometer. The electronic absorption spectra were obtained with UV-1800 Shimadzu UV spectrophotometer. Emission spectra were recorded with Shimadzu RF-5301PC spectrofluorimeter. Cyclic voltammetry (CV) was performed on CHI 620C electrochemical analyzer with a three-electrode cell in a solution of 0.1 M tetrabutylammonium perchlorate in tetrahydrofuran as the supporting electrolyte, with an Ag/AgNO_3 reference electrode, a platinum wire as the counter electrode, and a glassy carbon electrode as the working electrode. The $E_{1/2}$ values were determined as $(E_p^a + E_p^c)/2$, where E_p^a and E_p^c are the anodic and cathodic peak potentials, respectively. The potential are quoted against ferrocene internal standard, tetrahydrofuran was the solvent in all the experiments. The HOMO energy levels of the dyes were measured from the oxidation potentials, as obtained by cyclic voltammetry. The DSSCs fabrication and characterisation was done by the literature reported procedure.¹³

3.4.2 Computational details

All the computations were performed with the Gaussian 09 program package. The ground-state geometries were fully optimized without any symmetry constrains at the DFT level with Becke's three parameters hybrid functional and Lee, Yang and Parr's correlational functional using 6-31G(d,p) basis set on all atoms. Vibrational analysis on the optimized structures was performed to confirm the structure. The time-dependent DFT (TD-DFT) at the level of B3LYP or MPW1K/6-31G(d,p) was further carried out to determine at least 10 vertical excitations to the excited state of the molecules. Solvation effects were modeled using the polarizable continuum

model (PCM) implemented in the Gaussian program, for both geometry optimizations and TD-DFT calculations.

3.4.3 Synthesis

Synthesis of 4-bromo-7-morpholinobenzo[*c*][1,2,5]thiadiazole (2b): The reaction was carried under nitrogen atmosphere. 4,7-dibromobenzo[*c*][1,2,5]thiadiazole **4** (2.05 g, 7.0 mmol), morpholine (5 mL) were refluxed for 10 h and the reaction mixture was cooled to room temperature. The reaction mixture was poured in cold water and extracted with dichloromethane. The compound was purified by column chromatography on silica gel using hexane/dichloromethane mixture as eluant. Orange solid; Yield = 55%; m.p. 110-112 °C; IR (KBr, cm⁻¹): δ 2955, 1483, 1234, 1118; ¹H NMR (CDCl₃, 500.13 MHz): δ 3.50 (t, *J* = 5.0 Hz, 2H), 3.95 (t, *J* = 5.0 Hz, 2H), 6.58 (d, *J* = 8.0 Hz, 1H), 7.65 (d, *J* = 8.0 Hz, 1H); ¹³C NMR (CDCl₃, 125.75 MHz): δ 50.3, 66.8, 104.5, 111.9, 132.8, 143.6, 149.0, 154.5; HRMS (ESI) *m/z* calcd for C₁₀H₁₁BrN₃O_s (M+H) 299.9806, found 299.9805.

Synthesis of 4-(7-(piperidin-1-yl)benzo[*c*][1,2,5]thiadiazol-4-yl)benzaldehyde (3a): 4-bromo-7-(piperidin-1-yl)benzo[*c*][1,2,5]thiadiazole **2a** (2.1 g, 7 mmol), 4-formylphenylboronic acid (1.2 g, 8 mmol) were dissolved under nitrogen in dry THF (30 mL) and the solution was degassed. Now Pd(PPh₃)₄ (210 mg) was added, and the solution was degassed again. An aqueous solution of K₂CO₃ (2.9 g, 21 mmol) in 10 mL was added to the reaction mixture. This reaction mixture was kept on heating at 80 °C for 24 h under a nitrogen atmosphere. The reaction mixture was poured into a saturated NH₄Cl solution (100 mL) and extracted with DCM (3 × 25 mL). The combined organic phases were dried over Na₂SO₄ and the solvent was removed in vacuo. The resulting red solid was purified by column chromatography using hexanes/DCM. Red solid; m.p. 88-90 °C; IR (KBr, cm⁻¹): 2360, 1696, 1542, 1376, 1220; ¹H NMR (CDCl₃, 500.13 MHz): δ 1.71-1.75 (m, 2H), 1.86-1.88 (m, 4H), 3.61 (t, *J* = 5.5 Hz, 4H), 6.84 (d, *J* = 8.0 Hz, 1H), 7.69 (d, *J* = 8.0 Hz, 1H), 7.99 (d, *J* = 8.0 Hz, 2H), 8.11 (d, *J* = 8.0 Hz, 2H), 10.07 (s, 1H); ¹³C NMR (CDCl₃, 125.77 MHz): δ 24.6, 25.9, 51.4, 111.2, 123.4, 129.9, 129.9, 130.3, 134.9, 144.1, 145.3, 150.0, 154.7, 191.9. HRMS (ESI) *m/z* calcd for C₁₈H₁₈N₃O_s (M+H) 324.1170, found 324.1185.

Synthesis of 4-(7-morpholinobenzo[*c*][1,2,5]thiadiazol-4-yl)benzaldehyde (3b):

This was synthesized by a procedure similar to that of **3a** except that 4-(7-bromobenzo[*c*][1,2,5]thiadiazol-4-yl)morpholine **2b** was used in place of 4-bromo-7-(piperidin-

Amine Directly Attached Benzothiadiazole Sensitizers

1-yl)benzo[c][1,2,5]thiadiazole **2a**. Yellow solid; m.p. 170-172 °C; IR (KBr, cm^{-1}): 2357, 1691, 1621, 1552, 1220, 1114, 1017; ^1H NMR (CDCl_3 , 500.13 MHz): δ 3.65 (t, $J = 5.0$ Hz, 4H), 4.08 (t, $J = 5.0$ Hz, 4H), 6.86 (d, $J = 8.0$ Hz, 1H), 7.71 (d, $J = 8.0$ Hz, 1H), 8.0 (d, $J = 8.0$ Hz, 2H), 8.12 (d, $J = 8.0$ Hz, 2H), 10.08 (s, 1H); ^{13}C NMR (CDCl_3 , 125.77 MHz): δ 50.3, 66.9, 111.2, 124.7, 129.3, 129.9, 130.0, 135.2, 143.8, 144.2, 149.7, 154.7, 191.9; HRMS (ESI) m/z calcd for $\text{C}_{17}\text{H}_{16}\text{N}_3\text{O}_2\text{S}$ (M+H) 326.0963, found 326.0960

Synthesis of 5-(7-(piperidin-1-yl)benzo[c][1,2,5]thiadiazol-4-yl)thiophene-2-carbaldehyde (**5a**):

A round bottom flask was charged with **2a** (298.2 mg, 1 mmol), 2-tributylstannyl-5-dioxolanyl thiophene (1.1 mmol) and 2 ml DMF. Nitrogen was purged into this, followed by the addition of $\text{Pd}(\text{PPh}_3)_2\text{Cl}_2$ (7.0 mg). This was kept on heating at 80 °C for 16 h under a nitrogen atmosphere. After completion of time the reaction mixture was poured into cold water and extracted with dichloromethane and washed with brine solution. This was dried over anhydrous sodium sulfate. Then the solvent was evaporated by applying vacuum. The resultant liquid was dissolved in 5 ml acetic acid and heated to 60 °C for 30 min. Then 10 ml of water was added to it and heating was continued for 6 h. The resulting solution was extracted with dichloromethane and washed with brine solution and dried over anhydrous sodium sulfate. Further purification was performed by silica gel column chromatography using hexanes/chloroform. Black solid; Yield = 61%; m.p. 135-137 °C; IR (KBr, cm^{-1}): 2921, 1654, 1545, 1441; ^1H NMR (CDCl_3 , 500.13 MHz): δ 1.70-1.75 (m, 2H), 1.82-1.86 (m, 4H), 3.62 (t, $J = 5.5$ Hz, 4H), 6.74 (d, $J = 8.5$ Hz, 1H), 7.78 (d, $J = 4$ Hz, 1H), 7.83 (d, $J = 8$ Hz, 1H), 8.04 (d, $J = 4$ Hz, 1H), 9.91 (s, 1H); ^{13}C NMR (CDCl_3 , 125.77 MHz): δ 24.5, 25.9, 51.2, 110.4, 116.6, 125.7, 129.4, 137.3, 141.4, 145.5, 149.4, 150.5, 153.7, 182.8; HRMS (ESI) m/z calculated for $\text{C}_{16}\text{H}_{16}\text{N}_3\text{OS}_2$ (M+H), 330.0735 found 330.0690

Synthesis of 5-(7-morpholinobenzo[c][1,2,5]thiadiazol-4-yl)thiophene-2-carbaldehyde (**5b**):

This was synthesized by a procedure similar to that of **5a** except that 4-(7-bromobenzo[c][1,2,5]thiadiazol-4-yl)morpholine **2b** was used in place of 4-bromo-7-(piperidin-1-yl)benzo[c][1,2,5]thiadiazole **2a**. Red solid; Yield = 60%; m.p. 190-192 °C; IR (KBr, cm^{-1}): 2927, 1663, 1548, 1446; ^1H NMR (CDCl_3 , 500.13 MHz): δ 3.68 (t, $J = 5.0$ Hz, 4H), 3.95 (t, $J = 4.5$ Hz, 4H), 6.78 (d, $J = 8.0$ Hz, 1H), 7.79 (d, $J = 4.0$ Hz, 1H), 7.89 (d, $J = 8.0$ Hz, 1H), 8.07 (d, $J = 4.0$ Hz, 1H), 9.93 (s, 1H); ^{13}C NMR (CDCl_3 , 125.77 MHz): δ 50.1, 66.8, 110.7, 118.0, 126.0, 129.0, 137.2, 141.9, 144.5, 149.2, 153.6, 182.9. MALDI-TOF MS m/z : calculated for, $\text{C}_{15}\text{H}_{14}\text{N}_3\text{O}_2\text{S}_2$ (M+H), 332.0527 found 332.0673.

Synthesis of 5'-(7-(piperidin-1-yl)benzo[*c*][1,2,5]thiadiazol-4-yl)-2,2'-bithiophene-5-carbaldehyde (5c):

This was synthesized by a procedure similar to that of **5a** except that (5'-(1,3-dioxolan-2-yl)-2,2'-bithiophen-5-yl)tributylstannane was used in place of 2-tributylstannyl-5-dioxolanyl thiophene **2a**. Black solid; Yield = 75%; m.p. 180-182 °C; IR (KBr, cm⁻¹): 2921, 2808, 2352, 1657, 1580, 1444, 1390, 1228; ¹H NMR (CDCl₃, 500.13 MHz): δ 1.70-1.725 (m, 2H), 1.83-1.88 (m, 4H), 3.59 (t, *J* = 5.0 Hz, 4H), 6.77 (d, *J* = 8.0 Hz, 1H), 7.31 (d, *J* = 4.0 Hz, 1H), 7.41 (d, *J* = 4.0 Hz, 1H), 7.69 (d, *J* = 4.0 Hz, 1H), 7.78 (d, *J* = 8.0 Hz, 1H), 7.86 (d, *J* = 4.0 Hz, 1H), 9.86 (s, 1H); ¹³C NMR (CDCl₃, 125.77 MHz): δ 24.5, 25.9, 51.4, 111.1, 117.7, 123.8, 126.0, 126.8, 127.7, 134.7, 137.5, 141.2, 142.2, 144.7, 147.6, 149.7, 153.5, 182.4. HRMS (ESI) *m/z* calculated for, C₂₀H₁₇N₃OS₃ (M⁺), 411.0534; found 411.0522.

Synthesis of 5'-(7-morpholinobenzo[*c*][1,2,5]thiadiazol-4-yl)-2,2'-bithiophene-5-carbaldehyde (5d):

This was synthesized by a procedure similar to that of **5b** except that (5'-(1,3-dioxolan-2-yl)-2,2'-bithiophen-5-yl)tributylstannane was used in place of 2-tributylstannyl-5-dioxolanyl thiophene. Dark red solid; Yield = 69%; m.p. 208-201 °C; IR (KBr, cm⁻¹): 2361, 1656, 1582, 1444, 1397; ¹H NMR (CDCl₃, 500.13 MHz): δ 3.62 (t, *J* = 5.0 HZ, 4H), 3.99 (t, *J* = 5.0 HZ, 4H), 6.77 (d, *J* = 8.0 HZ, 1H), 7.31 (d, *J* = 4.0 HZ, 1H), 7.40 (d, *J* = 4.0 HZ, 1H), 7.68 (d, *J* = 4.0 HZ, 1H), 7.78 (d, *J* = 8.0 HZ, 1H), 7.87 (d, *J* = 4.0 HZ, 1H), 9.86 (s, 1H); ¹³C NMR (CDCl₃, 125.77 MHz): δ 50.3, 66.8, 111.2, 118.9, 124.0, 126.8, 127.3, 135.2, 137.5, 141.4, 141.7, 143.5, 147.4, 149.4, 153.5, 182.4; MALDI-TOF MS *m/z*: calculated for, C₁₉H₁₅N₃O₂S₃ (M⁺), 413.0326; found 413.0308.

Synthesis of (E)-2-cyano-3-(4-(7-(piperidin-1-yl)benzo[*c*][1,2,5]thiadiazol-4-yl)phenyl)acrylic acid (4a):

4-(7-(piperidin-1-yl)benzo[*c*][1,2,5]thiadiazol-4-yl)benzaldehyde (0.30 g, 0.96 mmol) (**3a**), cyanoacetic acid (0.12 g, 1.44 mmol), glacial acetic acid (5 ml) and ammonium acetate (5 mg) were mixed together and kept on reflux at 120 °C for 12 h. The resulting orange solution was poured into ice-cold water to produce an orange precipitate. This was filtered and washed thoroughly with water and dried. The solid was further recrystallized with dichloromethane/hexanes. Red solid; Yield = 92%; m.p. 170-172 °C; IR (KBr, cm⁻¹): 2929, 2217, 1709, 1593, 1546, 1485, 1367, 1229; ¹H NMR (DMSO-*d*₆, 500.13 MHz): δ 1.62 (s, 2H), 1.70 (s, 4H), 3.47 (s, 4H), 6.86-6.88 (m, 1H), 7.50 (d, *J* = 7.0 Hz, 1H), 7.69-7.82 (m, 2H), 7.90-

Amine Directly Attached Benzothiadiazole Sensitizers

8.10 (m, 2H), 8.23 (s, 1H); ^{13}C NMR (DMSO- d_6 , 125.77 MHz): δ 24.2, 25.6, 50.8, 111.6, 123.4, 128.8, 129.1, 130.1, 141.3, 144.0, 144.5, 149.5, 154.2, 154.4, 166.6.

Synthesis of (*E*)-2-cyano-3-(4-(7-morpholinobenzo[*c*][1,2,5]thiadiazol-4-yl)phenyl)acrylic acid (**4b**):

This was synthesized by a procedure similar to that of **4a** except that 4-(7-morpholinobenzo[*c*][1,2,5]thiadiazol-4-yl)benzaldehyde (**3b**) was used in place of 4-(7-(piperidin-1-yl)benzo[*c*][1,2,5]thiadiazol-4-yl)benzaldehyde (**3a**). Orange solid; Yield = 89%; m.p. 202-204 °C; IR (KBr, cm^{-1}): 2358, 1702, 1590, 1546, 1485, 1438, 1258; ^1H NMR (DMSO- d_6 , 500.13 MHz): δ 3.60 (t, $J = 5.0$ Hz, 4H), 3.86 (t, $J = 5.0$ Hz, 4H), 6.96 (t, $J = 8.0$ Hz, 1H), 7.52 (t, $J = 9.0$ Hz, 1H), 7.91-7.95 (m, 2H), 8.13-8.18 (m, 2H), 8.34 (s, 1H); ^{13}C NMR (DMSO- d_6 , 125.77 MHz): δ 49.8, 66.1, 111.5, 124.2, 128.9, 129.4, 130.2, 141.6, 143.0, 143.7, 149.0, 154.0, 154.2, 166.1.

Synthesis of (*E*)-2-cyano-3-(5-(7-(piperidin-1-yl)benzo[*c*][1,2,5]thiadiazol-4-yl)thiophen-2-yl)acrylic acid (**6a**):

This was synthesized by a procedure similar to that of **4a** except that 5-(7-(piperidin-1-yl)benzo[*c*][1,2,5]thiadiazol-4-yl)thiophene-2-carbaldehyde **5a** was used in place of 4-(7-(piperidin-1-yl)benzo[*c*][1,2,5]thiadiazol-4-yl)benzaldehyde **3a**. Dark black solid; Yield = 84%; m.p. 150-152 °C; IR (KBr, cm^{-1}): 2928, 2210, 1680, 1535, 1384, 1234; ^1H NMR (DMSO- d_6 , 500.13 MHz, CDCl_3): δ 1.67-1.73 (m, 6H), 3.71 (m, 4H), 6.92 (d, $J = 8.0$ Hz, 1H), 7.95 (d, $J = 4.0$ Hz, 1H), 8.1 (d, $J = 4.0$ Hz, 1H), 8.1 (d, $J = 8.0$ Hz, 2H), 8.4 (s, 1H); ^{13}C NMR (DMSO- d_6 , 125 MHz): δ 24.0, 25.4, 50.3, 110.2, 114.7, 117.4, 125.0, 129.8, 134.2, 139.4, 139.4, 144.7, 145.4, 148.1, 148.8, 152.8, 164.0; HRMS (ESI) m/z calculated for $\text{C}_{19}\text{H}_{15}\text{N}_4\text{O}_2\text{S}_2$ (M-H), 395.0636 found 395.0536.

Synthesis of (*E*)-2-cyano-3-(5-(7-morpholinobenzo[*c*][1,2,5]thiadiazol-4-yl)thiophen-2-yl)acrylic acid (**6b**):

This was synthesized by a procedure similar to that of **4a** except that 5-(7-morpholinobenzo[*c*][1,2,5]thiadiazol-4-yl)thiophene-2-carbaldehyde **5b** was used in place of 4-(7-(piperidin-1-yl)benzo[*c*][1,2,5]thiadiazol-4-yl)benzaldehyde **3a**. Dark black solid; Yield = 79%; m.p. 270-272 °C; IR (KBr, cm^{-1}): 2917, 2221, 1684, 1572, 1425, 1240; ^1H NMR (DMSO- d_6 , 500.13 MHz): δ 3.69 (t, $J = 5.0$ Hz, 4H), 3.95 (t, $J = 4.5$ Hz, 4H), 6.94 (d, $J = 8.0$ Hz, 1H), 7.99 (d, $J = 4.0$ Hz, 1H), 8.07 (d, $J = 4.0$ Hz, 1H), 8.14 (d, $J = 8.0$ Hz, 1H), 8.43 (s, 1H); ^{13}C NMR (DMSO- d_6 , 125.77 MHz): δ 49.5, 65.9, 110.4, 115.7, 116.8, 125.4, 129.6, 134.4, 140.2,

Amine Directly Attached Benzothiadiazole Sensitizers

144.0, 146.4, 148.0, 149.1, 152.7, 163.9. MALDI-TOF MS m/z : calculated for, $C_{18}H_{14}N_4O_3S_2$ 398.0507; found 398.0267.

Synthesis of (*E*)-2-cyano-3-(5'-(7-(piperidin-1-yl)benzo[*c*][1,2,5]thiadiazol-4-yl)-2,2'-bithiophen-5-yl)acrylic acid (**6c**):

This was synthesized by a procedure similar to that of **4a** except that 5'-(7-(piperidin-1-yl)benzo[*c*][1,2,5]thiadiazol-4-yl)-2,2'-bithiophene-5-carbaldehyde **5c** was used in place of 4-(7-(piperidin-1-yl)benzo[*c*][1,2,5]thiadiazol-4-yl)benzaldehyde **3a**. Dark black solid; Yield = 79%; m.p. 250-252 °C; IR (KBr, cm^{-1}): 2928, 2849, 2378, 2204, 1715, 1627, 1577, 1403; 1H NMR (DMSO- d_6 , 500.13 MHz, $CDCl_3$): δ 1.65-66 (m, 2H), 1.73 (m, 4H), 3.63 (t, $J = 5.0$ Hz, 4H), 6.88 (d, $J = 8.0$ Hz, 1H), 7.61-7.62 (d, $J = 4.0$ Hz, 1H), 7.68 (d, $J = 4.0$ Hz, 1H), 7.95-7.97 (m, 1H), 8.04 (d, $J = 8.0$ Hz, 1H) 8.46 (s, 1H); ^{13}C NMR (DMSO- d_6 , 125.77 MHz): δ 24.1, 25.4, 50.5, 110.8, 115.8, 116.8, 124.4, 125.7, 127.5, 128.0, 133.5, 133.9, 141.5, 141.6, 143.9, 146.1, 146.2, 148.6, 152.7, 163.8; HRMS (ESI) m/z calculated for, $C_{23}H_{19}N_4O_2S_3$ 479.0670 [M+H]; found 479.0649.

Synthesis of (*E*)-2-cyano-3-(5'-(7-morpholinobenzo[*c*][1,2,5]thiadiazol-4-yl)-2,2'-bithiophen-5-yl)acrylic acid (**6d**):

This was synthesized by a procedure similar to that of **4a** except 5'-(7-morpholinobenzo[*c*][1,2,5]thiadiazol-4-yl)-2,2'-bithiophene-5-carbaldehyde **5c** was used in place of 4-(7-(piperidin-1-yl)benzo[*c*][1,2,5]thiadiazol-4-yl)benzaldehyde **3a**. Dark black solid; Yield = 76%; m.p. 262-264 °C; IR (KBr, cm^{-1}): 2919, 2854, 2210, 1709, 1622, 1578, 1433, 1390, 1344, 1197; 1H NMR (DMSO- d_6 , 500.13 MHz, $CDCl_3$): δ 3.57-3.58 (m, 4H), 3.83-3.84 (m, 4H), 6.85 (d, $J = 8.0$ Hz, 1H), 7.54 (d, $J = 3.5$ Hz, 1H), 7.61 (d, $J = 3.5$ Hz, 1H), 7.90 (d, $J = 4.0$ Hz, 1H), 7.99 (d, $J = 8.0$ Hz, 1H), 8.43(s, 1H); ^{13}C NMR (DMSO- d_6 , 125.77 MHz): δ 49.7, 66.1, 111.1, 116.9, 124.5, 126.1, 127.5, 127.8, 134.3, 141.4, 141.6, 143.2, 146.1, 148.4, 152.6; HRMS (ESI) m/z calculated for, $C_{22}H_{17}N_4O_3S_3$ 481.0463 [M+H]; found 481.0449

Synthesis of 4-(piperidin-1-yl)-7-(thiophen-2-yl)benzo[*c*][1,2,5]thiadiazole (**7a**):

A round bottom flask was charged with 4-bromo-7-(piperidin-1-yl)benzo[*c*][1,2,5]thiadiazole **2a** (298.2 mg, 1 mmol), (thiophen-2-yl)stannane (1.1 mmol) and 2 ml DMF. Nitrogen was purged into this, followed by the addition of $Pd(PPh_3)_2Cl_2$ (7.0 mg). This was kept on heating at 80 °C for 16 h under a nitrogen atmosphere. After completion of time the reaction mixture was poured into cold water and extracted with dichloromethane and washed with brine solution. This was dried over anhydrous sodium sulfate. Further purification was performed by silica gel

column chromatography using hexane/chloroform. Red solid; Yield = 74%; m.p. 58-60 °C; IR (KBr, cm^{-1}): 2925, 2846, 2372, 1636, 1579, 1394, 1262, 1124; ^1H NMR (CDCl_3 , 500.13 MHz): δ 1.69-1.70 (m, 2H), 1.85 (m, 4H), 3.51(m, 4H), 6.73 (d, $J = 7.5$ Hz, 1H), 7.15 (s, 1H), 7.33 (d, $J = 5.0$ Hz, 1H), 7.71 (d, $J = 7.5$ Hz, 1H), 7.93 (s, 1H); ^{13}C NMR (CDCl_3 , 125.77 MHz): δ 24.6, 26.0, 51.6, 111.6, 119.2, 124.7, 125.5, 127.5, 127.7, 140.2, 144.2, 150.0, 153.8.

Synthesis of 4-(7-(thiophen-2-yl)benzo[*c*][1,2,5]thiadiazol-4-yl)morpholine (7b):

This was synthesized by a procedure similar to that of **7a** except that 4-(7-bromobenzo[*c*][1,2,5]thiadiazol-4-yl)morpholine **2b** was used in place of 4-bromo-7-(piperidin-1-yl)benzo[*c*][1,2,5]thiadiazole **2a**. Orange solid; Yield = 74%; m.p. 116-118 °C; IR (KBr, cm^{-1}): 2966, 2849, 2372, 2339, 1636, 1581, 1548, 1477, 1381, 1262; ^1H NMR (CDCl_3 , 500.13 MHz): δ 3.58 (d, $J = 4.5$ Hz, 4H), 4.01, (d, $J = 4.5$ Hz, 4H), 6.79 (d, $J = 8.0$ Hz, 1H), 7.17(t, $J = 4.0$ Hz, 1H), 7.36 (d, $J = 5.0$ Hz, 1H), 7.75 (d, $J = 7.5$ Hz, 1H), 7.95 (d, $J = 3.5$ Hz, 1H); ^{13}C NMR (CDCl_3 , 125.77 MHz): δ 50.5, 66.9, 111.7, 120.3, 125.2, 125.9, 127.1, 127.8, 139.8, 142.9, 149.7, 153.8.

3.5 References

- (1) H. S. Jung and J.-K. Lee, Dye Sensitized Solar Cells for Economically Viable Photovoltaic Systems. *The Journal of Physical Chemistry Letters* **2013**, *4*, 1682-93.
- (2) J. H. Heo, S. H. Im, J. H. Noh, T. N. Mandal, C.-S. Lim, J. A. Chang, Y. H. Lee, H.-j. Kim, A. Sarkar, K. NazeeruddinMd, M. Gratzel and S. I. Seok, Efficient inorganic-organic hybrid heterojunction solar cells containing perovskite compound and polymeric hole conductors. *Nat Photon* **2013**, *7*, 486-91.
- (3) T. Kinoshita, J. T. Dy, S. Uchida, T. Kubo and H. Segawa, Wideband dye-sensitized solar cells employing a phosphine-coordinated ruthenium sensitizer. *Nat Photon* **2013**, *7*, 535-9.
- (4) A. Yella, H.-W. Lee, H. N. Tsao, C. Yi, A. K. Chandiran, M. K. Nazeeruddin, E. W.-G. Diau, C.-Y. Yeh, S. M. Zakeeruddin and M. Grätzel, Porphyrin-Sensitized Solar Cells with Cobalt (II/III)-Based Redox Electrolyte Exceed 12 Percent Efficiency. *Science* **2011**, *334*, 629-34.
- (5) S. Haid, M. Marszalek, A. Mishra, M. Wielopolski, J. Teuscher, J.-E. Moser, R. Humphry-Baker, S. M. Zakeeruddin, M. Grätzel and P. Bäuerle, Significant Improvement of Dye-Sensitized Solar Cell Performance by Small Structural Modification in π -

Amine Directly Attached Benzothiadiazole Sensitizers

Conjugated Donor–Acceptor Dyes. *Adv. Funct. Mater.* **2012**, *22*, 1291-302.

- (6) A. Mishra, M. K. R. Fischer and P. Bäuerle, Metal-Free Organic Dyes for Dye-Sensitized Solar Cells: From Structure: Property Relationships to Design Rules. *Angew. Chem. Int. Ed.* **2009**, *48*, 2474-99.
- (7) P. Singh, A. Baheti, K. R. J. Thomas, C.-P. Lee and K.-C. Ho, Fluorene-based organic dyes containing acetylene linkage for dye-sensitized solar cells. *Dyes Pigm.* **2012**, *95*, 523-33.
- (8) A. Baheti, C. P. Lee, K. R. J. Thomas and K. C. Ho, Pyrene-based organic dyes with thiophene containing pi-linkers for dye-sensitized solar cells: optical, electrochemical and theoretical investigations. *Phys. Chem. Chem. Phys.* **2011**, *13*, 17210-21.
- (9) S. Tatay, S. A. Haque, B. O'Regan, J. R. Durrant, W. J. H. Verhees, J. M. Kroon, A. Vidal-Ferran, P. Gavina and E. Palomares, Kinetic competition in liquid electrolyte and solid-state cyanine dye sensitized solar cells. *J. Mater. Chem.* **2007**, *17*, 3037-44.
- (10) R. F. Fink, J. Seibt, V. Engel, M. Renz, M. Kaupp, S. Lochbrunner, H.-M. Zhao, J. Pfister, F. Würthner and B. Engels, Exciton Trapping in π -Conjugated Materials: A Quantum-Chemistry-Based Protocol Applied to Perylene Bisimide Dye Aggregates. *J. Am. Chem. Soc.* **2008**, *130*, 12858-59.
- (11) T. Sudyoasuk, S. Pansay, S. Morada, R. Rattanawan, S. Namuangruk, T. Kaewin, S. Jungsuttiwong and V. Promarak, Synthesis and Characterization of D-D- π -A-Type Organic Dyes Bearing Carbazole-Carbazole as a Donor Moiety (D-D) for Efficient Dye-Sensitized Solar Cells. *Eur. J. Org. Chem.* **2013**, *2013*, 5051-63.
- (12) K. R. J. Thomas, N. Kapoor, C. P. Lee and K. C. Ho, Organic dyes containing pyrenylamine-based cascade donor systems with different aromatic pi linkers for dye-sensitized solar cells: optical, electrochemical, and device characteristics. *Chem Asian J.* **2012**, *7*, 738-50.
- (13) A. Baheti, P. Singh, C. P. Lee, K. R. J. Thomas and K. C. Ho, 2,7-Diaminofluorene-based organic dyes for dye-sensitized solar cells: effect of auxiliary donor on optical and electrochemical properties. *J. Org. Chem.* **2011**, *76*, 4910-20.
- (14) L.-Y. Lin, C.-H. Tsai, F. Lin, T.-W. Huang, S.-H. Chou, C.-C. Wu and K.-T. Wong, 2,1,3-Benzothiadiazole-containing donor–acceptor–acceptor dyes for dye-sensitized solar cells. *Tetrahedron* **2012**, *68*, 7509-16.

- (15) Y. Wu and W. Zhu, Organic sensitizers from D- $[\pi]$ -A to D-A- $[\pi]$ -A: effect of the internal electron-withdrawing units on molecular absorption, energy levels and photovoltaic performances. *Chem. Soc. Rev.* **2013**, *42*, 2039-58.
- (16) X. Lu, G. Zhou, H. Wang, Q. Feng and Z. S. Wang, Near infrared thieno[3,4-*b*]pyrazine sensitizers for efficient quasi-solid-state dye-sensitized solar cells. *Phys. Chem. Chem. Phys.* **2012**, *14*, 4802-9.
- (17) X. Wang, J. Yang, H. Yu, F. Li, L. Fan, W. Sun, Y. Liu, Z. Y. Koh, J. Pan, W.-L. Yim, L. Yan and Q. Wang, A benzothiazole-cyclopentadithiophene bridged D-A- $[\pi]$ -A sensitizer with enhanced light absorption for high efficiency dye-sensitized solar cells. *Chem. Commun.* **2014**, *50*, 3965-68.
- (18) Q. Feng, X. Jia, G. Zhou and Z.-S. Wang, Embedding an electron donor or acceptor into naphtho[2,1-*b*:3,4-*b'*]dithiophene based organic sensitizers for dye-sensitized solar cells. *Chem. Commun.* **2013**, *49*, 7445-7.
- (19) W. Zhu, Y. Wu, S. Wang, W. Li, X. Li, J. Chen, Z.-s. Wang and H. Tian, Organic D-A- π -A Solar Cell Sensitizers with Improved Stability and Spectral Response. *Adv. Funct. Mater.* **2011**, *21*, 756-63.
- (20) Y. Wu, M. Marszalek, S. M. Zakeeruddin, Q. Zhang, H. Tian, M. Grätzel and W. Zhu, High-conversion-efficiency organic dye-sensitized solar cells: molecular engineering on D-A- π -A featured organic indoline dyes. *Energy & Environmental Science* **2012**, *5*, 8261-72.
- (21) T. Suzuki, T. Tsuji, T. Okubo, A. Okada, Y. Obana, T. Fukushima, T. Miyashi and Y. Yamashita, Preparation, Structure, and Amphoteric Redox Properties of p-Phenylenediamine-Type Dyes Fused with a Chalcogenadiazole Unit. *J. Org. Chem.* **2001**, *66*, 8954-60.
- (22) W. Lee, J. y. Seng and J.-I. Hong, Metal-free organic dyes with benzothiadiazole as an internal acceptor for dye-sensitized solar cells. *Tetrahedron* **2013**, *69*, 9175-82.
- (23) Z. M. Tang, T. Lei, K. J. Jiang, Y. L. Song and J. Pei, Benzothiadiazole containing D- π -A conjugated compounds for dye-sensitized solar cells: synthesis, properties, and photovoltaic performances. *Chem Asian J.* **2010**, *5*, 1911-17.
- (24) R. Y. Lin, C. P. Lee, Y. C. Chen, J. D. Peng, T. C. Chu, H. H. Chou, H. M. Yang, J. T. Lin and K. C. Ho, Benzothiadiazole-containing donor-acceptor-acceptor type organic

Amine Directly Attached Benzothiadiazole Sensitizers

- sensitizers for solar cells with ZnO photoanodes. *Chem Commun* **2012**, 48, 12071-73.
- (25) J.-J. Kim, H. Choi, J.-W. Lee, M.-S. Kang, K. Song, S. O. Kang and J. Ko, A polymer gel electrolyte to achieve 6% power conversion efficiency with a novel organic dye incorporating a low-band-gap chromophore. *J. Mater. Chem.* **2008**, 18, 5223-29.
- (26) K. R. J. Thomas, P. Singh, A. Baheti, Y.-C. Hsu, K.-C. Ho and J. T. s. Lin, Electro-optical properties of new anthracene based organic dyes for dye-sensitized solar cells. *Dyes Pigm.* **2011**, 91, 33-43.
- (27) M. Velusamy, K. R. J. Thomas, J. T. Lin, Y.-C. Hsu and K.-C. Ho, Organic Dyes Incorporating Low-Band-Gap Chromophores for Dye-Sensitized Solar Cells. *Org. Lett.* **2005**, 7, 1899-902.
- (28) K. Pilgram, M. Zupan and R. Skiles, Bromination of 2,1,3-benzothiadiazoles. *J. Heterocycl. Chem.* **1970**, 7, 629-33.
- (29) S. Chen, Y. Li, W. Yang, N. Chen, H. Liu and Y. Li, Synthesis and Tuning Optical Nonlinear Properties of Molecular Crystals of Benzothiadiazole. *J. Phys. Chem. C* **2010**, 114, 15109-15.
- (30) P. Singh, A. Baheti and K. R. J. Thomas, Synthesis and optical properties of acidochromic amine-substituted benzo[*a*]phenazines. *J. Org. Chem.* **2011**, 76, 6134-45.
- (31) Frisch, M. J.; Trucks, G. W.; Schlegel, H. B.; Scuseria, G. E.; Robb, M. A.; Cheeseman, J. R.; Scalmani, G.; Barone, V.; Mennucci, B.; Petersson, G. A.; Nakatsuji, H.; Caricato, M.; Li, X.; Hratchian, H. P.; Izmaylov, A. F.; Bloino, J.; Zheng, G.; Sonnenberg, J. L.; Hada, M.; Ehara, M.; Toyota, K.; Fukuda, R.; Hasegawa, J.; Ishida, M.; Nakajima, T.; Honda, Y.; Kitao, O.; Nakai, H.; Vreven, T.; Montgomery, J. A., Jr.; Peralta, J. E.; Ogliaro, F.; Bearpark, M.; Heyd, J. J.; Brothers, E.; Kudin, K. N.; Staroverov, V. N.; Kobayashi, R.; Normand, J.; Raghavachari, K.; Rendell, A.; Burant, J. C.; Iyengar, S. S.; Tomasi, J.; Cossi, M.; Rega, N.; Millam, N. J.; Klene, M.; Knox, J. E.; Cross, J. B.; Bakken, V.; Adamo, C.; Jaramillo, J.; Gomperts, R.; Stratmann, R. E.; Yazyev, O.; Austin, A. J.; Cammi, R.; Pomelli, C.; Ochterski, J. W.; Martin, R. L.; Morokuma, K.; Zakrzewski, V. G.; Voth, G. A.; Salvador, P.; Dannenberg, J. J.; Dapprich, S.; Daniels, A. D.; Farkas, Ö.; Foresman, J. B.; Ortiz, J. V.; Cioslowski, J.; Fox, D. J. Gaussian 09, revision A.02; Gaussian, Inc.: Wallingford, CT, 2009.
- (32) A. Baheti, P. Tyagi, K. R. J. Thomas, Y.-C. Hsu and J. T. s. Lin, Simple Triarylamine-

- Based Dyes Containing Fluorene and Biphenyl Linkers for Efficient Dye-Sensitized Solar Cells. *J. Phys. Chem. C* **2009**, *113*, 8541-47.
- (33) T. Khanasa, N. Jantasing, S. Morada, N. Leesakul, R. Tarsang, S. Namuangruk, T. Kaewin, S. Jungsuttiwong, T. Sudyoadsuk and V. Promarak, Synthesis and Characterization of 2D-D- π -A-Type Organic Dyes Bearing Bis(3,6-di-tert-butylcarbazol-9-ylphenyl)aniline as Donor Moiety for Dye-Sensitized Solar Cells. *Eur. J. Org. Chem.* **2013**, *2013*, 2608-20.
- (34) M. Gratzel, Photoelectrochemical cells. *Nature* **2001**, *414*, 338-44.
- (35) A. Hagfeldt and M. Graetzel, Light-Induced Redox Reactions in Nanocrystalline Systems. *Chem. Rev.* **1995**, *95*, 49-68.
- (36) P. Wang, S. M. Zakeeruddin, J.-E. Moser and M. Grätzel, A New Ionic Liquid Electrolyte Enhances the Conversion Efficiency of Dye-Sensitized Solar Cells. *J. Phys. Chem. B* **2003**, *107*, 13280-85.
- (37) R. G. Parr and W. Yang, Density-Functional Theory of the Electronic Structure of Molecules. *Annu. Rev. Phys. Chem.* **1995**, *46*, 701-28.
- (38) A. D. Becke, A new mixing of Hartree-Fock and local density-functional theories. *The Journal of Chemical Physics* **1993**, *98*, 1372-77.
- (39) C. Lee, W. Yang and R. G. Parr, Development of the Colle-Salvetti correlation-energy formula into a functional of the electron density. *Physical Review B* **1988**, *37*, 785-89.
- (40) B. J. Lynch, P. L. Fast, M. Harris and D. G. Truhlar, Adiabatic Connection for Kinetics. *J. Phys. Chem. A* **2000**, *104*, 4811-15.
- (41) Y.-F. Liu, X.-F. Ren, L.-Y. Zou, A.-M. Ren, J.-K. Feng and C.-C. Sun, Theoretical study on photophysical properties of 2,1,3-benzothiadiazole-based star-shaped molecules. *Theor. Chem. Acc.* **2011**, *129*, 833-45.

Chapter 4

Phenothiazine Donor Based Organic dye for Dye-Sensitized Solar Cells: Effect of Auxiliary Acceptors on Optical and Electrochemical Properties

4.1 Introduction

Recently the performance of solar cells based on metal free organic sensitizers has been remarkably improved and promising cell efficiencies in the range of 9-11% has been reported [1-3]. D- π -A configuration represents the most ubiquitous molecular architectures of the sensitizer in the dye-sensitized solar cells and a large variety of donors and π -conjugation bridges has been investigated [4-6]. The long π -conjugated spacers between the donor and acceptor in D- π -A configuration make the sensitizers to possess a rod-shape configuration, which can facilitate the recombination of the electrons with I^{3-} and enhances the aggregation between molecules on the semiconductor surface and leading to lower photovoltaic performance in DSSCs [7-10]. Because of such findings, organic dyes with auxiliary donor or auxiliary acceptor were employed as sensitizers, found to be fruitful for facile charge migration from the donor to the acceptor [11-14]. As a result, the dyes showed enhanced spectral response in the red region of the solar spectrum, and thus effectively improved the light-harvesting range [11, 15].

In this context it is found that for broadening of the absorption spectrum and improvement of the DSSC performance, embedding an electron acceptor is superior to that of an electron donor on the conjugation bridge [16]. A wide variety of electron withdrawing groups such as benzothiadiazole [3,13, 17-21], benzotriazole [22-24], diketopyrrolopyrrole [25-26], isoindigo[27], quinoxaline [28-32], phthalimide [33-34], thiazolo[5,4-*d*]thiazole [35-36], benzo[1,2-*d*:4,5-*d'*]bisthiazole[37], etc. are combined with various electron-donating arylamines and the energy levels, band-gaps of the dyes were readily modulated. Among these

Effect of auxiliary acceptor on optical properties

electron withdrawing groups, we have been attracted by the sensitizers containing benzothiadiazole (BTD) and benzotriazole (BTA) as auxiliary electron-accepting units. Recently benzothiadiazole and benzotriazole based derivatives have been vigorously investigated in dye-sensitized solar cells (DSSC) [33, 38], bulk heterojunction solar cells (BHJ) [39-46] and organic light emitting diodes (OLED) [47-50] etc due to their good electron affinity and unique properties. Structures and numbering scheme of BTD and BTA units were shown in Figure 4.1. However, to the best of our knowledge, there is no report on the insights of the choice of proper auxiliary acceptor in the D- π -A- π -A configuration and phenothiazine functionalized with low-band gap chromophores like benzothiadiazole and benzotriazole for DSSCs has not been explored. So it is interesting to study the consequences on the photophysical and electrochemical properties of the sensitizers by permutation of benzothiadiazole with benzotriazole as auxiliary acceptor.

Figure 4.1 Structures and numbering scheme of BTD and BTA

It is worth mentioning that, replacing the sulfur atom of the BTD unit with a nitrogen atom, new acceptor unit BTA was emerged [22, 51-52]. In a review on conjugated polymers for bulk-heterojunction photovoltaics, Huang and co-workers proposed an empirical chart showing the relative electron accepting ability of BTD and BTA analogues [51]. Since the lone pair of electron on the middle nitrogen atom of the benzotriazole unit easily donates into the triazole ring than, the lone pairs of electron on the sulfur atom of the benzothiadiazole, making it comparatively electron-rich when compared with the BTD [22-23, 53]. Thus BTA sensitizers usually show higher lowest unoccupied molecular orbital (LUMO) energy and a larger band gap than the benzothiadiazole analogs [22]. However, the 2-position nitrogen atom in BTA renders an additional position for incorporating solubilizing alkyl chain, diminishes the electron recombination effectively and inhibits the dye aggregation [22, 53]. Moreover 4-*tert*-butylpyridine, benzimidazole and pyrimidine etc. are commonly used additives in the electrolyte of DSSC for the sake of increasing V_{OC} . These additives by interacting with the

Effect of auxiliary acceptor on optical properties

TiO₂ film retard the charge recombination between the electrons in the conduction band of TiO₂ and I³⁻[22-24]. Similarly it was also proved that benzotriazole based sensitizers achieved high V_{OC} , than their benzothiadiazole-based analogs. Benzothiadiazole/benzotriazole auxiliary acceptors can stabilize the charge-separated excited-state. As well demonstrated in the literature, due to its strong electron-donating capability and high molar extinction coefficient of phenothiazine unit over triphenylamine, carbazole and tetrahydroquinoline units we choose phenothiazine as the donor segment [54-55]. Experimental and theoretical studies have manifested that the phenothiazine unit is expected to confine the cationic charge away from the nanocrystalline TiO₂ surface and efficiently hamper charge recombination [56-57]. The phenothiazine unit also possesses non-planar butterfly conformation which can impede unfavorable dye aggregation and formation of molecular excimers at the semiconductor surface [54, 58]. Indeed, the alkyl substitutions on the phenothiazine, benzotriazole units adequately improve the solubility, insulate the I³⁻ or cations approaching the semiconductor TiO₂ surface and enhance the open-circuit voltage (V_{OC}) [22, 40].

Herein, by preserving the same donor group throughout the series and permutation of the hetero atom on the auxiliary acceptor, π -spacer between acceptor and auxiliary acceptor we developed four new organic dyes. We investigated subtle changes in the photophysical, electronic energy levels and frontier molecular orbitals for the dyes. The newly developed phenothiazine donor based dyes displayed substantial improvement in their optical and electrochemical properties when compared to their congener derivatives that contained triphenylamine or indoline donors, consequently these dyes may serve as efficient sensitizers in DSSCs. To the best of our knowledge, sensitizers comprising phenothiazine as donor with auxiliary acceptor (benzothiadiazole/benzotriazole) have not been exploited. The General representation and structures of phenothiazine donor based BTD/BTA auxiliary acceptors based sensitizers are shown in Figures 4.2 and 4.3.



Figure 4.2 General representation of the benzothiadiazole/benzotriazole auxiliary acceptor based sensitizers

Figure 4.3 Molecular structures of dyes

4.2 Results and discussions

4.2.1 Design and synthesis

The synthetic strategy employed for the preparation of sensitizers with benzothiadiazole/benzotriazole moieties in the π -conjugated spacer is illustrated in Scheme 4.1.

Scheme 4.1 Synthetic routes to the benzothiadiazole/benzotriazole featured sensitizers

The synthesis was started from the lithiation of **8** with *n*-butyl lithium and subsequent quenching with tributyltin chloride (*n*-Bu₃SnCl) to afford stannyl derivative in quantitative

yield. The palladium-catalyzed Stille coupling reactions of stannane with **9a-b** [20], **12a-b** [59] yielded compounds **10a-b** and **13a-b**, respectively. Finally obtained precursor terminal aldehydes were converted to the corresponding sensitizer by Knoevenagel condensation with cyanoacetic acid in presence of ammonium acetate in acetic acid. The obtained sensitizers are deep red or black in colors. The final products were confirmed by the disappearance of the aldehyde proton, appearance of vinylic proton in NMR spectra. The molecular structures of the intermediates as well as sensitizers were characterized IR, NMR (^1H and ^{13}C) and high resolution mass spectrometry (HR-MS) and the obtained data were consistent with the proposed structures. All the sensitizers are air stable and fairly soluble in polar solvents like tetrahydrofuran, dimethylformamide, and moderately soluble in CH_2Cl_2 , CHCl_3 , acetonitrile and toluene.

4.2.2 Absorption spectra

The molecular-level capacity of the sensitizers for solar radiation capture was evaluated through measuring their UV-vis absorption spectra in THF (Figure 4.4). The optical data of the dyes were compiled in Table 4.1.

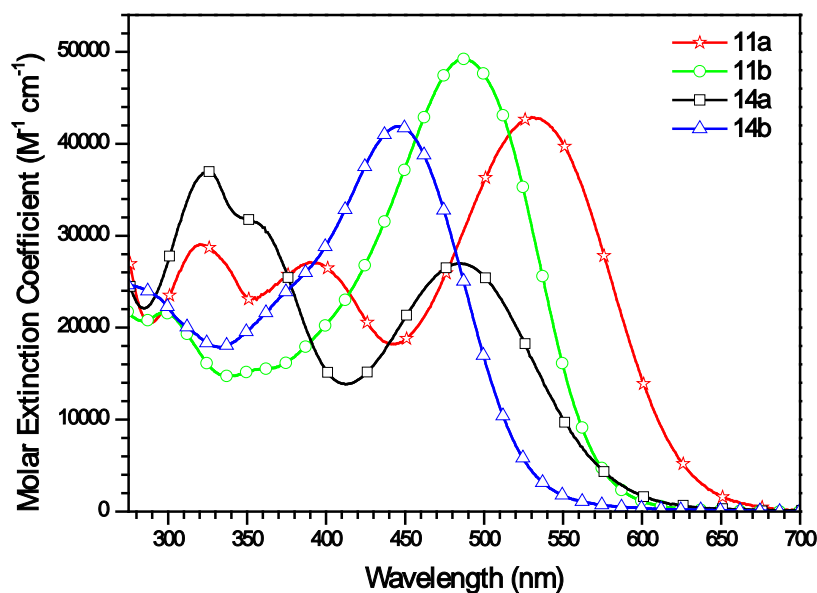


Figure 4.4 Absorption spectra of the dyes recorded in THF

All the studied sensitizers contain the same electron-donating moiety 10-butyl-3-(thiophen-2-yl)-10*H*-phenothiazine and differed by the auxiliary acceptor group and the nature of the π -linkers. In these D-A- π -A featured sensitizers, the two auxiliary acceptors benzothiadiazole and benzotriazole have a distinct result on optical properties. The benzothiadiazole,

Effect of auxiliary acceptor on optical properties

benzotriazole π -conjugated sensitizers displayed three, two major prominent bands in the absorption spectra, respectively. The prominent bands in the region below 400 nm are probably due to a localized aromatic π - π^* transition, whereas the band found in the visible region can be attributed to intramolecular charge transfer from the donor phenothiazine to the acceptor cyanoacrylic acid group. The maximum absorption wavelengths of dyes with molar extinction coefficients are **11a** : 530 nm ($42.9 \times 10^3 \text{ M}^{-1}\text{cm}^{-1}$); **11b** : 488 nm ($49.2 \times 10^3 \text{ M}^{-1}\text{cm}^{-1}$); **14a** : 485 nm ($27.0 \times 10^3 \text{ M}^{-1}\text{cm}^{-1}$); **14b** : 446 nm ($41.9 \times 10^3 \text{ M}^{-1}\text{cm}^{-1}$).

The absorption maximum and the molar extinction coefficient of the sensitizers are consistent with the electro negativity of the heteroatom present in the auxiliary acceptor unit and the electron richness of the π -linker. The BTD bridged dyes (**11a**, **14a**) displayed bathochromically shifted absorption profile when compared with its BTA congeners (**11b**, **14b**) which is attributable to the more electron-deficient character of BTD segment. The introduction of electron-rich thiophene unit in the conjugation pathway red shifted the absorption maxima and hiked the molar extinction coefficient, when compared with the phenyl analogs. Extension of conjugation by thienyl unit rather than phenyl unit, found to be beneficial to enhance the light harvesting capacity of the sensitizer. The diminished charge transfer transition in the phenyl π -conjugated derivatives is due to the non-planar structural feature which hampers donor-acceptor interactions and electron delocalization across the sensitizer. The comparison between dyes demonstrated the influence of the auxiliary acceptor group and the π -linker. Because of the judicious molecular design of the sensitizers based on phenothiazine, the molar extinction coefficient (ϵ) at the maximum absorption of the dyes falls in the range 27000 - $49200 \text{ M}^{-1} \text{ cm}^{-1}$, which are notably two fold larger than those of prominent Ru-based dyes **N3** [60] and **N719** [61-62] (13900 and $14000 \text{ M}^{-1}\text{cm}^{-1}$, respectively). It is worth mentioning that the absorption wavelengths and molar extinction coefficients of these benzothiadiazole dyes are significantly red-shifted when compared to the dyes containing triphenylamine [13], indoline [63], and coumarin [19] unit substituted for thienyl phenothiazine as electron donor in a similar structural composition.

Table 4.1 Absorption data of the dyes recorded in tetrahydrofuran

Dye	λ_{abs} , nm ($\epsilon \times 10^3 \text{ M}^{-1} \text{ cm}^{-1}$)
11a	320 (29.0), 390 (27.1), 530 (42.9)
11b	298 (21.6), 488 (49.2)
14a	326 (37.0), 351 (31.7), 485 (27.0)
14b	275 (24.7), 446 (41.9)

Effect of auxiliary acceptor on optical properties

Table 4.2 Absorption data for the dyes in various solvents.

Dye	$\lambda_{\text{abs, nm}}$								
	TOL	TOL+TFA	TOL+TEA	DCM	ACN	DMF	DMF+TFA	DMF+TEA	MeOH
11a	324, 393, 539	324, 538	323, 379, 520	318, 396, 537	316, 357, 508	332, 376, 517	320, 388, 531	379, 517	320, 377, 508
11b	301, 500	302, 520	290, 469	298, 501	296, 474	298, 462	296, 490	296, 463	294, 484
14a	327, 356, 496	326, 364, 502	329, 356, 485	324, 358, 490	317, 353, 473	328, 482	325, 353, 488	318, 483	320, 350, 474
14b	451	290, 453	288, 436	453	432	433	447	434	432

We have examined the electronic absorption spectra of the sensitizer in solvents with different dielectric constant such as toluene, THF, CH_2Cl_2 , DMF, MeCN and MeOH of the solvents, to realize the effect of solvent environments on the electronic absorption properties of the sensitizers. All the sensitizers showed alternations in the absorption maxima due to solvent polarity. The alterations in the absorption spectra for the sensitizers with solvent polarity are illustrated in Figure 4.6 and data is compiled in Table 4.2. Particularly, they displayed a blue-shifted absorption in the polar solvents such as DMF, ACN and MeOH as compared to the absorption maximum recognized in THF, DCM and TOL. Explanation for the blue shift observed for the sensitizers in polar solvents can be explained on the basis of protonation and deprotonation of carboxylic acid group in the sensitizers. Figure 4.6 shows the illustration of acid-base equilibrium in the sensitizers.

Figure 4.5 Illustration of acid-base equilibrium in the sensitizers

Effect of auxiliary acceptor on optical properties

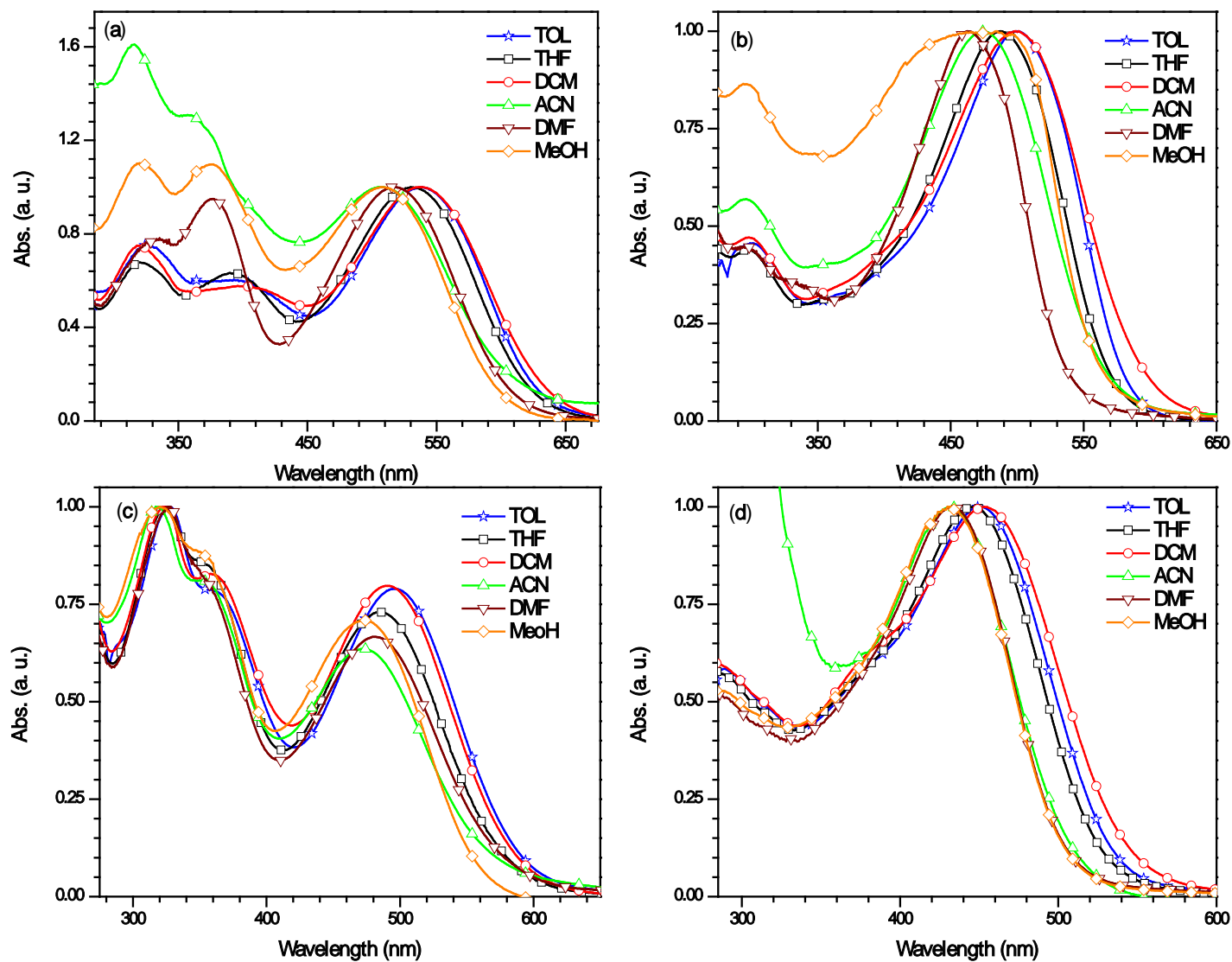


Figure 4.6 Absorption spectra of dyes (a) 11a (b) 11b (c) 14a (d) 14b recorded in different solvents.

Effect of auxiliary acceptor on optical properties

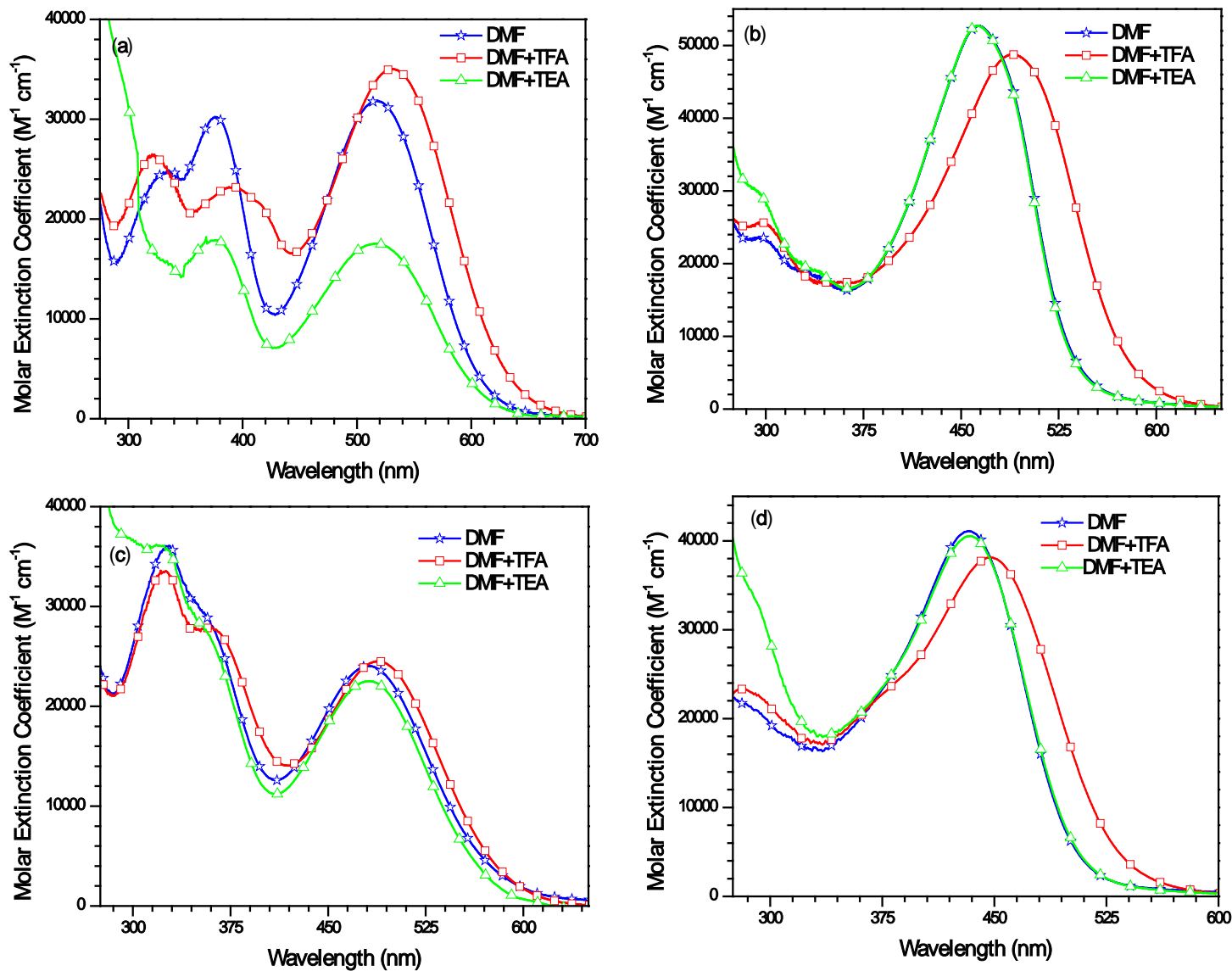


Figure 4.7 Absorption spectra of dyes (a) **11a** (b) **11b** (c) **14a** (d) **14b** in DMF recorded in the presence of TFA or TEA.

Effect of auxiliary acceptor on optical properties

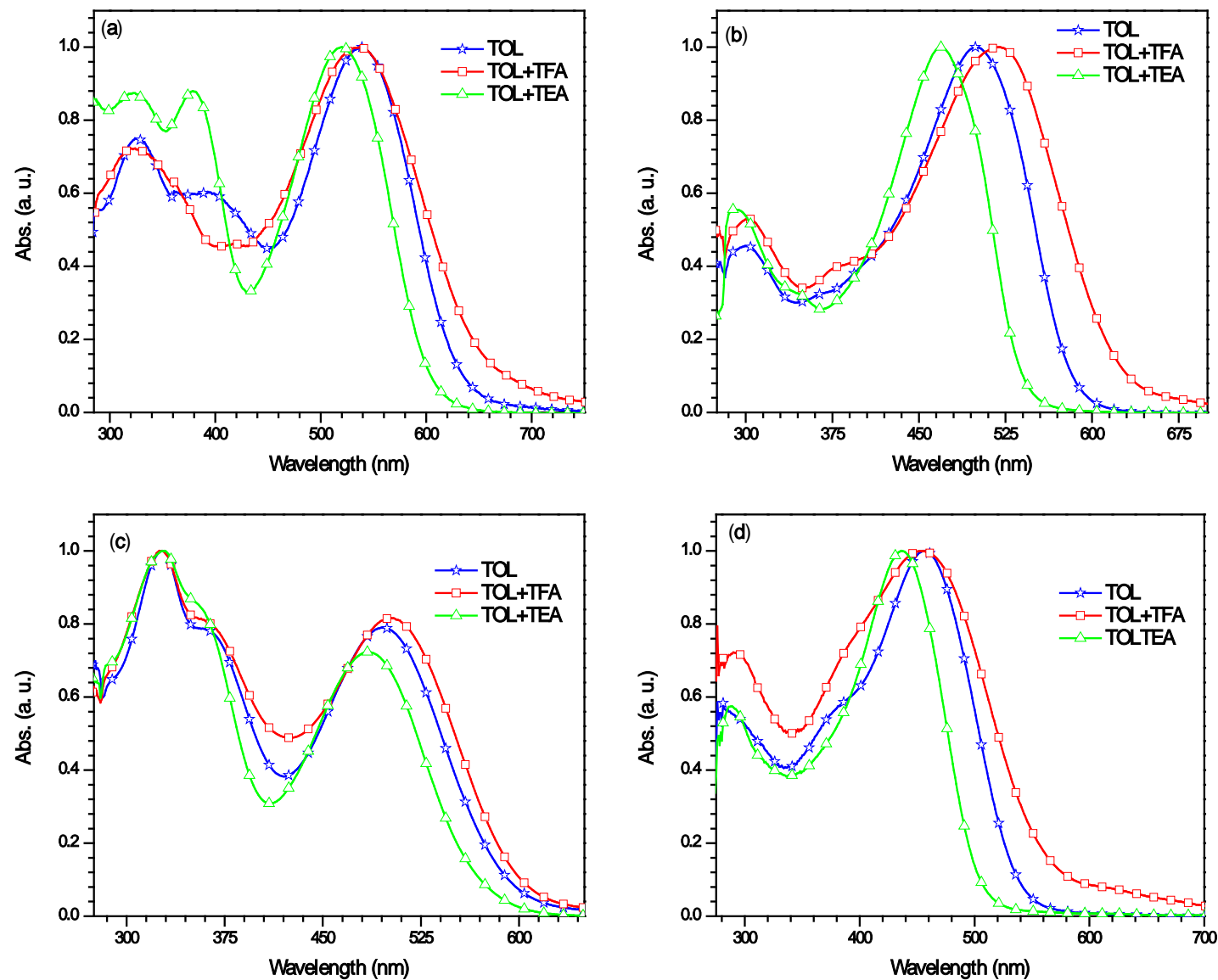


Figure 4.8 Absorption spectra of dyes (a) 11a (b) 11b (c) 14a (d) 14b in toluene recorded in the presence of TFA or TEA.

The solvents capable of coordinating with the carboxylic acid unit in the sensitizers can shift the acid-base equilibrium toward the deprotonated form (D^-). This deprotonation can diminish the electron-accepting nature of the acceptor group, which results in reduction of donor-acceptor interaction in the sensitizers [64]. This hypothesis of protonation and deprotonation of the sensitizers was further supported by the fact that addition of a base such as triethylamine to the dimethylformamide solutions of the sensitizers blue shifted the absorption maximum. The absorption spectra of the dyes recorded in DMF/TOL before and after addition of TFA or TEA were shown in Figures 4.7 & 4.8. As discussed earlier, the absorption spectra of the sensitizers recorded in basic solvents displayed a blue-shifted absorption. Hence, it was expected that in basic solvents, the deprotonated form might be present in greater quantity and the addition of TFA would push the equilibrium towards the protonated form DH. As anticipated, the addition of TFA to the DMF/TOL solution of the sensitizers resulted in a bathochromic-shift for the absorption maximum. Addition of TFA/TEA to the sensitizer solutions altered lower energy absorption because of the charge-transfer transition and no alterations were seen on the higher energy transitions

4. 2. 3 Emission spectra

Fluorescence emission spectra (Figure 4.9) of the sensitizers were recorded in THF by irradiating the samples at their maximum absorption wavelengths. Solvatochromic behavior of the dyes was illustrated in Figure 4.10 and relevant parameters are listed in Table 4.3. The sensitizers emit in the range of 552-631 nm. The maximum emission peaks are at 631, 612, 581 and 552 nm for **11a**, **11b**, **14a** and **14b**, respectively. The emission maximum of the sensitizers followed the same trend as the absorption spectra and more π -conjugated sensitizers are showing red-shifted emission. The sensitizers with thienyl π -conjugation (**11a-b**) displayed red shifted emission maximum than phenyl π -conjugated sensitizers (**14a-b**). In **11a** and **11b** through effective conjugation of thiophene linkage the acceptor strength was enhanced, while in **14a** and **14b** the twisted phenyl π -linker decouples the acceptor from the auxiliary acceptor. Thus in **11a**, and **11b** the electronic excitation which arises due to the charge transfer from the donor to the acceptor would cause a migration of electron density from the phenothiazine toward the cyanoacrylic acid acceptor, while this would be less pronounced in **11b** and **14b**. The net result is a more polar excited state for **11a-b** than **14a-b**. The larger Stokes shift observed for the phenyl based dyes (**14a-b**) when compared to the thienyl based dyes (**11a-b**) is likely to

Effect of auxiliary acceptor on optical properties

arise due to the twisting occurring in the phenyl conjugation on excitation while the thienyl will forbid thermal rotational relaxation. This clearly reveals that the nature of the π -conjugated unit that bridges the acceptor with the auxiliary acceptor plays a major role in the stabilization of excited state. The large Stokes shift ($> 3020 \text{ cm}^{-1}$) observed for the sensitizers confirms intramolecular charge-transfer nature of the excited state upon photo-excitation process. The thienyl bridge enhances the acceptor strength due to effective conjugation, whilst the phenyl bridge deteriorates the acceptor strength presumably due to the non-planar linkage.

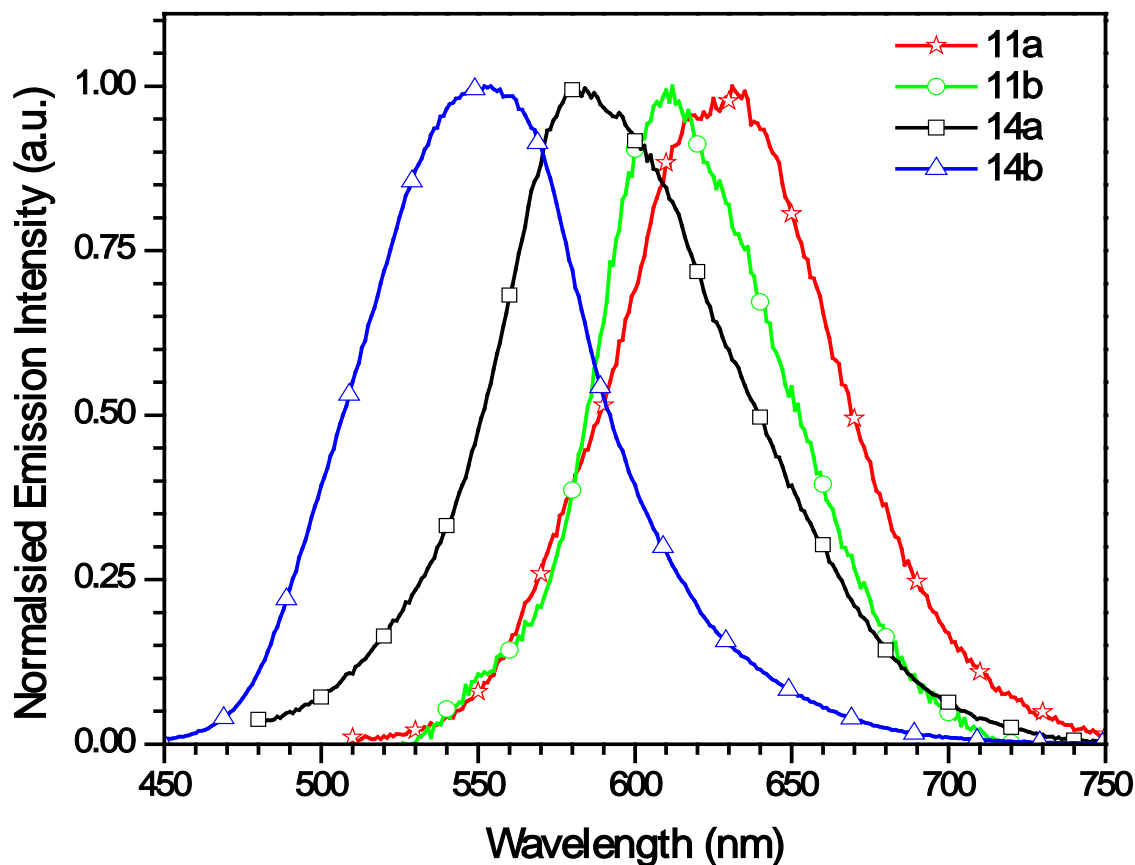


Figure 4.9 Emission spectra of the dyes recorded in THF

Table 4.3 Emission properties and Stokes shift observed for the dyes in the different solvents

Dye	λ_{em} , nm						Stokes shift (cm^{-1})					
	TOL	THF	DCM	ACN	DMF	MeOH	TOL	THF	DCM	ACN	DMF	MeOH
11a	652	631	579	608	580	576	3215	3020	1351	3238	2101	2324
11b	605	612	572	566	554	563	3471	4152	2478	3429	3594	2899
14a	612	581	571	587	571	577	3821	3407	2895	4106	3234	3766
14b	572	552	564	553	564	512	4690	4306	4345	5065	5364	3617

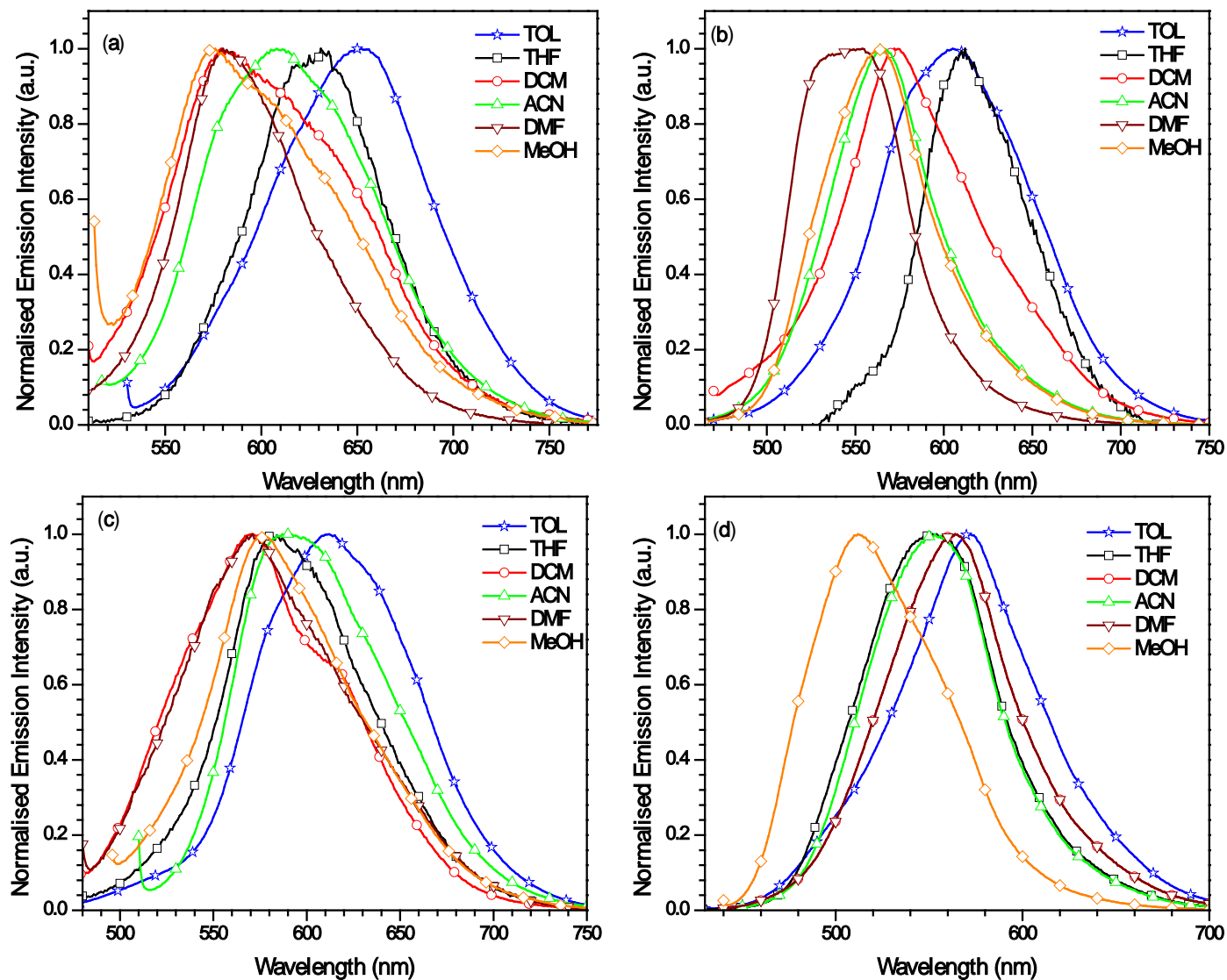


Figure 4.10 Emission spectra of dyes (a) 11a (b) 11b (c) 14a (d) 14b recorded in different solvents.

The fluorescence wavelength maximum of the dyes decreases as the solvent polarity increases from polar to non-polar, which is an indicative of negative solvatochromism. This negative solvatochromism further corroborates the presence of an ICT transition from the phenothiazine to cyanoacrylic acid acceptor. Generally polar solvents expected to stabilize the dipolar molecules in the excited state. However a significant hypso chromic shift was observed for polar solvents such as acetonitrile, dimethylformamide and methanol when compared to that of toluene is interesting and indicate a less polar excited state [65].

4.2.4 Electrochemistry

To probe the feasibility of electron transfer at the $\text{TiO}_2/\text{dye}/\text{redox}$ electrolyte interface, cyclic voltammetry was performed in tetrahydrofuran solution, using 0.1 M tetrabutylammonium perchlorate as the supporting electrolyte, Pt as working electrode at a scan rate 100 mV/s. The redox potentials were calibrated by using the ferrocene/ferrocenium redox couple as an external standard. The redox data of the dyes are compiled in Table 4.4, and the representative cyclic voltammograms are displayed in Figure 4.11.

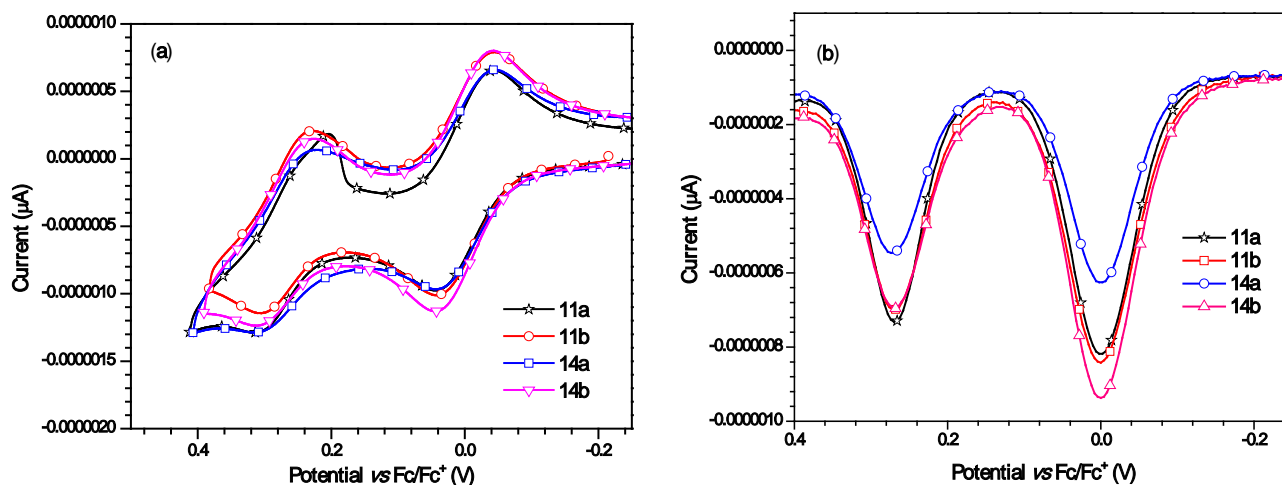


Figure 4.11 (a) Cyclic voltammograms recorded for the dyes in THF (b) Differential pulse voltammograms of the dyes recorded in THF

The HOMO-LUMO energy gap was estimated from the optical edge of the absorption spectra. All the dyes displayed a quasi-reversible one electron oxidation wave arising due to the removal of electron from the phenothiazine donor segment at potential higher than that observed for external ferrocene/ferrocenium couple. The oxidation potentials follow the order: **11b** (221 mV) > **14b** (215 mV) > **11a** (195 mV) > **14a** (190 mV). The HOMO levels of **11a**, **11b**, **14a** and **14b** are 0.97 V, 0.99 V, 0.97 V, and 0.99 V (*vs.* NHE), respectively.

It was observed that for similar structural organization modulation of π -linker in between the auxiliary acceptor and acceptor (cyanoacrylic acid) with phenyl, thiophene has no effect on the oxidation potential as well as HOMO energy level. Whilst modifying benzothiadiazole with benzotriazole auxiliary acceptor induced (≈ 25 mV) anodic shift in oxidation potential. As the donor group was preserved throughout the series, their HOMO energy levels show only minor differences. While modulation of the auxiliary acceptor by benzotriazole raised the LUMO energy level of the sensitizers, which is assigned to the less electron withdrawing nature of benzotriazole than the benzothiadiazole. The HOMO-LUMO energy gaps (E_{0-0}) of the dyes are 1.88 eV, 2.05 eV, 2.02 eV and 2.21 eV respectively, which are estimated from the optical edge of the absorption spectra. The estimated excited-state potentials for dyes calculated from the formula $E_{OX} - E_{0-0}$, are -0.91 V, -1.06 V, -1.05 V, and -1.22 V, respectively. Electron injection from the excited state of sensitizers to the conduction band of the nanocrystalline TiO₂ was energetically favorable, since E_{OX}^* energy levels of the sensitizers were more negative than that of the conduction band of TiO₂ (0.5 V). Recent studies revealed that for efficient regeneration of organic sensitizers from iodide/triiodide electrolyte 0.5 V driving force is necessary. Since all the dyes possess more than 0.5 V driving forces for dye regeneration from I⁻/I³⁻ redox couple. On this basis, it may be argued that the oxidized dyes may efficiently be regenerated by the redox electrolyte [66].

Table 4.4 Electrochemical properties of the benzothiadiazole based sensitizers

Dye	E_{OX} , mV (ΔE_p , mV) ^a	E_{OX} , mV ^b	E_{OX} vs NHE, V ^c	HOMO, eV ^d	LUMO, eV ^e	E_{0-0} , eV ^f	E_{OX}^* , V ^g
11a	260 (112)	270	1.03	5.06	3.18	1.88	-0.85
11b	267 (88)	270	1.04	5.07	3.02	2.05	-1.01
14a	269 (94)	272	1.04	5.07	3.05	2.02	-0.98
14b	272 (85)	268	1.04	5.07	2.86	2.21	-1.17

^a potentials with reference to ferrocene internal standard from CV; ^b potentials with reference to ferrocene internal standard from DPV; ^c Ground-state oxidation potential versus NHE; ^d Deduced from the equation HOMO = $E_{OX} + 4.8$; ^e Deduced from the equation LUMO = HOMO - E_{0-0} ; ^f Derived from optical edge; ^g Deduced from formula $E_{OX}^* = E_{OX} - E_{0-0}$

4.2.5. Molecular modeling

For a deeper understanding of the structural influences on the molecular orbital distributions and photophysical behavior of the sensitizers, we have performed the molecular structure optimization and molecular orbital calculations using density functional theory at the B3LYP [67-68], MPKW1K [69] level with the 6-31G(d,p) basis set by using the Gaussian 09 [70] program package. The electronic distributions observed for the frontier molecular orbitals of the sensitizers are shown in Figures 4.12 & 4.13. The computed excitation energies for the vertical

Effect of auxiliary acceptor on optical properties

transitions, their oscillator strengths (f), compositions in terms of molecular orbitals, the energies of the highest occupied molecular orbital (HOMO) and lowest unoccupied molecular orbital (LUMO) levels, and ground-state dipole moments computed for the sensitizers are compiled in Tables 4.5, 4.6 and 4.7. Notably, the electron clouds of the HOMO for all the sensitizers are mainly distributed on the thienylphenothiazine segment and HOMO-1 is delocalized over the entire molecule. Whilst the LUMO is largely dominated by orbitals from thiophene moiety attached to phenothiazine to the cyanoacrylic unit. The well-separated electron distribution of HOMO and LUMO orbitals on the auxiliary acceptor units, illustrate the role of the auxiliary acceptor on the charge migration from the HOMO to the LUMO on electronic excitation. Generally, this type of well separated electron distribution imparts an intrinsic intramolecular charge transfer property in the sensitizers and expected to yield a charge migration from the HOMO to the LUMO on electronic excitation. After photoexcitation, the electrons are from phenothiazine donor to the auxiliary acceptors (benzothiadiazole/benzotriazole) and then channeled to the cyanoacetic acid subunit, subsequently transferred into TiO_2 .

According to the B3LYP computations, the low energy vertical transitions in the sensitizers originate from the HOMO to LUMO electronic excitations with reasonable oscillator strengths. However, the MPKW1K suggested this higher wave length absorption resulted from the electronic promotion from the HOMO to LUMO (major) and HOMO-1 \rightarrow LUMO (minor). This clearly reveals that the longer wavelength transition is due to the charge transfer from the phenothiazine moiety to (A- π -A) segment. Since the calculated transitions by MPKW1K are closely matching to the experimentally observed optical data for the sensitizers in THF, we presume that the composition of the transitions predicted by the MPW1K is more reliable than B3LYP. The two electronic transitions corresponding to the low energy transition are positively contributed to electron injection, since they transfer electron density from the whole molecule (HOMO and HOMO-1) to the anchoring group (LUMO), which is in closest proximity to the TiO_2 semiconductor surface. The introduction of benzothiadiazole moiety unit into the molecular structure bathochromically-shifted the ICT absorption peak when compared with the benzotriazole congeners, which is consistent with our experimental results.

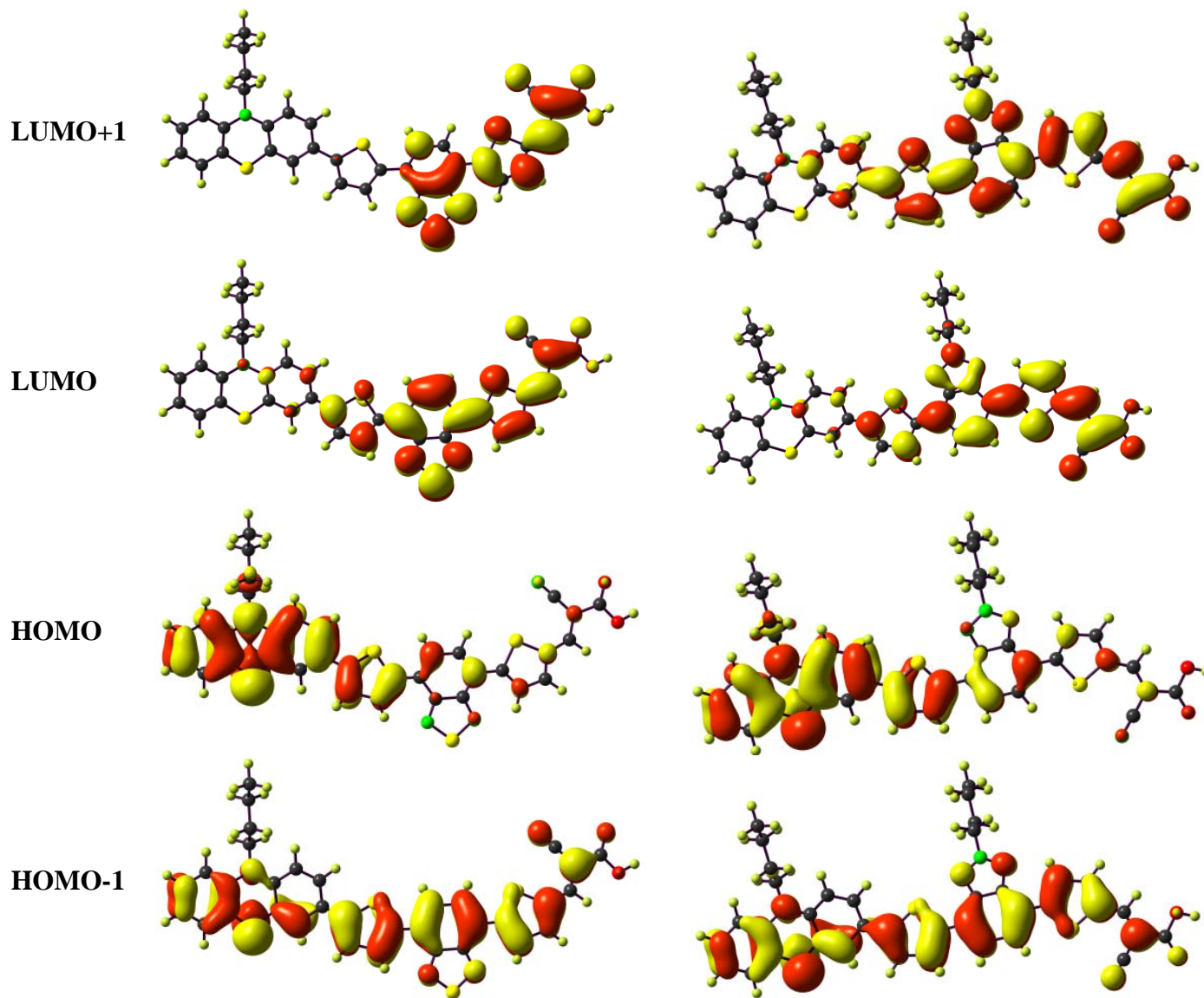


Figure 4.12 Frontier molecular orbitals of the dyes **11a** (left) and **11b** (right)

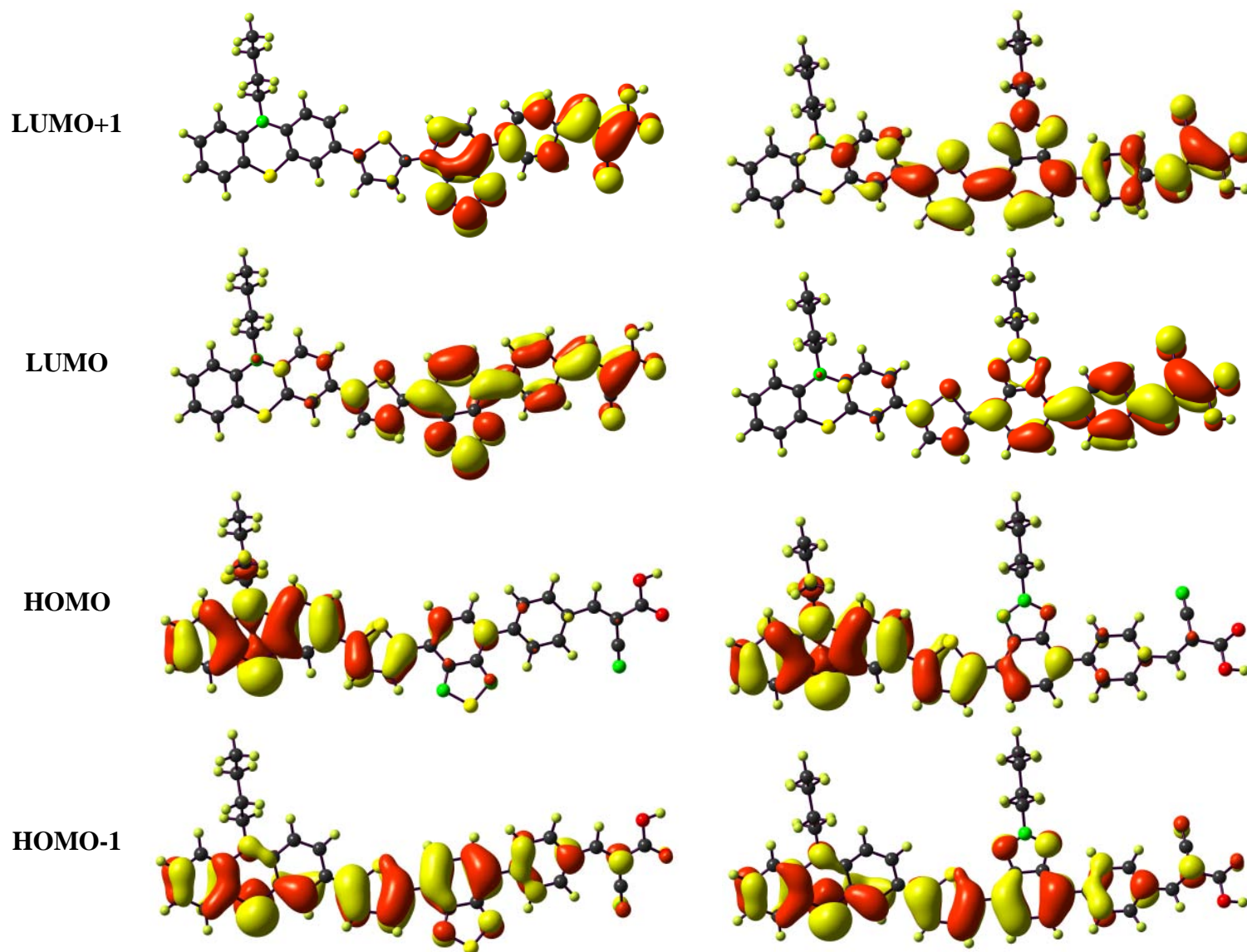


Figure 4.13 Frontier molecular orbitals of the dyes **14a** (right) and **14b** (left)

Table 4.5 Computed vertical transition energies, oscillator strengths (f), and their assignment for the dyes^[a] using B3LYP (gas).

Dyes	$\lambda_{\text{abs}}/\text{nm}$	f	Configuration	HOMO, ev	LUMO, ev	$\mu_{\text{g}}, [\text{D}]$
11a	742.0	0.50	HOMO→LUMO (100%)	-5.00	-3.11	6.09
	559.3	0.50	HOMO-1→LUMO (90%)			
	506.2	0.18	HOMO→LUMO+1 (88%)			
	419.9	0.38	HOMO-1→LUMO+1 (49%), HOMO→LUMO+2 (24%) HOMO-2→LUMO (20%)			
	400.6	0.14	HOMO→LUMO+2 (58%), HOMO-3→LUMO (21%) HOMO-2→LUMO (10%)			
	387.8	0.11	HOMO-3→LUMO (66%), HOMO-1→LUMO+1 (12%) HOMO→LUMO+2 (10%)			
	342.7	0.30	HOMO-1→LUMO+2 (42%), HOMO-2→LUMO+1 (38%)			
	11b	643.5	0.67	HOMO →LUMO (99%)	-4.89	-2.77
500.6		1.00	HOMO-1→LUMO (98%)			
444.0		0.10	HOMO→LUMO+1 (91%)			
14a	677.2	0.47	HOMO→LUMO (99%)	-5.00	-2.92	11.28
	516.6	0.13	HOMO→LUMO+1 (67%), HOMO-1→LUMO (29%)			
	502.9	0.51	HOMO-1→LUMO (69%), HOMO→LUMO+1(30%)			
	416.1	0.15	HOMO-1→LUMO+1 (86%)			
	404.2	0.32	HOMO→LUMO+2 (58%), HOMO-2→LUMO (35%)			
	362.2	0.14	HOMO-3→LUMO (85%)			
	335.7	0.47	HOMO →LUMO+3 (40%), HOMO-2→LUMO+1 (25%) HOMO-1→LUMO+2 (22%)			
14b	611.7	0.58	HOMO→LUMO (99%)	-4.88	-2.64	7.75
	475.2	0.87	HOMO-1→LUMO (99%)			
	448.2	0.19	HOMO→LUMO+1 (96%)			
	374.2	0.30	HOMO-1→LUMO+1(54%), HOMO-2→LUMO (40%)			

[a] Contributions of less than 10% are omitted.

Table 4.6 Computed vertical transition energies, oscillator strengths (*f*), and their assignment for the dyes^[a] using MPW1K (gas).

Dye	$\lambda_{\text{abs}}/\text{nm}$	<i>f</i>	Configuration	HOMO, ev	LUMO, ev	μ_{g} , [D]
11a	518.9	1.09	HOMO→LUMO (77%), HOMO-1→LUMO (19%)	-5.87	-2.61	4.99
	418.6	0.21	HOMO-1→LUMO (74%), HOMO→LUMO (19%)			
	364.1	0.24	HOMO→LUMO+1 (66%), HOMO-1→LUMO+1(27%)			
	335.7	0.19	HOMO→LUMO+2 (52%), HOMO-2→LUMO (19%)			
	331.4	0.17	HOMO-2→LUMO (51%), HOMO →LUMO+2(19%)			
	292.2	0.37	HOMO-1→LUMO+2 (28%), HOMO→LUMO+3(19%), HOMO-4→LUMO (11%)			
11b	467.4	1.60	HOMO→LUMO (75%), HOMO-1→LUMO (19%)	-5.77	-2.25	11.54
	382.8	0.22	HOMO-1→LUMO (73%), HOMO→LUMO (18%)			
	339.5	0.15	HOMO→LUMO+1(65%), HOMO→LUMO+2(16%)			
	275.7	0.12	HOMO-7→LUMO (21%), HOMO-1→LUMO+1(14%), HOMO→LUMO+3 (12%), HOMO→LUMO+2(10%)			
14a	270.6	0.12	HOMO→LUMO+4 (38%), HOMO-8→LUMO (11%), HOMO-1→LUMO+2(10%)	-5.88	-2.38	10.72
	472.6	1.06	HOMO→LUMO (75%), HOMO-1→LUMO (17%)			
	383.7	0.23	HOMO-1→LUMO (70%), HOMO→LUMO (19%)			
	351.0	0.16	HOMO→LUMO+1(75%), HOMO-1→LUMO+1(14%)			
	331.1	0.35	HOMO→LUMO+2 (70%), HOMO→LUMO+3(12%)			
	306.3	0.19	HOMO-1→LUMO+1(43%), HOMO-2→LUMO (16%), HOMO→LUMO+1 (15%) HOMO-3→LUMO (12%)			
14b	290.2	0.26	HOMO→LUMO+3(49%), HOMO-1→LUMO+2 (12%), HOMO→LUMO+2 (11%)	-5.77	-2.08	7.02
	283.3	0.28	HOMO-1→LUMO+2 (31%), HOMO-3→LUMO (23%), HOMO→LUMO+5 (14%)			
	430.7	1.49	HOMO→LUMO (72%), HOMO-1→LUMO (16%)			
	356.3	0.38	HOMO-1→LUMO (71%), HOMO→LUMO (15%)			
	338.2	0.16	HOMO→LUMO+1(61%), HOMO→LUMO+2 (18%), HOMO→LUMO (11%)			
	291.9	0.11	HOMO-2→LUMO (41%), HOMO-3→LUMO (19%), HOMO→LUMO+3 (16%)			
268.8	0.10	HOMO→LUMO+5 (61%)				
265.9	0.16	HOMO-4→LUMO (21%), HOMO-6→LUMO (12%), HOMO-3→LUMO (11%)				

[a] Contributions of less than 10% are omitted

Table 4.7 Computed vertical transition energies, oscillator strengths (*f*), and their assignment for the dyes^[a] MPW1K (THF)

Dye	$\lambda_{\text{abs}}/\text{nm}$	<i>f</i>	Configuration	HOMO, ev	LUMO, ev	μ_{g} , [D]
11a	526.6	1.23	HOMO→LUMO (73%), HOMO-1→LUMO (21%)	-5.87	-2.61	4.99
	416.2	0.23	HOMO-1→LUMO (71%), HOMO→LUMO (22%)			
	369.0	0.18	HOMO→LUMO+1(65%), HOMO-1→LUMO+1(27%)			
	336.4	0.29	HOMO→LUMO+2 (64%)			
	330.6	0.16	HOMO-2→LUMO (55%), HOMO-3→LUMO (24%)			
	292.2	0.33	HOMO-1→LUMO+2 (25%), HOMO-3→LUMO (20%), HOMO→LUMO+3(16%)			
11b	493.6	1.78	HOMO→LUMO (72%), HOMO-1→LUMO (22%)	-5.86	-2.42	14.14
	393.3	0.17	HOMO-1→LUMO (69%), HOMO→LUMO (20%)			
	347.3	0.22	HOMO→LUMO+1 (68%), HOMO→LUMO+2(13%)			
	319.4	0.11	HOMO-2→LUMO (37%), HOMO-3→LUMO (16%), HOMO-1→LUMO+1(15%) HOMO→LUMO+2 (15%)			
14a	277.8	0.22	HOMO→LUMO+3 (29%), HOMO→LUMO+2(19%), HOMO-8→LUMO (13%)	-5.88	-2.38	10.72
	474.8	1.24	HOMO→LUMO (72%), HOMO-1→LUMO (18%)			
	378.3	0.23	HOMO-1→LUMO (67%), HOMO→LUMO (20%)			
	357.4	0.11	HOMO→LUMO+1 (73%), HOMO-1→LUMO+1(14%)			
	333.4	0.46	HOMO→LUMO+2 (72%)			
	309.1	0.13	HOMO-1→LUMO+1 (41%), HOMO→LUMO+1 (17%), HOMO-3→LUMO (14%) HOMO-2→LUMO (13%)			
14b	291.9	0.32	HOMO→LUMO+3 (54%), HOMO-1→LUMO+2 (13%)	-5.86	-2.20	8.40
	282.6	0.31	HOMO-1→LUMO+2 (30%), HOMO-3→LUMO (18%), HOMO→LUMO+4 (15%)			
	442.5	1.67	HOMO→LUMO (69%), HOMO-1→LUMO (18%)			
	360.2	0.28	HOMO-1→LUMO (67%), HOMO→LUMO (15%)			
	344.1	0.24	HOMO→LUMO+1 (61%), HOMO→LUMO (15%), HOMO→LUMO+2 (14%)			
	294.0	0.14	HOMO-2→LUMO (33%), HOMO-3→LUMO (23%), HOMO→LUMO+3 (14%)			
269.2	0.28	HOMO→LUMO+5 (24%), HOMO-4→LUMO (14%), HOMO-5→LUMO (14%), HOMO-1→LUMO+2 (10%)				

[a] Contributions of less than 10% are omitted

Effect of auxiliary acceptor on optical properties

On altering the conjugation pathway of the π -linker that connects the auxiliary acceptor and cyanoacrylic acid from thiophene to phenyl, decreased the oscillator strength of the lower energy transition. However, the oscillator strengths for the lower energy transitions for benzotriazole dyes (1.67-1.78) are higher when compared with benzothiadiazole analogs (1.24-1.30), which are in good agreement with the parameters observed experimentally. The TD-DFT calculations evoked that the introduction of thiophene unit decreases the LUMO energy level and reduces the energy gap for the HOMO \rightarrow LUMO transition. It appears that by altering the auxiliary acceptor and π -linker in a D- π -A- π -A architecture, the LUMO levels can be adjusted while retaining the HOMO levels. The HOMO and LUMO energy levels of the sensitizers present in the narrow ranges 5.88-5.86 and 2.20-2.61 eV, respectively. The HOMO-LUMO gap of the dyes ranged 3.26-3.66 eV and slightly decreased on the extension of the conjugation with thiophene. These subtle differences in the photophysical properties and electrochemical properties resulted from modulation of auxiliary acceptor and π -linker may contribute to the different DSSC performance based on these four dyes.

Figure 4.14 Computed dihedral angles between the different aryl groups in the dyes.

Figure 4.14 displays the dihedral angles between neighboring aromatic segments in the sensitizers. The dihedral angles between the phenothiazine moiety and the thienyl ring in all molecules were as large as 23.45-25.24° and butterfly geometry of the phenothiazine and persists good amount of non-planarity, which could help to suppress dye aggregation when sensitizers were loaded on TiO₂ films. Because of a relatively smaller dihedral angle between the thienyl segment and auxiliary acceptor moieties, π -electrons from the donor moiety can delocalize effectively to the acceptor moiety. The dihedral angles between auxiliary acceptors and phenyl ring (26.31-33.57°) are larger than those between auxiliary acceptors and thienyl ring (0.15-0.93°). The lower dihedral angle ensured good molecular co-planarity and resulted in

the larger red-shift of the absorption band in the optical spectra of **11a-b**. Whilst due to the larger dihedral angle in the dyes **14a-b**, the charge transfer was jeopardized and resulted blue-shifted absorption profile. These results reveal that the sensitizers bearing thiophene segment as a π -linker shows excellent planarity and may be beneficial for intramolecular charge transfer. In all the sensitizers, the cyanoacrylic acid segment is found to be coplanar with the adjacent π -spacer unit (thiophene/phenyl), pointing a facile extension of conjugation between the π -spacer and cyanoacrylic acid groups.

4.3 Conclusions

In summary, we have synthesized four new phenothiazine donor based sensitizers, comprising benzothiadiazole/benzotriazole auxiliary acceptors and the cyanoacrylic acid unit as an electron acceptor to form D- π -A- π -A conjugated systems. The sensitizers synthesized in good yields using standard synthetic protocols and analytically characterized with IR, NMR (^1H & ^{13}C) and HR-MS. The magnitude of light harvesting property was highly dependent on the nature of the auxiliary acceptor and π -bridge which connects the auxiliary acceptor and cyanoacrylic acid (acceptor) units. As thiophene unit enhances the conjugation and facilitates charge-transfer process than phenyl unit, dyes **11a** and **11b** showed better photophysical properties than that of phenyl conjugated dyes **14a** and **14b**, respectively. As manifested by the absorption properties, the increase in the electron-accepting strength and conjugation length ensued in the broadening and the enhancement of the ICT transition. Compared to benzotriazole bridged sensitizers, benzothiadiazole sensitizers displayed lower band gap owing to the low LUMO energy level. Interestingly, the two auxiliary acceptors played different roles in absorption and electro chemistry. The absorption, electrochemical properties and TDDFT computations of the dyes were in accordance with the electron-withdrawing ability of the auxiliary acceptor and π -conjugating segment. However, trends in the oscillator strengths of the lower energy transitions from benzothiadiazole dyes to benzotriazole dyes are in the increasing order, which are well match with the trend of increasing molar extinction coefficients. Similar structures of auxiliary acceptors which differ only the hetero atom present on the 2-position allowed a systematic comparative investigations in choice of the auxiliary acceptors in D-A- π -A dyes for DSSCs. The HOMO and LUMO energy levels of the four sensitizers are ideal to be promising material for DSSC devices. These findings will shed light to understand the crucial

importance of molecular engineering with auxiliary acceptor for high efficient dye-sensitized solar cells.

4.4 Experimental section

4.4.1 Materials and physical methods

Materials and physical methods are similar as in chapter 3.

Synthesis of 5-(7-(5-(10-butyl-10*H*-phenothiazin-3-yl)thiophen-2-yl)benzo[*c*][1,2,5]thiadiazol-4-yl)thiophene-2-carbaldehyde (10a)

A round bottom flask was charged with 5-(7-bromobenzo[*c*][1,2,5]thiadiazol-4-yl)thiophene-2-carbaldehyde (0.14 g, 0.4 mmol), 10-butyl-3-(5-(tributylstannyl)thiophen-2-yl)-10*H*-phenothiazine (0.5 mmol) and 5 mL DMF. Nitrogen was purged into this, followed by the addition of Pd(PPh₃)₂Cl₂ (4.0 mg). This was kept on heating at 80 °C for 16 h under a nitrogen atmosphere. After completion of reaction time, the mixture was poured into cold water and extracted with dichloromethane followed by washing with brine solution and dried over anhydrous Na₂SO₄. Then the solvent was evaporated by applying vacuum. The resultant liquid was dissolved in 5 ml acetic acid and heated to 60 °C for 30 min. Then 10 mL of water was added to it and heating was continued for 6h. The resulting solution was extracted with dichloromethane and washed with brine solution and dried over anhydrous sodium sulfate. Further purification was performed by silica gel column chromatography using hexane/dichloromethane. Black solid; Yield = 0.13 g (57%); m.p. 90-92 °C; IR (KBr, cm⁻¹): $\bar{\nu}$ = 1659 (C=O); ¹H NMR (CDCl₃, 500.13 MHz): δ = 0.96 (t, *J* = 7.5 Hz, 3H), 1.48-1.49 (m, 2H), 1.79-1.85 (m, 2H), 3.88 (t, *J* = 7.0 Hz, 2H), 6.87-6.89 (m, 2H), 6.92-6.95 (m, 1H), 7.14-7.19 (m, 2H), 7.31 (d, *J* = 4.0 Hz, 1H), 7.46-7.49 (m, 2H), 7.84 (d, *J* = 4.0 Hz, 1H) 7.89 (d, *J* = 7.5 Hz, 1H), 8.00 (d, *J* = 7.5 Hz, 1H), 8.14 (d, *J* = 2.0 Hz, 1H), 8.21 (d, *J* = 4 Hz, 1H), 9.97 (s, 1H); ¹³C NMR (CDCl₃, 125.77 MHz): δ = 13.9, 20.2, 29.0, 47.3, 115.4, 115.5, 122.6, 123.2, 123.9, 124.0, 124.4, 124.8, 125.4, 127.38, 127.40, 127.5, 127.8, 127.9, 128.2, 129.5, 136.8, 137.2, 143.2, 144.7, 145.1 145.8, 148.7, 152.3, 152.4, 183.0; HRMS (ESI): *m/z* calcd for C₃₁H₂₃N₃OS₄: 581.0724 [M⁺]; found: 581.0704.

Synthesis of 5-(2-butyl-7-(5-(10-butyl-10*H*-phenothiazin-3-yl)thiophen-2-yl)-2*H*-benzo[*d*][1,2,3]triazol-4-yl)thiophene-2-carbaldehyde (10b)

Compound **10b** was prepared from **9b** by following a similar procedure as described for **10a**. Red solid; Yield = 71%; m.p. 148-150 °C; IR (KBr, cm⁻¹): $\bar{\nu}$ = 1660 (C=O); ¹H NMR (CDCl₃,

500.13 MHz): δ = 0.99 (t, J = 7 Hz, 3H), 1.06 (t, J = 7 Hz, 3H), 1.47-1.54 (m, 4H), 1.78-1.88 (m, 2H), 2.22-2.25 (m, 2H), 3.91 (t, J = 7.0 Hz, 2H), 4.88 (t, J = 7.0 Hz, 2H), 6.93-6.95 (m, 2H), 6.97 (t, J = 6.5 Hz, 1H), 7.17-7.19 (m, 2H), 7.32 (d, J = 3.5 Hz, 1H), 7.48-7.50 (m, 2H), 7.67 (d, J = 7.5 Hz, 1H), 7.80 (d, J = 8.0 Hz, 1H), 7.85 (d, J = 4.0 Hz, 1H), 8.14 (d, J = 4.0 Hz, 1H), 8.19 (d, J = 4.0 Hz, 1H), 9.98 (s, 1H); ^{13}C NMR (CDCl_3 , 125.770 MHz): δ = 13.5, 13.8, 19.9, 20.2, 28.9, 32.1, 47.2, 56.7, 115.4, 115.4, 121.6, 121.9, 122.6, 123.4, 124.1, 124.4, 124.4, 124.8, 125.3, 125.9, 127.2, 127.3, 127.5, 128.5, 129.0, 137.8, 141.8, 142.4, 144.5, 144.8, 144.9, 149.7, 182.9; HRMS (ESI): m/z calcd for $\text{C}_{35}\text{H}_{32}\text{N}_4\text{NaOS}_3$: 643.1636 $[\text{M}+\text{Na}]^+$; found: 643.1615.

Synthesis of 4-(7-(5-(10-butyl-10*H*-phenothiazin-3-yl)thiophen-2-yl)benzo[*c*][1,2,5]thiadiazol-4-yl)benzaldehyde (13a)

Compound **13a** was prepared from **12a** by following a similar procedure as described for **10a**. Dark red solid; Yield = 58%; m.p. 90-92 °C; IR (KBr, cm^{-1}): $\bar{\nu}$ = 1636 (C=O); ^1H NMR (CDCl_3 , 500.13 MHz): δ = 0.89 (t, J = 8 Hz, 3H), 1.38-1.45 (m, 2H), 1.66-1.72 (m, 2H), 3.91 (t, J = 7.0 Hz, 3H), 6.97 (t, J = 7.0 Hz, 3H), 7.05-7.09 (m, 2H), 7.17 (d, J = 7.0 Hz, 1H), 7.22 (t, J = 7.0 Hz, 1H), 7.54 (s, 1H), 7.56-7.60 (m, 2H), 8.04-8.08 (m, 3H), 8.20 (t, J = 4.0 Hz, 2H), 8.26 (d, J = 8.0 Hz, 2H), 10.10 (s, 1H); ^{13}C NMR ($\text{DMSO}-d_6$, 125.77 MHz): δ = 13.6, 19.3, 28.3, 46.8, 115.9, 116.1, 122.6, 122.8, 123.5, 123.8, 124.3, 124.8, 125.0, 126.3, 127.1, 127.7, 127.8, 129.1, 129.3, 129.6, 129.9, 135.4, 136.6, 142.3, 144.1, 144.5, 144.6, 151.7, 152.9, 192.6; HRMS (ESI): m/z calcd for $\text{C}_{33}\text{H}_{25}\text{N}_3\text{OS}_3$: 575.1160 $[\text{M}]^+$; found: 575.1133.

Synthesis of 4-(2-butyl-7-(5-(10-butyl-10*H*-phenothiazin-3-yl)thiophen-2-yl)-2*H*-benzo[*d*][1,2,3]triazol-4-yl)benzaldehyde (13b)

Compound **13b** was prepared from **12b** by following a similar procedure as described for **10a**. Orange solid; Yield = 66%; m.p. 125-127 °C; IR (KBr, cm^{-1}): $\bar{\nu}$ = 1645 (C=O); ^1H NMR (CDCl_3 , 500.13 MHz): δ = 0.90 (t, J = 7.0 Hz, 3H), 1.05 (t, J = 7.0 Hz, 3H), 1.49-1.54 (m, 4H), 1.82 (t, J = 7.0 Hz, 2H), 2.19 (t, J = 7.5 Hz, 2H), 3.88 (t, J = 7.0 Hz, 2H), 4.84 (t, J = 7.0 Hz, 2H), 6.90-6.92 (m, 2H), 6.93 (t, J = 7.0 Hz, 1H), 7.16 (d, J = 7.5 Hz, 2H), 7.30 (d, J = 3.5 Hz, 1H), 7.46-7.48 (m, 2H), 7.66-7.72 (m, 2H), 8.02 (d, J = 8.5 Hz, 2H), 8.11 (d, J = 3.5 Hz, 1H), 8.27 (d, J = 8.0 Hz, 2H), 10.09 (s, 1H); ^{13}C NMR (CDCl_3 , 125.770 MHz): δ = 13.4, 13.7, 19.8, 20.0, 28.8, 32.0, 47.1, 56.5, 115.3, 122.0, 122.4, 123.2, 124.0, 124.3, 124.6, 125.1, 125.3, 127.2, 127.3, 127.6, 128.5, 128.7, 129.9, 135.2, 137.9, 142.0, 143.0, 143.1, 143.9, 144.7, 191.8; HRMS (ESI): m/z calcd for $\text{C}_{37}\text{H}_{35}\text{N}_4\text{OS}_2$: 615.2252 $[\text{M}+\text{H}]^+$; found: 615.2225.

Synthesis of (*E*)-3-(5-(7-(5-(10-butyl-10*H*-phenothiazin-3-yl)thiophen-2-yl)benzo[*c*][1,2,5]thiadiazol-4-yl)thiophen-2-yl)-2-cyanoacrylic acid (11a)

A mixture of **10a** (0.105 g, 0.18 mmol), cyanoacetic acid (0.03 g, 0.36 mmol), ammonium acetate (10 mg), and glacial acetic acid (15 mL) were heated under reflux for 12 h. Cooling the reaction mixture to room temperature produced a black precipitate, which was filtered and washed with water for several times. The analytically pure product was obtained by recrystallization from a DCM/hexanes mixture (1:3, 10 mL) as a black solid; Yield = 0.106 g (91%); m.p. 250-252 °C; IR (KBr, cm⁻¹): $\bar{\nu}$ = 2209 (C=N); ¹H NMR (DMSO-*d*₆, 500.13 MHz): δ = 0.90 (t, *J* = 7.0 Hz, 3H), 1.39-1.44 (m, 2H), 1.66-1.70 (m, 2H), 3.90 (t, *J* = 6.5 Hz, 2H), 6.97 (t, *J* = 7.4 Hz, 1H), 7.04-7.06 (m, 2H), 7.18 (d, *J* = 7.5 Hz, 1H), 7.22 (t, *J* = 7.5 Hz, 1H), 7.51-7.58 (m, 3H), 8.07 (s, 1H), 8.14 (d, *J* = 7.5 Hz, 1H), 8.19 (s, 1H), 8.27-8.31 (m, 2H), 8.52 (s, 1H); ¹³C NMR (DMSO-*d*₆, 125.77 MHz): δ = 13.7, 19.4, 28.3, 46.3, 115.9, 116.1, 116.6, 122.7, 122.8, 123.1, 123.6, 124.0, 124.3, 124.9, 126.8, 127.2, 127.7, 127.8, 129.6, 136.5, 136.7, 139.9, 144.2, 144.6, 145.2, 146.4, 147.4, 151.4, 151.9, 163.6; HRMS (ESI):m/z calcd for C₃₄H₂₄N₄NaO₂S₄: 671.0680 [M+Na]⁺; found: 671.0680.

Synthesis of (*E*)-3-(5-(2-butyl-7-(5-(10-butyl-10*H*-phenothiazin-3-yl)thiophen-2-yl)-2*H*-benzo[*d*][1,2,3]triazol-4-yl)thiophen-2-yl)-2-cyanoacrylic acid (11b)

Compound **11b** was prepared from **10b** by following a similar procedure as described for **11a**. Black solid; Yield = 93%; m.p. 240-242 °C; IR (KBr, cm⁻¹): $\bar{\nu}$ = 2219 (C=N); ¹H NMR (DMSO-*d*₆, 500.13 MHz): δ = 0.88 (t, *J* = 7.0 Hz, 3H), 0.95 (t, *J* = 7.0 Hz, 3H), 1.36-1.40 (m, 2H), 1.65-1.67 (m, 2H), 2.10 (t, *J* = 7 Hz, 2H), 3.86 (m, 2H), 4.86 (m, 2H), 6.94-7.03 (m, 3H), 7.15-7.26 (m, 2H), 7.46-7.51 (m, 3H), 7.72 (s, 1H), 7.88 (s, 1H), 8.03-8.07 (m, 2H), 8.17 (s, 1H), 8.48 (s, 1H); ¹³C NMR (DMSO-*d*₆, 125.770 MHz): δ = 13.4, 13.6, 19.4, 19.4, 28.3, 31.2, 46.3, 56.1, 115.8, 116.5, 120.5, 121.8, 122.7, 122.8, 123.4, 123.8, 124.1, 124.4, 124.6, 124.7, 127.2, 127.3, 127.7, 129.1, 135.3, 136.9, 140.2, 140.7, 141.0, 143.7, 144.1, 144.3, 146.2, 148.2, 163.7; HRMS (ESI): m/z calcd for C₃₈H₃₃N₅NaO₂S₃: 710.1694 [M+Na]⁺; found: 710.1652.

Synthesis of (*E*)-3-(4-(7-(5-(10-butyl-10*H*-phenothiazin-3-yl)thiophen-2-yl)benzo[*c*][1,2,5]thiadiazol-4-yl)phenyl)-2-cyanoacrylic acid (14a)

Compound **14a** was prepared from **13a** by following a similar procedure as described for **11a**. Black solid; yield = 81 %; m.p. 188-190 °C; IR (KBr, cm⁻¹): $\bar{\nu}$ = 2213 (C=N); ¹H NMR (DMSO-*d*₆, 500.13 MHz): δ = 0.90 (t, *J* = 7.0 Hz, 3H), 1.40-1.45 (m, 2H), 1.70 (t, *J* = 7.0 Hz, 2H), 3.91 (t, *J* = 7.0 Hz, 3H), 6.97 (t, *J* = 7.0 Hz, 1H), 7.05-7.09 (m, 2H), 7.17-7.24 (m, 2H),

7.54-7.61 (m, 3H), 8.06 (d, $J = 7.0$ Hz, 1H), 8.14-8.26 (m, 7H); ^{13}C NMR (DMSO- d_6 , 125.77 MHz): $\delta = 13.5, 19.3, 28.3, 46.2, 115.8, 116.0, 122.6, 122.8, 123.5, 123.7, 124.3, 124.7, 125.0, 126.1, 127.1, 127.7, 127.8, 128.9, 129.0, 129.4, 129.8, 130.3, 136.6, 144.1, 144.4, 144.5, 151.7, 152.9, 163.1$; HRMS (ESI): m/z calcd for $\text{C}_{36}\text{H}_{26}\text{N}_4\text{NaO}_2\text{S}_3$: 665.1116 $[\text{M}+\text{Na}]^+$; found: 665.1147.

Synthesis of (*E*)-3-(4-(2-butyl-7-(5-(10-butyl-10*H*-phenothiazin-3-yl)thiophen-2-yl)-2*H*-benzo[*d*][1,2,3]triazol-4-yl)phenyl)-2-cyanoacrylic acid (14b**)**

Compound **14b** was prepared from **13b** by following a similar procedure as described for **11a**. Black solid; Yield = 63 %; m.p. 230-232 °C; IR (KBr, cm^{-1}): $\bar{\nu} = 2217$ (C=N); ^1H NMR (DMSO- d_6 , 500.13 MHz): $\delta = 0.89$ (t, $J = 7.5$ Hz, 3H), 0.94 (t, $J = 7.5$ Hz, 3H), 1.35-1.44 (m, 4H), 1.67-1.70 (m, 2H), 2.05-2.10 (m, 2H), 3.90 (t, $J = 6.5$ Hz, 2H), 4.90 (t, $J = 7.0$ Hz, 2H), 6.95-6.98 (m, 1H), 7.04-7.08 (m, 2H), 7.17-7.18 (m, 1H), 7.21-7.24 (m, 1H), 7.51-7.55 (m, 2H), 7.58 (d, $J = 4.0$ Hz, 1H), 7.85 (d, $J = 7.5$ Hz, 1H), 7.92 (d, $J = 8.0$ Hz, 1H), 8.13 (d, $J = 3.5$ Hz, 1H), 8.18 (d, $J = 8.5$ Hz, 2H), 8.35-8.37 (m, 3H); ^{13}C NMR (DMSO- d_6 , 125.770 MHz): $\delta = 13.4, 13.7, 19.3, 19.4, 28.3, 31.6, 42.7, 56.2, 115.9, 116.1, 116.7, 122.2, 122.7, 122.8, 123.6, 124.1, 124.3, 124.8, 125.4, 126.8, 127.2, 127.8, 127.9, 128.5, 128.9, 131.0, 137.2, 140.4, 141.3, 142.4, 143.4, 144.2, 144.4, 152.8, 163.4$; HRMS (ESI): m/z calcd for $\text{C}_{40}\text{H}_{35}\text{N}_5\text{NaO}_2\text{S}_2$: 704.2130 $[\text{M}+\text{Na}]^+$; found: 704.2130.

4.5 References

- (1) A. Yella, R. Humphry-Baker, B. F. E. Curchod, N. Ashari Astani, J. Teuscher, L. E. Polander, S. Mathew, J.-E. Moser, I. Tavernelli, U. Rothlisberger, M. Grätzel, M. K. Nazeeruddin and J. Frey, Molecular Engineering of a Fluorene Donor for Dye-Sensitized Solar Cells. *Chem. Mater.* **2013**, *25*, 2733-9.
- (2) R. Yeh-Yung Lin, H.-W. Lin, Y.-S. Yen, C.-H. Chang, H.-H. Chou, P.-W. Chen, C.-Y. Hsu, Y.-C. Chen, J. T. Lin and K.-C. Ho, 2,6-Conjugated anthracene sensitizers for high-performance dye-sensitized solar cells. *Energy & Environmental Science* **2013**, *6*, 2477-86.
- (3) M. Zhang, Y. Wang, M. Xu, W. Ma, R. Li and P. Wang, Design of high-efficiency organic dyes for titania solar cells based on the chromophoric core of cyclopentadithiophene-benzothiadiazole. *Energy & Environmental Science* **2013**, *6*, 2944-9.

- (4) A. Mishra, M. K. R. Fischer and P. Bäuerle, Metal-Free Organic Dyes for Dye-Sensitized Solar Cells: From Structure: Property Relationships to Design Rules. *Angew. Chem., Int. Ed.* **2009**, *48*, 2474-99.
- (5) M. Liang and J. Chen, Arylamine organic dyes for dye-sensitized solar cells. *Chem. Soc. Rev.* **2013**, *42*, 3453-88.
- (6) X. Qian, Y.-Z. Zhu, J. Song, X.-P. Gao and J.-Y. Zheng, New Donor- π -Acceptor Type Triazatruxene Derivatives for Highly Efficient Dye-Sensitized Solar Cells. *Org. Lett.* **2013**, *15*, 6034-7.
- (7) R. F. Fink, J. Seibt, V. Engel, M. Renz, M. Kaupp, S. Lochbrunner, H.-M. Zhao, J. Pfister, F. Würthner and B. Engels, Exciton Trapping in π -Conjugated Materials: A Quantum-Chemistry-Based Protocol Applied to Perylene Bisimide Dye Aggregates. *J. Am. Chem. Soc.* **2008**, *130*, 12858-9.
- (8) S. Tatay, S. A. Haque, B. O'Regan, J. R. Durrant, W. J. H. Verhees, J. M. Kroon, A. Vidal-Ferran, P. Gavina and E. Palomares, Kinetic competition in liquid electrolyte and solid-state cyanine dye sensitized solar cells. *J. Mater. Chem.* **2007**, *17*, 3037-44.
- (9) Y. Hua, S. Chang, D. Huang, X. Zhou, X. Zhu, J. Zhao, T. Chen, W.-Y. Wong and W.-K. Wong, Significant Improvement of Dye-Sensitized Solar Cell Performance Using Simple Phenothiazine-Based Dyes. *Chem. Mater.* **2013**, *25*, 2146-53.
- (10) T. Sudyoasuk, S. Pansay, S. Morada, R. Rattanawan, S. Namuangruk, T. Kaewin, S. Jungsuttiwong and V. Promarak, Synthesis and Characterization of D-D- π -A-Type Organic Dyes Bearing Carbazole-Carbazole as a Donor Moiety (D-D) for Efficient Dye-Sensitized Solar Cells. *Eur. J. Org. Chem.* **2013**, *2013*, 5051-63.
- (11) A. Baheti, P. Singh, C. P. Lee, K. R. Thomas and K. C. Ho, 2,7-Diaminofluorene-based organic dyes for dye-sensitized solar cells: effect of auxiliary donor on optical and electrochemical properties. *J. Org. Chem.* **2011**, *76*, 4910-20.
- (12) K. R. J. Thomas, N. Kapoor, C. P. Lee and K. C. Ho, Organic dyes containing pyrenylamine-based cascade donor systems with different aromatic pi linkers for dye-sensitized solar cells: optical, electrochemical, and device characteristics. *Chem.-Asian J.* **2012**, *7*, 738-50.
- (13) M. Velusamy, K. R. Justin Thomas, J. T. Lin, Y.-C. Hsu and K.-C. Ho, Organic Dyes Incorporating Low-Band-Gap Chromophores for Dye-Sensitized Solar Cells. *Org. Lett.* **2005**, *7*, 1899-902.

- (14) M. D. Zhang, H. X. Xie, X. H. Ju, L. Qin, Q. X. Yang, H. G. Zheng and X. F. Zhou, D- π -A organic dyes containing 4,4'-di(2-thienyl)triphenylamine moiety for efficient dye-sensitized solar cells. *Phys. Chem. Chem. Phys.* **2013**, *15*, 634-41.
- (15) A. Baheti, K. R. J. Thomas, C.-P. Lee and K.-C. Ho, Fine Tuning the Performance of DSSCs by Variation of the π -Spacers in Organic Dyes that Contain a 2,7-Diaminofluorene Donor. *Chem.-Asian J.* **2012**, *7*, 2942-54.
- (16) Q. Feng, X. Jia, G. Zhou and Z.-S. Wang, Embedding an electron donor or acceptor into naphtho[2,1-*b*:3,4-*b'*]dithiophene based organic sensitizers for dye-sensitized solar cells. *Chem. Commun.* **2013**, *49*, 7445-7.
- (17) K. R. J. Thomas, P. Singh, A. Baheti, Y.-C. Hsu, K.-C. Ho and J. T. Lin, Electro-optical properties of new anthracene based organic dyes for dye-sensitized solar cells. *Dyes Pigm.* **2011**, *91*, 33-43.
- (18) D. H. Lee, M. J. Lee, H. M. Song, B. J. Song, K. D. Seo, M. Pastore, C. Anselmi, S. Fantacci, F. De Angelis, M. K. Nazeeruddin, M. Grätzel and H. K. Kim, Organic dyes incorporating low-band-gap chromophores based on π -extended benzothiadiazole for dye-sensitized solar cells. *Dyes Pigm.* **2011**, *91*, 192-8.
- (19) K. D. Seo, I. T. Choi, Y. G. Park, S. Kang, J. Y. Lee and H. K. Kim, Novel D-A- π -A coumarin dyes containing low band-gap chromophores for dye-sensitised solar cells. *Dyes Pigm.* **2012**, *94*, 469-74.
- (20) S. Cai, X. Hu, Z. Zhang, J. Su, X. Li, A. Islam, L. Han and H. Tian, Rigid triarylamine-based efficient DSSC sensitizers with high molar extinction coefficients. *J. Mater. Chem. A* **2013**, *1*, 4763.
- (21) S. Cai, G. Tian, X. Li, J. Su and H. Tian, Efficient and stable DSSC sensitizers based on substituted dihydroindolo[2,3-*b*]carbazole donors with high molar extinction coefficients. *J. Mater. Chem. A* **2013**, *1*, 11295.
- (22) J. Mao, F. Guo, W. Ying, W. Wu, J. Li and J. Hua, Benzotriazole-bridged sensitizers containing a furan moiety for dye-sensitized solar cells with high open-circuit voltage performance. *Chem.-Asian J.* **2012**, *7*, 982-91.
- (23) Y. S. Yen, C. T. Lee, C. Y. Hsu, H. H. Chou, Y. C. Chen and J. T. Lin, Benzotriazole-containing D- π -A conjugated organic dyes for dye-sensitized solar cells. *Chem.-Asian J.* **2013**, *8*, 809-16.

- (24) Y. Cui, Y. Wu, X. Lu, X. Zhang, G. Zhou, F. B. Miapah, W. Zhu and Z.-S. Wang, Incorporating Benzotriazole Moiety to Construct D-A- π -A Organic Sensitizers for Solar Cells: Significant Enhancement of Open-Circuit Photovoltage with Long Alkyl Group. *Chem. Mater.* **2011**, *23*, 4394-401.
- (25) S. Qu, C. Qin, A. Islam, J. Hua, H. Chen, H. Tian and L. Han, Tuning the electrical and optical properties of diketopyrrolopyrrole complexes for panchromatic dye-sensitized solar cells. *Chem.-Asian J.* **2012**, *7*, 2895-903.
- (26) T. W. Holcombe, J. H. Yum, J. Yoon, P. Gao, M. Marszalek, D. Di Censo, K. Rakstys, M. K. Nazeeruddin and M. Graetzel, A structural study of DPP-based sensitizers for DSC applications. *Chem. Commun.* **2012**, *48*, 10724-6.
- (27) W. Ying, F. Guo, J. Li, Q. Zhang, W. Wu, H. Tian and J. Hua, Series of new D-A- π -A organic broadly absorbing sensitizers containing isoindigo unit for highly efficient dye-sensitized solar cells. *ACS Appl. Mater. Interfaces* **2012**, *4*, 4215-24.
- (28) K. Pei, Y. Wu, A. Islam, Q. Zhang, L. Han, H. Tian and W. Zhu, Constructing high-efficiency D-A- π -A-featured solar cell sensitizers: a promising building block of 2,3-diphenylquinoxaline for antiaggregation and photostability. *ACS Appl. Mater. Interfaces* **2013**, *5*, 4986-95.
- (29) S. R. Li, C. P. Lee, H. T. Kuo, K. C. Ho and S. S. Sun, High-performance dipolar organic dyes with an electron-deficient diphenylquinoxaline moiety in the π -conjugation framework for dye-sensitized solar cells. *Chem.-Eur. J.* **2012**, *18*, 12085-95.
- (30) K. Pei, Y. Wu, W. Wu, Q. Zhang, B. Chen, H. Tian and W. Zhu, Constructing organic D-A- π -A-featured sensitizers with a quinoxaline unit for high-efficiency solar cells: the effect of an auxiliary acceptor on the absorption and the energy level alignment. *Chem.-Eur. J.* **2012**, *18*, 8190-200.
- (31) S.-R. Li, C.-P. Lee, H.-T. Kuo, K.-C. Ho and S.-S. Sun, High-Performance Dipolar Organic Dyes with an Electron-Deficient Diphenylquinoxaline Moiety in the π -Conjugation Framework for Dye-Sensitized Solar Cells *Chem.-Eur. J.* **2012**, *18*, 12085-95.
- (32) J. Shi, Z. Chai, J. Su, J. Chen, R. Tang, K. Fan, L. Zhang, H. Han, J. Qin, T. Peng, Q. Li and Z. Li, New sensitizers bearing quinoxaline moieties as an auxiliary acceptor for dye-sensitized solar cells. *Dyes Pigm.* **2013**, *98*, 405-13.
- (33) W. Li, Y. Wu, Q. Zhang, H. Tian and W. Zhu, D-A- π -A featured sensitizers bearing phthalimide and benzotriazole as auxiliary acceptor: effect on absorption and charge

- recombination dynamics in dye-sensitized solar cells. *ACS Appl. Mater. Interfaces* **2012**, *4*, 1822-30.
- (34) Y. Wu and W. Zhu, Organic sensitizers from D- π -A to D-A- π -A: effect of the internal electron-withdrawing units on molecular absorption, energy levels and photovoltaic performances. *Chem. Soc. Rev.* **2013**, *42*, 2039-58.
- (35) W. Zhang, Q. Feng, Z. S. Wang and G. Zhou, Novel thiazolo[5,4-*d*]thiazole-based organic dyes for quasi-solid-state dye-sensitized solar cells. *Chem.-Asian J.* **2013**, *8*, 939-46.
- (36) L. Zani, G. Reginato, A. Mordini, M. Calamante, M. Peruzzini, M. Taddei, A. Sinicropi, M. L. Parisi, F. Fabrizi de Biani, R. Basosi, A. Cavallaro and M. Bruzzi, An unusual thiazolo[5,4-*d*]thiazole sensitizer for dye-sensitized solar cells. *Tetrahedron Lett.* **2013**, *54*, 3944-8.
- (37) A. Dessì, G. Barozzino Consiglio, M. Calamante, G. Reginato, A. Mordini, M. Peruzzini, M. Taddei, A. Sinicropi, M. L. Parisi, F. Fabrizi de Biani, R. Basosi, R. Mori, M. Spatola, M. Bruzzi and L. Zani, Organic Chromophores Based on a Fused Bis-Thiazole Core and Their Application in Dye-Sensitized Solar Cells. *Eur. J. Org. Chem.* **2013**, *2013*, 1916-28.
- (38) Y. Wu and W. Zhu, Organic sensitizers from D- π -A to D-A- π -A: effect of the internal electron-withdrawing units on molecular absorption, energy levels and photovoltaic performances. *Chem. Soc. Rev.* **2013**, *42*, 2039-58.
- (39) Y. H. Chen, L. Y. Lin, C. W. Lu, F. Lin, Z. Y. Huang, H. W. Lin, P. H. Wang, Y. H. Liu, K. T. Wong, J. Wen, D. J. Miller and S. B. Darling, Vacuum-deposited small-molecule organic solar cells with high power conversion efficiencies by judicious molecular design and device optimization. *J. Am. Chem. Soc.* **2012**, *134*, 13616-23.
- (40) P. Li, H. Tong, J. Ding, Z. Xie and L. Wang, Small molecules based on 2,7-carbazole for efficient solution-processed organic solar cells. *J. Mater. Chem. A* **2013**, *1*, 8805.
- (41) S. Steinberger, A. Mishra, E. Reinold, J. Levichkov, C. Uhrich, M. Pfeiffer and P. Bauerle, Vacuum-processed small molecule solar cells based on terminal acceptor-substituted low-band gap oligothiophenes. *Chem Commun* **2011**, *47*, 1982-4.
- (42) J. J. Chen, T. L. Chen, B. Kim, D. A. Poulsen, J. L. Mynar, J. M. Frechet and B. Ma, Quinacridone-based molecular donors for solution processed bulk-heterojunction organic solar cells. *ACS Appl. Mater. Interfaces* **2010**, *2*, 2679-86.

- (43) P. Dutta, J. Kim, S. H. Eom, W. H. Lee, I. N. Kang and S. H. Lee, An easily accessible donor-pi-acceptor-conjugated small molecule from a 4,8-dialkoxybenzo[1,2-*b*:4,5-*b'*]dithiophene unit for efficient solution-processed organic solar cells. *ACS Appl. Mater. Interfaces* **2012**, *4*, 6669-75.
- (44) L. Zhang, C. He, J. Chen, P. Yuan, L. Huang, C. Zhang, W. Cai, Z. Liu and Y. Cao, Bulk-Heterojunction Solar Cells with Benzotriazole-Based Copolymers as Electron Donors: Largely Improved Photovoltaic Parameters by Using PFN/Al Bilayer Cathode. *Macromolecules* **2010**, *43*, 9771-8.
- (45) Y. Dong, W. Cai, X. Hu, C. Zhong, F. Huang and Y. Cao, Synthesis of novel narrow-band-gap copolymers based on [1,2,5]thiadiazolo[3,4-*f*]benzotriazole and their application in bulk-heterojunction photovoltaic devices. *Polymer* **2012**, *53*, 1465-72.
- (46) J. Min, Z.-G. Zhang, S. Zhang and Y. Li, Conjugated Side-Chain-Isolated D–A Copolymers Based on Benzo[1,2-*b*:4,5-*b'*]dithiophene-alt-dithienylbenzotriazole: Synthesis and Photovoltaic Properties. *Chem. Mater.* **2012**, *24*, 3247-54.
- (47) B. A. D. Neto, A. A. M. Lapis, E. N. da Silva Júnior and J. Dupont, 2,1,3-Benzothiadiazole and Derivatives: Synthesis, Properties, Reactions, and Applications in Light Technology of Small Molecules. *Eur. J. Org. Chem.* **2013**, *2013*, 228-55.
- (48) T. Khanasa, N. Prachumrak, R. Rattanawan, S. Jungsuttiwong, T. Keawin, T. Sudyoadsuk, T. Tuntulani and V. Promarak, An efficient solution processed non-doped red emitter based on carbazole-triphenylamine end-capped di(thiophen-2-yl)benzothiadiazole for pure red organic light-emitting diodes. *Chem Commun* **2013**, *49*, 3401-3.
- (49) Z. Zhao, J. Geng, Z. Chang, S. Chen, C. Deng, T. Jiang, W. Qin, J. W. Y. Lam, H. S. Kwok, H. Qiu, B. Liu and B. Z. Tang, A tetraphenylethene-based red luminophor for an efficient non-doped electroluminescence device and cellular imaging. *J. Mater. Chem.* **2012**, *22*, 11018.
- (50) D. Tomkute-Luksiene, J. Keruckas, T. Malinauskas, J. Simokaitiene, V. Getautis, J. V. Grazulevicius, D. Volyniuk, V. Cherpak, P. Stakhira, V. Yashchuk, V. Kosach, G. Luka and J. Sidaravicius, 2-Phenyl-1,2,3-benzotriazole Ir(III) complexes with additional donor fragment for single-layer PhOLED devices. *Dyes Pigm.* **2013**, *96*, 278-86.
- (51) C. Duan, F. Huang and Y. Cao, Recent development of push–pull conjugated polymers for bulk-heterojunction photovoltaics: rational design and fine tailoring of molecular structures. *J. Mater. Chem.* **2012**, *22*, 10416.

- (52) A. Tanimoto and T. Yamamoto, Synthesis of n-Type Poly(benzotriazole)s Having p-Conducting and Polymerizable Carbazole Pendants. *Macromolecules* **2006**, *39*, 3546-52.
- (53) S. C. Price, A. C. Stuart, L. Yang, H. Zhou and W. You, Fluorine Substituted Conjugated Polymer of Medium Band Gap Yields 7% Efficiency in Polymer-Fullerene Solar Cells. *J. Am. Chem. Soc.* **2011**, *133*, 4625-31.
- (54) Z. Iqbal, W.-Q. Wu, H. Zhang, P.-L. Hua, X. Fang, D.-B. Kuang, L. Wang, H. Meier and D. Cao, Impact of hydroxy and octyloxy substituents of phenothiazine based dyes on the photovoltaic performance. *Dyes Pigm.* **2013**, *99*, 299-307.
- (55) H. Tian, X. Yang, J. Cong, R. Chen, C. Teng, J. Liu, Y. Hao, L. Wang and L. Sun, Effect of different electron donating groups on the performance of dye-sensitized solar cells. *Dyes Pigm.* **2010**, *84*, 62-8.
- (56) T. Okamoto, M. Kuratsu, M. Kozaki, K. Hirotsu, A. Ichimura, T. Matsushita and K. Okada, Remarkable Structure Deformation in Phenothiazine Trimer Radical Cation. *Org. Lett.* **2004**, *6*, 3493-6.
- (57) S. Agrawal, M. Pastore, G. Marotta, M. A. Reddy, M. Chandrasekharam and F. De Angelis, Optical Properties and Aggregation of Phenothiazine-Based Dye-Sensitizers for Solar Cells Applications: A Combined Experimental and Computational Investigation. *J. Phys. Chem. C* **2013**, *117*, 9613-22.
- (58) X. Kong, A. P. Kulkarni and S. A. Jenekhe, Phenothiazine-Based Conjugated Polymers: Synthesis, Electrochemistry, and Light-Emitting Properties. *Macromolecules* **2003**, *36*, 8992-9.
- (59) S. Haid, M. Marszalek, A. Mishra, M. Wielopolski, J. Teuscher, J.-E. Moser, R. Humphry-Baker, S. M. Zakeeruddin, M. Grätzel and P. Bäuerle, Significant Improvement of Dye-Sensitized Solar Cell Performance by Small Structural Modification in π -Conjugated Donor-Acceptor Dyes. *Adv. Funct. Mater.* **2012**, *22*, 1291-302.
- (60) M. K. Nazeeruddin, A. Kay, I. Rodicio, R. Humphry-Baker, E. Mueller, P. Liska, N. Vlachopoulos and M. Graetzel, Conversion of light to electricity by cis-X₂bis(2,2'-bipyridyl-4,4'-dicarboxylate)ruthenium(II) charge-transfer sensitizers (X = Cl-, Br-, I-, CN-, and SCN-) on nanocrystalline titanium dioxide electrodes. *J. Am. Chem. Soc.* **1993**, *115*, 6382-90.

Effect of auxiliary acceptor on optical properties

- (61) M. K. Nazeeruddin, R. Humphry-Baker, P. Liska and M. Grätzel, Investigation of Sensitizer Adsorption and the Influence of Protons on Current and Voltage of a Dye-Sensitized Nanocrystalline TiO₂ Solar Cell. *J. Phys. Chem. B* **2003**, *107*, 8981-7.
- (62) C. Pérez León, L. Kador, B. Peng and M. Thelakkat, Influence of the Solvent on the Surface-Enhanced Raman Spectra of Ruthenium(II) Bipyridyl Complexes. *J. Phys. Chem. B* **2005**, *109*, 5783-9.
- (63) W. Zhu, Y. Wu, S. Wang, W. Li, X. Li, J. Chen, Z.-s. Wang and H. Tian, Organic D-A- π -A Solar Cell Sensitizers with Improved Stability and Spectral Response. *Adv. Funct. Mater.* **2011**, *21*, 756-63.
- (64) A. Baheti, P. Tyagi, K. R. J. Thomas, Y.-C. Hsu and J. T. s. Lin, Simple Triarylamine-Based Dyes Containing Fluorene and Biphenyl Linkers for Efficient Dye-Sensitized Solar Cells. *J. Phys. Chem. C* **2009**, *113*, 8541-7.
- (65) P. Singh, A. Baheti, K. R. J. Thomas, C.-P. Lee and K.-C. Ho, Fluorene-based organic dyes containing acetylene linkage for dye-sensitized solar cells. *Dyes Pigm.* **2012**, *95*, 523-33.
- (66) M. Gratzel, Photoelectrochemical cells. *Nature* **2001**, *414*, 338-44.
- (67) C. Lee, W. Yang and R. G. Parr, Development of the Colle-Salvetti correlation-energy formula into a functional of the electron density. *Physical Review B* **1988**, *37*, 785-9.
- (68) A. D. Becke, A new mixing of Hartree-Fock and local density-functional theories. *The Journal of Chemical Physics* **1993**, *98*, 1372-7.
- (69) B. J. Lynch, P. L. Fast, M. Harris and D. G. Truhlar, Adiabatic Connection for Kinetics. *J. Phys. Chem. A* **2000**, *104*, 4811-5.
- (70) Gaussian 09, Revision A.02, M. J. Frisch, G. W. Trucks, H. B. Schlegel, G. E. Scuseria, M. A. Robb, J. R. Cheeseman, G. Scalmani, V. Barone, B. Mennucci, G. A. Petersson, H. Nakatsuji, M. Caricato, X. Li, H. P. Hratchian, A. F. Izmaylov, J. Bloino, G. Zheng, J. L. Sonnenberg, M. Hada, M. Ehara, K. Toyota, R. Fukuda, J. Hasegawa, M. Ishida, T. Nakajima, Y. Honda, O. Kitao, H. Nakai, T. Vreven, J. A., Jr., Montgomery, J. E. Peralta, F. Ogliaro, M. Bearpark, J. J. Heyd, E. Brothers, K. N. Kudin, V. N. Staroverov, R. Kobayashi, J. Normand, K. Raghavachari, A. Rendell, J. C. Burant, S. S. Iyengar, J. Tomasi, M. Cossi, N. Rega, N. J. Millam, M. Klene, J. E. Knox, J. B. Cross, V. Bakken, C. Adamo, J. Jaramillo, R. Gomperts, R. E. Stratmann, O. Yazyev, A. J. Austin, R. Cammi, C. Pomelli, J. W. Ochterski, R. L. Martin, K. Morokuma, V. G. Zakrzewski, G. A. Voth, P. Salvador, J. J.

Effect of auxiliary acceptor on optical properties

Dannenberg, S. Dapprich, A. D. Daniels, Farkas, J. B. Foresman, J. V. Ortiz, J. Cioslowski, D. J. Fox, Gaussian, Inc., Wallingford, CT, 2009.

Chapter 5

Benzothiadiazole Based Pyridine Anchoring Organic Dyes for Dye-Sensitized Solar Cells: Effect of Donor on Optical and Photovoltaic Properties

5.1 Introduction

Electron acceptors like carboxylic acid, cyanoacrylic acid and rhodanine-3-acetic acid moieties have been successfully used as acceptors/anchoring groups in DSSCs, as they can bind to the nanocrystalline TiO_2 [1-5]. Among these acceptors, cyanoacrylic acid is by far the most common used acceptor in DSSCs presumably due to its good electron injection efficiency with enhanced spectral response through intramolecular charge transfer and affording energy conversion efficiencies of up to 10.0% for metal-free organic sensitizers [6-8]. The carboxyl group in the cyanoacrylic acid forms a strong ester linkage with the nanocrystalline TiO_2 surface, and renders good electronic communication between TiO_2 and dye [2,9]. Despite the superior performance and ubiquitous use of cyanoacrylic acid acceptor in organic sensitizer for DSSCs, this acceptor has some well-established drawbacks [1, 10-11]. Recently Sun and co-workers found that the cyanoacrylic acid unit transform into the aldehyde group with the synergy of water and UV light, by which performance and stability of solar cells deteriorated [12]. Thus, identifying an ideal acceptor to replace cyanoacrylic acid is one of the most important problems in advancing DSSCs for long-term photo-stability. However, the research devoted for improvement of the efficiency in organic dyes for DSSCs by regulating electron donors and π -conjugated bridges are quite adequate, especially when compared to the amount of research devoted to electron acceptor/anchoring group development. Recently, organic dyes featuring various electron acceptor/anchoring groups such as pyridine [9, 13-15], hydroxypyridium [16], pyridine-N-oxide [17], pyrimidine, 2-cyanopyridine [18], acetylacetone [19], 2-(1,1-dicyanomethylene) rhodanine [1], phosphinic acid [20], hydroxamate [21], and 8-

Effect of Donor on Optical Properties

hydroxylquinoline [10] etc. have been developed, explored as anchoring groups and examined as sensitizers in DSSCs. The structures of the dyes with various anchoring groups were shown in Figure 5.1.



Figure 5.1 Structures of the dyes with various anchoring groups known in the literature

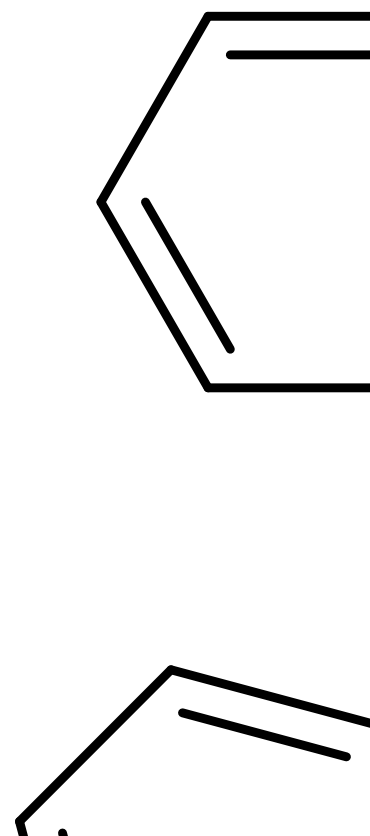


Figure 5.2 Structures of the pyridine anchoring sensitizers known in the literature

Since Harima and co-workers reported the use of pyridine anchoring dyes in 2011 [9], dyes containing pyridine anchoring group have received considerable attention. Reported examples of dyes containing pyridine anchoring unit are shown in Figure 5.2. The relationship between

the chemical structures of the dye and the performance of the DSSCs still needs to be revealed. Pyridine is a π -deficient heteroaromatic ring with much higher electron withdrawing power than that of sulfoxide, cyano, sulfones moieties and comparable to that of carboxyl and carbonyl groups [22]. Pyridine ring can form strong coordinate bonding with the Lewis acid sites of TiO_2 by lone pair of electrons on the nitrogen atom and affords comparable electron injection efficiencies to carboxyl group [14, 23]. Nevertheless, due to limited broadening of absorption spectra and low photocurrent response, these pyridine anchoring group sensitizers achieved lower efficiencies [17, 24-25]. Recently, Ooyama and colleagues have reported a new series of sensitizers with two pyridyl groups as an electron withdrawing-injecting anchoring group featured with electron donor carbazole moiety, which showed an efficiency of 1.61% [13]. To achieve the red-shifted and broadened absorption profile in the red/NIR region, Ohshita and co-workers [15] developed a dye comprising two pyridyl groups as electron withdrawing-anchoring groups, carbazole-diphenylamine moiety as an electron donor with boron dipyrromethene (BODIPY) in the π -conjugated bridge and yielded good light-harvesting properties. Unfortunately, due to the electrostatic interactions between the BODIPY core and I^{3-} ions achieved low photovoltaic performance.

We envisioned a new class of benzothiadiazole sensitizer with pyridine as a anchoring/acceptor group and hypothesized to display increased spectral response arising from elongated π -conjugation due to vinyl linkage and intramolecular charge transfer (ICT) caused by low band gap benzothiadiazole. Benzothiadiazole is well-known excellent acceptor utilized in low band-gap small molecules and polymers for organic solar cells due to its excellent electron transporting capability and facile functionalization possibilities at 4,7-positions [26-33]. We have inserted benzothiadiazole as auxiliary acceptor in between donor moieties and pyridine anchoring group to extend the absorption window and to achieve good light-harvesting response in the visible region by lowering its LUMO level. To the best of our knowledge, organic sensitizers composed of benzothiadiazole and pyridine anchoring group were not exploited before for DSSCs application. We have designed and synthesized a series of organic dyes possessing donors such as piperidine, morpholine, carbazole, phenothiazine and ferrocene (Figure 5.3). In addition the introduction of the vinyl bridges was expected to enhance the conjugation degree and may lead to broad and red-shifted absorption profile. Structure-property relationship studies with different donors segments were also proposed. The optical properties were correlated by DFT calculations. Since these π -conjugated materials possess terminal

pyridyl substituent which can form intermolecular interactions such as hydrogen bonding and coordination bonds with metals, expected to be alligator clips for the synthesis of supramolecular building blocks [34]. Especially the dipyriddy derivative **17** can be employed for building of self-assembling macrocyclic architectures by hydrogen bonding and metal coordination with nitrogen atoms of dipyriddy groups [35-36].

Generally, intramolecular charge transfer process is mainly dependent on the donor-acceptor interactions. We modulated the donor segment in the dyes to fine tune the optical and electrochemical properties, the introduction of stronger donor segment was expected to red shift the absorption and reduce the energy gap by raising the HOMO energy level. Alkyl and aryl amines were utilized to illustrate the variations in the optical properties arising due to the change in the donor strength and π -conjugation. Thus the direct attachment of the amine functionality on the benzothiadiazole core in **15a-b** is believed to play concerted role on the electro-optical properties and different from **19a-c** in which donor is attached to benzothiadiazole core by vinyl linkage. This subtle difference in the donor strength and conjunction path may tune the photophysical and electrochemical properties of these six dyes. The intensity and absorption maximum of the ICT transition was affected by the choice of donor within the dye.

Figure 5.3 Structures of pyridine anchoring sensitizers featured with benzothiadiazole

5.2 Results and discussion

5.2.1 Synthesis

The general representation and numbering of the pyridine featured benzothiadiazole sensitizers is as shown in Figure 5.4.

Figure 5.4 General representation and numbering of the pyridine featured benzothiadiazole sensitizers

The synthetic pathways employed to synthesize benzothiadiazole sensitizers with pyridine anchoring are shown in Scheme 5.1. To synthesize amine directly attached benzothiadiazole sensitizers (**15a-b**), in the first step the donor is attached to the core benzothiadiazole by reacting with piperidine/morpholine. In the second step, pyridine anchoring group was attached by the Heck-coupling protocol to yield targeted dyes (**15a-b**). The π -extended pyridine dyes (**19a-c**) were synthesized by two consecutive Heck coupling reactions. In the first step, Heck coupling reaction between 4,7-dibromobenzo[*c*][1,2,5]thiadiazole (**1**) with vinylpyridine produced the mono-substituted product **16**. This reaction also produced the disubstituted product (**17**) as well. However monocapped compound (**16**) can be easily separated by column chromatography. In the next step, the mono substituted derivative converted to a series of dyes **19a-c** by Heck-coupling reaction with different vinyl derivatives (**18a-c**). The structures of all of these new sensitizers were characterized by ^1H NMR, ^{13}C NMR, FT-IR spectroscopy and HR-MS. Apart from these characterizations, single crystal X-ray structure determination of an intermediate (**16**) was performed. The FT-IR results of the powders of the six dyes reveals existence of the characteristic stretching band for the C=N or C=C at about 1590, 1540 and 1470 cm^{-1} , which can be assigned to the pyridine ring in the sensitizers [9, 13-15, 37]. The NMR spectra of the new pyridine sensitizers are consistent with their proposed structures and showing the expected features with the correct integration ratios. From ^1H NMR, all the alkene -CH=CH- units appear as doublets with coupling constant of 16 Hz, which establishes an (*E*) configuration for the double bond(s) produced by Heck coupling reaction. All the sensitizers are highly

soluble in common organic solvents like dichloromethane, chloroform, toluene, dimethylformamide and tetrahydrofuran etc.

Scheme 5.1 Synthetic pathway leading to benzothiadiazole containing pyridine anchoring sensitizers

5.2.2 Single-Crystal X-ray Structural Analysis of **16**

The single crystals of **16** (Figure 5.5) suitable for analysis by X-ray crystallography were grown by slow evaporation of a concentrated acetonitrile solution at room temperature. The derivative **16** crystallizes in the orthorhombic space group *Pbcn*. The vinylpyridine was exclusively mono coupled to the benzothiadiazole unit confirming the formation of newly introduced C-C bonding by Heck coupling protocol and our proposed structure from solution characterization. And also, the (*E*) configuration of the double bond introduced by Heck coupling protocol was confirmed by the crystal structure of **16**. At the termini of the alkene, BTD moiety and the pyridine ring are disposed in a mutual anti manner with respect to each other, which is in agreement with the NMR assignment. The vinylpyridine segment is slightly deviated from planarity with respect to benzothiadiazole ring by 2.57°. The bond lengths of C11-Br (1.884 Å) and C6=C7 (1.321 Å) are shorter than the localized C-Br (1.91 Å), C=C (1.34 Å) bond lengths, indicating the π -conjugation within the molecule.

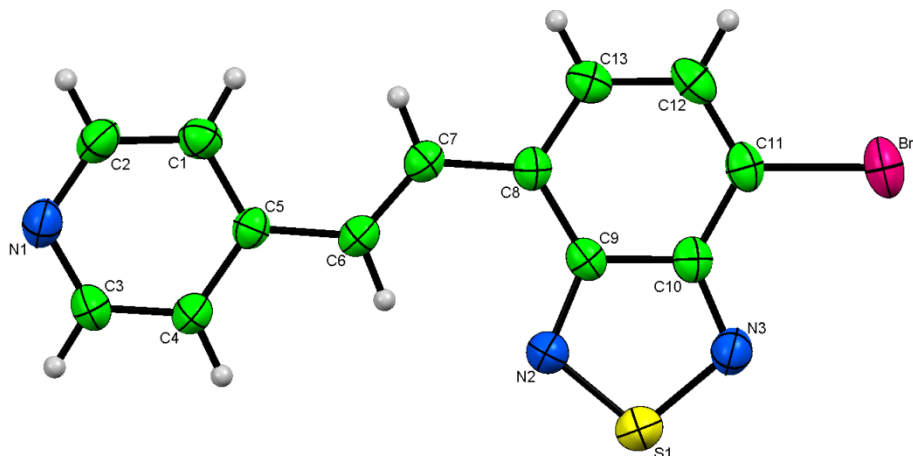


Figure 5.5 ORTEP diagram of **16** with the atom-numbering scheme.

5.2.3 Optical Properties

To probe the light absorption properties and donor-acceptor interactions of the new benzothiadiazole based pyridine anchoring sensitizers we have recorded the absorption spectra of the dyes in dichloromethane. Figure 5.6 shows the UV-vis absorption spectra of the dyes in dilute dichloromethane solution and on thin film, respectively. The optical absorption maxima (λ_{abs}) are summarized in Table 5.1.

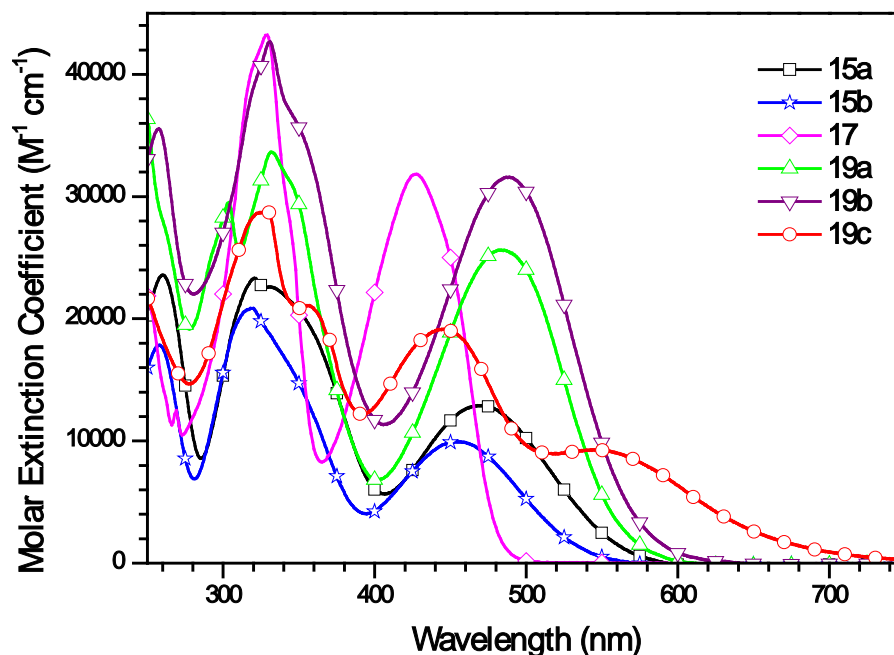


Figure 5.6 Absorption spectra of dyes recorded in dichloromethane

All the dyes show strong and broad absorption bands in the range of 250 to 600 nm. The absorption spectra of dyes except **19c** exhibited two absorption peaks in the wavelength range 250–600 nm. The lower wavelength absorption in the range of 250–400 nm is corresponding to

the π - π^* absorption of the molecules and the absorption band at longer wavelength range 400-600 nm could be assigned to the intramolecular charge transfer transition between the donor and acceptor.

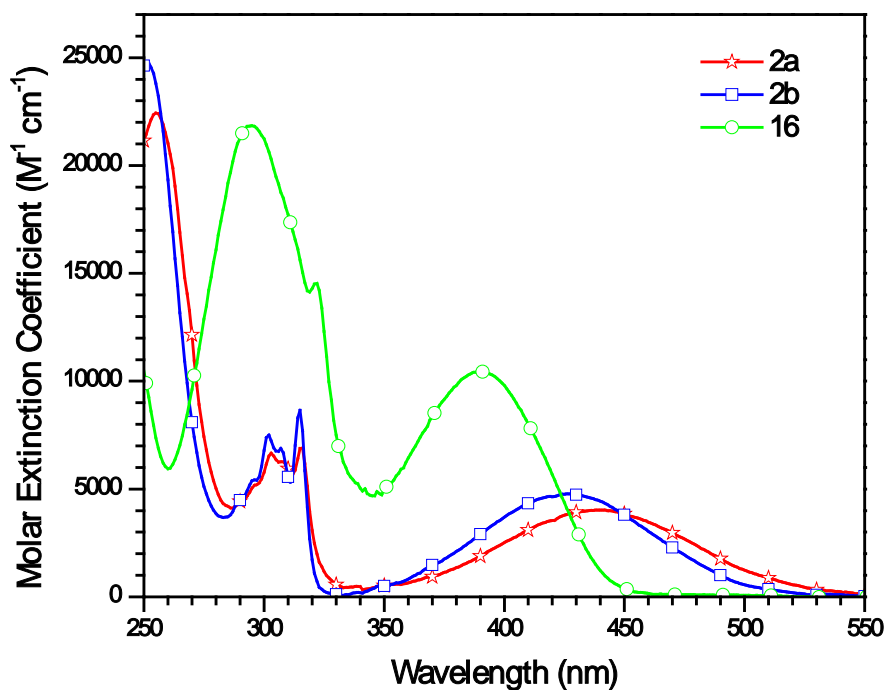


Figure 5.7 Absorption spectra of intermediates **2a**, **2b** and **16** recorded in dichloromethane

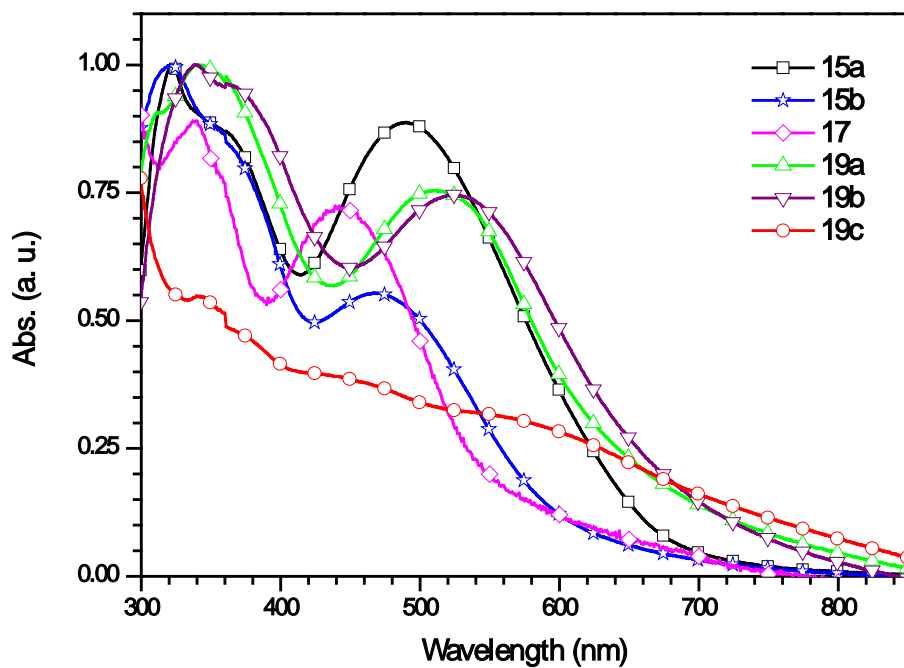


Figure 5.8 Absorption spectra of dyes recorded on thin film

Effect of Donor on Optical Properties

Especially the lower energy transition in **15a** and **15b** is assigned to the intramolecular charge transfer transition with contribution from the π - π^* transition character. The dipyridyl derivative **17** inherits the most blue-shifted absorption profile with two transition bands below 450 nm assigned to the π - π^* transitions in the dye and does not show ICT transition due to lack of donor segment in the dye structure. Among **15a** and **15b**, the piperidine donor based sensitizers **15a** was showing red shifted absorption owing the higher electron donating ability. The derivatives **19a**, **19b**, and **19c** showed the red-shifted absorption profiles when compared to the alkylamine derivatives **15a** and **15b**. The peak positions of the lower-energy band in the dyes follow the order **19c** > **19b** > **19a** > **15a** > **15b** > **17**.

It is interesting to compare the absorption spectra (Figure 5.7) of the dyes with the precursor bromides (**2a**, **2b**, **16**) as they reveal the impact of the electron-accepting group and electron-donating group. The Absorption data of the bromides (**2a**, **2b**, **16**) compiled in Table 5.2. The absorption spectra of **15a**, **15b** were red-shifted on comparison with **2a**, **2b** due to extension of conjugation with electron-withdrawing vinylpyridine unit. All the dyes showing bathochromic shift when compared to the bromo derivative **16**, due to the introduction of donor segment on benzothiadiazole segment. Among all, the ferrocene based dye **19c** showed red shifted absorption due to strong MLCT from ferrocene to benzothiadiazole-vinylpyridine. Whereas the dye **19b** showing red shifted absorption maxima with high molar extinction coefficient than **19a**, due to pronounced electron donating ability of phenothiazine than carbazole. The introduction of phenothiazine moiety as electron donor increased the extent of electron delocalization over the whole molecule due to higher electron donating ability than the carbazole, thus the maximum absorption peaks of **19b** is red-shifted. These results showed that the introduction of carbazole, phenothiazine and ferrocene by vinyl linkage expanded the π -conjugation in the dyes and broadened the ICT band with enhancement in the molar extinction coefficient. Consequently these dyes can absorb a larger portion of the solar spectrum, which may increase its photocurrent response in the low energy regime. In comparison with their absorption spectra in solution, the absorption bands of the dyes in films were red-shifted and the absorption onset was broadened to the longer wave length region due to the strong intermolecular π - π interactions in the solid state (Figure 5.8).

Effect of Donor on Optical Properties

Here an interesting comparison can be made to see the effect of different donor groups on the absorption profile of the dyes (Figure 5.9). The optical properties of this family of dyes were sensitive to the nature of the donor segment that was attached onto the benzothiadiazole moiety. A stronger electron-donating strength can result in a higher degree of electronic delocalization and hence a stronger ICT effect in the molecule. As identified from their absorption spectra, the features of the π - π^* and charge transfer bands undoubtedly depend on the nature of the electron-donating segment. These new pyridine-anchored benzothiadiazole-based sensitizers have a higher light-harvesting capacity than other previously reported organic sensitizers that incorporated pyridine as an anchoring group. The optical data of the organic dyes with a pyridine anchoring group for DSSCs was shown in Table 5.3. The difference in the dipole moments of the molecules in the ground state and the excited states originates solvatochromism in the donor-acceptor compounds. So to investigate solvatochromism of the dyes in the ground state, we have recorded the absorption spectra in various solvents with different dielectric constants viz. CH₂Cl₂, TOL, THF, DCM, ACN and DMF. The changes in the absorption profiles for the dyes with solvent polarity are illustrated in Figures 5.10, 5.11 (a) and (b). The absorption maxima of the dyes remain fairly insensitive to the solvent polarity, which indicates that in the ground state the interaction of the dyes with the solvents is less significant.

Figure 5.9 Effect of the donor attached to benzothiadiazole unit and effect of addition of TFA on absorption maximum

Table 5.1 Absorption properties of dyes in different solvents

Dye	$\lambda_{\text{abs, nm}} (\epsilon \times 10^3 \text{ M}^{-1} \text{ cm}^{-1})$						
	CH	TOL	THF	DCM	ACN	DMF	Film
15a	259, 319, 465 ^a	322 (23.4), 470 (11.7)	320 (25.1), 468 (12.2)	260 (23.6), 321 (23.3), 470 (12.9)	258, 319, 466 ^a	321 (22.5), 472 (11.5)	322, 490
15b	258, 314, 454 ^a	319 (33.7), 457 (15.0)	256 (28.7), 319 (33.1), 459 (14.7)	258 (17.8), 319 (20.9), 454 (9.9)	256, 317, 452 ^a	320 (25.0), 462 (11.5)	321, 471
17	326, 429 ^a	329 (36.7), 431 (26.6)	328 (44.3), 428 (30.7)	329 (43.2), 428 (31.8)	327, 423 ^a	330 (44.2), 428 (31.3)	339, 442
19a	302, 328, 477 ^a	304 (29.1), 334 (32.5), 490 (26.1)	303 (35.5), 332 (45.5), 482 (32.9)	304 (29.5), 332 (33.7), 482 (25.6)	301, 330, 472 ^a	304 (28.2), 333 (36.1), 483 (25.7)	340, 512
19b	259, 328, 480 ^a	333 (33.4), 492 (25.4)	330 (40.6), 488 (28.3)	257 (35.5), 331 (42.7), 488 (31.6)	255, 327, 474 ^a	331 (40.2), 487 (29.2)	339, 525
19c	317, 355, 441, 543 ^a	330 (33.4), 358 (26.0), 442 (19.8), 549 (11.1)	329 (33.3), 354 (25.4), 442 (18.9), 546 (9.9)	329 (22.2), 356 (18.1), 437 (7.3), 548 (9.6)	328, 437, 535 ^a	330 (38.0), 354 (28.1), 443 (21.2), 540 (10.4)	-

^a Molar extinction coefficient values could not be obtained owing to poor solubility

Table 5.2 Absorption data of the dyes recorded in dichloromethane

Compound	$\lambda_{\text{abs, nm}} (\epsilon \times 10^3 \text{ M}^{-1} \text{ cm}^{-1})$
2a	255 (26.5), 303 (7.2), 316 (7.5), 439 (4.8)
2b	302 (7.5), 316 (7.7), 427 (4.8)
16	295 (21.8), 322 (14.5), 390 (10.5)

Table 5.3 Optical, electrochemical and DSSC data for organic dyes having pyridine anchoring group for DSSCs

Dye	$\lambda_{\text{abs/nm}}$	$E_{\text{OX}}/\text{V}(\text{NHE})$	$E_{\text{OX}}^*/\text{V}(\text{NHE})$	V_{OC}/mV	$J_{\text{SC}}/\text{mA cm}^{-2}$	ff	$\eta/\%$	Ref
P1	375 (33000) ^a	1.02	-2.07	522	3.35	0.62	1.15	9
P2	396 (49600) ^a	0.97	-1.87	548	5.63	0.60	1.84	9
P3	327 (21900) ^b	1.54	-1.95	492	1.84	0.63	0.57	13
P4	378 (46100) ^b	1.22	-1.75	520	4.48	0.63	1.47	13
P5	377 (72600), 673 (80900) ^a	1.22	-0.58	320	1.85	0.67	0.39	15
P6	473 (19900) ^c	1.01	-1.20	600	9.45	0.70	4.02	18
P7	519 (33300) ^c	1.00	-0.96	450	0.62	0.60	0.17	18
P8	461 (18900) ^c	1.03	-1.22	570	5.24	0.70	2.10	18
P9	408 (56400) ^b	0.87	-1.84	548	3.12	0.67	1.11	38
P10	393 (50700) ^d	1.04	-1.13	118	4.05	0.34	0.16	39

^a 1,4-dioxane ^b THF ^c CH₂Cl₂ ^d MeCN

To probe the donor-acceptor interactions and charge transfer nature of the pyridine dyes protonation-deprotonation study was performed by the addition of TFA and TEA to the toluene solutions of the dyes (Table 5.4). The cartoon representation of acid-base equilibrium in the dyes was shown in Figure 5.9. The addition of TFA led to a significant red-shift in the absorption except the dye **17**, owing to the protonation occurred on nitrogen atom of the pyridine ring. Now this positive charge on the pyridinium cation makes it more electron deficient and enhanced intermolecular charge transfer occurred from donor moieties to benzothiadiazole-vinylpyridinium cation, TEA addition resorted the original absorption. The changes in the absorption spectra of the dyes upon addition of TFA or TEA in toluene solutions were displayed in Figures 5.11 (c), (d) and 5.12.

Table 5.4 Absorption data of the dyes recorded in toluene before and after addition of TFA or TEA

Dye	$\lambda_{\text{abs}}, \text{nm} (\epsilon \times 10^3 \text{M}^{-1} \text{cm}^{-1})$			
	TOL	TOL+TFA	TOL+TFA+TEA	TOL+TEA
15a	322 (23.4),	322 (21.5),	321 (23.7),	320 (22.8),
	470 (11.7)	379 (19.3),	466 (11.0)	469 (9.7)
		516 (5.8)		
15b	319 (33.7),	322 (19.1),	317 (34.6),	319 (34.5),
	457 (15.0)	395 (20.3),	457 (15.2)	459 (15.3)
		482 (23.8)		
17	329 (36.7),	344 (20.9),	329 (21.8),	344 (21.3),
	431 (26.6)	435 (47.4),	431 (15.1)	435 (47.0),
		458 (41.8)		458 (41.3)
19a	304 (29.1),	303 (31.6),	304 (30.3),	304 (30.3),
	334 (32.5),	383 (16.7),	334 (35.9),	334 (36.2),
	490 (26.1)	540 (32.6),	484 (25.3)	483 (25.9)
19b	333 (33.4),	326 (23.7),	332 (34.8),	332 (35.4),
	492 (25.4)	544 (24.5)	485 (23.9)	493 (25.6)
19c	330 (24.7),	331 (17.4),	331 (24.7),	331 (25.1),
	356 (19.1),	449 (21.2),	355 (19.1),	357 (19.2),
	442 (14.5),	624 (3.0)	441 (14.5),	441 (14.5),
	546 (8.0)		547 (8.1)	547 (8.0)

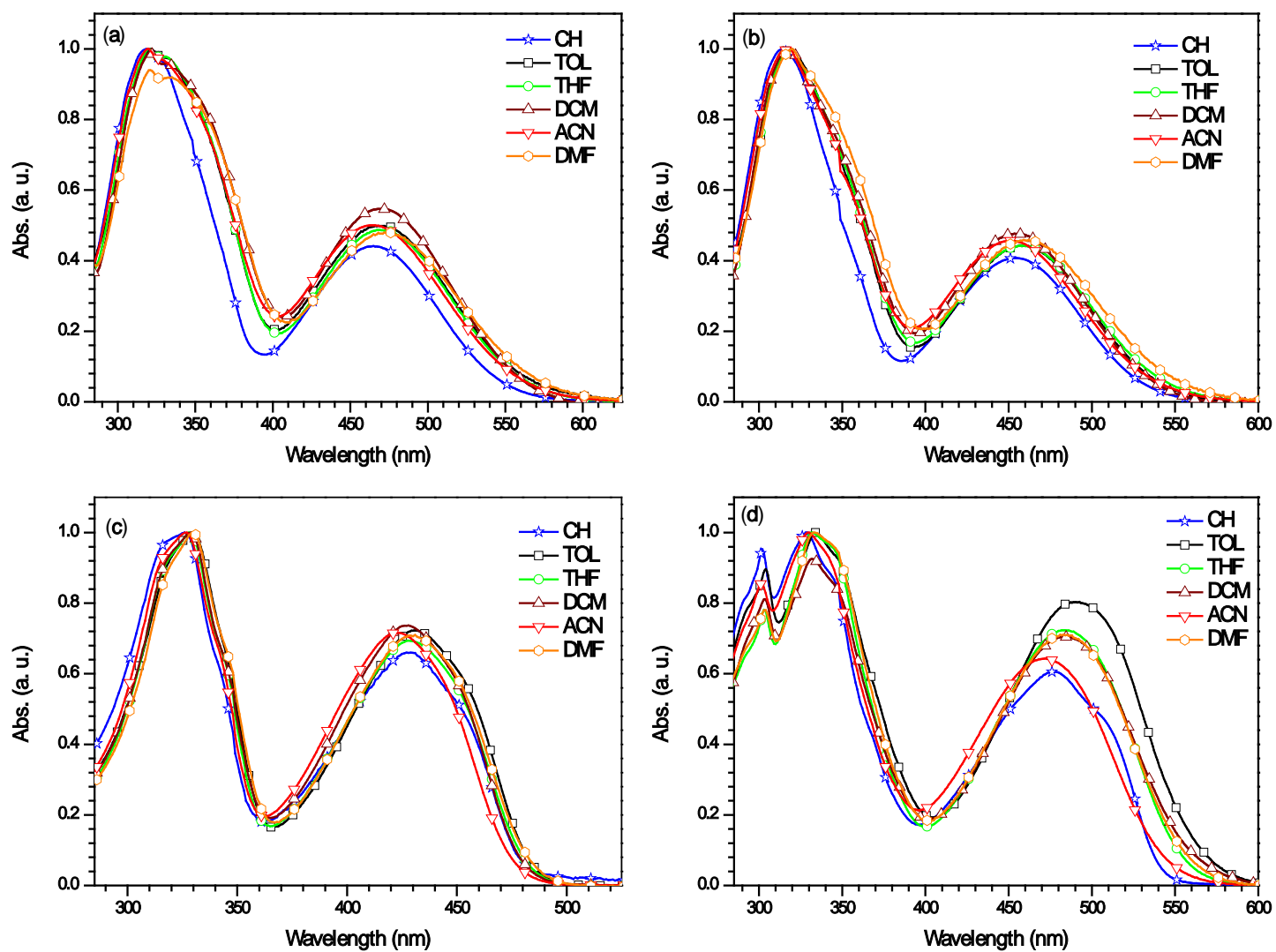


Figure 5.10 Absorption spectra of (a) 15a (b) 15b (c) 17 (d) 19a recorded in different solvents

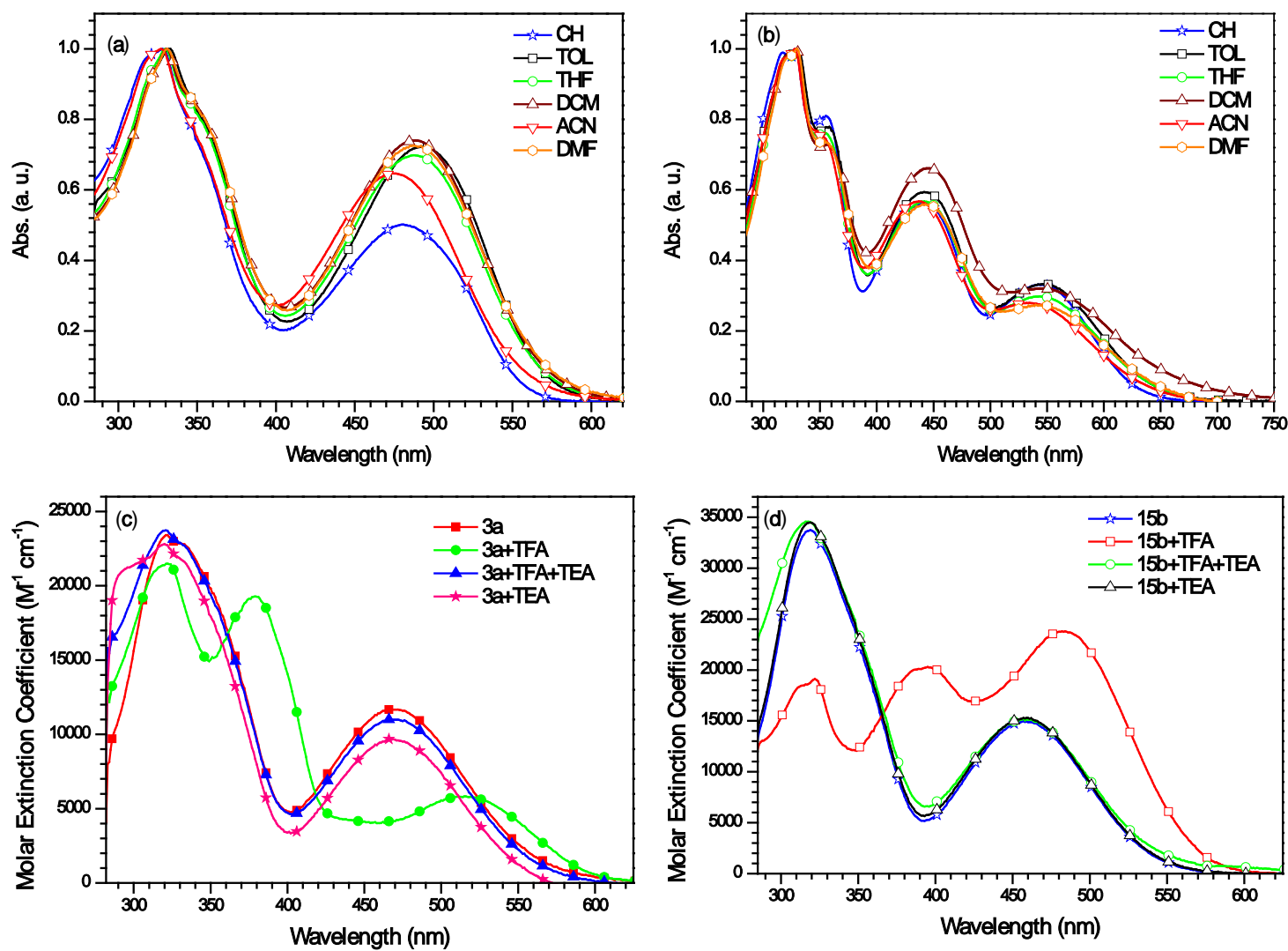


Figure 5.11 Absorption spectra of (a) **19b** (b) **19c** recorded in different solvents and (c) **15a** (d) **15b** recorded in toluene before and after addition of TFA and TEA

Effect of Donor on Optical Properties

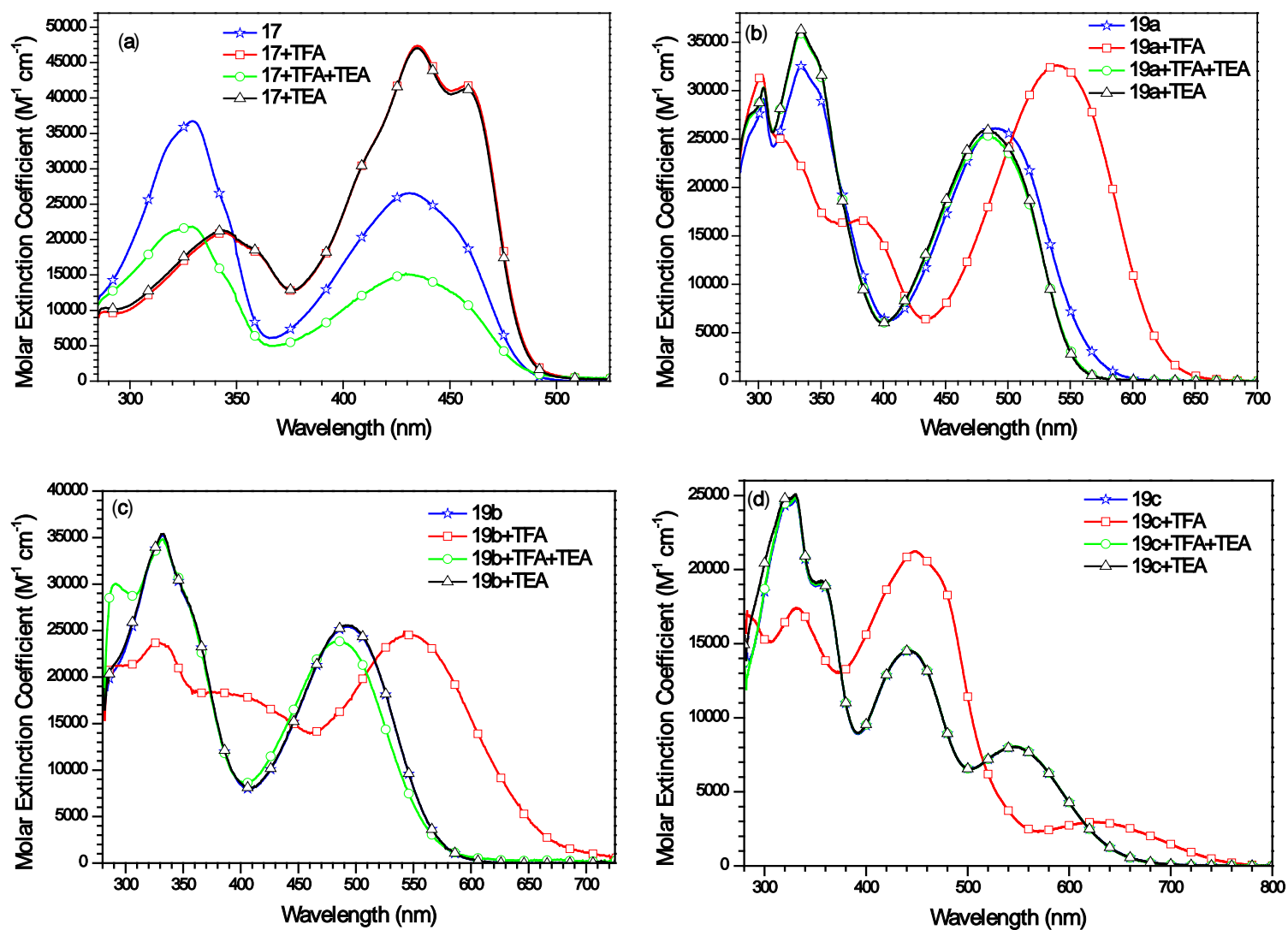


Figure 5.12 Changes in the absorption spectra of (a) 17 (b) 19a (c) 19b (d) 19c upon addition of TFA and TEA recorded in toluene

The emission spectra of the dyes were recorded by irradiating the toluene solutions of the dyes at their absorption maximum. The emission spectra are displayed in Figure 5.13 and the pertinent data with Stokes shift compiled in Tables 5.5. The derivative **19c** was non-emissive in nature due to the effective excited state quenching nature of ferrocene. The emission range for all the dyes are 505-645 nm in toluene solution. The emission wavelength of the dyes increased in the order of **17** (505 nm) < **19a** (584 nm) < **19b** (626 nm) < **15b** (635 nm) < **15a** (645 nm). As like in the ground state the dipyriddy derivative **17** acquires most blue shifted emission, due to lack intra molecular charge transfer transition in the molecule. In comparison with dyes **19a-b**, the dyes **15a-b** exhibited red shifted emission profile and larger Stokes shifts, owing to the large differences (vibrational, electronic, geometric) between the Franck-Condon state and the excited state [40]. Fluorescence spectra of the compounds were also examined in a series of solvents with varying polarity index $E_T(30)$ to identify the impact of the polarity of the solvent on the excited state of the dyes and to identify the nature of the molecules in the excited state. Representative illustrations showing the influence of the solvent polarity on the emission profile are displayed in Figure 5.14 & 5.15 (a).

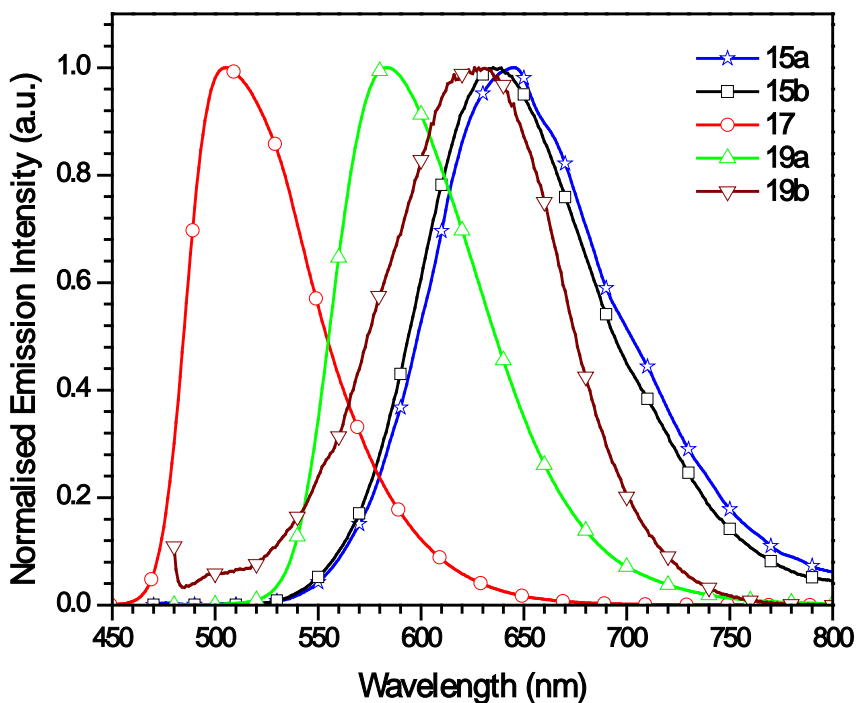


Figure 5.13 Emission spectra of the dyes recorded in toluene

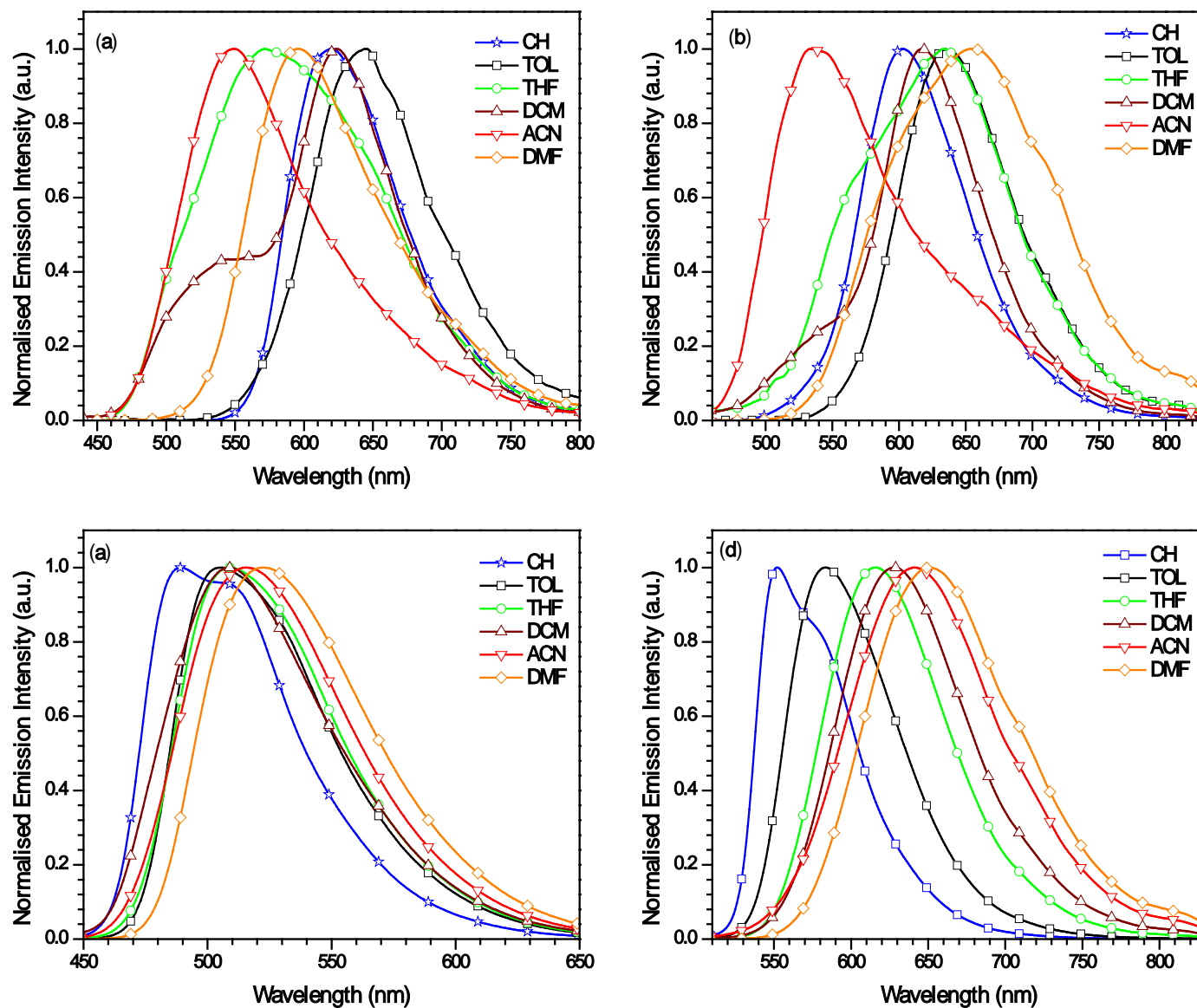


Figure 5.14 Emission spectra of the dyes recorded in different solvents (a) 15a (b) 15b (c) 17 (d) 19a

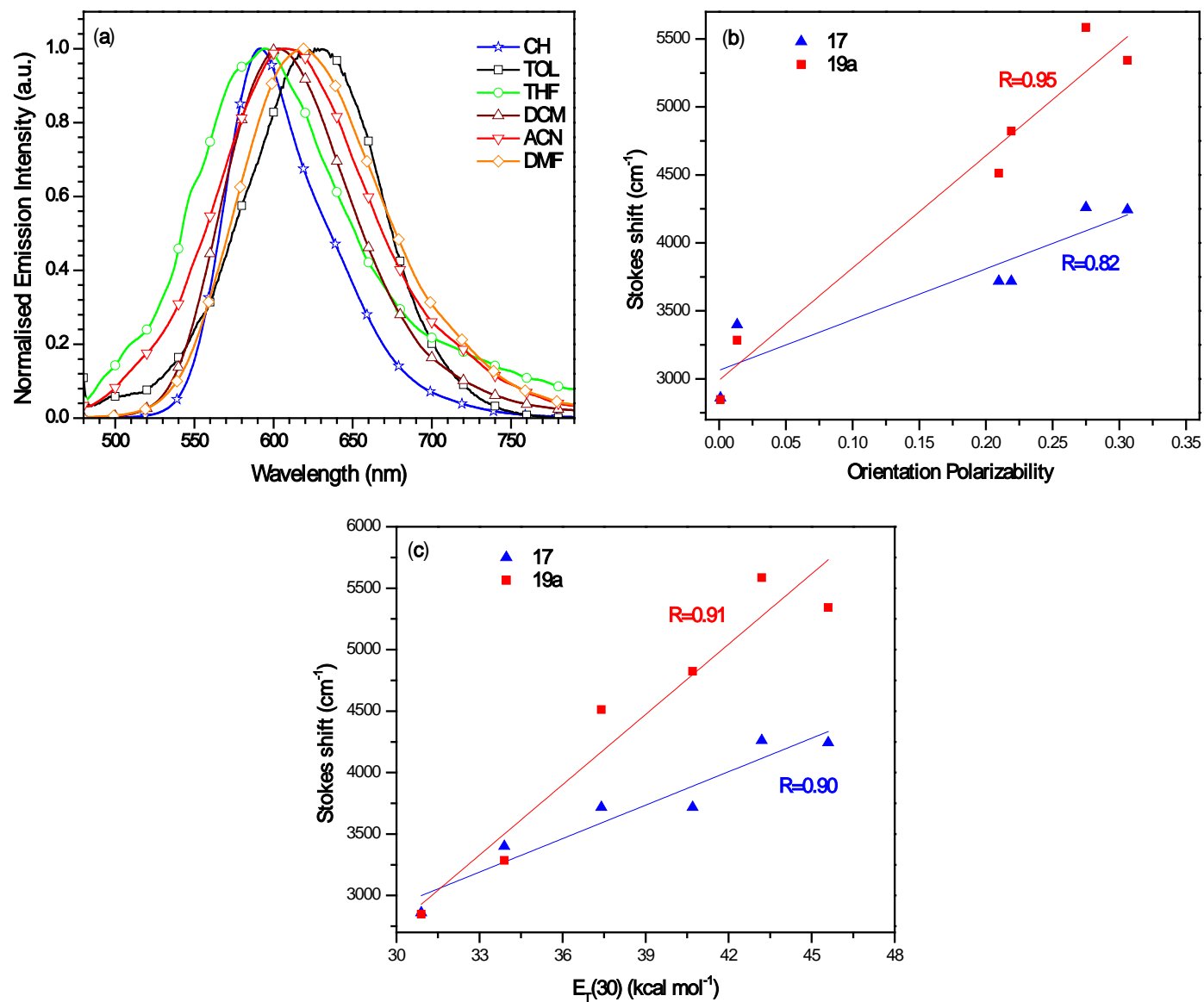


Figure 5.15 (a) Emission spectra of the dye **19b** recorded in different solvents. Correlation of solvent-induced Stokes shift with (b) orientation polarizability (c) $E_T(30)$ parameter for compounds **17** and **19a**

Effect of Donor on Optical Properties

The effect of the solvent polarity on the excited state is more pronounced than that on the ground state. The emission spectra of the dyes exhibited pronounced positive solvatochromism with the bathochromically shifted emission maxima and increased Stokes shift from nonpolar to polar solvents. This solvatochromic behavior is consistent with the charge-transfer characteristics of donor-acceptor substituted benzothiadiazole dyes. For instance, the emission maxima of **17**, **19a** and **19b** exhibited a positive solvatochromatic shift of 34, 99, and 26 nm, respectively, changing from cyclohexane to DMF. In the polar solvents due to the more efficient solvation and stabilization of the excited state than the ground state, the dyes displayed positive solvatochromism in the excited state. As discussed above the absorption spectra of all the dyes are less dependent on the polarity of the solvent, in contrast emission spectra showed significant solvent-dependent bathochromic shift with the increased polarity.

The emission was totally quenched on the addition of TFA to toluene solutions. It appears that in the protonated species, due to the presence of strong donor-acceptor interactions experiences a more pronounced dipolar relaxation from the excited state [41]. The solvent-dependent fluorescence properties of dyes were explained on the basis of general solvation effects with the Lippert–Mataga equation [42-44] and the $E_T(30)$ parameter [45] (Figures 5.15 (b) & (c)). Near linear correlation was observed in all of the solvents for **17** and **19a** in the Lippert-Mataga plot, which revealed existence of general solvent-solute interactions. Also it is worth mentioning that there is linear correlation in the plot of Stokes shifts versus the $E_T(30)$ parameter, which further affirms the positive solvatochromic behavior of the dyes.

Table 5.5 Emission properties and Stokes shift observed for the dyes in the different solvents

Dye	λ_{em} , nm						Stokes shift (cm^{-1})					
	CH	TOL	THF	DCM	ACN	DMF	CH	TOL	THF	DCM	ACN	DMF
15a	620	645	572	624	549	596	5376	5773	3885	5251	3244	4408
15b	603	635	634	617	534	655	5443	6134	6014	5819	3397	6378
17	489	505	509	509	516	523	2860	3400	3718	3718	4261	4244
19a	552	584	616	628	641	651	2848	3285	4513	4823	5586	5343
19b	592	626	595	603	607	618	3941	4351	3685	3908	4623	4353

5.2.4 Electrochemical Properties

To investigate the possibility of the photogenerated electron injection and the sensitizer regeneration from the redox electrolyte, differential pulse voltammetry (DPV) experiment was performed in their 1.0×10^{-4} M solutions in dichloromethane solution using tetraethyl ammonium perchlorate (Et_4NClO_4) in a typical three-electrode electrochemical cell with a scan rate of 100

mV s^{-1} . The potentials were calibrated to ferrocene/ferrocenium (Fc/Fc^+) as an internal reference in each measurement and the pertinent data compiled in Table 5.6. Except **17**, all the dyes displayed oxidation peak (0.053-0.616 V), which is more positive than the Fc/Fc^+ redox couple is attributed to the removal of an electron from the donor segment (Figure 5.16).

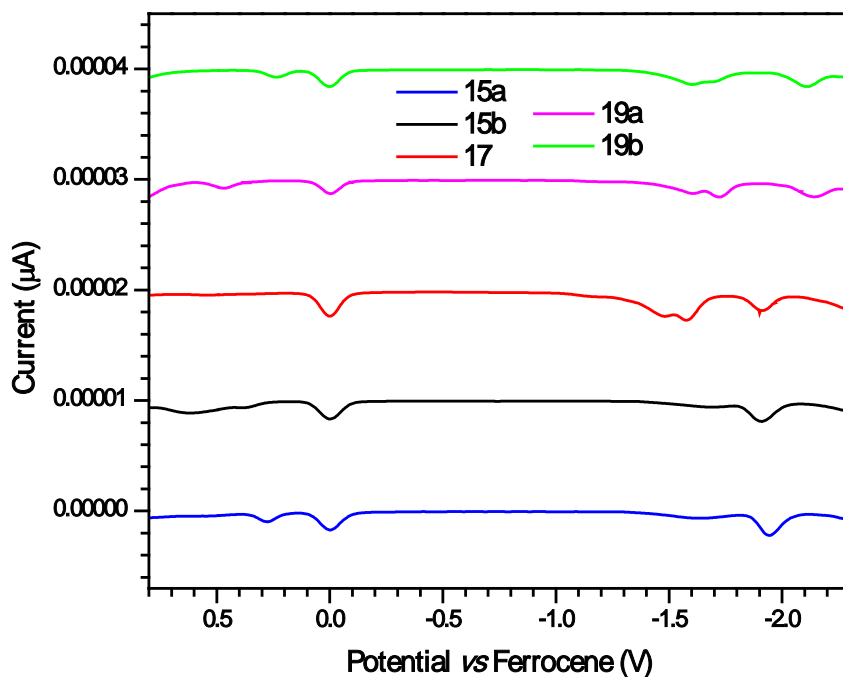


Figure 5.16 Differential pulse voltammograms recorded for dyes in dichloromethane

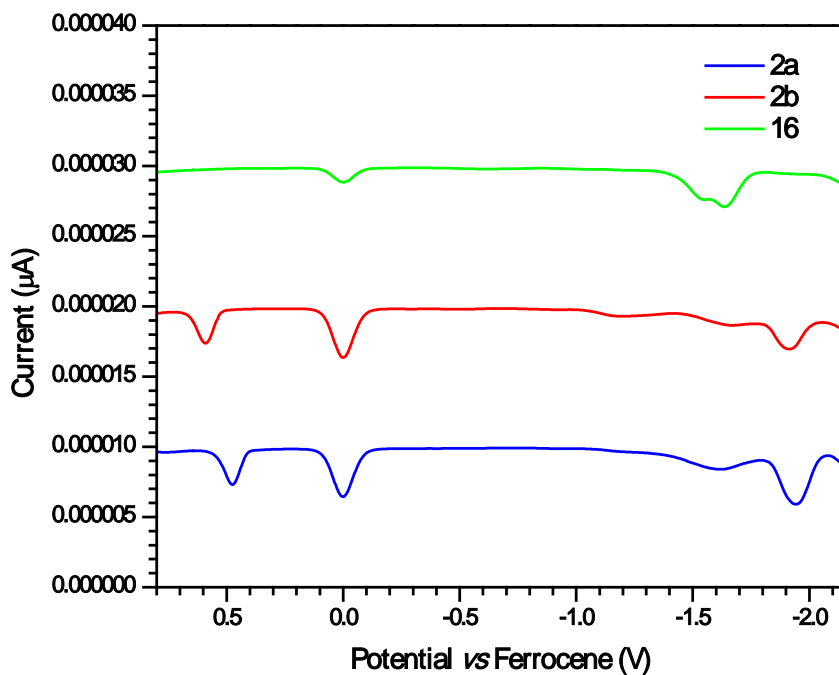


Figure 5.17 Differential pulse voltammograms recorded for intermediates **2a**, **2b** and **16** in dichloromethane

Effect of Donor on Optical Properties

The oxidation potentials follow the order **19c** < **19b** < **15a** < **19a** < **15b**, which are reminiscent to the nature of amine unit connected to the benzothiadiazole segment. The oxidation potentials are fairly in agreement with the electron-richness of the amine unit. The HOMO energy levels of dyes was measured relative to the ferrocene/ferrocenium (Fc/Fc⁺) couple for which an energy level of 4.8 eV versus vacuum was assumed and were within the range 4.853-5.418 eV. The dye **15a** was exhibited the cathodically shifted oxidation potential than **15b** due to the more electron rich piperidine donor segment. Whereas phenothiazine based dye (**19b**) showed cathodically shifted oxidation with respect to carbazole based dye (**19a**), due to the presence of electron rich phenothiazine unit. It is interesting to note that the dye **19c** exhibited anodically shifted oxidation potential with respect to ferrocene, confirms the strong electronic communication between the ferrocenyl unit and the benzothiadiazole-vinylpyridine segments. The dyes exhibited reduction wave due to the presence of electron deficient benzo[*c*][1,2,5]thiadiazole segment and the reduction potentials of the dyes follow the trend **15b** < **17** < **15a** < **19b** < **19a**. The LUMO energy levels were calculated from the reduction potential by referencing to ferrocene (4.8 eV) and the electrochemical band gap (E_{0-0}) was derived from the difference between the HOMO and LUMO energy. As expected, the band gaps of the dyes are progressively reduced with increasing electron donating strength from the donor. The trends in the absorption and electrochemical profiles of the dyes are in accordance with the electron-donating ability of donor. The Differential pulse voltammograms recorded for intermediates **2a**, **2b** and **16** in dichloromethane were shown in Figure 5.17.

Table 5.6 Electrochemical data of complexes recorded in dichloromethane

Dye	E_{OX} , V ^a (ΔE_p , mV)	E_{red} , V ^a	E_{OX} vs NHE, V ^b	HOMO, eV ^b	LUMO, eV ^b	E_{0-0} , eV	E_{OX}^* , V ^c
2a	0.476	1.944	1.246	5.276	2.856	2.340	1.094
2b	0.596	1.912	1.366	5.396	2.888	2.410	1.044
16	-	1.636	-	-	3.164	2.810	-
15a	0.276	1.944	1.046	5.076	2.856	2.220	-1.174
15b	0.616	1.908	1.386	5.416	2.892	2.524	-1.138
17	-	1.912	-	5.418	2.888	2.530	-
19a	0.476	2.144	1.246	5.276	2.656	2.620	-1.374
19b	0.236	2.108	1.006	5.036	2.692	2.344	-1.338
19c	0.053(155)	-	0.823	4.853	3.082	1.771	-0.948

^a Redox potentials are reported with reference to the ferrocene internal standard. ^b Ground state oxidation potential vs NHE ^c Deduced from the equations HOMO = E_{OX} + 4.8 and LUMO = E_{red} + 4.8 ^c Excited-state oxidation potential vs NHE

To probe the feasibility of dye regeneration and electron injection in DSSCs, we have evaluated the ground-state oxidation potentials and excited-state oxidation potentials (E_{OX}^*) of

the dyes. The ground state oxidation potentials of the dyes fall in the range 0.823-1.386 V versus the normal hydrogen electrode (NHE), more positive than the iodide/triiodide redox couple (0.4 V vs NHE) [46] and ensure the efficient regeneration of the dye from the oxidized dye [47]. The E_{OX}^* values determined for the dyes (-0.948-1.374 V vs NHE) are more negative than the conduction-band-edge energy level of the TiO_2 (-0.5 V vs NHE) [48] and expected have an efficient electron injection to the TiO_2 conduction band.

5.2.5 Quantum chemical calculations

Density functional theory (DFT) [49] calculations were carried out for the new benzothiadiazole-vinylpyridine sensitizers to correlate the structures of the sensitizers with their absorption bands and electronic transition processes upon photoexcitation. The ground-state geometries of dyes were optimized in the gas phase by DFT by using the hybrid B3LYP [50-51] functional and the standard 6-31G(d,p) basis set (Figures 5.18 & 5.19). The TD-DFT calculations were performed on the B3LYP-optimized ground-state geometries, with the hybrid B3LYP and MPW1K [52] functions using the 6-31G(d,p) basis set.

Electronic density distribution of the frontier molecular orbitals revealed that the HOMO is extended throughout the molecule in **15a-b**, **17** and in **19a-c** the HOMO is extended up to vinyl segment near the anchoring pyridine ring from donor. In all the dyes LUMO is mainly localized on benzothiadiazole with a significant contribution from vinyl pyridine. While LUMO+1 mostly distributed on vinylpyridine with a significant contribution from benzothiadiazole. The lowest energy peak position predicted by the B3LYP (Table 5.7) model is of the charge transfer character and overestimated from experimental result. Overestimation of charge transfer transitions in donor-acceptor compounds at the B3LYP level is quite expected and it is well documented in the literature [53-54]. The vertical excitations predicted by the MPW1K (Tables 5.8 & 5.9) model closely resembled those observed experimentally. It was clear that the distribution of HOMO and LUMO are not well separated within the molecule for **15a-b** and a significant overlap is present. The changes in the electron density associated by the first electron excitation (HOMO→LUMO) reveal that, the lower energy transition cannot be considered as a pure charge transfer transition and has a contribution from the π - π^* transition as well. It was notable that by careful scrutiny of the frontier molecular orbitals in **19a-c**, the distribution of the HOMO and LUMO of the dyes are well-separated.

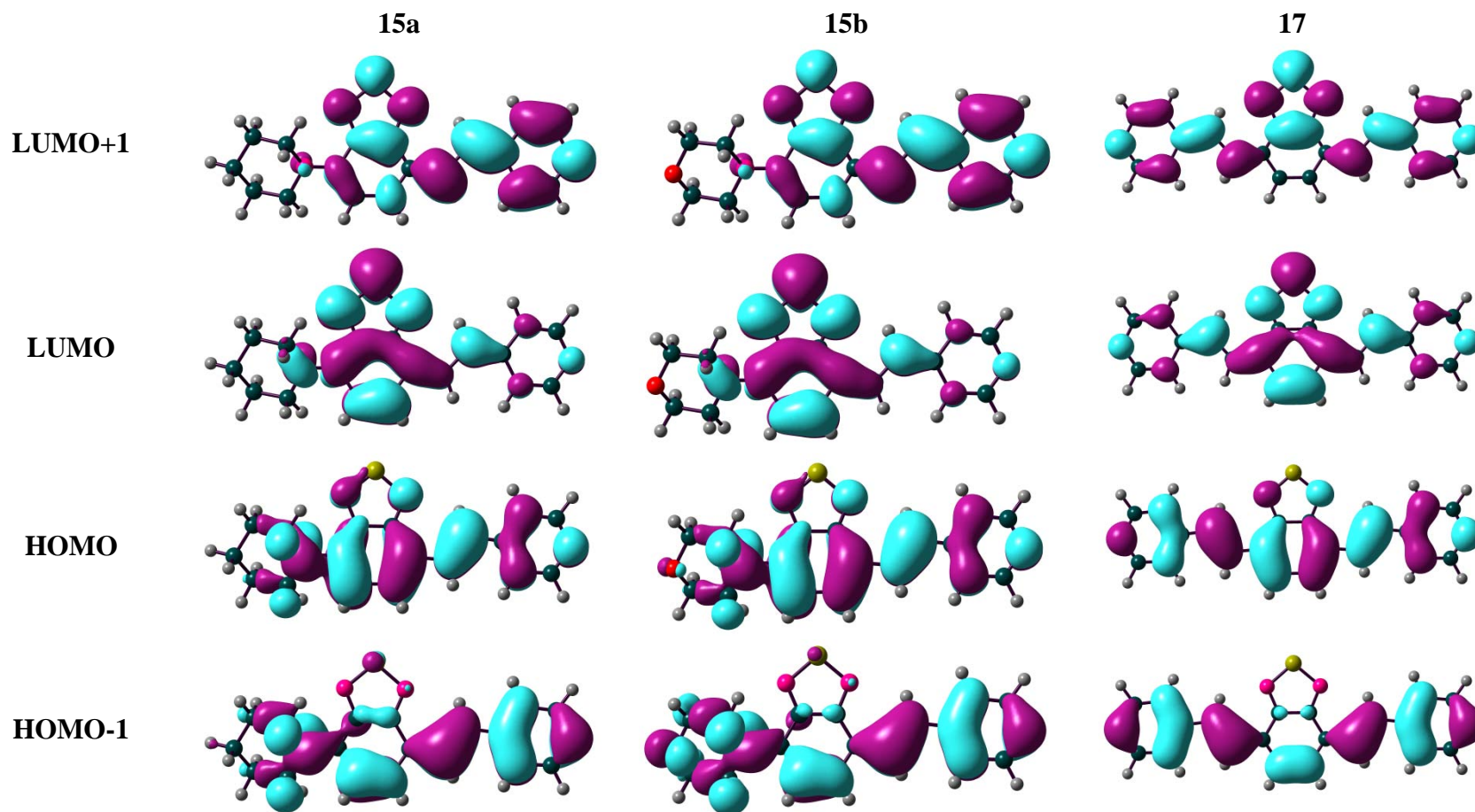


Figure 5.18 Frontier molecular orbitals of dyes **15a**, **15b** and **17** computed by using TDDFT at the B3LYP level

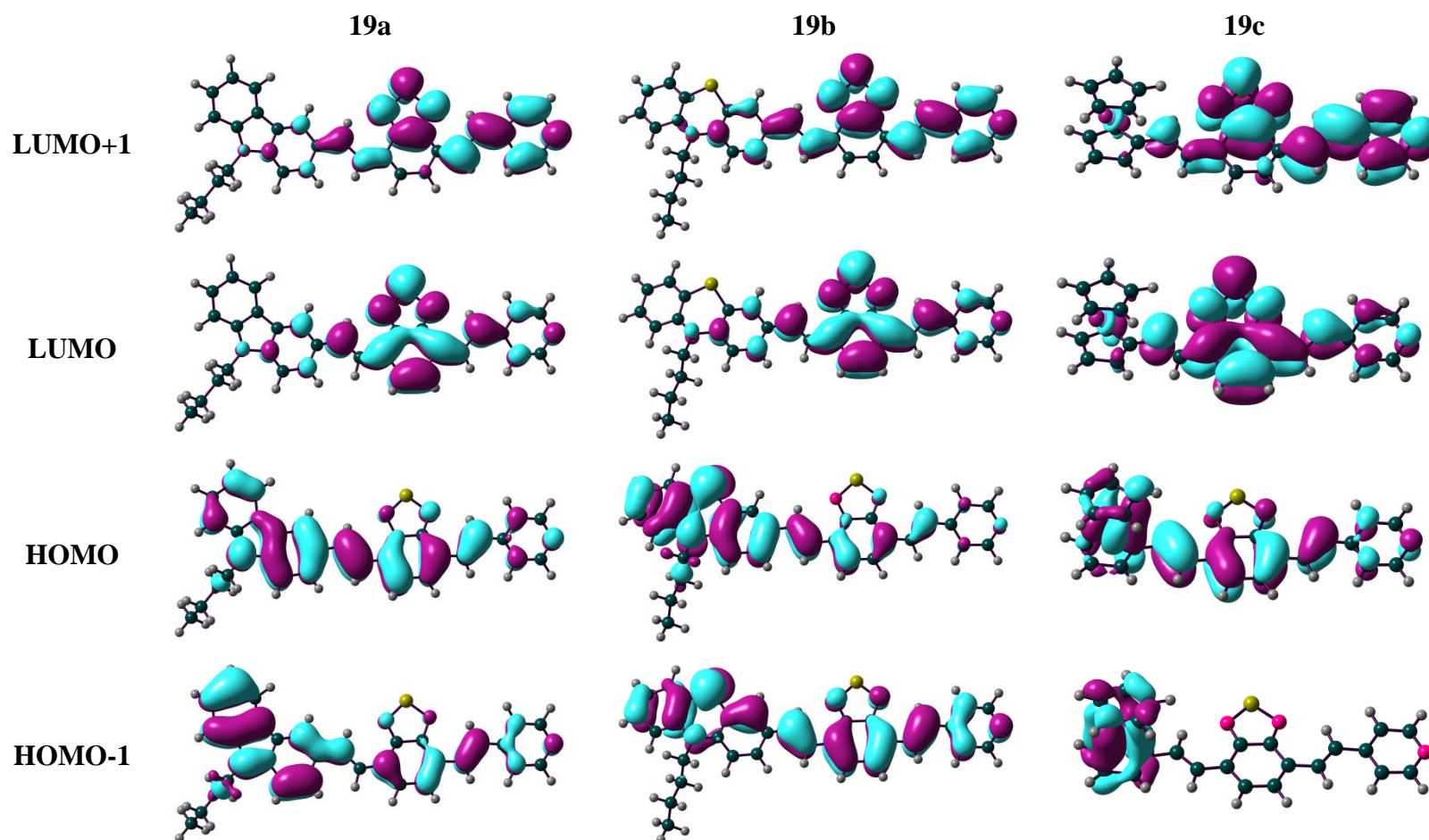


Figure 5.19 Frontier molecular orbitals of dyes **19a**, **19b** and **19c** computed by using TDDFT at the B3LYP level

Table 5.7 Predicted vertical transitions, oscillator strength, configurations^[a], orbital energies, and dipole moments using B3LYP (gas)

Dye	$\lambda_{\text{abs}}/\text{nm}$	f	Configuration	HOMO, eV	LUMO, eV	μ_g (D)
15a	520.3	0.21	HOMO→LUMO (96%)	-5.22	-2.40	6.49
	347.2	0.52	HOMO→LUMO+1 (63%), HOMO-1→LUMO (34%)			
	330.6	0.36	HOMO-1→LUMO (64%), HOMO→LUMO+1 (32%)			
	251.9	0.15	HOMO-1→LUMO+1 (73%), HOMO→LUMO+4 (13%)			
15b	517.6	0.21	HOMO→LUMO (96%)	-5.34	-2.51	4.63
	346.2	0.34	HOMO-1→LUMO (53%), HOMO→LUMO+1 (45%)			
	330.6	0.52	HOMO→LUMO+1 (50%), HOMO-1→LUMO (45%)			
	251.9	0.14	HOMO-1→LUMO+1 (76%), HOMO→LUMO+4 (12%)			
17	421.4	0.88	HOMO→LUMO (98%)	-6.66	-2.46	1.02
	294.2	0.98	HOMO→LUMO+1 (95%)			
19a	583.4	0.72	HOMO→LUMO (98%)	-5.05	-2.64	7.73
	378.3	1.19	HOMO→L+1 (89%)			
	280.8	0.10	HOMO-1→LUMO+2 (58%), HOMO-2→LUMO+1 (9%) HOMO→LUMO+3 (7%), HOMO-1→LUMO+3 (6%)			
19b	655.2	0.50	HOMO→LUMO (99%)	-4.87	-2.71	7.17
	490.8	0.26	HOMO-1→LUMO (95%)			
	411.4	0.68	HOMO→LUMO+1 (87%)			
	338.4	0.77	HOMO-1→LUMO+1 (90%)			
19c	609.3	0.21	HOMO→LUMO (72%)	5.21	2.72	4.80
	521.5	0.22	HOMO-2→LUMO (28%), HOMO→LUMO (23%) HOMO-1→LUMO+4 (17%)			
	374.5	0.30	HOMO-4→LUMO (52%), HOMO→LUMO+1 (42%)			
	361.6	0.36	HOMO→LUMO+1 (45%), HOMO-4→LUMO (39%)			
	345.9	0.13	HOMO-3→LUMO+6 (19%), HOMO-1→LUMO+4 (18%) HOMO-3→LUMO+2 (12%)			
	326.3	0.32	HOMO-2→LUMO+1 (80%)			

^[a] Contributions of less than 10% are omitted

Table 5.8 Predicted vertical transitions, oscillator strength, configurations ^[a], orbital energies, and dipole moments using MPW1K (gas)

Dye	λ_{abs} /nm	f	Configuration	HOMO, ev	LUMO, ev	μ_g (D)
15a	421.6	0.37	HOMO→LUMO (97%)	-6.18	-1.79	6.12
	292.9	0.82	HOMO→LUMO+1(94%)			
	257.5	0.14	HOMO-4→LUMO (71%), HOMO→LUMO+3 (18%)			
15b	419.0	0.36	HOMO→LUMO (97%)	-6.30	-1.90	4.28
	290.5	0.81	HOMO→LUMO+1 (93%)			
	257.3	0.15	HOMO-4→LUMO (71%), HOMO→LUMO+3(18%)			
17	421.4	0.88	HOMO→LUMO (98%)	-6.66	-2.46	1.02
	294.2	0.98	HOMO→LUMO+1 (95%)			
19a	467.2	1.05	HOMO→LUMO (95%)	-5.90	-2.10	7.15
	310.6	1.20	HOMO→LUMO+1 (78%), HOMO→LUMO+3 (6%)			
	250.6	0.51	HOMO-1→LUMO+2 (27%), HOMO→LUMO+3 (25%) HOMO-1→LUMO+3(13%), HOMO-2→LUMO+2 (11%)			
19b	483.5	0.97	HOMO→LUMO (89%)	-5.74	-2.18	6.66
	380.6	0.11	HOMO-1→LUMO (85%)			
	332.0	0.46	HOMO→LUMO+1 (45%), HOMO→LUMO+2 (37%)			
	305.1	0.26	HOMO-2→LUMO (50%), HOMO-1→LUMO+1 (13%) HOMO-3→LUMO (10%)			
	300.7	0.44	HOMO-2→LUMO (25%), HOMO→LUMO+1 (19%) HOMO-1→LUMO+1(14%), HOMO→LUMO+2 (14%) HOMO→LUMO+4 (10%)			
	272.7	0.16	HOMO-7→LUMO (43%), HOMO→LUMO+4 (20%) HOMO-1→LUMO+2 (12%)			
	261.5	0.28	HOMO-1→LUMO+1 (25%), HOMO→LUMO+2 (19%) HOMO-7→LUMO (17%), HOMO→LUMO+1 (16%)			

^[a] Contributions of less than 10% are omitted

Table 5.9 Predicted vertical transitions, oscillator strength, configurations ^[a], orbital energies, and dipole moments using MPW1K (THF)

Dye	λ_{abs} /nm	f	Configuration	HOMO, ev	LUMO, ev	μ_{g} (D)
15a	430.4	0.49	HOMO→LUMO (98%)	-6.20	-1.83	7.70
	307.0	0.84	HOMO→LUMO+1 (94%)			
	261.2	0.19	HOMO-3→LUMO (73%), HOMO→LUMO+3 (13%) HOMO-1→LUMO (10%)			
15b	425.3	0.48	HOMO→LUMO (98%)	-6.29	-1.88	5.55
	303.6	0.83	HOMO→LUMO+1 (94%)			
	261.3	0.20	HOMO-3→LUMO (74%), HOMO→LUMO+3 (12%)			
17	428.9	1.10	HOMO→LUMO (98%)	-6.61	-2.37	1.52
	298.1	0.91	HOMO→LUMO+1 (96%)			
	278.2	0.14	HOMO-4→LUMO (67%), HOMO→LUMO+2 (20%)			
	259.7	0.12	HOMO-3→LUMO (39%), HOMO→LUMO+2 (38%)			
19a	479.1	1.24	HOMO→LUMO (94%)	-5.98	-2.18	8.49
	315.6	1.13	HOMO→LUMO+1 (77%), HOMO→LUMO+3 (6%)			
	265.5	0.13	HOMO-5→LUMO (29%), HOMO→LUMO+3 (24%) HOMO-3→LUMO (24%)			
	254.6	0.54	HOMO-1→LUMO+2 (29%), HOMO-4→LUMO (14%) HOMO-1→LUMO+3 (14%), HOMO-2→LUMO+2 (12%) HOMO→LUMO+3 (10%)			
	254.0	0.11	HOMO-4→LUMO (60%)			
19b	491.6	1.18	HOMO →LUMO (87%), HOMO-1→LUMO (10%)	-5.82	-2.23	8.15
	332.3	0.54	HOMO→LUMO+1 (43%), HOMO→LUMO+2 (39%)			
	305.8	0.52	HOMO-1→LUMO+1 (26%), HOMO→LUMO+1 (26%) HOMO→LUMO+2 (24%)			
	275.4	0.22	HOMO-6→LUMO (37%), HOMO-1→LUMO+2 (13%) HOMO-3→LUMO (11%), HOMO→LUMO+4 (11%)			
	267.1	0.15	HOMO→LUMO+4 (34%), HOMO-3→LUMO (12%) HOMO-2→LUMO (12%), HOMO-6→LUMO (10%)			
	263.6	0.24	HOMO-1→LUMO+1 (29%), HOMO→LUMO+1 (16%) HOMO→LUMO+2 (16%), HOMO-1→LUMO+2 (13%)			

^[a] Contributions of less than 10% are omitted

Effect of Donor on Optical Properties

The HOMO→LUMO transition can be considered as an ICT transition, which is shifted towards the lower energy region on the increment of electron donating ability of the donor. The transition occurring next to low energy transition in the dyes is HOMO→LUMO+1 with high oscillator strength. Therefore, it is believed that the donor characteristic HOMO, the BTD and vinylpyridine characteristics LUMO, LUMO+1 indicate that the HOMO→LUMO (or) LUMO+1 transitions bears a significant intramolecular charge-transfer (ICT) character from donor units to the benzothiadiazole-vinylpyridine. The S2 (HOMO→LUMO+1) and S1 (HOMO→LUMO) transition states has a charge shift mainly from donor moieties to the benzothiadiazole-vinylpyridine unit. From this, we conclude that both transitions can inject electrons into the conduction band of the TiO₂. When these pyridine anchoring dyes applied in DSSCs, electrons from donor part sequentially transferred to benzothiadiazole moiety, then shifted to the pyridine anchoring unit, and finally to nanocrystalline TiO₂ surface. The experimental photophysical and energy levels of the dyes is consistent with the trends observed by quantum chemical calculations and, in turn supports a progressive change in the electron richness of the donor unit. The dihedral angle between two adjacent conjugated segments in the ground-state of the dyes was showed in Figure 5.20.

Figure 5.20 Calculated dihedral angle angles (°) between various aromatic segments and vinyl pyridine planes in the optimized geometries of the dyes

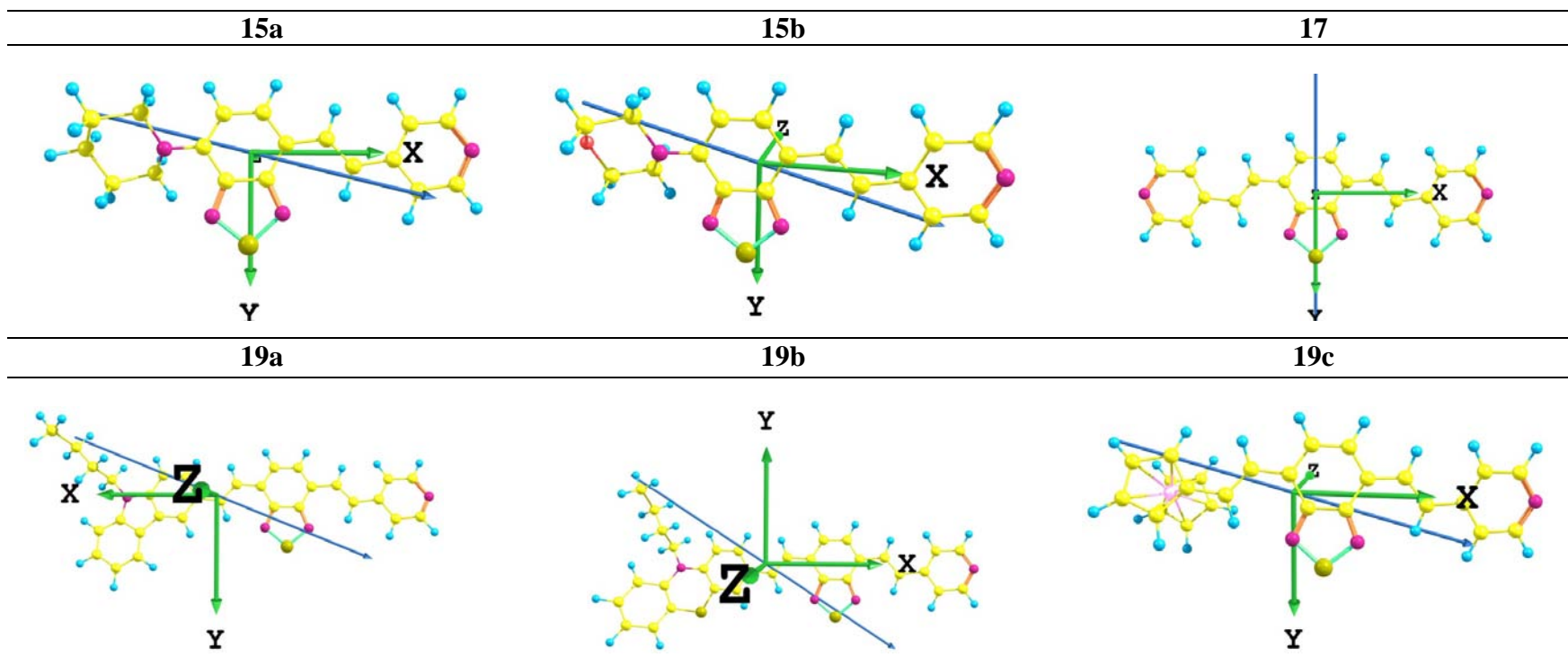


Figure 5.21 Direction of the dipole moment of the dyes

The dihedral angle between the benzothiadiazole and vinyl phenothiazine entity is higher than that of vinyl carbazole by 8.23°. Even with high dihedral angle between benzothiadiazole and vinyl phenothiazine, the dye **19b** attained the red shifted absorption by raising HOMO level. This may be attributed to the high electron donating ability of phenothiazine donor over carbazole. It should be noted that in this case **19c**, the MLCT of ferrocene play a role in the lowering the energy gap of the dye. In the optimized structures, the dihedral angle between the auxiliary acceptor BTD unit and anchoring pyridine moieties are smaller than 5°. Hence the coplanarity between these segments will help for the good electronic communication and efficient photoinduced electron transfer to TiO₂ film via the terminal pyridine anchoring group. It is also anticipated that the different electron donating abilities of the donor segment, will affect the direction and size of the dipole moment of the derivatives. Figure 5.21 shows the direction of the dipole moment of the benzothiadiazole-vinylpyridine dyes calculated by TD-DFT. The order of the dipole moment of the dyes as follows **17** < **15b** < **15a** < **19b** < **19a**. In the dipyrindyl derivative **17** which does not contain the donor segment, the dipole moment directed from benzene ring (δ^+) to thiadiazole (δ^-). While by the introduction of donor segments in the remaining dyes, the dipole moment is directed towards electron deficient pyridine ring (δ^-) from donor segments (δ^+). The π -extended dyes **19a** and **19b** acquired larger theoretically computed dipole moment compared to **15a** and **15b**, thus implying strong dipolar interactions in π -extended dyes.

5.2.6 Thermal properties

Thermal stability of the dye has significant impact on the life of the solar cell and one of the most essential parameters for applicability in DSSCs. So the thermal stability and the decomposition temperatures (T_d) of the new pyridine anchoring benzothiadiazole dyes were determined by the thermal gravimetric analysis (TGA) under nitrogen atmosphere, with a heating rate of 10 °C/min; the pertinent data are presented in Table 5.10. All the compounds showed excellent thermal stability (Figure 5.22) and their thermal decomposition temperatures are in the range 355-407 °C. In particular, the highest T_d value for the **19a** dye is 407 °C, indicative of excellent thermal stability. The carbazole featuring dye **19a** have been demonstrated to display high thermal robustness, due to the rigid and planar conformation than butterfly structured phenothiazine analogue **19b**.

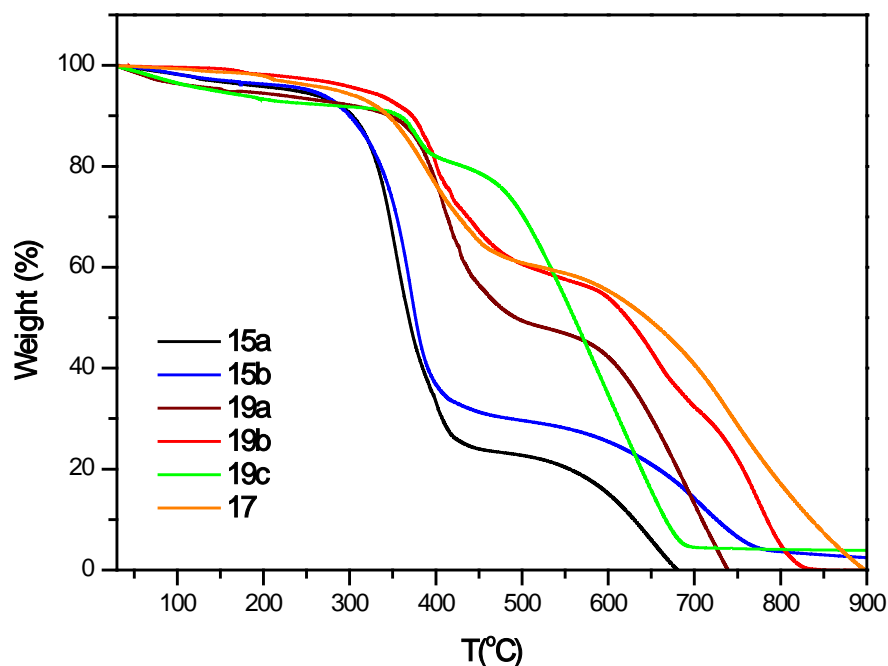


Figure 5.22 Thermograms of the benzothiadiazole-vinylpyridine dyes

Table 5.10 Thermal properties of the benzothiadiazole-pyridine anchoring sensitizers

Dye	T_{onset} °C ^a	T_d °C ^b
15a	303	355
15b	300	374
17	345	395
19a	347	407
19b	372	400
19c	358	371

^aTemperature corresponding to 10% weight loss. ^bHeating rate 10 °C/min in nitrogen.

5.2.7 Photovoltaic performances

The photovoltaic performances of the solar cells fabricated from these pyridine anchoring dye-sensitized TiO₂ electrodes were measured under simulated AM 1.5G irradiation (100 mW·cm⁻²). DSSCs were fabricated using I⁻/I³⁺ redox couple containing electrolyte 0.1 M LiI, 0.6 M 1,2-dimethyl-3-*n*-propylimidazolium iodide, 0.05 M I₂ and 0.5 M 4-*tert*-butylpyridine in a mixing solvent of ACN/MPN with a volume ratio of 1:1. The photocurrent-voltage (I-V) curves, the incident photon-to-current conversion efficiencies (IPCE) of the DSSCs are plotted in Figures 5.23 and photovoltaic performance parameters for the dyes are collected in Table 5.11. Depending on electron donor group tethered on the BTD unit, these dyes showed distinguishing and interesting results.

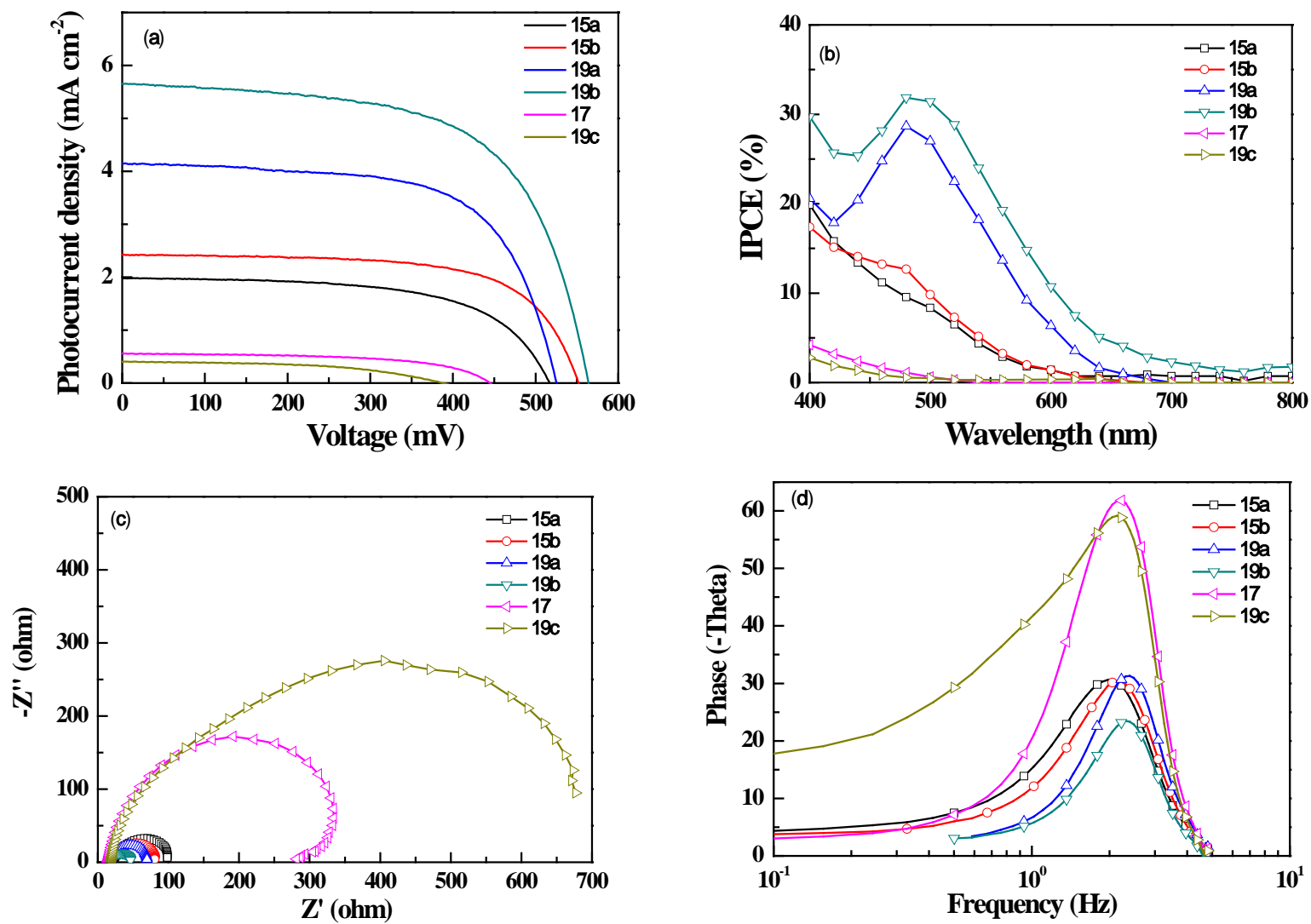


Figure 5.23 (a) I-V characteristics (b) IPCE plots (c) Nyquist plots (d) Bode phase plots for the DSSCs that were fabricated by using these dyes under illumination at 100 mW cm^{-2}

The IPCE spectra show maximum conversion efficiencies in the region 400-550 nm. The IPCEs of dyes **19a** and **19b** are more than 29% and 32%, respectively, in the range 450-500 nm. The onset IPCE for dyes **19a**, **19b** starts close to about 680 nm. The short-circuit current is associated to the molar extinction coefficient of the dyes. The short-circuit photocurrent density and efficiency for the devices increase in the order **19c** < **17** < **15a** < **15b** < **19a** < **19b**. For dyes **19a-b**, higher molar extinction coefficients yielded higher short-circuit current. The DSSCs sensitized by the dyes **19a** and **19b** have exhibited the higher η values 1.31% ($J_{sc} = 3.96 \text{ mA cm}^{-2}$, $V_{oc} = 516 \text{ mV}$, $ff = 0.64$) and 1.97% ($J_{sc} = 5.65 \text{ mA cm}^{-2}$, $V_{oc} = 564 \text{ mV}$, $ff = 0.62$), respectively. The π - extended dyes featuring arylamine donors (**19a-b**) showed higher power conversion efficiencies when compared to the alkylamine dyes (**15a-b**), owing to the lower molar coefficients of the later dyes. In addition, **19a-b** showed broader absorption bands than the dyes **15a-b** when adsorbed onto a TiO_2 surface (Figure 5.24 (b)). The derivatives **17** and **19c** achieved low efficiencies in the series, which are attributed to the low J_{sc} and V_{oc} values.

The V_{oc} value can be different for cells that are made from different sensitizers. This was mainly attributed to the difference in the electronic coupling between the TiO_2 nanoparticles and the sensitizer, which can change the quasi-Fermi level of TiO_2 . To elucidate the effect of the nature of the donor unit on the V_{oc} value, electrochemical impedance spectroscopy (EIS) measurements were conducted. Figure 5.24(a) shows Nyquist plots for DSSCs that were constructed from the sensitizers under dark conditions. It may be appropriate to discuss the photovoltaic properties of the sensitizers in two different categories: **15a-b**, **19a-b**. The Nyquist plot shows two semicircles, which assigned to the charge-transfer resistances at the counter electrode (R_{ct1}) and TiO_2 /dye/electrolyte interface (R_{rec}), respectively. The charge-transfer resistance assumes the order of **15a** < **15b** and indicates that the dye **15b** have high charge-recombination resist. The V_{oc} for the devices increases in the order of **15a** < **15b**. Where as in **19a-b**, the charge-transfer resistance assumes the order of **19a** < **19b** and supports the higher V_{oc} for **19b**. Upon illumination at 100 mWcm^{-2} under open-circuit conditions, from the radius of the intermediate-frequency semicircle in the Nyquist plot (Figure 5.23(c)), we found that the electron-transport resistance (R_{ct2}) followed the order **15b** < **15a** and **19b** < **19a**. Lower values of electron-transfer resistances for **15b** and **19b** would support the electron collection and consequently, would play an important role in increasing the efficiency of a cell.

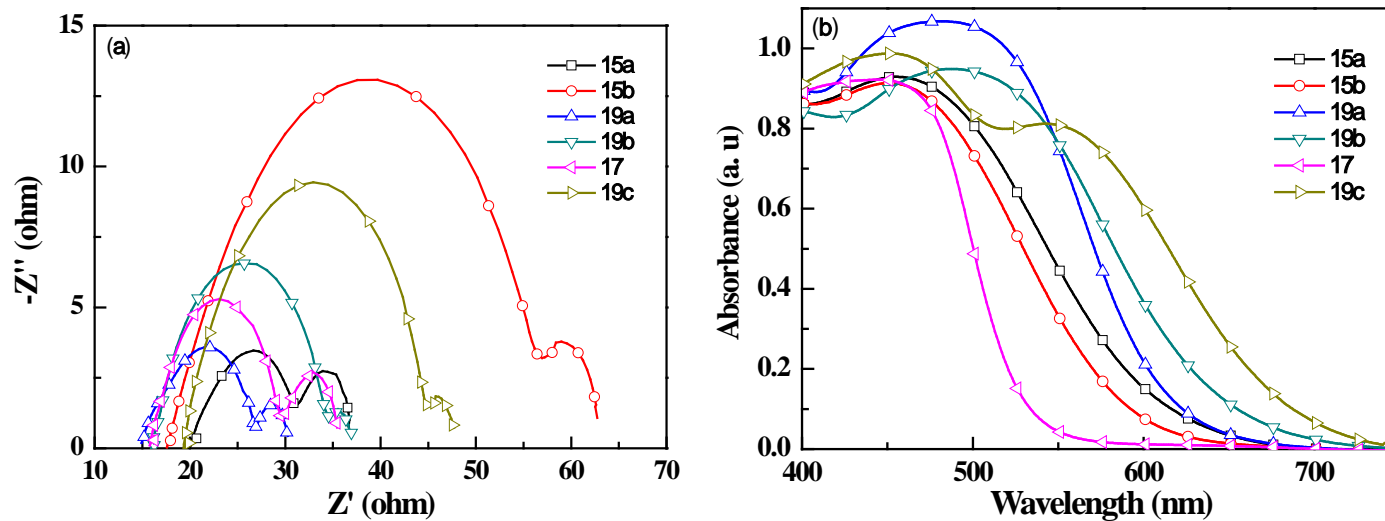


Figure 5.24 (a) Nyquist plots of the DSSCs fabricated using the dyes under dark conditions (b) Absorption spectra of the dyes anchored on nanocrystalline TiO₂

Table 5.11 Photovoltaic-performance parameters of the dyes.

Dye	η (%)	V_{OC} (mV)	J_{SC} (mA cm ⁻²)	ff	R_{rec} (ohm)	R_{ct2} (ohm)	τ_e (ms)
15a	0.62	516	1.99	0.61	12.29	80.67	1.41
15b	0.89	552	2.42	0.66	41.19	56.76	1.16
19a	1.31	516	3.96	0.64	12.11	54.12	0.64
19b	1.97	564	5.65	0.62	19.73	30.60	0.78
19c	0.08	387	0.40	0.51	25.80	512.28	1.16
17	0.14	445	0.56	0.58	14.77	317.26	0.95

The electron lifetime can be extracted from the angular frequency (ω_{\min}) at the mid-frequency peak in the Bode phase plot (Figure 5.23(d)) by using $\tau_e = 1/\omega_{\min}$. The obtained τ_e values follow the order **15a** > **15b** > **19b** > **19a**. Shorter electron life time and enhanced dark current observed for the carbazole containing dye is responsible for the low Voc than phenothiazine based dye. Despite the higher electron lifetime, the lower device efficiency observed for **17**, **19c** dyes is attributed to the lower number of photoinduced electron generation and high electron-transport resistance (R_{ct2}). These results revealed that the presence of the benzothiadiazole moiety in between electron donor and pyridine anchoring group is beneficial for enhancement of the light harvesting property and the onset IPCE for dyes extended up to 700 nm. The DSSCs sensitized by the dye **19b** showed promising efficiency of 1.97%, when compared to the dyes containing pyridine anchoring group. The promising performance of the dyes **19a**, **19b** as sensitizers is intriguing as they do not possess cyanoarylic acid anchoring/acceptor group.

5.3 Conclusions

In summary, we have designed and synthesized a series of benzothiadiazole sensitizers with pyridine terminal anchoring group, tethered with different electron donating segments by palladium catalyzed Heck-cross coupling reactions. The π -extended dyes **19a-c** displayed bathochromically shifted absorption profiles as compared to amine directly attached to benzothiadiazole dyes **15a-b**, due to the elongated conjugation and greater electron donating ability of donors. The ferrocenyl derivative (**19c**) displayed the most red shifted absorption profile due to the MLCT and non-emissive in nature. The modulation of donor segment successfully led to structure-dependent optical, electronic, and redox properties. Using the benzothiadiazole group as exciton confinement center, we have extended the absorption onset into the long-wavelength range beyond 600 nm by introducing strong ICT in the pyridine anchoring sensitizers. The dyes reported in this work showed higher light-harvesting properties when compared with the previously reported pyridine anchoring sensitizer, which illustrate the benefits of the benzothiadiazole unit as an efficient auxiliary acceptor on the π -conjugating bridge. Except **17**, all the dyes exhibited bathochromic shift in the absorption spectra upon addition of TFA. Enhanced charge transfer from the donors to the pyridium moiety justifies the bathochromic shift and it is reversible by neutralization with a base, such as Et_3N . The absorption maxima for all the dyes remain fairly constant, while their fluorescence maxima increased progressively by increasing the solvent polarity. Due to the stabilization of the excited

state in polar solvents as compared to the ground state, the dyes showed positive solvatochromism, which is attributed to the more-efficient solvation of the molecules in the excited state. The photophysical properties of the dyes were computed theoretically using TDDFT simulations employing B3LYP and MPW1K models, and the best resemblance has been found with MPW1K calculations. In addition, the TD-DFT calculations indicated that the LUMOs are highly localized on the benzothiadiazole and vinyl pyridine units, which could facilitate the electron transfer to the nanocrystalline TiO₂ via auxiliary acceptor/anchor groups from the donor segments. These materials exhibited good thermal stability and their thermal-decomposition temperatures fell within the range 355-407 °C, the highest decomposition temperature was displayed by carbazole comprising dye. The DSSC characteristics of the dyes are improved on incorporation of benzothiadiazole segment in the conjugation pathway. The π -extended arylamine dyes achieved higher efficiency than the alkylamine dyes, due to the red shifted absorption profiles and high molar extension coefficients. The DSSC device with the phenothiazine based sensitizer **19b** showed a power conversion efficiency of 1.97%, which is a promising efficiency with pyridine anchoring group under AM 1.5 G simulated solar light at a light intensity of 100 mW cm⁻². Tuning of the optical and photovoltaic properties of these dyes has been achieved by the modulation of donor segments with varied donor strength and conjugation pathway length. Thus, these finding may pave the new way to develop high light harvesting and stable pyridine anchoring sensitizers for DSSCs. Overall, the introduction benzothiadiazole in the π -conjugated bridge is not jeopardized for improvement of optical properties as well as the efficiency of the pyridine anchoring sensitizers. The promising performance of the dye **19b** as sensitizer is intriguing as it does not possess cyanoarylic acid anchoring/acceptor group.

5.4 Experimental section

5.4.1 Material and Methods

Thermogravimetric analysis/differential thermal analysis/differential thermogravimetry (TGA-DTA-DTG) measurements were performed on a Perkin-Elmer Pyris Diamond at a heating rate of 10°C min⁻¹ under a flow of nitrogen. Materials and physical methods are similar as in chapter 3.

5.4.2 Synthesis

Synthesis of (*E*)-4-bromo-7-(2-(pyridin-4-yl)vinyl)benzo[*c*][1,2,5]thiadiazole (16) and 4,7-bis((*E*)-2-(pyridin-4-yl)vinyl)benzo[*c*][1,2,5]thiadiazole (17): In a 100 ml pressure tube mixture of 4,7-dibromobenzo[*c*][1,2,5]thiadiazole (**2**) (2.94 g, 10 mmol), 4-vinylpyridine (1.05 g, 10 mmol), Pd(OAc)₂ (22.45 mg, 0.1 mmol), NaOAc (4.1 g, 50 mmol), and n-Bu₄NBr (0.65 g, 2 mmol) were dissolved in degassed *N,N*-dimethylformamide (50 mL). The solution was kept under a nitrogen atmosphere at 100 °C for 24 h with stirring. The mixture was poured into water. The precipitate was filtered, washed with water, dissolved in dichloromethane, and dried over anhydrous sodium sulfate. After evaporation of the solvent, the residue was purified by column chromatography on silica gel, using dichloromethane and hexane as eluant to obtain **16** and **17**.

16: Light yellow solid; Yield = 33%; mp 202-204 °C; IR (KBr, cm⁻¹): 2923, 2855, 2359, 1588, 1481, 1261; ¹H NMR (CDCl₃, 500.13 MHz): δ 7.49 (d, *J* = 5.5 Hz, 2H), 7.58 (d, *J* = 7.5 Hz, 1H), 7.69 (d, *J* = 16.5 Hz 1H), 7.87 (d, *J* = 7.5 Hz, 1H), 7.98 (d, *J* = 16.5 Hz, 1H), 8.64 (s, 2H); ¹³C NMR (125.75 MHz, CDCl₃): δ 114.2, 121.1, 128.2, 128.6, 129.0, 131.7, 132.3, 144.5, 150.3, 152.7, 153.9. HRMS (ESI) *m/z*: calculated for C₁₃H₈BrN₃NaS 339.9520 (M+Na)⁺; found 339.9503

17: Yellow solid; Yield = 31%; mp 230-232 °C; IR (KBr, cm⁻¹): 2968, 2923, 2357, 1585, 1544, 1407, 1229; ¹H NMR (CDCl₃, 500.13 MHz): δ 7.505 (d, *J* = 5.0 Hz, 4H), 7.768 (m, 4H), 8.033 (d, *J* = 16 Hz, 2H), 8.641 (d, *J* = 5 Hz, 4H); ¹³C NMR (125.75 MHz, CDCl₃): δ 121.1, 128.4, 128.6, 129.2, 131.4, 144.5, 150.3, 153.7. HRMS (ESI) *m/z* calculated for C₂₀H₁₅N₄S (M+H)⁺ 343.1017 observed 343.1015

Synthesis of (*E*)-4-(piperidin-1-yl)-7-(2-(pyridin-4-yl)vinyl)benzo[*c*][1,2,5]thiadiazole (15a)

In a 100 ml pressure tube mixture 4-bromo-7-(piperidin-1-yl)benzo[*c*][1,2,5]thiadiazole (**2a**) (0.298 g, 1 mmol), 4-vinylpyridine (0.115 g, 1.1 mmol), Pd(OAc)₂ (5 mg, 0.022mmol), NaOAc (0.82 g, 10 mmol), and n-Bu₄NBr (0.065 g, 0.2 mmol) was dissolved in degassed *N,N*-dimethylformamide (10 mL). The solution was kept under a nitrogen atmosphere at 100 °C for 24 h. The mixture was poured into water. The precipitate was filtered, washed with water, dissolved in dichloromethane, and dried over anhydrous sodium sulfate. After evaporation of the solvent, the residue was purified by column chromatography on silica gel, using a hexane/dichloromethane mixture as eluant. A red solid weighing 0.307 g (95%) was obtained. mp 108-110 °C; IR (KBr, cm⁻¹):2932, 2849, 2802, 1623, 1592, 1542,1385; ¹H NMR (500.13

MHz, CDCl₃): δ 1.72 (m, 2H), 3.60 (t, J = 5.0 Hz, 4H), 6.74 (d, J = 8.0 Hz 1H), 7.44 (d, J = 5.0 Hz, 2H), 7.58 (d, J = 8.0 Hz, 1H), 7.65 (d, J = 16.0 Hz, 1H), 7.83 (d, J = 16.0 Hz, 1H), 8.57 (d, J = 4.0 Hz, 2H); ¹³C NMR (125.75 MHz, CDCl₃): δ 24.5, 25.8, 51.3, 110.9, 120.5, 120.7, 126.7, 129.6, 130.9, 145.0, 145.7, 149.9, 154.7. HRMS (ESI) m/z calculated for C₁₈H₁₉N₄S, 323.1330 (M+H)⁺ found 323.1327

Synthesis of (*E*)-4-morpholino-7-(2-(pyridin-4-yl)vinyl)benzo[*c*][1,2,5]thiadiazole (**15b**)

Complex **15b** was prepared by following a procedure similar to that described above for **15a**, by taking one equivalent of 4-bromo-7-morpholinobenzo[*c*][1,2,5]thiadiazole (**2b**). Orange solid; Yield = 91%; mp 156-158 °C; IR (KBr, cm⁻¹): 2950, 2923, 2856, 1596, 1542, 1380, 1122; ¹H NMR (500.13 MHz, CDCl₃): δ 3.64 (t, J = 5.0 Hz, 4H), 4.00 (t, J = 5.0 Hz, 4H), 6.77 (d, J = 8.0 Hz 1H), 7.45 (d, J = 6.0 Hz, 2H), 7.61 (d, J = 8.0 Hz, 1H), 7.66 (d, J = 16.0 Hz, 1H), 7.86 (d, J = 16.0 Hz, 1H), 8.59 (dd, J = 5.0 Hz, 2H); ¹³C NMR (125.75 MHz, CDCl₃): δ 50.2, 66.8, 111.0, 120.8, 121.7, 127.6, 129.1, 130.4, 143.9, 145.3, 150.1, 154.7; HRMS (ESI) m/z calculated for C₁₇H₁₇N₄OS, 325.1123 (M+H)⁺ found 325.1156

Synthesis of 9-butyl-3-((*E*)-2-(7-((*E*)-2-(pyridin-4-yl)vinyl)benzo[*c*][1,2,5]thiadiazol-4-yl)vinyl)-9H-carbazole (**19a**)

In a 100 ml pressure tube mixture (*E*)-4-bromo-7-(2-(pyridin-4-yl)vinyl)benzo[*c*][1,2,5]thiadiazole (**16**) (0.240 g, 0.75 mmol), 9-butyl-3-vinyl-9H-carbazole (**18a**) (0.199 g, 0.8 mmol), Pd(OAc)₂ (5 mg, 0.022 mmol), NaOAc (0.82 g, 10 mmol), and n-Bu₄NBr (0.065 g, 0.2 mmol) was dissolved in degassed *N,N*-dimethylformamide (10 mL). The solution was kept under a nitrogen atmosphere at 100 °C for 24 h. The mixture was poured into water. The precipitate was filtered, washed with water, dissolved in dichloromethane, and dried over anhydrous sodium sulfate. After evaporation of the solvent, the residue was purified by column chromatography on silica gel, using a hexane/dichloromethane mixture as eluant. A red solid weighing 0.237 g (65%, 0.80 mmol) was obtained. mp 100-102 °C; IR (KBr, cm⁻¹): 3040, 2917, 2865, 1594, 1479, 1337, 1210, 1150, 1064, 961; ¹H NMR (CDCl₃, 500.13 MHz): δ 0.96 (t, J = 7.0 Hz, 3H), 1.41 (m, 2H), 1.86 (m, 2H), 4.29 (t, J = 7.0 Hz, 2H), 7.25 (m, 2H), 7.40 (m, 2H), 7.46 (d, J = 5.0 Hz, 3H), 7.68 (m, 3H), 7.78 (d, J = 7.0 Hz, 1H), 7.93 (m, 1H), 8.16 (m, 2H), 8.34 (s, 1H), 8.59 (s, 1H); ¹³C NMR (125.75 MHz, CDCl₃): δ 13.7, 20.4, 31.0, 42.9, 108.8, 119.1, 119.3, 120.3, 120.9, 121.2, 122.7, 123.2, 124.7, 125.4, 125.8, 127.0, 128.2, 128.9, 129.7, 131.2, 135.0, 140.6, 140.8, 144.8, 150.1, 153.6, 153.8; HRMS (ESI) m/z calculated for C₃₁H₂₇N₄S (M+H)⁺ 487.1956, found 487.1964

Synthesis of 10-butyl-3-((*E*)-2-(7-((*E*)-2-(pyridin-4-yl)vinyl)benzo[*c*][1,2,5]thiadiazol-4-yl)vinyl)-10*H*-phenothiazine (**19b**)

Complex **19b** was prepared by following a procedure similar to that described above for **19a**, by taking one equivalent of 10-butyl-3-vinyl-10*H*-phenothiazine (**18b**). Black solid; Yield = 61%; mp 150-152 °C; IR (KBr, cm⁻¹): 2924, 2860, 2359, 1587, 1459, 1385, 1330, 1249, 967; ¹H NMR (CDCl₃, 500.13MHz): δ 0.96 (t, *J* = 6.0 Hz, 3H), 1.48 (m, 2H), 1.80 (m, 2H), 3.86 (t, *J* = 6.0 Hz, 2H), 6.86 (t, *J* = 8.0 Hz, 2H), 6.92 (t, *J* = 7.0 Hz, 1H), 7.14 (m, 2H), 7.43 (m, 5H), 7.65 (m, 2H), 7.73 (d, *J* = 16.0 Hz, 1H), 7.88 (d, *J* = 16.0 Hz, 1H), 7.96 (d, *J* = 16.0 Hz, 1H), 8.61 (d, *J* = 4.0 Hz, 2H); ¹³C NMR (125.75 MHz, CDCl₃): δ 13.8, 20.1, 28.9, 47.3, 115.3, 115.4, 121.0, 122.4, 122.6, 124.1, 125.0, 125.3, 126.1, 126.5, 127.3, 127.4, 128.9, 129.0, 130.1, 130.8, 131.7, 132.8, 144.6, 144.9, 145.3, 150.2, 153.7, 153.8; HRMS (ESI) *m/z* calculated for C₃₁H₂₇N₄S (M+H) 519.1677 observed 519.1703

4-((*E*)-2-ferrocenylvinyl)-7-((*E*)-2-(pyridin-4-yl)vinyl)benzo[*c*][1,2,5]thiadiazole (**19c**)

Complex **19c** was prepared by following a procedure similar to that described above for **19a**, by taking one equivalent of vinyl ferrocene (**18c**). Dark black solid; Yield = 61%; mp 184-186 °C; IR (KBr, cm⁻¹): 2924, 2847, 1622, 1380, 1100, 965, 810; ¹H NMR (CDCl₃, 500.13MHz): δ 4.19 (s, 5H), 4.40 (s, 2H), 4.62 (s, 2H), 7.22 (s, 1H), 7.50 (s, 2H), 7.61 (s, 2H), 7.69 (d, *J* = 6.0 Hz, 1H), 7.75 (d, *J* = 16.0 Hz, 1H), 7.84 (d, *J* = 16.0 Hz, 1H), 7.99 (d, *J* = 16.0 Hz, 1H), 8.6 (s, 2H); ¹³C NMR (125.75 MHz, CDCl₃): δ 67.5, 69.5, 69.9, 83.0, 121.0, 121.5, 125.2, 126.8, 129.1, 129.2, 129.8, 131.2, 134.0, 145.0, 150.2, 153.7, 153.9. HRMS (ESI) *m/z* calculated for C₂₅H₁₉FeN₃S (M)⁺ 449.0649 observed 449.0625

5.5 References

- (1) J. Mao, N. He, Z. Ning, Q. Zhang, F. Guo, L. Chen, W. Wu, J. Hua and H. Tian, Stable dyes containing double acceptors without COOH as anchors for highly efficient dye-sensitized solar cells. *Angew. Chem., Int. Ed.*, **2012**, *51*, 9873-76.
- (2) Y. Ooyama and Y. Harima, Photophysical and Electrochemical Properties, and Molecular Structures of Organic Dyes for Dye-Sensitized Solar Cells. *ChemPhysChem* **2012**, *13*, 4032-80.
- (3) S. Urnikaite, T. Malinauskas, V. Gaidelis, I. Bruder, R. Send, R. Sens and V. Getautis, Simple and Inexpensive Organic Dyes with Hydrazone Moiety as π-Conjugation Bridge for Solid-State Dye-Sensitized Solar Cells. *Chem. Asian J.* **2013**, *8*, 538-41.

- (4) J. Wiberg, T. Marinado, D. P. Hagberg, L. Sun, A. Hagfeldt and B. Albinsson, Effect of Anchoring Group on Electron Injection and Recombination Dynamics in Organic Dye-Sensitized Solar Cells. *J. Phys. Chem. C* **2009**, *113*, 3881-86.
- (5) S. S. Park, Y. S. Won, Y. C. Choi and J. H. Kim, Molecular Design of Organic Dyes with Double Electron Acceptor for Dye-Sensitized Solar Cell. *Energy Fuels* **2009**, *23*, 3732-6.
- (6) W. Zeng, Y. Cao, Y. Bai, Y. Wang, Y. Shi, M. Zhang, F. Wang, C. Pan and P. Wang, Efficient Dye-Sensitized Solar Cells with an Organic Photosensitizer Featuring Orderly Conjugated Ethylenedioxythiophene and Dithienosilole Blocks. *Chem. Mater.* **2010**, *22*, 1915-25.
- (7) A. Yella, R. Humphry-Baker, B. F. E. Curchod, N. Ashari Astani, J. Teuscher, L. E. Polander, S. Mathew, J.-E. Moser, I. Tavernelli, U. Rothlisberger, M. Grätzel, M. K. Nazeeruddin and J. Frey, Molecular Engineering of a Fluorene Donor for Dye-Sensitized Solar Cells. *Chem. Mater.* **2013**, *25*, 2733-39.
- (8) R. Yeh-Yung Lin, H.-W. Lin, Y.-S. Yen, C.-H. Chang, H.-H. Chou, P.-W. Chen, C.-Y. Hsu, Y.-C. Chen, J. T. Lin and K.-C. Ho, 2,6-Conjugated anthracene sensitizers for high-performance dye-sensitized solar cells. *Energy & Environmental Science* **2013**, *6*, 2477-86.
- (9) Y. Ooyama, S. Inoue, T. Nagano, K. Kushimoto, J. Ohshita, I. Imae, K. Komaguchi and Y. Harima, Dye-sensitized solar cells based on donor-acceptor pi-conjugated fluorescent dyes with a pyridine ring as an electron-withdrawing anchoring group. *Angew. Chem., Int. Ed.*, **2011**, *50*, 7429-33.
- (10) H. He, A. Gurung and L. Si, 8-Hydroxylquinoline as a strong alternative anchoring group for porphyrin-sensitized solar cells. *Chem Commun* **2012**, *48*, 5910-12.
- (11) B. Zietz, V. Johansson, E. Gabrielsson, A. M. El-Zohry, L. Sun and L. Kloo, Photoisomerization of the Cyanoacrylic Acid Acceptor Group - A Potential Problem for Organic Dyes in Solar Cells. *Phys. Chem. Chem. Phys.* **2014**, *16*, 2251-2255.
- (12) C. Chen, X. Yang, M. Cheng, F. Zhang and L. Sun, Degradation of cyanoacrylic acid-based organic sensitizers in dye-sensitized solar cells. *ChemSusChem* **2013**, *6*, 1270-75.
- (13) Y. Ooyama, N. Yamaguchi, I. Imae, K. Komaguchi, J. Ohshita and Y. Harima, Dye-sensitized solar cells based on D- π -A fluorescent dyes with two pyridyl groups as an electron-withdrawing-injecting anchoring group. *Chem Commun* **2013**, *49*, 2548-50.

- (14) Y. Ooyama, T. Nagano, S. Inoue, I. Imae, K. Komaguchi, J. Ohshita and Y. Harima, Dye-sensitized solar cells based on donor- π -acceptor fluorescent dyes with a pyridine ring as an electron-withdrawing-injecting anchoring group. *Chem. Eur. J.* **2011**, *17*, 14837-43.
- (15) Y. Ooyama, Y. Hagiwara, T. Mizumo, Y. Harima and J. Ohshita, Photovoltaic performance of dye-sensitized solar cells based on D- π -A type BODIPY dye with two pyridyl groups. *New J. Chem.* **2013**, *37*, 2479-85.
- (16) J. Zhao, X. Yang, M. Cheng, S. Li and L. Sun, Molecular design and performance of hydroxypyridium sensitizers for dye-sensitized solar cells. *ACS Appl. Mater. Interfaces* **2013**, *5*, 5227-31.
- (17) L. Wang, X. Yang, S. Li, M. Cheng and L. Sun, A new type of organic sensitizers with pyridine-N-oxide as the anchoring group for dye-sensitized solar cells. *RSC Advances* **2013**, *3*, 13677-80.
- (18) J. Mao, D. Wang, S.-H. Liu, Y. Hang, Y. Xu, Q. Zhang, W. Wu, P.-T. Chou and J. Hua, Dye-Sensitized Solar Cells Based on Functionally Separated D- π -A Dyes with 2-Cyanopyridine as an Electron-Accepting and Anchoring Group. *Asian Journal of Organic Chemistry* **2014**, *3*, 153-60.
- (19) J. Warnan, V.-M. Guerin, F. B. Anne, Y. Pellegrin, E. Blart, D. Jacquemin, T. Pauporté and F. Odobel, Ruthenium Sensitizer Functionalized by Acetylacetonate Anchoring Groups for Dye-Sensitized Solar Cells. *J. Phys. Chem. C* **2013**, *117*, 8652-60.
- (20) Lopez-Duarte, M. Wang, R. Humphry-Baker, M. Ince, M. V. Martinez-Diaz, M. K. Nazeeruddin, T. Torres and M. Gratzel, Molecular engineering of zinc phthalocyanines with phosphinic acid anchoring groups. *Angew. Chem., Int. Ed.*, **2012**, *51*, 1895-98.
- (21) T. P. Brewster, S. J. Konezny, S. W. Sheehan, L. A. Martini, C. A. Schmuttenmaer, V. S. Batista and R. H. Crabtree, Hydroxamate anchors for improved photoconversion in dye-sensitized solar cells. *Inorg. Chem.* **2013**, *52*, 6752-64.
- (22) A. Abbotto, S. Bradamante and G. A. Pagani, Pyridoneimines and Pyridonemethides: Substituent- and Solvent-Tunable Intramolecular Charge Transfer and Geometric Isomerism. *J. Org. Chem.* **2001**, *66*, 8883-92.
- (23) Y. Harima, T. Fujita, Y. Kano, I. Imae, K. Komaguchi, Y. Ooyama and J. Ohshita, Lewis-Acid Sites of TiO₂ Surface for Adsorption of Organic Dye Having Pyridyl Group as Anchoring Unit. *J. Phys. Chem. C* **2013**, *117*, 16364-70.

- (24) M. D. Zhang, H. Pan, X. H. Ju, Y. J. Ji, L. Qin, H. G. Zheng and X. F. Zhou, Improvement of dye-sensitized solar cells' performance through introducing suitable heterocyclic groups to triarylamine dyes. *Phys. Chem. Chem. Phys.* **2012**, *14*, 2809-15.
- (25) M. D. Zhang, H. X. Xie, X. H. Ju, L. Qin, Q. X. Yang, H. G. Zheng and X. F. Zhou, D-D- π -A organic dyes containing 4,4'-di(2-thienyl)triphenylamine moiety for efficient dye-sensitized solar cells. *Phys. Chem. Chem. Phys.* **2013**, *15*, 634-41.
- (26) J. You, L. Dou, K. Yoshimura, T. Kato, K. Ohya, T. Moriarty, K. Emery, C. C. Chen, J. Gao, G. Li and Y. Yang, A polymer tandem solar cell with 10.6% power conversion efficiency. *Nature communications* **2013**, *4*, 1446.
- (27) W. Li, A. Furlan, K. H. Hendriks, M. M. Wienk and R. A. Janssen, Efficient tandem and triple-junction polymer solar cells. *J. Am. Chem. Soc.* **2013**, *135*, 5529-32.
- (28) M. Velusamy, K. R. J. Thomas, J. T. Lin, Y.-C. Hsu and K.-C. Ho, Organic Dyes Incorporating Low-Band-Gap Chromophores for Dye-Sensitized Solar Cells. *Org. Lett.* **2005**, *7*, 1899-902.
- (29) P. E. Schwenn, K. Gui, A. M. Nardes, K. B. Krueger, K. H. Lee, K. Mutkins, H. Rubinstein-Dunlop, P. E. Shaw, N. Kopidakis, P. L. Burn and P. Meredith, A Small Molecule Non-fullerene Electron Acceptor for Organic Solar Cells. *Advanced Energy Materials* **2011**, *1*, 73-81.
- (30) K. R. J. Thomas, J. T. Lin, M. Velusamy, Y. T. Tao and C. H. Chuen, Color Tuning in Benzo[1,2,5]thiadiazole-Based Small Molecules by Amino Conjugation/Deconjugation: Bright Red-Light-Emitting Diodes. *Adv. Funct. Mater.* **2004**, *14*, 83-90.
- (31) Y. H. Chen, L. Y. Lin, C. W. Lu, F. Lin, Z. Y. Huang, H. W. Lin, P. H. Wang, Y. H. Liu, K. T. Wong, J. Wen, D. J. Miller and S. B. Darling, Vacuum-deposited small-molecule organic solar cells with high power conversion efficiencies by judicious molecular design and device optimization. *J. Am. Chem. Soc.* **2012**, *134*, 13616-23.
- (32) Y. Sun, G. C. Welch, W. L. Leong, C. J. Takacs, G. C. Bazan and A. J. Heeger, Solution-processed small-molecule solar cells with 6.7% efficiency. *Nat. Mater.* **2012**, *11*, 44-8.
- (33) S. H. Park, A. Roy, S. Beaupré, S. Cho, N. Coates, J. S. Moon, D. Moses, M. Leclerc, K. Lee and A. J. Heeger, Bulk heterojunction solar cells with internal quantum efficiency approaching 100%. *Nat. Photonics* **2009**, *3*, 297-302.
- (34) M. Akhtaruzzaman, M. Tomura, M. B. Zaman, J.-i. Nishida and Y. Yamashita, Synthesis

- and Characterization of New Linear π -Conjugated Molecules Containing Bis(ethynylpyridine) Units with a Benzothiadiazole Spacer. *J. Org. Chem.* **2002**, *67*, 7813-18.
- (35) M. Akhtaruzzaman, M. Tomura, J.-i. Nishida and Y. Yamashita, Synthesis and Characterization of Novel Dipyridylbenzothiadiazole and Bisbenzothiadiazole Derivatives. *J. Org. Chem.* **2004**, *69*, 2953-58.
- (36) K. R. J. Thomas, J. T. Lin, Y.-Y. Lin, C. Tsai and S.-S. Sun, Self-Assembly Molecular Architectures Incorporating Fluorene- and Carbazole-Based Bichromic Oligopyridines. Novel Photoactive Materials. *Organometallics* **2001**, *20*, 2262-69.
- (37) Y. Ooyama, T. Nagano, S. Inoue, I. Imae, K. Komaguchi and Y. Harima, Dye-Sensitized Solar Cells Based on D- π -A Fluorescent Dyes with Pyridine Ring Forming Strong Interaction with Nanocrystalline TiO₂. *Bull. Chem. Soc. Jpn.* **2010**, *83*, 1113-21.
- (38) Y. Ooyama, T. Sato, Y. Harima and J. Ohshita, Development of a D- π -A dye with benzothienopyridine as the electron-withdrawing anchoring group for dye-sensitized solar cells. *J. Mater. Chem. A* **2014**, *2*, 3293-96.
- (39) J. Cui, J. Lu, X. Xu, K. Cao, Z. Wang, G. Alemu, H. Yuang, Y. Shen, J. Xu, Y. Cheng and M. Wang, Organic Sensitizers with Pyridine Ring Anchoring Group for p-Type Dye-Sensitized Solar Cells. *J. Phys. Chem. C* **2014**, dx.doi.org/10.1021/jp410829c.
- (40) S. Achelle, A. Barsella, C. Baudequin, B. Caro and F. Robin-le Guen, Synthesis and photophysical investigation of a series of push-pull arylvinylidiazine chromophores. *J. Org. Chem.* **2012**, *77*, 4087-96.
- (41) P. Singh, A. Baheti and K. R. J. Thomas, Synthesis and Optical Properties of Acidochromic Amine-Substituted Benzo[*a*]phenazines. *J. Org. Chem.* **2011**, *76*, 6134-45.
- (42) B. Valeur, *Molecular Fluorescence: Principles and Applications*, WILEY-VCH Verlag GmbH, Weinheim, 2002.
- (43) M. Jozefowicz, J.R. Heldt, Dipole moments studies of fluorenone and 4-hydroxyfluorenone, *Spectrochim. Acta A* *67* (2007) 316-20.
- (44) G.V. Loukova, A.A. Milov, V.P. Vasiliev, V.A. Smirnov, Dipole moment of a metallocene precatalyst in the ground and excited states, *Russ. Chem. Bull. Int. Ed.* *57* (2008) 1166-71.
- (45) C. Reichardt, Solvatochromic Dyes as Solvent Polarity Indicators. *Chem. Rev.* **1994**, *94*,

2319-58.

- (46) M. Gratzel, Photoelectrochemical cells. *Nature* **2001**, *414*, 338-44.
- (47) A. Mishra, M. K. R. Fischer and P. Bäuerle, Metal-Free Organic Dyes for Dye-Sensitized Solar Cells: From Structure: Property Relationships to Design Rules. *Angew. Chem., Int. Ed.*, **2009**, *48*, 2474-99.
- (48) P. Wang, S. M. Zakeeruddin, J.-E. Moser and M. Grätzel, A New Ionic Liquid Electrolyte Enhances the Conversion Efficiency of Dye-Sensitized Solar Cells. *J. Phys. Chem. B* **2003**, *107*, 13280-85.
- (49) R. G. Parr and W. Yang, Density-Functional Theory of the Electronic Structure of Molecules. *Annu. Rev. Phys. Chem.* **1995**, *46*, 701-28.
- (50) A. D. Becke, A new mixing of Hartree–Fock and local density-functional theories. *The Journal of Chemical Physics* **1993**, *98*, 1372-77.
- (51) C. Lee, W. Yang and R. G. Parr, Development of the Colle-Salvetti correlation-energy formula into a functional of the electron density. *Physical Review B* **1988**, *37*, 785-89.
- (52) B. J. Lynch, P. L. Fast, M. Harris and D. G. Truhlar, Adiabatic Connection for Kinetics. *J. Phys. Chem. A* **2000**, *104*, 4811-15.
- (53) Y.-F. Liu, X.-F. Ren, L.-Y. Zou, A.-M. Ren, J.-K. Feng and C.-C. Sun, Theoretical study on photophysical properties of 2,1,3-benzothiadiazole-based star-shaped molecules. *Theor. Chem. Acc.* **2011**, *129*, 833-45.
- (54) K. R. J. Thomas, P. Singh, A. Baheti, Y.-C. Hsu, K.-C. Ho and J. T. Lin, Electro-optical properties of new anthracene based organic dyes for dye-sensitized solar cells. *Dyes Pigm.* **2011**, *91*, 33-43.

Chapter 6

Benzothiadiazole-Phenothiazine Vinyl Conjugates: Effect of Conjugation on Optical and Electrochemical properties

6.1 Introduction

Over the last decade, organic materials with a donor-acceptor configuration in a conjugated system have received much attention due to the potential applications in various fields, such as organic light-emitting devices (OLEDs) [1-3], organic field-effect transistors (OFETs) [4-5], dye- sensitized solar cells (DSSCs) [6-7], bulk heterojunction organic solar cells (BHJs) [8], nonlinear optics [9-11] and sensors [12-13] etc. For instance, many scientific efforts have been made to fine-tune optoelectronic applicability with triaryl amines [14-17], carbazole [18-22], phenothiazine [23-30] and indoline [31-37] etc as donor segments and quinoxaline/pyrazine [38-45], benzo[*a*]phenazines [46], oxadiazole [47-50], benzothiadiazole [2, 51-55], triazine [56-58], cyanoacrylic acid [59-62] and imidazole [9, 20, 63-65] etc as an acceptor groups. Benzothiadiazole and phenothiazine based heterocyclic derivatives have been comprehensively proved as excellent active ingredients for electronic devices individually.

Benzothiadiazole (BTD) is one of the most intensively investigated electron-accepting heterocyclic system due to its intrinsic properties such as high reduction potential and electron affinity. By the incorporation of the BTD moiety in the π -conjugated system we can custom the highest occupied molecular orbital (HOMO) and the lowest unoccupied molecular orbital (LUMO). Due to the intermolecular interactions such as heteroatom contacts and π - π interactions BTD based materials expected to render well-ordered crystal with highly polarized properties [66]. Indeed benzothiadiazole based organic dyes are the special class of compounds which have the red shifted absorption and emission profiles due to the low lying LUMO level and low energy gap. In general, benzothiadiazole derivatives show low energy gap (band gap) due to the existence of the quinoid ring configuration Figure 6.1.

Figure 6.1 Resonance structures (aromatic and quinoid) of BTD

Recently, integration of benzothiadiazole with strong π donor that can be reversibly transform into its radical cation (TTF^+) and dication (TTF^{2+}) tetrathiafulvalene (Figure 6.2) demonstrated to have optimized absorption properties, charge transfer states in the visible and near-IR regions, along with improved photochemical stabilities [67].

Figure 6.2 Structures of the tetrathiafulvalene-benzothiadiazole based derivatives

Li et al. reported a series of dyes comprising triphenylamine and benzo[1,2,5]thiadiazole units linked through double bonds (Figure 6.3) [68-70]. The absorption spectra of the dyes in solution covered the visible region and the BHJs fabricated using dye **E6** achieved efficiency up to 2.39% with (6,6)-phenyl C70 butyric acid methyl ester (PC_{70}BM) as acceptor.

Figure 6.3 Structures of triphenylamine-benzothiadiazole reported vinyl derivatives

Benzothiadiazole-phenothiazine conjugates

Phenothiazine is a tricyclic heterocyclic compound containing electron rich sulphur and nitrogen [23,30]. Phenothiazine can preclude the molecular aggregation, formation of intermolecular excimers due to the non-planar butterfly conformation in the ground state [71]. It was also expected that inclusion phenothiazine into the molecular structure may improve the hole transporting ability as well as the performance of the organic device. The pronounced propensity of phenothiazine derivatives to form stable radical cations was described by Okada and co-workers [72]. Interestingly, Son and co-workers achieved excellent low turnover number (TON) due to the intriguing stability of their cationic radical formed by one electron oxidation of phenothiazine in visible light-induced water splitting [23]. Figure 6.4 shows the phenothiazine based vinyl derivatives known in the literature.

Figure 6.4 Structures of the phenothiazine based vinyl derivatives known in the literature.

To the best of our knowledge small molecules containing phenothiazine moiety attached to a low band chromophore like benzothiadiazole with vinyl linkage have been not exploited. So, we decided to explore the effect of phenothiazine unit on the photophysical and electrochemical

Benzothiadiazole-phenothiazine conjugates

behaviors of the benzothiadiazole. Because of paramount π -conjugation and red shifted absorption profiles we choose vinyl linkage over the rigid and electron deficient acetylene linkage. Further, introduction of vinyl linkage between phenothiazine and benzothiadiazole not only increases the conjugation but also increases the electronic coupling between them and may leads to enhanced charge transporting properties. The stronger electron donating ability of phenothiazine may help to achieve facile charge transfer to electron deficient benzothiadiazole. This may be beneficial to red shift the electronic absorption band and the molecular HOMO-LUMO energy levels can be tuned by the proper molecular design. In this context to evaluate the electronic communication between phenothiazine and benzothiadiazole donor-acceptor compounds, in this chapter we systematically designed and synthesised a new family of phenothiazine-benzothiadiazole hybrids (Figure 6.5) and established the structure-property relationships. We systematically varied the electron donors to tune the optical, electrochemical and thermal properties. These five dyes can be divided in to three categories. The dyes **26a**, **26b** are considered as D-A-D¹ and dyes **28a**, **28b** treated as D¹-A-D-A-D¹. The dye **27** is treated as D-A-D, where 10-butyl-10*H*-phenothiazine (D), piperidine/morpholine (D¹) acts as electron-rich units and benzo[*c*][1,2,5]thiadiazole (A) serve as electro-deficient unit.

Figure 6.5 Structures of the benzothiadiazole-phenothiazine vinyl conjugated derivatives

6.2 Results and Discussion

6.2.1 Synthesis and Characterization

The benzothiadiazole-phenothiazine conjugates were prepared by the protocol depicted in the Scheme 6.1.

Scheme 6.1 Synthetic pathways leading to benzothiadiazole-phenothiazine hybrids

All the derivatives were synthesised by palladium-catalyzed Heck coupling reaction in high yields. The vinyl derivatives 10-butyl-3-vinyl-10*H*-phenothiazine (**18b**) and 10-butyl-3,7-divinyl-10*H*-phenothiazine (**25**) have been synthesised by a three-step protocol involving butylation of 10*H*-phenothiazine, formylation by Vilsmeier-Haack reaction followed by Wittig reaction according to reported procedures [73-74]. Bromo derivatives of benzothiadiazole **2a** and **2b** were synthesised from dibromo benzothiadiazole (**1**). The derivative **2a** was synthesised according to reported procedure [75] and derivative **2b** was made from the reaction of dibromo benzothiadiazole with morpholine. The mono-substituted phenothiazine dyes (**26a** & **26b**) were obtained from **18b** by reacting with one equivalent of **2a** & **2b**. The di-substituted phenothiazine derivatives (**28a** & **28b**) were obtained from **25** by reacting with two equivalents **2a** & **2b**. By

the reaction of **1** with two equivalents of **18b**, the derivative **27** was obtained. All the derivatives were purified by column chromatography using appropriate eluant and well characterised by IR, ^1H NMR, ^{13}C NMR and HR-MS, the data was consistent with the proposed structures. The coupling constant (J) in ^1H NMR indicates that in all the derivatives the double bond(s) introduced by Heck coupling are in (*E*) configuration. Except **27**, all dyes showed the characteristic two doublet for the BTB protons in the region 6.75-7.70 ppm. The symmetrical nature of the benzothiadiazole in **27** was confirmed by the presence of a singlet at 7.62 ppm for the BTB protons. All the derivatives are intensely colored (orange or red) and soluble in common solvents such as CH_2Cl_2 , CHCl_3 , tetrahydrofuran, toluene but insoluble in alcohols.

6.2.2 Photophysical Properties

To probe the presence of donor-acceptor interactions and the absorption characteristics, we have recorded the absorption spectra of the dyes in dichloromethane and shown in Figure 6.6.

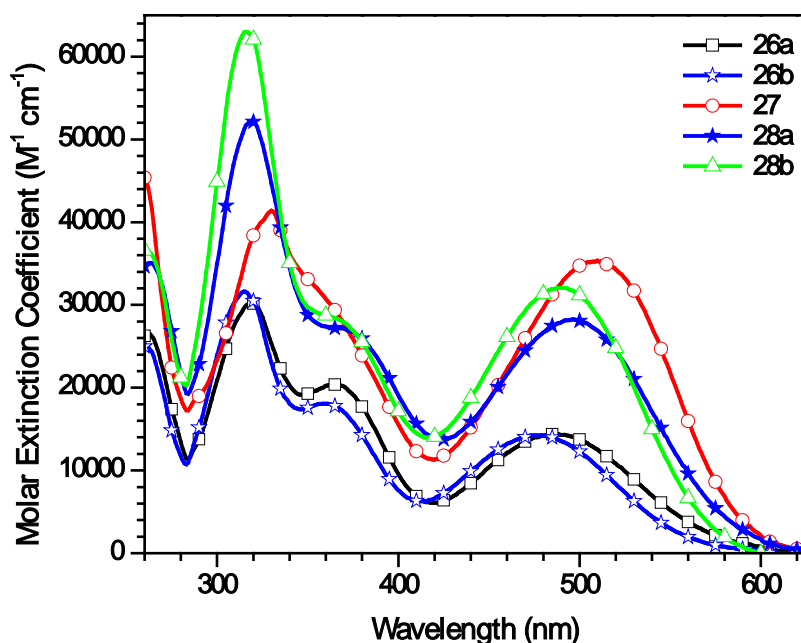


Figure 6.6 Absorption spectra of the dyes recorded in dichloromethane

The derivatives were showing two major absorption bands. The higher energy absorption band (280-420 nm) corresponds to $\pi-\pi^*$ transition and the low energy absorption band (420-600 nm) was attributed to the charge transfer from phenothiazine to BTB unit. Within the same class, the derivatives (**26a** and **28a**) containing electron rich piperidine unit tethered at 4th position of BTB showed red shifted absorption than the morpholine dyes (**26b** and **28b**). The molar extinction coefficient was raised nearly 1.75 fold from **26a** to **28a**, 1.69 fold from **26b** to **28b**, the increment in the molar extinction coefficient is due to the extension in conjugation.

Among all the derivatives, **27** showed red shifted absorption with high molar extinction coefficient due to the presence of two strong electron donating phenothiazine units. Figure 6.7 shows the absorption spectra of the derivatives recorded on thin films. The absorption pattern was similar to that observed for solutions. Small red shift in absorption peak position and large extent of broadening of the absorption edges in films as compared to solution was observed due to the existence of strong intermolecular interaction in the solid state. The absorption edges of the derivatives **26a**, **26b**, **27**, **28a** and **28b** are 660 nm, 625 nm, 720 nm, 650 nm and 710 nm, respectively. The optical band gaps of the derivatives were derived from the absorption edge of the thin film spectra. The optical band gaps for **26a**, **26b**, **27**, **28a**, and **28b** are 1.86 eV, 1.98 eV, 1.72 eV, 1.91 eV and 1.75 eV, respectively. The optical band gaps in the solid state were in the order **27** < **28a** < **26a** < **28b** < **26b**. From the absorption features of the thin film it was clear that, the derivatives cover the region from 250 nm to 700 nm. This broad absorption features may greatly enhance the photo current response and power-conversion efficiency in bulk heterojunction solar cell.

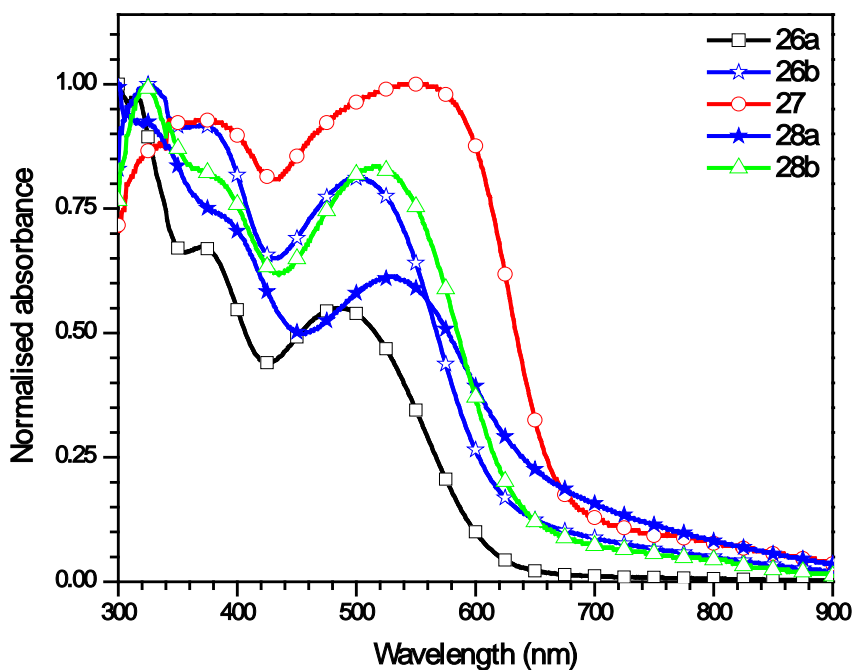


Figure 6.7 Absorption spectra of the dyes recorded on thin film

Solvent polarity plays a major role in tuning of the photophysical properties of the dyes. So to probe the effect of solvent polarity on the photophysical behavior of the dyes, we have examined absorption and fluorescence spectra in six different solvents with different dielectric constants viz. CH, TOL, THF, DCM, ACN and DMF (Figures 6.8, 6.9, 6.12, 6.13 (a)) and the pertinent data are collected in Tables 6.1 & 6.2.

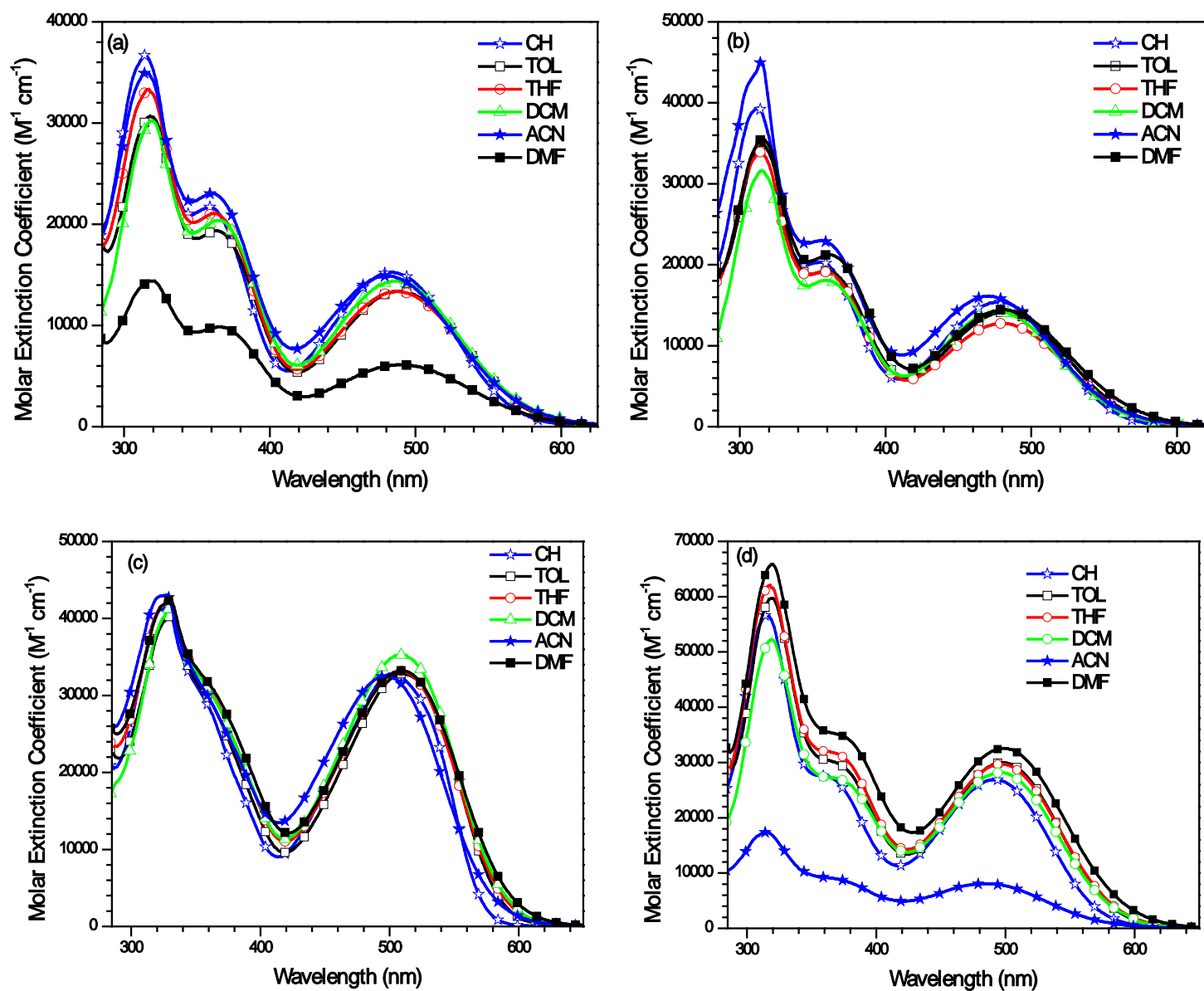


Figure 6.8 Absorption spectra of the dyes (a) 26a (b) 26b (c) 27 (d) 28a recorded in different solvents

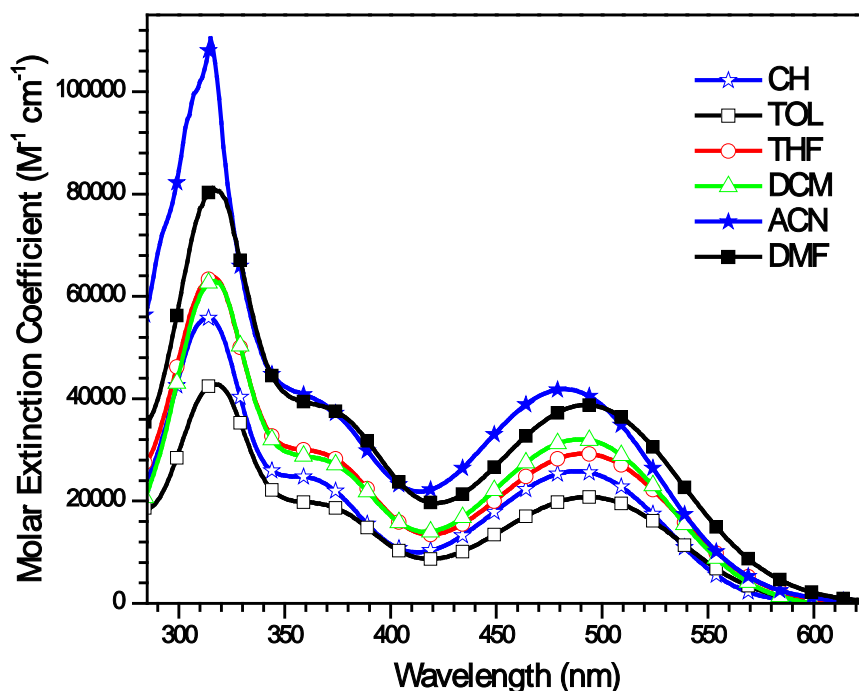


Figure 6.9 Absorption spectra of **28b** recorded in different solvents

The absorption spectra of the new benzothiadiazole-phenothiazine conjugates showed no significant difference by changing the solvent polarity. This indicates that in the ground state, there is no appreciable interaction between solvents and dye molecules.

Table 6.1 Absorption data of the dyes recorded in different solvents

Dye	λ_{abs} , nm ($\epsilon \times 10^3$ M ⁻¹ cm ⁻¹)						Film
	CH	TOL	THF	DCM	ACN	DMF	
26a	260 (37.0),	318 (30.7),	317 (33.3),	319 (30.2),	260 (35.7),	319,	371,
	314 (36.7),	363 (19.4),	363 (21.0),	365 (20.3),	316 (35.0),	366,	486
	351 (21.7),	489 (13.4)	489 (15.9)	486 (14.3)	361 (23.0),	490 ^a	
	484 (15.3)				481 (14.9)		
26b	260 (37.0),	315 (34.8),	315 (33.9),	315 (31.6),	259 (39.0),	316,	325,
	312 (39.3),	363 (19.4),	357 (19.1),	361 (18.0),	315 (45.0),	361,	373,
	355 (20.3),	482 (14.1)	480 (12.8)	476 (14.2)	356 (23.0),	481 ^a	501
	478 (15.4)				471 (16.1)		
27	259 (51.5),	331 (40.4),	330 (42.2),	330 (41.3),	258,	330 (42.4),	343,
	328 (41.4),	511 (32.8)	509 (33.2)	510 (35.3)	327,	510 (33.2)	547
	502 (32.8)				497 ^a		
28a	262 (42.9),	320 (59.7),	318 (62.0),	319 (52.2),	291,	320 (65.8),	392,
	315 (56.8),	374 (29.4),	496 (29.7)	374 (26.8) (sh),	316,	499 (32.6)	534
	492 (26.9)	498 (30.0)		497 (28.2)	486 ^a		
28b	261 (37.2),	316 (42.8),	317 (63.7),	316 (63.0),	263,	316 (81.1),	324,
	313 (55.8),	371 (19.0),	492 (29.3)	372 (25.6) (sh),	315,	492 (38.8)	386,
	488 (25.8)	493 (20.8)		490 (32.0)	482 ^a		517

^a Molar extinction coefficient could not be obtained due to poor solubility

Benzothiadiazole-phenothiazine conjugates

The emission spectra of the compounds were recorded in dichloromethane and displayed in Figure 6.10 and relevant data was collected in Tables 6.2. All the new phenothiazine-benzothiadiazole dyes were emitting orange-red fluorescence at the wavelength region of 563-611 nm.

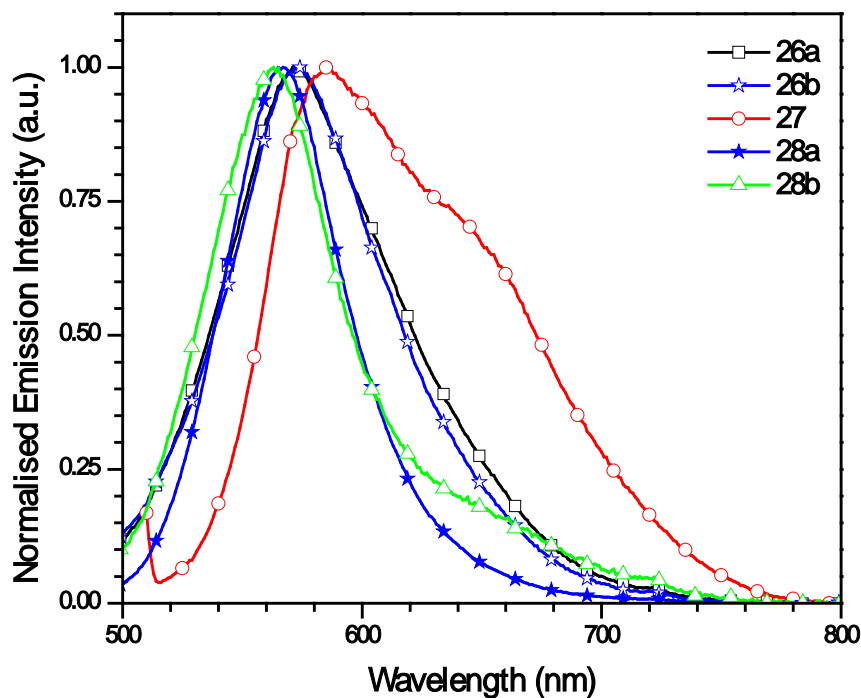


Figure 6.10 Emission spectra of the dyes recorded in DCM

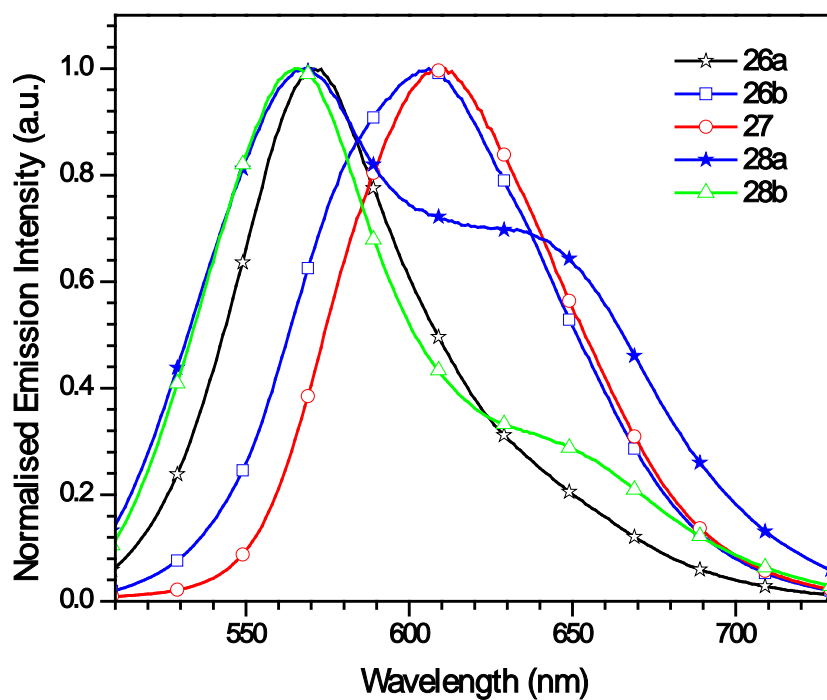


Figure 6.11 Emission spectra of the dyes recorded in toluene

It may be appropriate to discuss the emission spectra of the compounds in three different categories: **26a** and **26b** as (D-A-D¹), **28a** and **28b** as (¹D-A-D-A-D¹) and **27** as (D-A-D). Within a series (**26&28**), there is no appreciable change in the emission profile of the dyes in DCM. But the dye **27** possesses broad red shifted emission profile, which is attributed to the more elongated conjugation and strong ICT among the compounds. Interestingly **28a** and **28b** showed two emission bands in toluene (Figure 6.11), higher energy emission band centred at 560-570 nm and lower energy emission band peaking at 640-660 nm. To identify the origin of this dual emission observed for compounds **28a** and **28b**, the emission spectra of the dyes were measured in toluene with different concentrations (10 μ M to 1000 μ M) by exciting at 480 nm (Figures 6.13 (b) & (c)). The longer wavelength emission band starts appearing at a concentration of 10 μ M. As the concentration of the dye increases, the longer wavelength emission band grown in intensity. At the very high concentrations (500-1000 μ M) only the low energy emission band was observed. This observation is correlated with the formation of aggregation. However the nature of aggregation is not clear. It is probable that extended inter-chain donor-acceptor interactions may stabilize such aggregates. Despite the presence of non-planar butterfly like phenothiazine unit the formation of aggregates for the dyes **28a** and **28b** is intriguing.

Table 6.2 Emission properties and Stokes shift observed for the dyes in different solvents

Dye	λ_{em} , nm						Stokes shift (cm ⁻¹)					
	CH	TOL	THF	DCM	ACN	DMF	CH	TOL	THF	DCM	ACN	DMF
26a	574	606	589	571	598	603	3240	3948	3472	3063	4068	3824
26b	566	570	583	572	585	597	3253	3203	3681	3526	4137	4040
27	577	611	642	585	575	610	2589	3241	4070	2514	2729	3214
28a	616	565	586	567	575	603	4091	2381	3096	2484	3185	3456
28b	610	568	638	563	573	602	4098	2678	4651	2646	3295	3741

Unlike the minor shifts in the absorption spectra, the extent of the bathochromic shifts in fluorescence spectra of these dyes mainly depend on the solvent polarities. Commonly, these dyes exhibited larger Stokes shift values in the polar solvents due to the more favorable solvation-assisted ICT relaxation. With minor variations in cyclohexane and tetrahydrofuran, symmetrical (A-D-A) dyes **28a** and **28b** exhibited smaller Stokes shift than unsymmetrical (D-A) dyes **26a** and **26b** due to the associated small dipole moments. It is worth noting that the dyes **26a** (3063 cm⁻¹) and **26b** (3526 cm⁻¹) with asymmetrical structures exhibited larger Stokes shift than the dyes **28a** (2484 cm⁻¹) and **28b** (2646 cm⁻¹) with symmetrical structures in DCM.

This result probably indicates that asymmetrical dyes induce the larger dipole moment relative to those symmetrical dyes upon excitation from ground state to excited state [76]. The solvatochromic effects in the emission strongly propose a more polar electronic structure in the excited state than in the ground state for the dyes.

We have also attempted to correlate the solvent-dependent emission properties of the dyes using Lippert-Mataga equation [77-79], $E_T(30)$ parameter [80] and Kamlet-Taft equation [81-82]. The Lippert-Mataga equation provides information regarding the change in the dipole moment of the dye from ground state to the excited state and this correlation is useful if the solvent-dependent shift of the emission maximum is insensitive to non-specific interactions.

$$\bar{\nu}_A - \bar{\nu}_F = \frac{2}{hc} \left(\frac{\varepsilon - 1}{2\varepsilon + 1} - \frac{n^2 - 1}{2n - 1} \right) \frac{(\mu_E - \mu_G)^2}{a^3} + \text{constant}$$

In this equation h ($= 6.6256 \times 10^{-27}$ ergs) is Planck's constant, c ($= 2.9979 \times 10^{10}$ cm/s) is the speed of light, and a is the radius of the solvent cavity in which the fluorophore resides. $\bar{\nu}_A$, $\bar{\nu}_F$ are the wave numbers (cm^{-1}) of the absorption and emission, respectively. ε is dielectric constant and n is refractive index of the solvent. The orientation polarizability is defined as

$$\Delta f = \frac{2}{hc} \left(\frac{\varepsilon - 1}{2\varepsilon + 1} - \frac{n^2 - 1}{2n - 1} \right)$$

The Lippert-Mataga, Stokes' shift vs $E_T(30)$ parameter and wave number vs Kamlet-Taft parameter (π^*) plots for the derivatives were shown in Figures 6.14-6.18. The dye **26b** showing appreciable linearity in Lippert-mataga and $E_T(30)$, which is indicative of the existence of general solvent-solute interactions (Figure 6.15). Lippert-Mataga, $E_T(30)$, Kamlet-Taft plots for the dyes were displayed in the Figures 6.14-6.18.

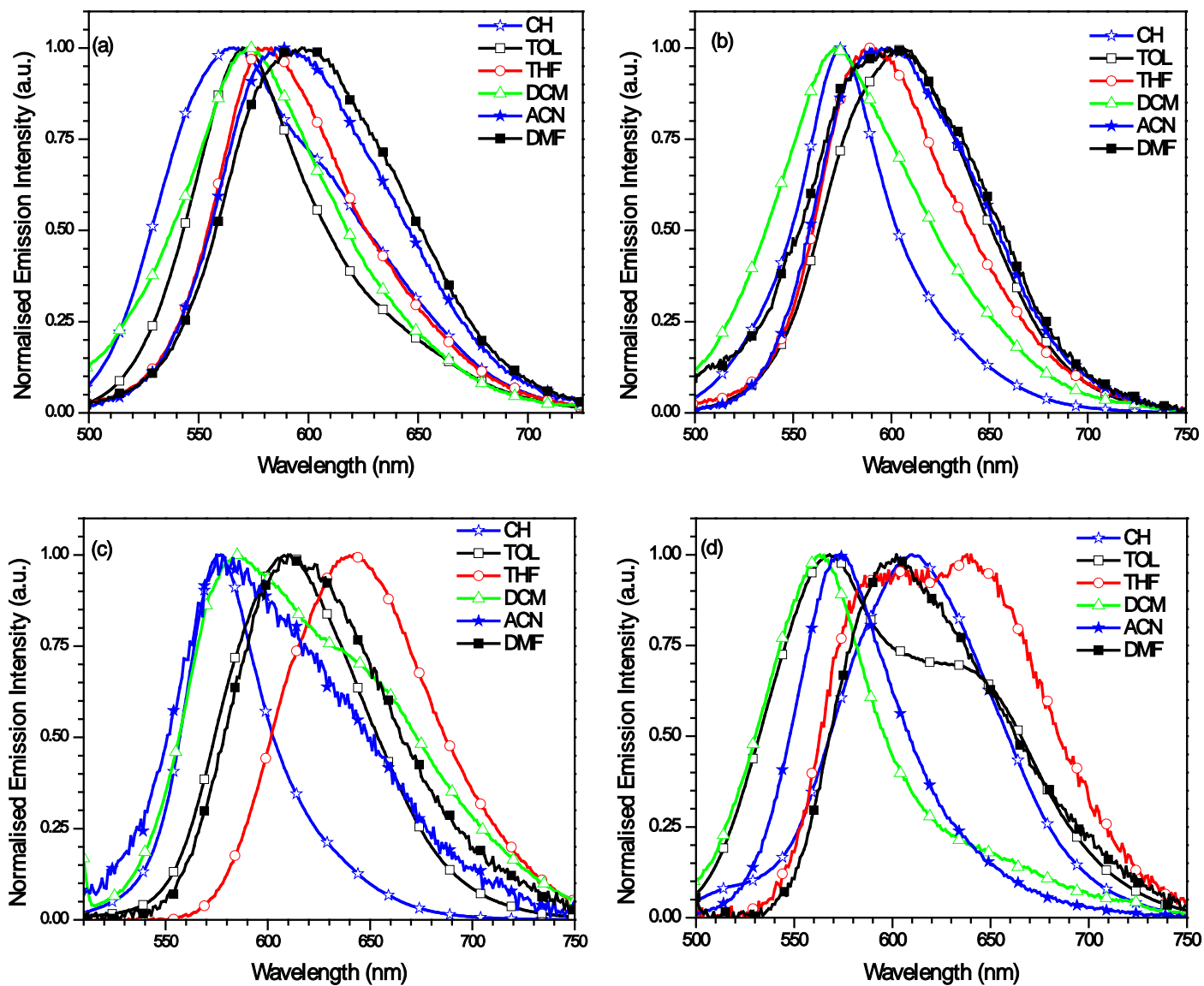


Figure 6.12 Emission spectra of the dye (a) 26a, (b) 26b, (c) 27 and (d) 28a recorded in different solvents

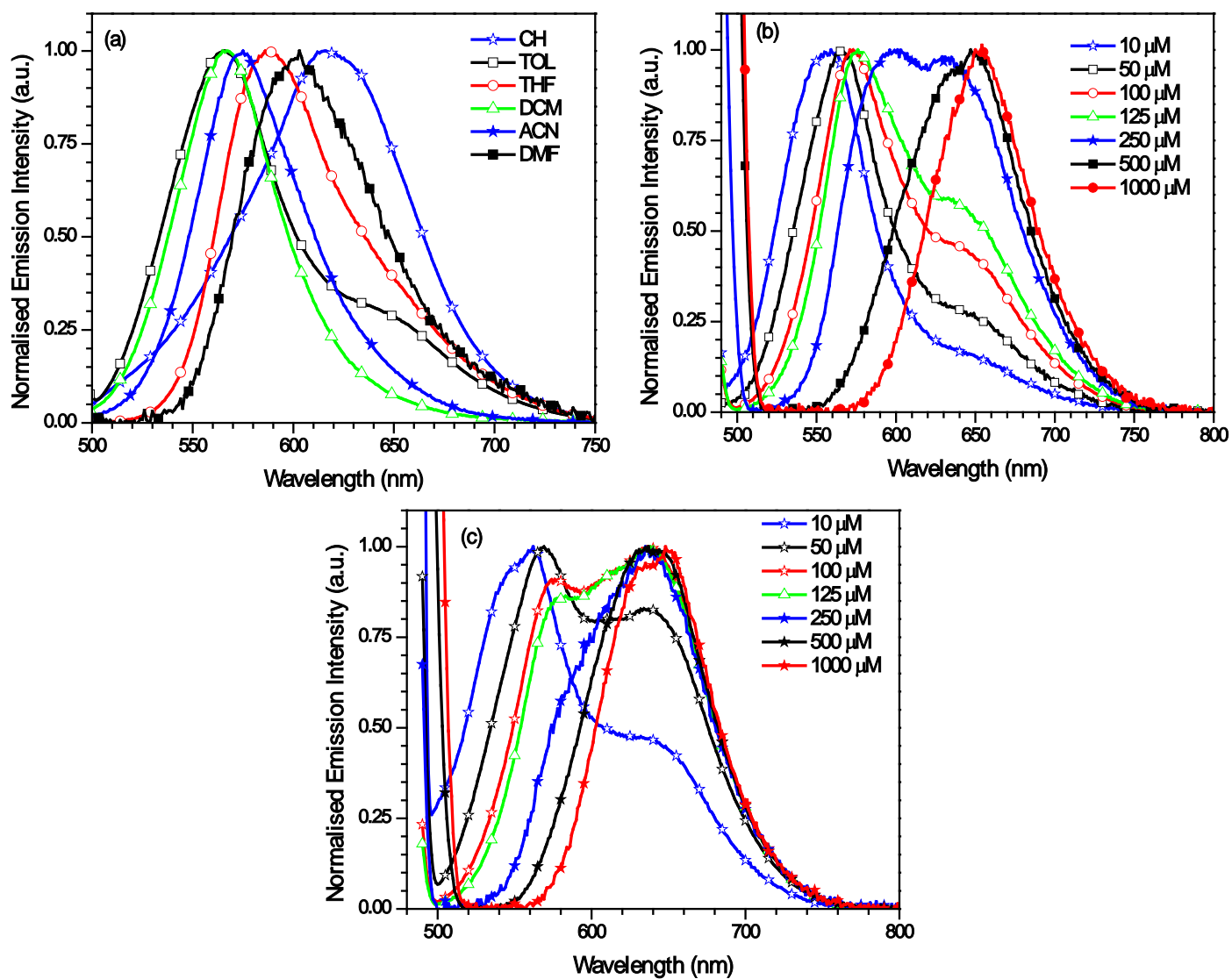


Figure 6.13 Emission spectra of the dye (a) **28b** recorded in different solvents, (b) **28a** recorded at various concentrations in toluene and (c) **28b** recorded at various concentrations in toluene

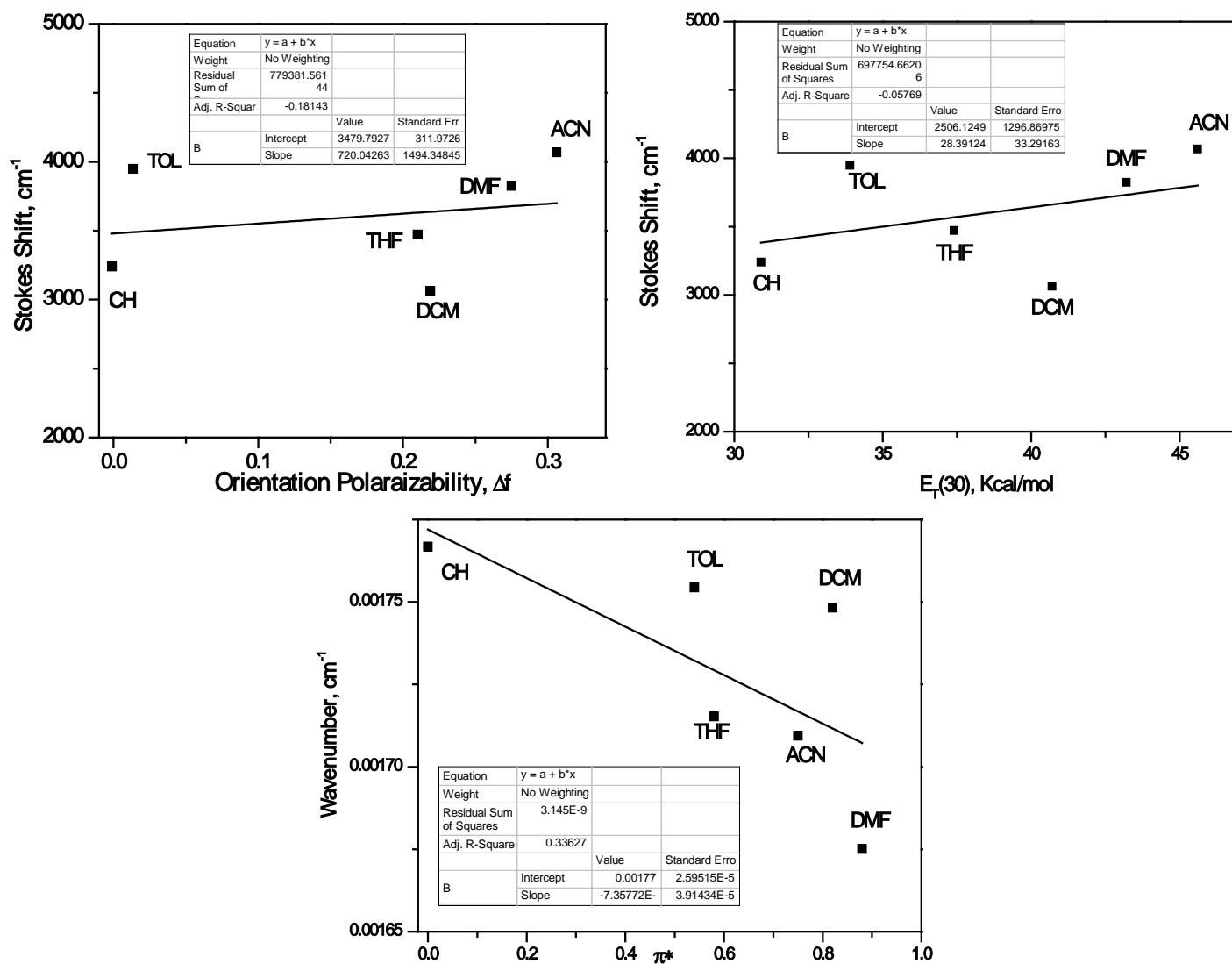


Figure 6.14 Plots for **26a** in different solvents (a) Lippert-Mataga plot showing Stokes' shift vs orientation polarizability of the solvents, (b) Stokes' shift vs $E_T(30)$ parameter, (c) Emission maxima (in wavenumber unit) vs Kamlet-Taft solvent polarity parameter.

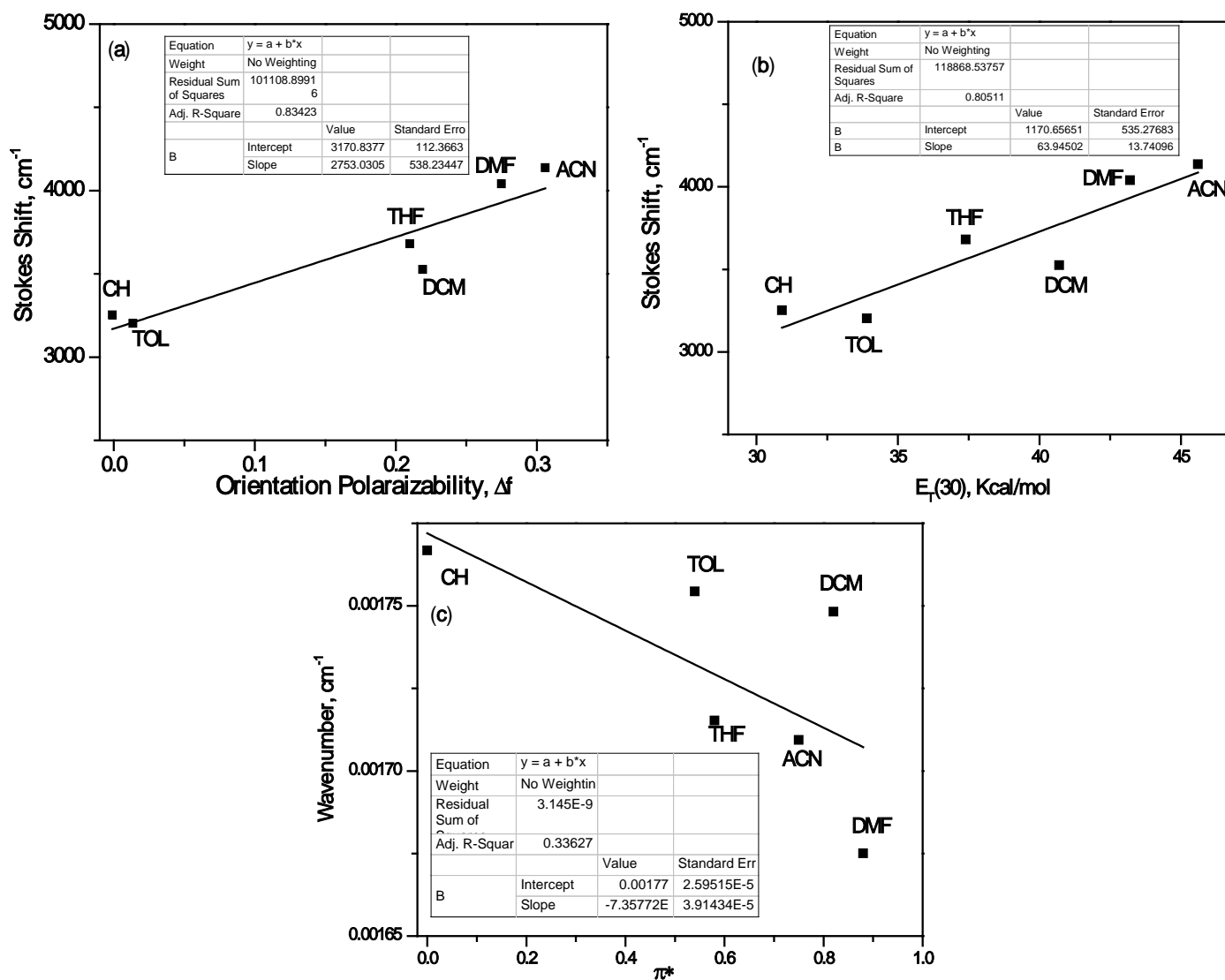


Figure 6.15 16 Plots for **27** in different solvents (a) Lippert-Mataga plot showing Stokes' shift vs orientation polarizability of the solvents, (b) Stokes' shift vs $E_T(30)$ parameter, (c) Emission maxima (in wavenumber unit) vs Kamlet-Taft solvent polarity parameter

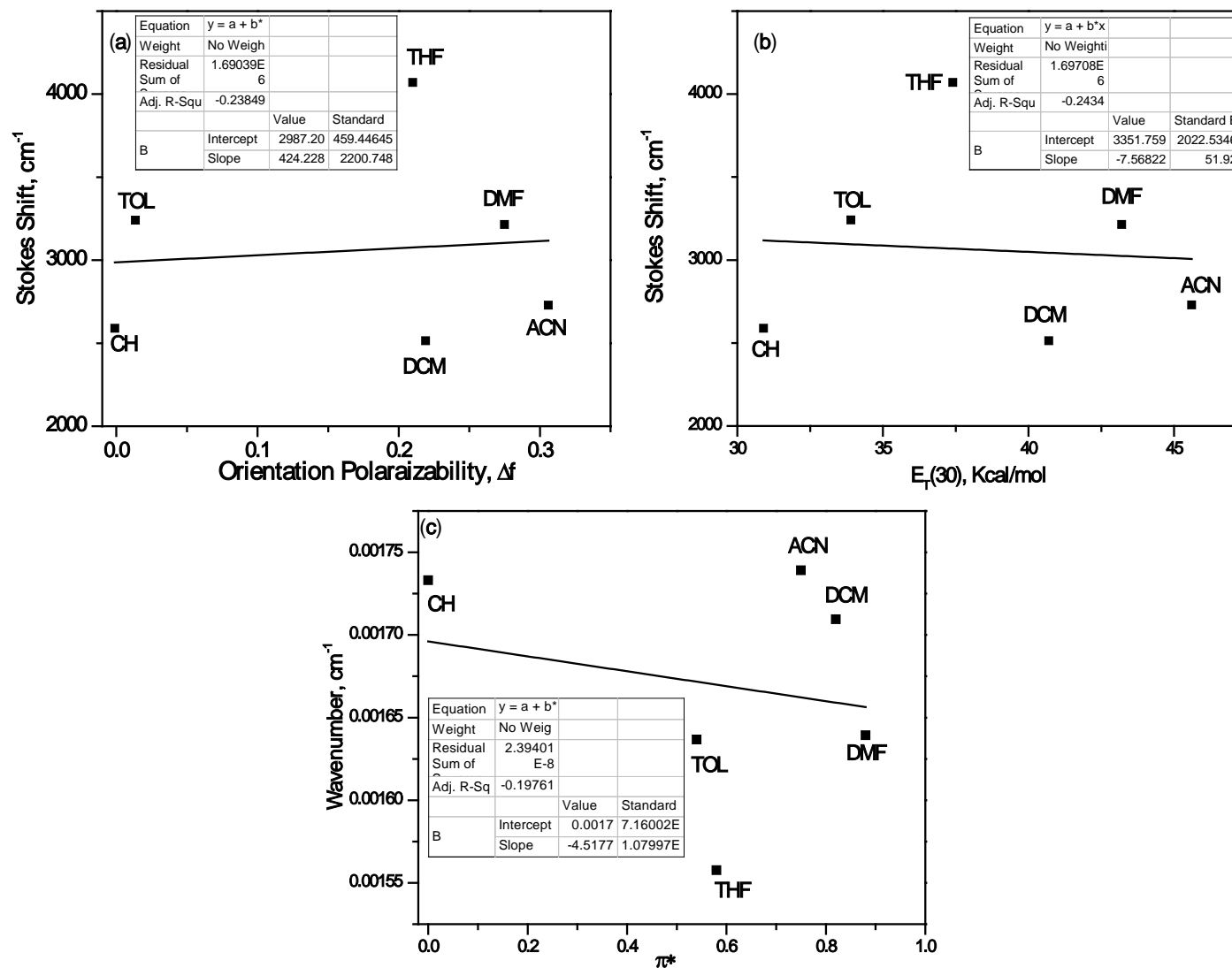


Figure 6.16 Plots for **27** in different solvents (a) Lippert-Mataga plot showing Stokes' shift vs orientation polarizability of the solvents, (b) Stokes' shift vs $E_T(30)$ parameter, (c) Emission maxima (in wavenumber unit) vs Kamlet-Taft solvent polarity parameter

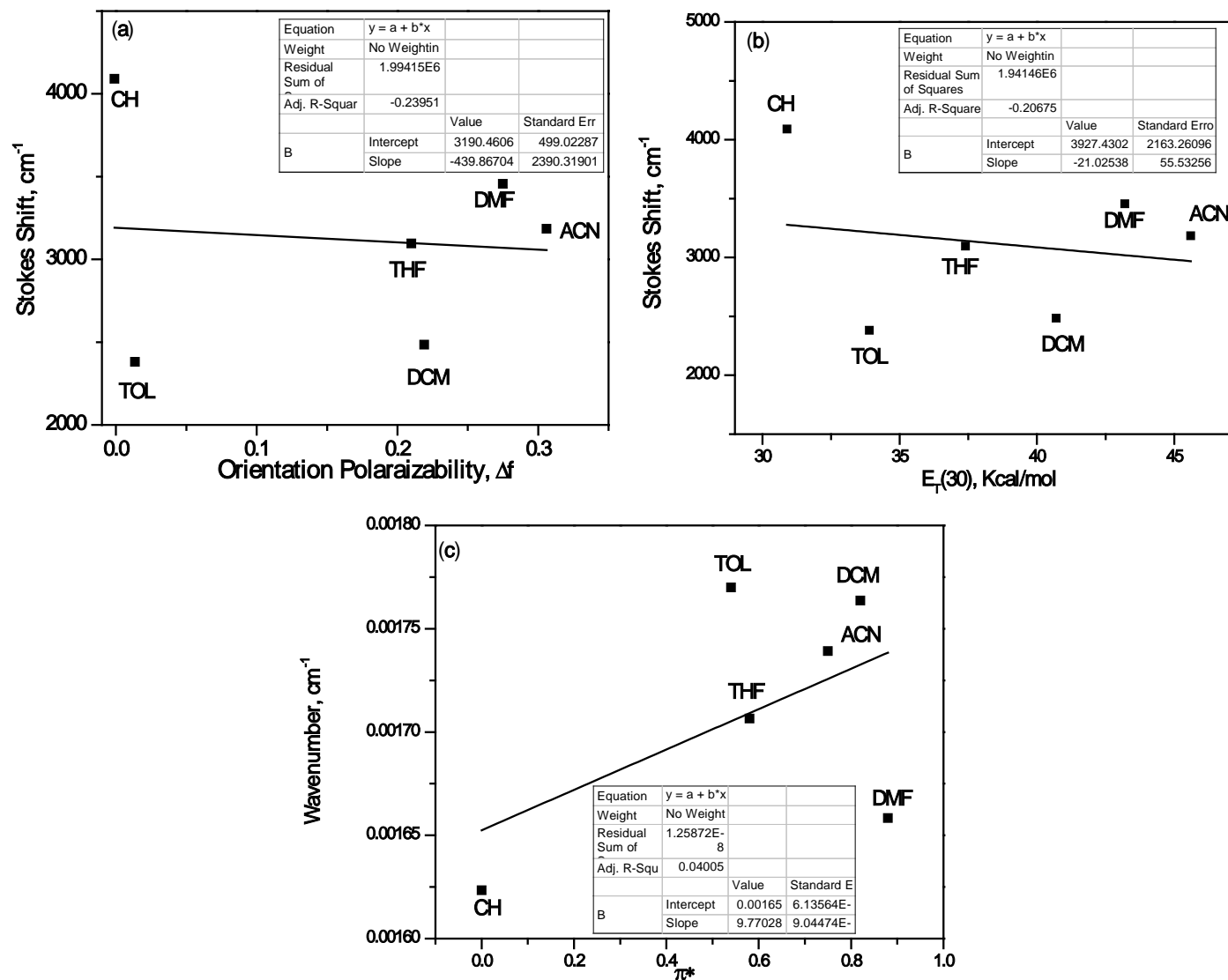


Figure 6.17 Plots for **28a** in different solvents (a) Lippert-Mataga plot showing Stokes' shift vs orientation polarizability of the solvents, (b) Stokes' shift vs $E_T(30)$ parameter, (c) Emission maxima (in wavenumber unit) vs Kamlet-Taft solvent polarity parameter

Benzothiadiazole-phenothiazine conjugates

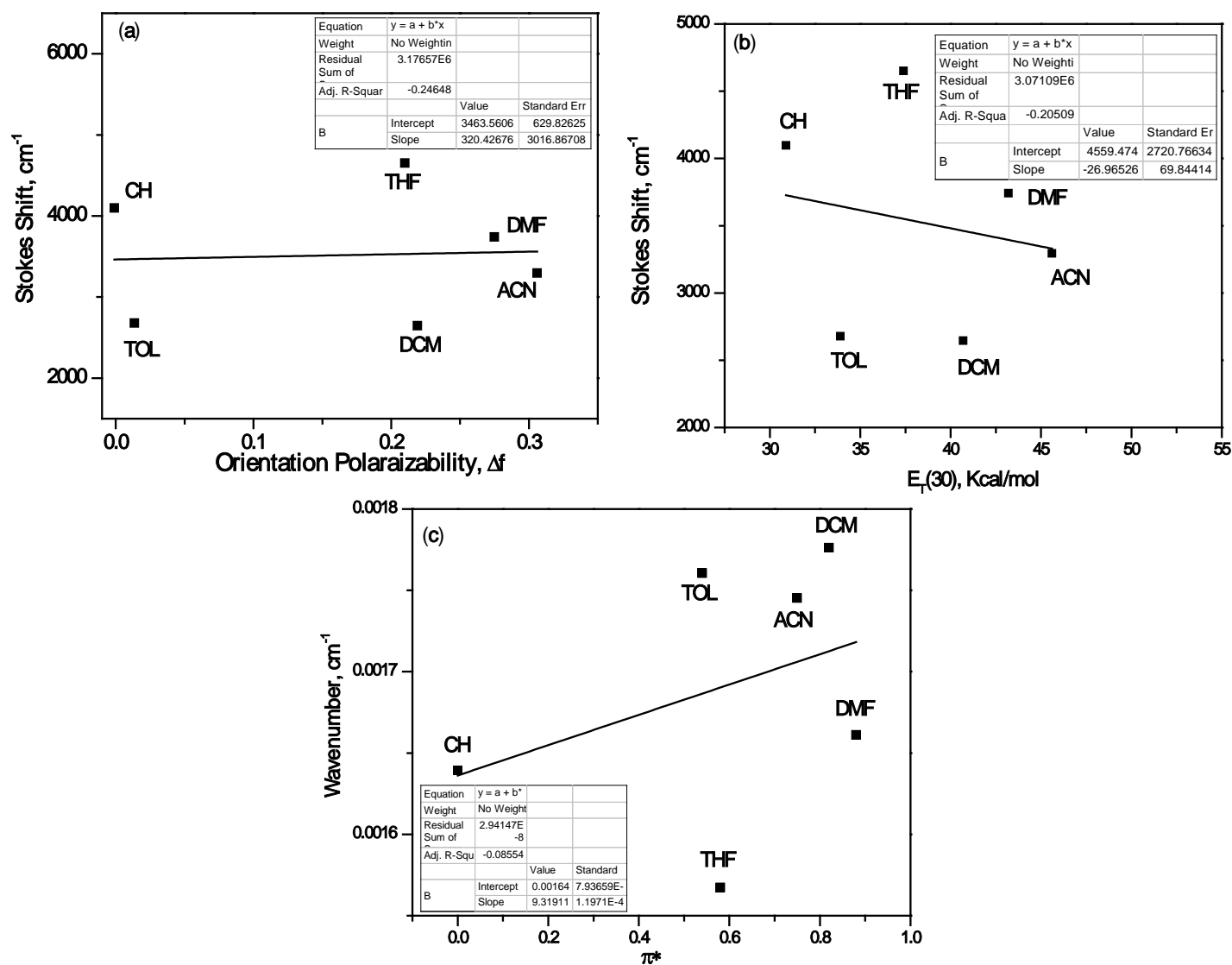


Figure 6.18 Plots for **28b** in different solvents (a) Lippert-Mataga plot showing Stokes' shift vs orientation polarizability of the solvents, (b) Stokes' shift vs $E_T(30)$ parameter, (c) Emission maxima (in wavenumber unit) vs Kamlet-Taft solvent polarity parameter

6.2.3 Electrochemical Properties

The redox stability plays a pivotal role in the optoelectronic device performance and lifetime, since the organic material is repeatedly oxidized and reduced. Hence to probe the redox stability and electronic communication between phenothiazine and benzothiadiazole units, cyclic and differential pulse voltammetric studies were performed. The electrochemical analysis was done in dichloromethane solution (2×10^{-4} M) using tetrabutylammonium perchlorate as a supporting electrolyte. The electrochemical data of the dyes are listed in Table 6.3, the cyclic voltammograms and differential pulse voltammogram are shown in Figure 6.19. Ferrocene was served as internal standard to calibrate the redox potentials. All the derivatives displayed a quasi reversible oxidation wave (120-232 mV) due to the oxidation of the conjugated pathway spread over the entire system. This is further support by the theoretical computation. The oxidation potentials of the dyes follows the order as **26a** > **28a** > **26b** > **27** > **28b**. These result reveals that within the same class, the oxidation potential of the phenothiazine mainly depend on the amine group tethered at 4-position of the benzothiadiazole moiety.

The strong donating ability of piperidine cathodically shifted oxidation potential of **26a**, **28a** than **26b**, **28b** respectively. The phenothiazine substituted benzothiadiazoles, exhibit one irreversible reduction wave due to the reduction of BTD unit in the region (-1760) mV to (-2088) mV. The reduction potential of the dyes follows the tread **27** < **26b** < **28b** < **26a** < **28a**. Within the same class, the dyes with morpholine donor tethered at 4th position of BTD were easily reduced than the dyes with piperidine donor, because of the inferior donating ability. Since all the dyes except **27** possess piperidine/morpholine unit directly attached to BTD unit and make them difficult to reduce. The dye **27** possesses low band gap in the series, presumably due to the low reduction potential and the low lying LUMO level. The HOMO and LUMO energy levels of the dyes were evaluated by standard equations $HOMO = E_{OX} + 4.8$ and $LUMO = E_{red} + 4.8$. And $E_{0.0}$ was calculated from HOMO-LUMO. The band gap of the newly synthesized phenothiazine-benzothiadiazole conjugates were in the range 1.988-2.268 eV. To correlate their electronic properties and identify their potential for use in organic photovoltaic devices, the HOMO and LUMO energy levels of the new phenothiazine-benzothiadiazole conjugates were estimated and shown in Figure 6.20.

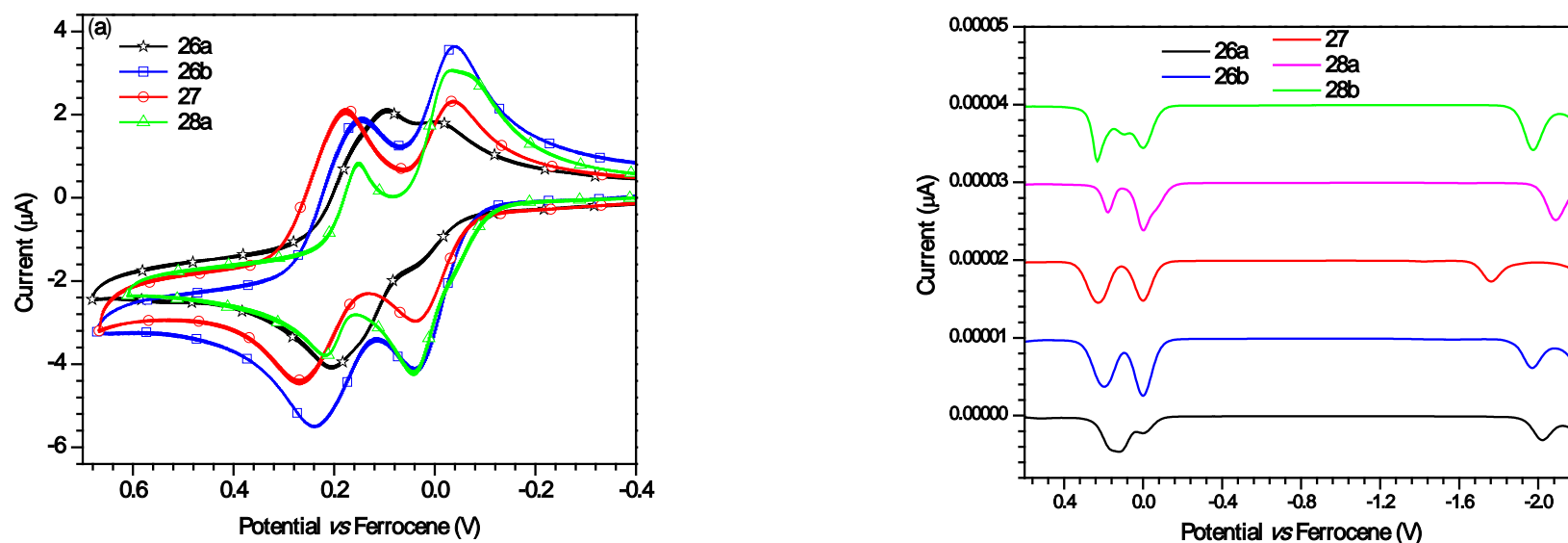


Figure.6.19 (a) Cyclic voltammograms recorded for the dyes **26a-b**, **27**, **28a** (b) Differential pulse voltammograms of the dyes recorded in dichloromethane solution

Table 6.3 Electrochemical properties of the dyes in dichloromethane solution

Dye	$E_{OX}(\Delta E_p)$, mV ^a	E_{red} , mV ^a	HOMO, eV ^b	LUMO, eV ^b	E_{0-0} , eV	E_{OX} vs NHE, V ^c	E_{0-0}^* , V ^d
26a	120 (107), 916, 1060	2020	4.920	2.780	2.140	0.890	-1.250
26b	196 (92), 900	1968	4.996	2.832	2.164	0.966	-1.198
27	228 (91), 824, 1724	1760	5.028	3.040	1.988	0.998	-0.990
28a	180 (68), 852, 948	2088	4.980	2.712	2.268	0.950	-1.318
28b	232, 808, 968	1976	5.032	2.824	2.208	1.002	-1.206

^a Measured for dichloromethane solutions using tetrabutylammonium perchlorate (TBAP) as the supporting electrolyte at a scan rate of 100 mV/s. ^b Deduced from the equations HOMO = E_{OX} + 4.8 and LUMO = E_{red} + 4.8. ^c Ground-state oxidation potential *versus* NHE. ^d Excited state oxidation potential *versus* NHE

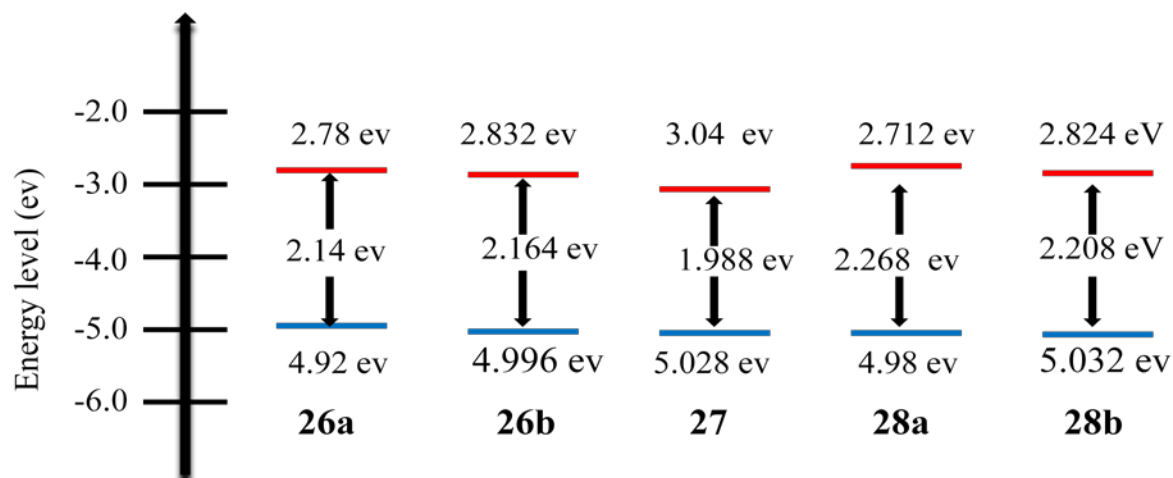


Figure 6.20 Energy-level diagram of the phenothiazine-benzothiadiazole hybrids

Figure 6.21 Snap shot of the trends in absorption and electrochemical data of the new benzothiadiazole-phenothiazine dyes

It is interesting to compare the band gap of the P3HT which is used as an efficient donor in BHJ solar cells. The band gap of the P3HT is 1.9-2.0 eV [83]. From this comparison we can conclude that these materials can serve as efficient donors in BHJs. In an attempt to establish structure-property relationship in the new family of benzothiadiazole-phenothiazine vinyl conjugates we correlated the electronic absorption maxima of the lower energy transition with

the first oxidation potentials of the dyes recorded in dichloromethane and the trends are displayed in Figure 6.21. The trends of the absorption maxima and first oxidation potential of the dyes correlated with the help of arrows. Both the absorption maxima and oxidation potentials trends were highly depended on the conjugation length and electron donating ability of the donor attached to benzothiadiazole.

6.2.4 Theoretical Calculations

To probe in more detail the influence of the structure on the geometry and electronic properties of the new phenothiazine-benzothiadiazole conjugates by theoretically, density functional theory (DFT) [84] calculations were performed using B3LYP [85-86], MPW1K [87] models and 6-31G(d,p) basis set. The transition energies, oscillator strengths, and assignments for the dyes are compiled in Tables 6.4, 6.5 and 6.6. Electronic distributions in the frontier molecular orbitals of the dyes are displayed in Figures 6.22 and 6.23. The simulated absorption spectra from the computed parameters are displayed in Figure 6.24. Some of the silent features emerged from the theoretical computations are:

In **26a** and **26b**,

- HOMO, HOMO-1 was distributed on entire molecule.
- LUMO was located mainly on benzothiadiazole moiety.
- LUMO+1 was located mainly on benzothiadiazole, double bond and significant contribution from phenothiazine also.

In **27**,

- HOMO was distributed on entire molecule.
- HOMO-1 was located on both the phenothiazines.
- LUMO, LUMO+1 were located on benzothiadiazole and double bond attached to the benzothiadiazole.

In **28a** and **28b**,

- HOMO was distributed on entire molecule.
- HOMO-1 was mainly located on benzothiadiazole and minor contribution from phenothiazine.
- LUMO, LUMO+1 were mainly located on both of benzothiadiazoles.

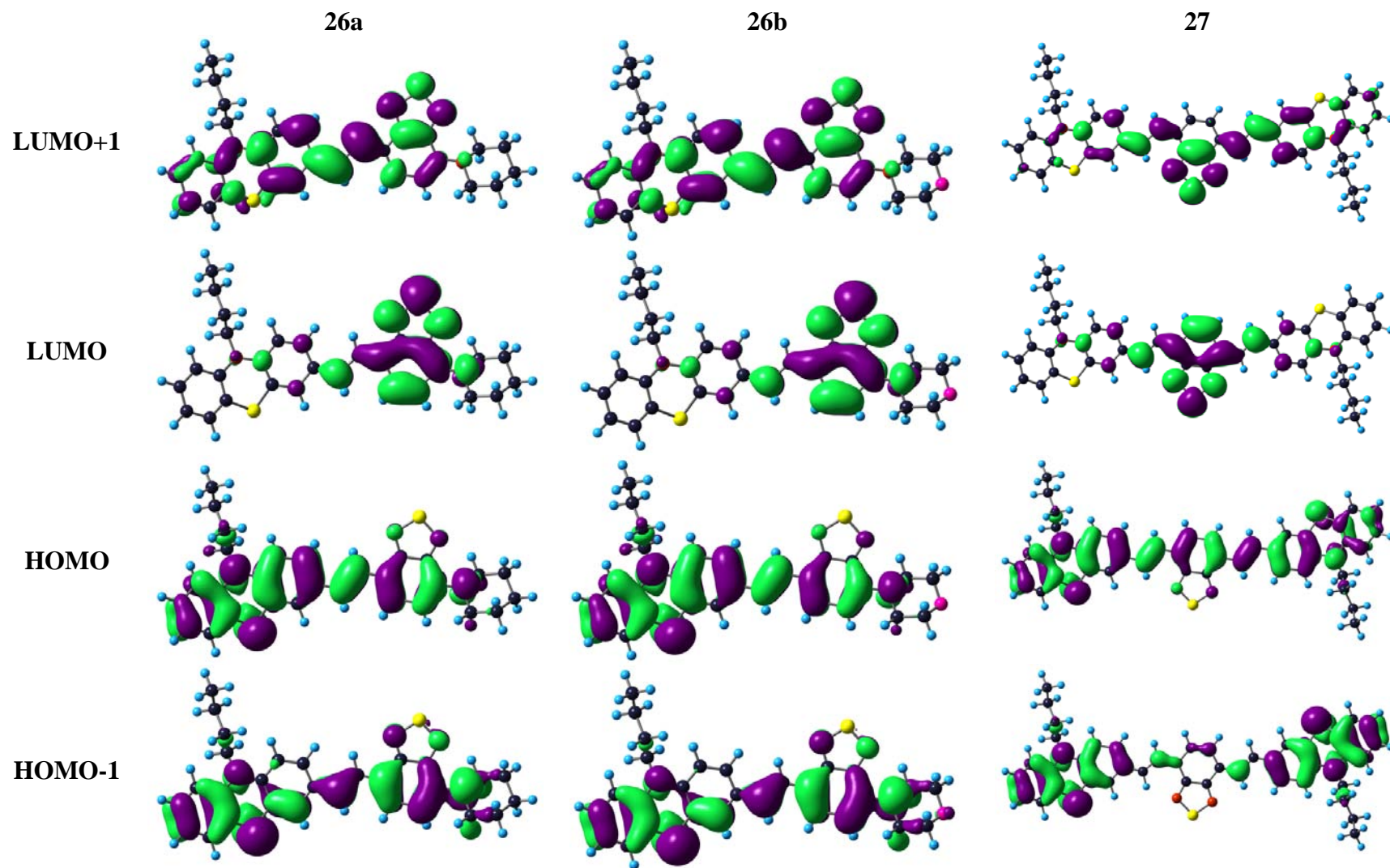


Figure 6.22 Electronic distribution observed for the frontier molecular orbitals of the dyes 20a, 20b and 21

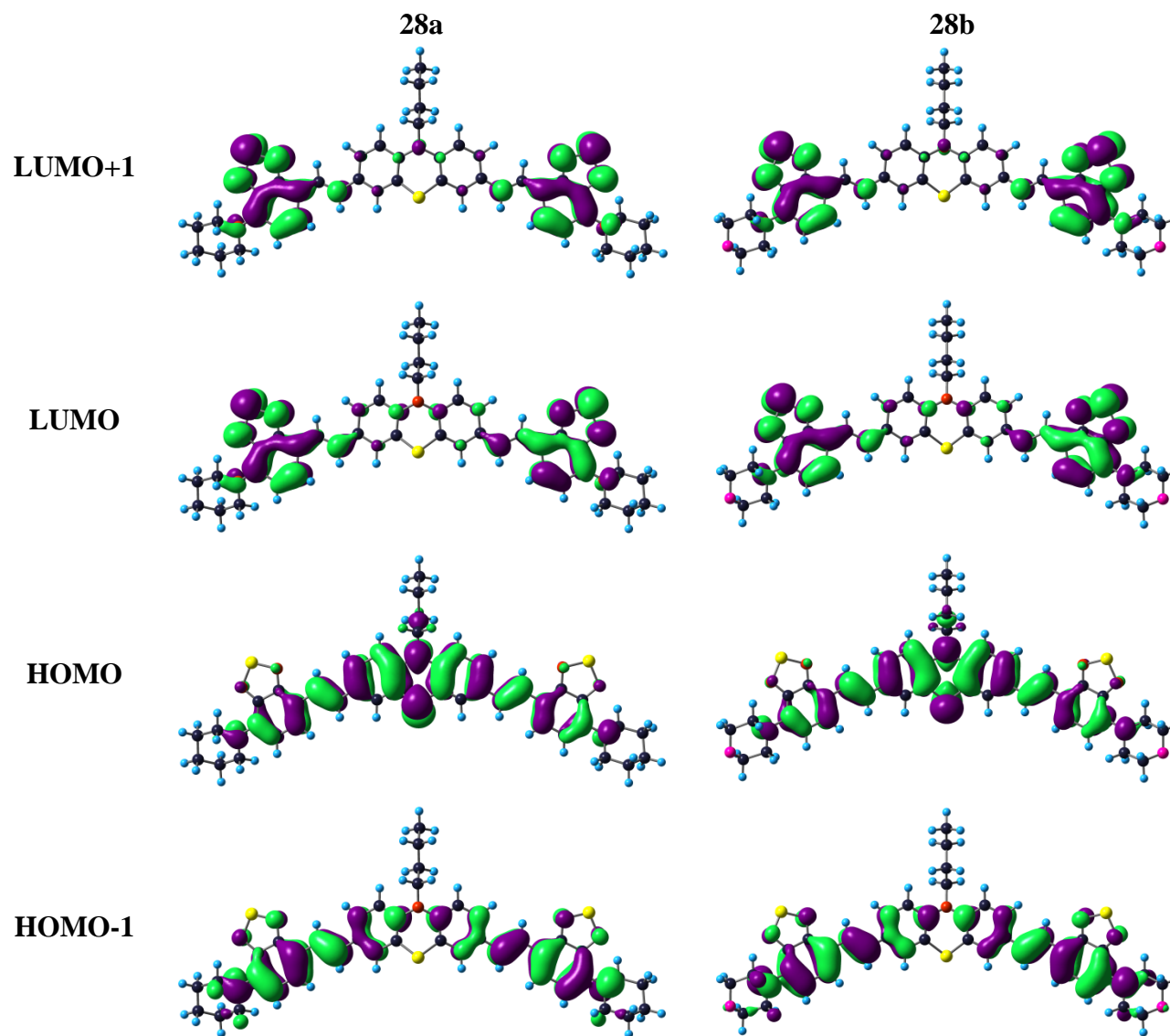


Figure 6.23 Electronic distribution observed for the frontier molecular orbitals of the dyes **23a** and **23b**

Table 6.4 Predicted vertical transitions and their assignments by B3LYP (gas)

Dye	$\lambda_{\text{abs}}/\text{nm}$	f	Configuration	HOMO, eV	LUMO, eV	$\mu_{\text{g}} [\text{D}]$
26a	598.0	0.29	HOMO→LUMO (98%)	-4.58	-2.15	0.78
	400.1	0.53	HOMO→LUMO+1 (90%)			
	338.6	0.56	HOMO-1→LUMO+1 (83%)			
	328.7	0.20	HOMO→LUMO+2 (76%)			
26b	605.7	0.28	HOMO→LUMO (98%)	-4.65	-2.25	1.59
	401.0	0.50	HOMO→LUMO+1 (90%)			
	337.0	0.54	HOMO-1→LUMO+1 (80%)			
	328.8	0.23	HOMO→LUMO+2 (78%)			
27	662.3	0.88	HOMO→LUMO (99%)	-4.60	-2.45	1.90
	421.2	1.14	HOMO→LUMO+1 (89%)			
	350.0	0.31	HOMO-1→LUMO+2 (55%), HOMO→LUMO+3 (14%), HOMO-2→LUMO+1(10%)			
28a	636.8	0.61	HOMO→LUMO (96%)	-4.46	-2.18	2.49
	434.1	0.76	HOMO→LUMO+2 (77%), HOMO-2→LUMO (20%)			
28b	641.5	0.58	HOMO→LUMO (97%)	-4.55	-2.29	0.07
	433.9	0.73	HOMO→LUMO+2 (78%), HOMO-2→LUMO (19%)			

Table 6.5 Predicted vertical transitions and their assignments by MPW1K (gas)

Dye	$\lambda_{\text{abs}}/\text{nm}$	f	Configuration	HOMO, eV	LUMO, eV	μ_g [D]
26a	446.2	0.55	HOMO→LUMO (81%), HOMO-1→LUMO (17%)	-5.51	-1.53	1.16
	327.1	0.32	HOMO→LUMO+1 (60%), HOMO-1→LUMO (20%)			
	289.7	0.82	HOMO-1→L+1 (42%), HOMO→L+3 (27%)			
	257.5	0.16	HOMO-5→L (69%), HOMO→L+5 (11%)			
26b	453.7	0.56	HOMO→LUMO (82%), HOMO-1→LUMO (15%)	-5.55	-1.65	1.75
	329.9	0.36	HOMO→LUMO+1 (63%), HOMO-1→LUMO (19%)			
	290.4	0.80	HOMO-1→LUMO+1 (42%), HOMO→LUMO+2 (28%)			
	257.7	0.16	HOMO-5→LUMO (65%), HOMO-0→LUMO+5 (12%)			
27	495.5	1.36	HOMO→LUMO (92%)	-5.49	-1.92	1.59
	334.4	0.81	HOMO→LUMO+1 (57%), HOMO-2→LUMO (20%), HOMO-1→LUMO+2 (10%)			
28a	469.0	1.18	HOMO→LUMO (71%), HOMO-1→LUMO+1 (22%)	-5.34	-1.59	2.43
	446.1	0.15	HOMO→LUMO+1 (64%), HOMO-1→LUMO (29%)			
	341.6	0.49	HOMO→LUMO+2 (55%), HOMO→LUMO (16%), HOMO-1→LUMO+1 (14%)			
	308.4	0.13	HOMO-2→LUMO (55%), HOMO-1→LUMO+1 (28%)			
	306.9	0.14	HOMO→LUMO+3 (32%), HOMO-2→LUMO+1 (27%), HOMO-1→LUMO+2 (20%), HOMO-1→LUMO (16%)			
	291.0	1.33	HOMO→LUMO+5 (38%), HOMO-2→LUMO+2 (21%), HOMO-1→LUMO+3 (20%)			
28b	464.5	1.12	HOMO→LUMO (72%), HOMO-1→LUMO+1 (20%)	-5.45	-1.69	0.62
	441.8	0.15	HOMO→LUMO+1 (64%), HOMO-1→LUMO (26%)			
	341.0	0.47	HOMO-0→LUMO+2 (56%), HOMO→LUMO (16%), HOMO-1→LUMO+1 (12%)			
	297.3	0.14	HOMO→LUMO+3 (36%), HOMO-2→LUMO+1 (31%), HOMO-1→LUMO+2 (14%)			
	289.2	1.37	HOMO→LUMO+5 (39%), HOMO-2→LUMO+2 (21%), HOMO-1→LUMO+3 (19%)			

Table 6.6 Predicted vertical transitions and their assignments by MPW1K (THF)

Dye	$\lambda_{\text{abs}}/\text{nm}$	f	Configuration	HOMO, eV	LUMO, eV	$\mu_{\text{g}}[\text{D}]$
26a	454.2	0.64	HOMO→LUMO (81%), HOMO-1→LUMO (16%)	-5.69	-1.69	1.51
	354.6	0.14	HOMO-1→LUMO (51%), HOMO→LUMO+1 (33%)			
	328.1	0.37	HOMO→LUMO+1 (55%), HOMO-1→LUMO (27%)			
	293.2	0.71	HOMO-1→LUMO+1 (43%), HOMO→LUMO+2 (20%), HOMO→LUMO+3 (16%)			
	261.1	0.19	HOMO-5→LUMO (74%)			
26b	459.5	0.67	HOMO→LUMO (83%), HOMO-1→LUMO (15%)	-5.69	-1.75	2.07
	356.7	0.12	HOMO-1→LUMO (52%), HOMO→LUMO+1 (33%)			
	330.2	0.39	HOMO→LUMO+1 (55%), HOMO-1→LUMO (27%)			
	293.7	0.69	HOMO-1→LUMO+1(42%), HOMO→LUMO+2 (27%), HOMO→LUMO+3 (12%)			
	261.3	0.20	HOMO-5→LUMO (72%)			
27	508.1	1.51	HOMO→LUMO (91%)	-5.65	-2.07	2.20
	336.2	0.84	HOMO→LUMO+1 (54%), HOMO-2→LUMO (26%)			
	299.0	0.43	HOMO-3→LUMO (23%), HOMO-1→LUMO+2 (15%), HOMO→LUMO+3 (14%) HOMO-2→LUMO+1 (13%)			
28a	297.6	0.17	HOMO-3→LUMO (51%), HOMO→LUMO+3 (10%)	-5.53	-1.74	3.07
	475.7	1.34	HOMO→LUMO (69%), HOMO-1→LUMO+1 (24%)			
	454.4	0.18	HOMO→LUMO+1 (60%), HOMO-1→LUMO (32%)			
	378.8	0.13	HOMO→LUMO+2 (35%), HOMO-1→LUMO+1 (28%), HOMO-2→LUMO (21%)			
	341.9	0.49	HOMO→LUMO+2 (49%), HOMO→LUMO (19%), HOMO-1→LUMO+1 (16%)			
	313.9	0.20	HOMO→LUMO+3 (44%), HOMO-1→LUMO+2 (33%)			
	308.0	0.15	HOMO-2→LUMO (53%), HOMO-1→LUMO+1 (27%)			
293.9	1.22	HOMO→LUMO+5 (35%), HOMO-2→LUMO+2 (21%), HOMO-1→LUMO+3 (19%)				
28b	468.5	1.28	HOMO→LUMO (70%), HOMO-1→LUMO+1 (22%)	-5.59	-1.78	0.72
	447.3	0.19	HOMO→LUMO+1 (61%), HOMO-1→LUMO (30%)			
	375.6	0.11	HOMO→LUMO+2 (35%), HOMO-1→LUMO+1 (28%), HOMO-2→LUMO (22%)			
	340.2	0.46	HOMO→LUMO+2 (49%), HOMO→LUMO (19%), HOMO-1→LUMO+1 (15%)			
	309.7	0.20	HOMO→LUMO+3 (44%), HOMO-1→LUMO+2 (31%), HOMO-2→LUMO+1 (10%)			
	304.7	0.15	HOMO-2→LUMO (52%), HOMO-1→LUMO+1 (28%)			
	291.6	1.27	HOMO→LUMO+5 (37%), HOMO-2→LUMO+2 (21%), HOMO-1→LUMO+3 (19%)			

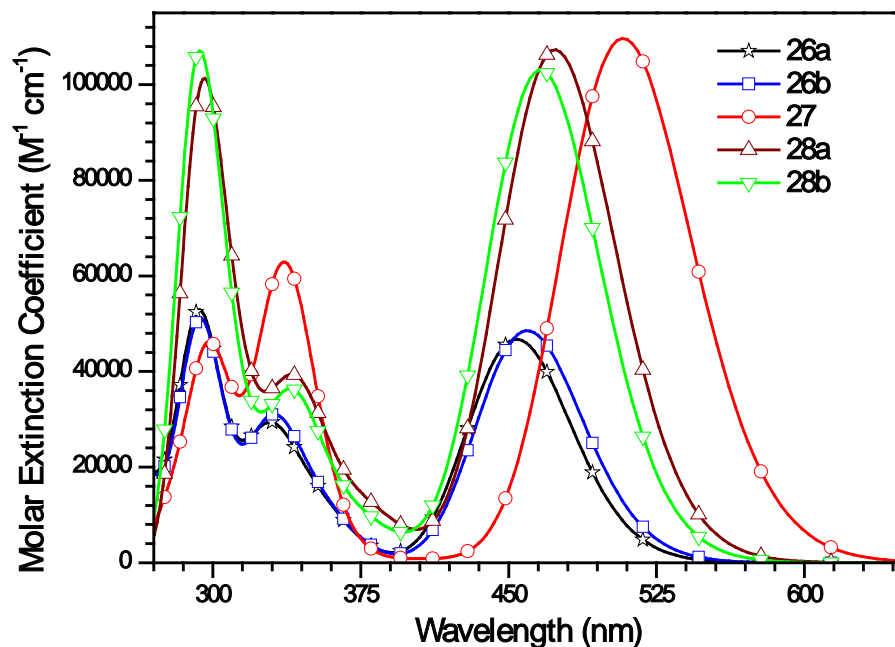


Figure 6.24 Simulated electronic transitions for the dyes by MPW1K

Appreciable overestimation (+50 nm) - (+100 nm) of absorption wavelengths for the dyes at the TDDFT level using B3LYP correlation functional's attributed to the flaws in modelling the long range charge transfer interactions [88-89]. However, the charge transfer transition as well as higher energy transition calculated in the presence of tetrahydrofuran using MPW1K showed close agreement to the experimentally observed values for tetrahydrofuran. In **26a** and **26b** the lower energy transition has major (81-83%) contribution from HOMO to LUMO and minor (15-16%) contribution from HOMO-1 to LUMO. As both HOMO and HOMO-1 were localised on entire molecule and LUMO is mainly localised on BTB unit, we can consider in the excited state there is an ICT from donor moieties to BTB unit. The longer wavelength vertical transition of **27** is mainly due to the electronic excitation from HOMO to LUMO, this clearly suggests that in **27** the prominent excitation leads to the charge transfer from the phenothiazine units to benzothiadiazole segment, as the HOMO, HOMO-1 are mainly localised on entire molecule (major contribution from phenothiazine) and LUMO, LUMO+1 are localised on benzothiadiazole unit. The low energy transition in the dyes **28** has a configuration from HOMO→LUMO (major) and HOMO-1→LUMO+1 (minor) excitation. This clearly indicates that in **28a**, **28b** the longer wavelength transition is due to the charge transfer from the donor segments to benzothiadiazole acceptor.

6.2.5 Thermal Properties

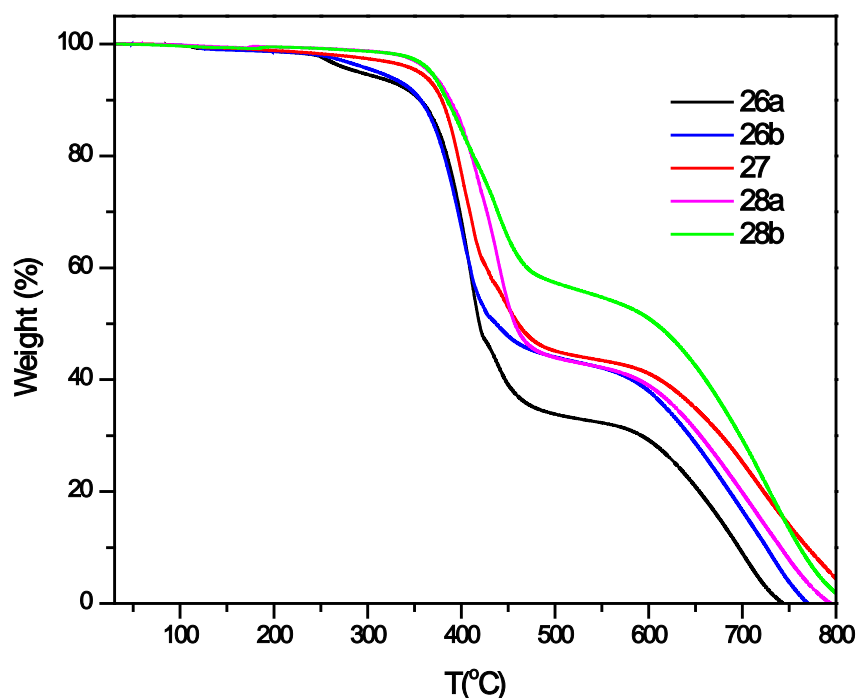


Figure 6.25 TGA plots for the dyes

Thermal stability of the dye plays crucial role in the device performance of any optoelectronic material. So to evaluate thermal properties of the dyes thermogravimetric analysis (TGA) was performed under nitrogen atmosphere, with a heating rate of 10 °C/min (Figure 6.25). All of the materials showed very good thermal stability. The temperature with 10% weight loss lies in the range from 356 to 387 °C Table 6.7. There is no difference in the onset decomposition temperature for dyes within the same class (**26a, 26b**) & (**28a, 28b**). This may be attributed to the presence of similar structural features in the dyes. Among all, the dye **27** exhibited poor thermal stability, which is attributable to the fragile butyl chains in the dye. The onset decomposition temperature of **27** is in between mono (**26a, 26b**) and di-substituted (**28a, 28b**) phenothiazine derivatives. Among the dyes, the dyes **28a, 28b** exhibited higher decomposition temperatures. The thermal stability trends revealed that the dyes with two BTB units have higher thermal stability. The decomposition temperatures of the newly synthesised phenothiazine-benzothiadiazole derivatives were in range 401-438 °C, which are quite good enough for the applications in opto-electronic devices.

Table 6.7 Thermal properties of the benzothiadiazole-phenothiazine conjugates

Dye	T _{onset} , °C ^a	T _d , °C ^b
26a	356	411
26b	356	404
27	379	401
28a	387	438
28b	384	437

^a Temperature corresponding to 10% weight loss ^b Heating rate 10 °C/min in nitrogen

6.3 Conclusions

In summary, we have successfully designed, synthesized and characterized a series of donor-acceptor compounds containing phenothiazine donor, benzothiadiazole acceptor and double bonds as the π -bridge. The compounds were synthesized by palladium-catalyzed Heck cross coupling reactions and isolated in moderate to good yields. The new phenothiazine-benzothiadiazole dyes were thoroughly characterized by UV-vis absorption, emission, electrochemical, theoretical calculations and thermal studies. The compounds exhibited good solubility in common organic solvents, which is beneficial to apply them in solution-processable electronic devices. The dyes exhibited interesting photophysical, electrochemical properties which are highly dependent on the conjugation length and the donor attached to benzothiadiazole unit. The extended conjugation in the dyes **28a**, **28b** contributed to the red shifted absorptions with high molar extension coefficients and anodically shifted oxidation potentials than **26a**, **26b**. The results of solvatochromism studies reveal the formation of polar excited intramolecular charge transfer states for the dyes. All the dyes displayed one-electron quasi-reversible oxidation couple and an irreversible reduction wave, which are attributable to the oxidation of the sulphur atom in phenothiazine unit and reduction of benzothiadiazole unit, respectively. Among all, the dye **27** exhibited low reduction potential and low band gap due to the presence of two strong electron donating phenothiazine units. There is a reasonable correlation between the optical properties proposed by TDDFT and the experimental data. The decomposition temperatures of the dyes are quite good enough to apply in any opto-electronic device. Finally, in this work we established the structure-property relationships in the new phenothiazine-benzothiadiazole dyes extended through vinyl spacer, which are suitable in electronic devices such as OLEDs, BHJ solar cells and nonlinear optics etc.

6.4 Experimental Section

6.4.1 Material and Methods

General methods are similar to those described in the earlier chapters.

6.4.2 Synthesis

Synthesis of 4-bromo-7-morpholinobenzo[*c*][1,2,5]thiadiazole (2b). The reaction was carried under nitrogen atmosphere. 4,7-dibromobenzo[*c*][1,2,5]thiadiazole (**1**) (2.05 g, 7.0 mmol), morpholine (5 mL) were refluxed for 10 h and the reaction mixture was cooled to room temperature. The reaction mixture was poured in cold water and extracted with dichloromethane. The compound was purified by column chromatography on silica gel using hexane/dichloromethane mixture as eluant. Orange solid; Yield = 1.15 g (55%, 3.83 mmol); m.p. 110-112 °C; IR (KBr, cm⁻¹): 2955, 1483, 1234, 1118; ¹H NMR (500.13 MHz, CDCl₃): δ 3.50 (t, *J* = 5.0 Hz, 2H), 3.95 (t, *J* = 5.0 Hz, 2H), 6.58 (d, *J* = 8.0 Hz, 1H), 7.65 (d, *J* = 8.0 Hz, 1H); ¹³C NMR (125.75 MHz, CDCl₃): δ 50.3, 66.8, 104.5, 111.9, 132.8, 143.6, 149.0, 154.5; HRMS (ESI) *m/z* calcd for C₁₀H₁₁BrN₃O_s (M+H) 299.9806, found 299.9805.

Synthesis of (*E*)-10-butyl-3-(2-(7-(piperidin-1-yl)benzo[*c*][1,2,5]thiadiazol-4-yl)vinyl)-10*H*-phenothiazine (26a). In a 100 ml pressure tube mixture of 4-bromo-7-(piperidin-1-yl)benzo[*c*][1,2,5]thiadiazole (**2a**) (0.3 g, 1 mmol), 10-butyl-3-vinyl-10*H*-phenothiazine (**18b**) (0.309 g, 1.1 mmol), Pd(OAc)₂ (2.245 mg, 0.01 mmol), NaOAc (0.82 g, 10 mmol), and *n*-Bu₄NBr (0.065 g, 0.2 mmol) was dissolved in degassed *N,N*-dimethylformamide (5 mL). The solution was kept under a nitrogen atmosphere at 100 °C for 24 h. The mixture was poured into water. The precipitate was filtered, washed with water, dissolved in dichloromethane, and dried over anhydrous sodium sulfate. After evaporation of the solvent, the residue was purified by column chromatography on silica gel, using a hexane/dichloromethane mixture as eluant. Dark red solid; Yield = 0.3 g (65%, 0.58 mmol); m.p. 115-117 °C; IR (KBr, cm⁻¹): 2925, 1462, 1383, 1239; ¹H NMR (500.13 MHz, CDCl₃): δ 0.95 (t, *J* = 7.5 Hz, 3H), 1.44-1.49 (m, 2H), 1.69-1.70 (m, 2H), 1.79-1.85 (m, 6H), 3.50-3.52 (m, 4H), 3.86 (t, *J* = 7.0 Hz, 2H), 6.75 (d, *J* = 8.0 Hz, 1H), 6.85 (t, *J* = 10.0 Hz, 2H), 6.90 (t, *J* = 7.5 Hz, 1H), 7.13-7.16 (m, 2H), 7.35-7.39 (m, 3H), 7.50 (d, *J* = 7.5 Hz, 1H), 7.70 (d, *J* = 16.0 Hz, 1H); ¹³C NMR (125.75 MHz, CDCl₃): δ 13.8, 20.2, 22.9, 24.6, 26.0, 29.0, 47.2, 51.6, 100.1, 112.0, 115.3, 122.3, 122.6, 123.3, 124.4, 124.9, 125.0, 125.9, 127.2, 127.4, 128.2, 128.7, 132.6, 144.0, 145.0, 150.3, 154.8; HRMS (ESI): *m/z* calculated for C₂₉H₃₁N₄S₂ 499.1990; found 499.1980

Synthesis of (*E*)-10-butyl-3-(2-(7-morpholinobenzo[*c*][1,2,5]thiadiazol-4-yl)vinyl)-10*H*-phenothiazine (26b). Compound **26b** was prepared from **2b** by following a similar procedure as described for **26a**. Orange solid; Yield = 74%; m.p. 120-122 °C; IR (KBr, cm⁻¹): 2926, 1470, 1380, 1245; ¹H NMR (500.13 MHz, CDCl₃): δ 0.95 (t, *J* = 7.5 Hz, 3H), 1.45-1.48 (m, 2H), 1.79-1.80 (m, 2H), 3.56 (t, *J* = 4.5 Hz, 4H), 3.87 (t, *J* = 4.5 Hz, 2H), 3.99-4.01 (t, *J* = 4.5 Hz, 4H), 6.76 (d, *J* = 8.0 Hz, 1H), 6.85 (t, *J* = 9.0 Hz, 2H), 6.91 (t, *J* = 7.5 Hz, 1H), 7.14 (d, *J* = 7.5 Hz, 2H), 7.35-7.40 (m, 3H), 7.53 (d, *J* = 8 Hz, 1H), 7.74 (d, *J* = 16.5 Hz, 1H); ¹³C NMR (125.75 MHz, CDCl₃): δ 13.7, 20.0, 28.8, 47.0, 50.3, 66.7, 111.7, 115.1, 122.2, 122.8, 123.4, 124.2, 124.8, 124.8, 125.8, 127.2, 127.0, 127.3, 127.7, 129.3, 132.3, 142.6, 144.5, 144.8, 149.7, 154.6; HRMS (ESI): m/z calculated for C₂₈H₂₉N₄OS₂ 501.1783; found 501.1753.

Synthesis of 10-butyl-3-((*E*)-2-(7-((*E*)-2-(10-butyl-10*H*-phenothiazin-3-yl)vinyl)benzo[*c*][1,2,5]thiadiazol-4-yl)vinyl)-10*H*-phenothiazine (27). Compound **27** was prepared from **1** (0.5 equivalent) by following a similar procedure as described for **26a**; Red solid; Yield = 78%; m.p. 135-137 °C; IR (KBr, cm⁻¹): 2951, 1465, 1360; ¹H NMR (500.13 MHz, CDCl₃): δ 0.96 (t, *J* = 7.5 Hz, 6H), 1.45-1.50 (m, 4H), 1.80-1.83 (m, 4H), 3.88 (t, *J* = 7.0 Hz, 4H), 6.86 (t, *J* = 7.0 Hz, 8.5 Hz, 4H), 6.92 (t, *J* = 7.5 Hz, 2H), 7.14-7.15 (m, 4H), 7.39-7.43 (m, 4H), 7.49 (d, *J* = 16.5 Hz, 2H), 7.86 (d, *J* = 16.5 Hz, 2H); ¹³C NMR (125.75 MHz, CDCl₃): δ 13.8, 20.0, 28.9, 47.2, 115.2, 115.3, 122.4, 122.7, 124.1, 124.3, 125.1, 126.3, 126.5, 127.7, 127.4, 129.0, 131.6, 131.9, 144.7, 145.0, 153.8; HRMS (ESI) m/z calculated for C₄₂H₃₈N₄S₃, 694.2259 [M⁺] found 694. 2222.

Synthesis of 10-butyl-3,7-bis((*E*)-2-(7-(piperidin-1-yl)benzo[*c*][1,2,5]thiadiazol-4-yl)vinyl)-10*H*-phenothiazine (28a). Compound **28a** was prepared from **25** (0.5 equivalent) by following a similar procedure as described for **26a**. Dark red solid; Yield = 89%; m.p. 138-140 °C; IR (KBr, cm⁻¹): 2921, 1476, 1388, 1254; ¹H NMR (500.13 MHz, CDCl₃): δ 0.97 (t, *J* = 7.5 Hz, 3H), 1.46-1.50 (m, 2 H), 1.67-1.71 (m, 4H), 1.79-1.87 (m, 10H), 3.50 (t, *J* = 5.0 Hz, 8H), 3.87 (t, *J* = 7.5 Hz, 2H), 6.75 (d, *J* = 7.5 Hz, 2H), 6.83 (d, *J* = 8.5 Hz, 2H), 7.35-7.37 (m, 3H), 7.4 (t, *J* = 2.0 Hz, 3H), 7.51 (d, *J* = 7.5 Hz, 2H), 7.72 (d, *J* = 16.0 Hz, 2H); ¹³C NMR (125.75 MHz, CDCl₃): δ 13.9, 20.2, 24.6, 26.0, 29.0, 47.5, 51.6, 112.0, 115.2, 122.6, 122.8, 123.3, 124.9, 125.9, 128.3, 128.7, 132.7, 144.0, 144.1, 150.3, 154.8; HRMS m/z: calculated for, C₄₂H₄₃N₇S₃ 741.2742 [M⁺]; found 741.2734.

Synthesis of 4,4'-(7,7'-((1E,1'E)-(10-butyl-10H-phenothiazine-3,7-diyl)bis(ethene-2,1-diy))bis(benzo[c][1,2,5]thiadiazole-7,4-diyl))dimorpholine (28b). Compound **28b** was prepared from **25** (0.5 equivalent) by following a similar procedure as described for **26a**; Red solid; Yield = 90%; m.p. 108-110 °C; IR (KBr, cm⁻¹): 2980, 2925, 1631, 1472, 1383, 1118; ¹H NMR (500.13 MHz, CDCl₃): δ 0.97 (t, *J* = 7.5 Hz, 3H), 1.49-1.50 (m, 2H), 1.80-1.83 (m, 2H), 3.58 (t, *J* = 4.0 Hz, 8H), 3.89 (t, *J* = 6.5 Hz, 7.5 Hz, 2H), 4.00 (t, *J* = 4.0 Hz, 5.0 Hz, 8H), 6.77 (d, *J* = 8.0 Hz, 2H), 6.85 (d, *J* = 8.5 Hz, 2H), 7.36-7.42 (m, 6H), 7.54 (d, *J* = 8.0 Hz, 2H), 7.75 (d, *J* = 16.0 Hz, 2H); ¹³C NMR (125.75 MHz, CDCl₃): δ 13.8, 20.1, 28.9, 47.3, 50.4, 66.9, 111.8, 115.2, 123.0, 123.5, 124.3, 124.9, 125.9, 127.8, 129.3, 132.4, 142.7, 144.1, 149.8, 154.7; HRMS m/z: calculated for, C₄₀H₃₉N₇NaO₂S₃ 768.2225 [M+Na⁺]; found 768.2205.

6.5 References

- (1) A. Chaskar, H. F. Chen and K. T. Wong, Bipolar host materials: a chemical approach for highly efficient electrophosphorescent devices. *Adv Mater* **2011**, *23*, 3876-95.
- (2) K. R. JustinThomas, J. T. Lin, M. Velusamy, Y. T. Tao and C. H. Chuen, Color Tuning in Benzo[1,2,5]thiadiazole-Based Small Molecules by Amino Conjugation/Deconjugation: Bright Red-Light-Emitting Diodes. *Adv. Funct. Mater.* **2004**, *14*, 83-90.
- (3) Y. Qiu, P. Wei, D. Q. Zhang, J. Qiao, L. Duan, Y. K. Li, Y. D. Gao and L. D. Wang, Novel Naphtho[2,3-*c*][1,2,5]thiadiazole Derivative for Non-doped Small Molecular Organic Red-Light-Emitting Diodes. *Adv. Mater.* **2006**, *18*, 1607-11.
- (4) K. Mutkins, K. Gui, M. Aljada, P. E. Schwenn, E. B. Namdas, P. L. Burn and P. Meredith, A solution processable fluorene-benzothiadiazole small molecule for n-type organic field-effect transistors. *Appl. Phys. Lett.* **2011**, *98*, 153301.
- (5) G. Yang, C.-a. Di, G. Zhang, J. Zhang, J. Xiang, D. Zhang and D. Zhu, Highly Sensitive Chemical-Vapor Sensor Based on Thin-Film Organic Field-Effect Transistors with Benzothiadiazole-Fused-Tetrathiafulvalene. *Adv. Funct. Mater.* **2013**, *23*, 1671-76.
- (6) J. Zhao, X. Yang, M. Cheng, S. Li and L. Sun, Molecular design and performance of hydroxypyridium sensitizers for dye-sensitized solar cells. *ACS Appl. Mater. Interfaces* **2013**, *5*, 5227-31.
- (7) A. Mishra, M. K. R. Fischer and P. Bäuerle, Metal-Free Organic Dyes for Dye-Sensitized Solar Cells: From Structure: Property Relationships to Design Rules. *Angew. Chem. Int. Ed.* **2009**, *48*, 2474-99.

- (8) A. Mishra and P. Bauerle, Small molecule organic semiconductors on the move: promises for future solar energy technology. *Angew. Chem. Int. Ed.* **2012**, *51*, 2020-67.
- (9) J. Kulhanek, F. Bures, W. Kuznik, I. V. Kityk, T. Mikysek and A. Ruzicka, Ferrocene-donor and 4,5-dicyanoimidazole-acceptor moieties in charge-transfer chromophores with pi linkers tailored for second-order nonlinear optics. *Chem. Asian J.* **2013**, *8*, 465-75.
- (10) S. Ellinger, K. R. Graham, P. Shi, R. T. Farley, T. T. Steckler, R. N. Brookins, P. Taranekar, J. Mei, L. A. Padilha, T. R. Ensley, H. Hu, S. Webster, D. J. Hagan, E. W. Van Stryland, K. S. Schanze and J. R. Reynolds, Donor–Acceptor–Donor-based π -Conjugated Oligomers for Nonlinear Optics and Near-IR Emission. *Chem. Mater.* **2011**, *23*, 3805-17.
- (11) A. R. Morales, A. Frazer, A. W. Woodward, H. Y. Ahn-White, A. Fonari, P. Tongwa, T. Timofeeva and K. D. Belfield, Design, synthesis, and structural and spectroscopic studies of push-pull two-photon absorbing chromophores with acceptor groups of varying strength. *J. Org. Chem.* **2013**, *78*, 1014-25.
- (12) N. Kumari, S. Jha and S. Bhattacharya, Colorimetric probes based on anthraimidazolediones for selective sensing of fluoride and cyanide ion via intramolecular charge transfer. *J. Org. Chem.* **2011**, *76*, 8215-22.
- (13) A. Thakur, S. Sardar and S. Ghosh, A highly selective redox, chromogenic, and fluorescent chemosensor for Hg^{2+} in aqueous solution based on ferrocene-glycine bioconjugates. *Inorg. Chem.* **2011**, *50*, 7066-73.
- (14) L. Cai, H. N. Tsao, W. Zhang, L. Wang, Z. Xue, M. Grätzel and B. Liu, Organic Sensitizers with Bridged Triphenylamine Donor Units for Efficient Dye-Sensitized Solar Cells. *Advanced Energy Materials* **2013**, *3*, 200-5.
- (15) E. Ripaud, T. Rousseau, P. Leriche and J. Roncali, Unsymmetrical Triphenylamine-Oligothiophene Hybrid Conjugated Systems as Donor Materials for High-Voltage Solution-Processed Organic Solar Cells. *Advanced Energy Materials* **2011**, *1*, 540-45.
- (16) Y. Lin, P. Cheng, Y. Li and X. Zhan, A 3D star-shaped non-fullerene acceptor for solution-processed organic solar cells with a high open-circuit voltage of 1.18 V. *Chem Commun* **2012**, *48*, 4773-75.
- (17) K. R. J. Thomas, N. Kapoor, M. N. K. P. Bolisetty, J.-H. Jou, Y.-L. Chen and Y.-C. Jou, Pyrene-Fluorene Hybrids Containing Acetylene Linkage as Color-Tunable Emitting Materials for Organic Light-Emitting Diodes. *J. Org. Chem.* **2012**, *77*, 3921-32.
- (18) . Li, H. Tong, J. Ding, Z. Xie and L. Wang, Small molecules based on 2,7-carbazole for

Benzothiadiazole-phenothiazine conjugates

- efficient solution-processed organic solar cells. *J. Mater. Chem. A* **2013**, *1*, 8805-12.
- (19) M. D. Zhang, H. X. Xie, X. H. Ju, L. Qin, Q. X. Yang, H. G. Zheng and X. F. Zhou, D-D- π -A organic dyes containing 4,4'-di(2-thienyl)triphenylamine moiety for efficient dye-sensitized solar cells. *Phys. Chem. Chem. Phys.* **2013**, *15*, 634-41.
- (20) D. Kumar, K. R. Thomas, C. C. Lin and J. H. Jou, Pyrenoimidazole-based deep-blue-emitting materials: optical, electrochemical, and electroluminescent characteristics. *Chem. Asian J.* **2013**, *8*, 2111-24.
- (21) T. Khanasa, N. Prachumrak, R. Rattanawan, S. Jungstittiwong, T. Keawin, T. Sudyoadsuk, T. Tuntulani and V. Promarak, An efficient solution processed non-doped red emitter based on carbazole-triphenylamine end-capped di(thiophen-2-yl)benzothiadiazole for pure red organic light-emitting diodes. *Chem Commun* **2013**, *49*, 3401-3.
- (22) P. Moonsin, N. Prachumrak, S. Namuangruk, S. Jungstittiwong, T. Keawin, T. Sudyoadsuk and V. Promarak, Novel bis(fluorenyl)benzothiadiazole-cored carbazole dendrimers as highly efficient solution-processed non-doped green emitters for organic light-emitting diodes. *Chem Commun* **2013**, *49*, 6388-90.
- (23) J. Lee, J. Kwak, K. C. Ko, J. H. Park, J. H. Ko, N. Park, E. Kim, H. Ryu do, T. K. Ahn, J. Y. Lee and S. U. Son, Phenothiazine-based organic dyes with two anchoring groups on TiO₂ for highly efficient visible light-induced water splitting. *Chem Commun* **2012**, *48*, 11431-33.
- (24) H. Tian, X. Yang, R. Chen, Y. Pan, L. Li, A. Hagfeldt and L. Sun, Phenothiazine derivatives for efficient organic dye-sensitized solar cells. *Chem. Commun.* **2007**, 3741-43.
- (25) M. Hauck, R. Turdean, K. Memminger, J. Schönhaber, F. Rominger and T. J. J. Müller, Luminescent, Redox-Active Diphenothiazine Dumbbells Expanded by Conjugated Arenes and Heteroarenes. *J. Org. Chem.* **2010**, *75*, 8591-603.
- (26) X. Zhang, Z. Chi, J. Zhang, H. Li, B. Xu, X. Li, S. Liu, Y. Zhang and J. Xu, Piezofluorochromic Properties and Mechanism of an Aggregation-Induced Emission Enhancement Compound Containing N-Hexyl-phenothiazine and Anthracene Moieties. *J. Phys. Chem. B* **2011**, *115*, 7606-11.
- (27) Z. Iqbal, W.-Q. Wu, H. Zhang, L. Han, X. Fang, L. Wang, D.-B. Kuang, H. Meier and D. Cao, Influence of spatial arrangements of π -spacer and acceptor of phenothiazine based dyes on the performance of dye-sensitized solar cells. *Organic Electronics* **2013**, *14*, 2662-72.
- (28) C. S. Krämer, K. Zeitler and T. J. J. Müller, Synthesis of Functionalized Ethynylphenothiazine Fluorophores. *Org. Lett.* **2000**, *2*, 3723-26.

- (29) M. Cheng, X. Yang, C. Chen, J. Zhao, Q. Tan and L. Sun, Effect of the acceptor on the performance of dye-sensitized solar cells. *Phys. Chem. Chem. Phys.* **2013**, *15*, 17452-59.
- (30) V. P. Barberis and J. A. Mikroyannidis, Novel blue luminescent twin molecules containing fluorene, carbazole or phenothiazine units. *Synth. Met.* **2006**, *156*, 1408-14.
- (31) W. Zhu, Y. Wu, S. Wang, W. Li, X. Li, J. Chen, Z.-s. Wang and H. Tian, Organic D-A- π -A Solar Cell Sensitizers with Improved Stability and Spectral Response. *Adv. Funct. Mater.* **2011**, *21*, 756-63.
- (32) S. Qu, C. Qin, A. Islam, J. Hua, H. Chen, H. Tian and L. Han, Tuning the electrical and optical properties of diketopyrrolopyrrole complexes for panchromatic dye-sensitized solar cells. *Chem. Asian J.* **2012**, *7*, 2895-903.
- (33) K. Pei, Y. Wu, W. Wu, Q. Zhang, B. Chen, H. Tian and W. Zhu, Constructing organic D-A- π -A-featured sensitizers with a quinoxaline unit for high-efficiency solar cells: the effect of an auxiliary acceptor on the absorption and the energy level alignment. *Chem. Eur. J.* **2012**, *18*, 8190-200.
- (34) Y. Wu, M. Marszalek, S. M. Zakeeruddin, Q. Zhang, H. Tian, M. Grätzel and W. Zhu, High-conversion-efficiency organic dye-sensitized solar cells: molecular engineering on D-A- π -A featured organic indoline dyes. *Energy & Environmental Science* **2012**, *5*, 8261-72.
- (35) B. Liu, Q. Liu, D. You, X. Li, Y. Naruta and W. Zhu, Molecular engineering of indoline based organic sensitizers for highly efficient dye-sensitized solar cells. *J. Mater. Chem.* **2012**, *22*, 13348-56.
- (36) W.-L. Ding, D.-M. Wang, Z.-Y. Geng, X.-L. Zhao and Y.-F. Yan, Molecular Engineering of Indoline-Based D-A- π -A Organic Sensitizers toward High Efficiency Performance from First-Principles Calculations. *J. Phys. Chem. C* **2013**, *117*, 17382-98.
- (37) B. Liu, W. Wu, X. Li, L. Li, S. Guo, X. Wei, W. Zhu and Q. Liu, Molecular engineering and theoretical investigation of organic sensitizers based on indoline dyes for quasi-solid state dye-sensitized solar cells. *Phys. Chem. Chem. Phys.* **2011**, *13*, 8985-92.
- (38) D. Kekuda, J.-S. Huang, M. Velusamy, J. T. Lin and C.-W. Chu, Dibenzo[*f,h*]thieno[3,4-*b*] quinoxaline-fullerene heterojunction bilayer solar cells with complementary spectrum coverage. *Sol. Energy Mater. Sol. Cells* **2010**, *94*, 1767-71.
- (39) T. L. Dexter Tam, T. Salim, H. Li, F. Zhou, S. G. Mhaisalkar, H. Su, Y. M. Lam and A. C. Grimsdale, From benzobisthiadiazole, thiadiazoloquinoxaline to pyrazinoquinoxaline based polymers: effects of aromatic substituents on the performance of organic photovoltaics. *J.*

Benzothiadiazole-phenothiazine conjugates

Mater. Chem. **2012**, *22*, 18528-34.

- (40) J. P. Nietfeld, R. L. Schwiderski, T. P. Gonnella and S. C. Rasmussen, Structural effects on the electronic properties of extended fused-ring thieno[3,4-*b*]pyrazine analogues. *J. Org. Chem.* **2011**, *76*, 6383-88.
- (41) S. Steinberger, A. Mishra, E. Reinold, E. Mena-Osteritz, H. Müller, C. Uhrich, M. Pfeiffer and P. Bäuerle, Synthesis and characterizations of red/near-IR absorbing A–D–A–D–A-type oligothiophenes containing thienothiadiazole and thienopyrazine central units. *J. Mater. Chem.* **2012**, *22*, 2701-12
- (42) Z. Kong, H. Zhou, J. Cui, T. Ma, X. Yang and L. Sun, A new class of organic dyes based on acenaphthopyrazine for dye-sensitized solar cells. *Journal of Photochemistry and Photobiology A: Chemistry* **2010**, *213*, 152-57.
- (43) P. Shen, X. Liu, P. Tang, B. Zhao, L. Wang, C. Weng, J. Cao, Y. Wu, Y. Chen and S. Tan, Bandgap and Molecular-Energy-Level Control of Conjugated-Polymer Photovoltaic Materials Based on 6,12-Dihydro-diindeno[1,2-*b*;10,20-*e*]pyrazine. *Macromol. Chem. Phys.* **2013**, *214*, 1147-57.
- (44) X. Lu, G. Zhou, H. Wang, Q. Feng and Z. S. Wang, Near infrared thieno[3,4-*b*]pyrazine sensitizers for efficient quasi-solid-state dye-sensitized solar cells. *Phys. Chem. Chem. Phys.* **2012**, *14*, 4802-9.
- (45) J. A. Mikroyannidis, P. Suresh and G. D. Sharma, Synthesis of a perylene bisimide with acenaphthopyrazine dicarbonitrile terminal moieties for photovoltaic applications. *Synth. Met.* **2010**, *160*, 932-38.
- (46) P. Singh, A. Baheti and K. R. J. Thomas, Synthesis and Optical Properties of Acidochromic Amine-Substituted Benzo[*a*]phenazines. *J. Org. Chem.* **2011**, *76*, 6134-45.
- (47) M.-k. Leung, W.-H. Yang, C.-N. Chuang, J.-H. Lee, C.-F. Lin, M.-K. Wei and Y.-H. Liu, 1,3,4-Oxadiazole Containing Silanes as Novel Hosts for Blue Phosphorescent Organic Light Emitting Diodes. *Org. Lett.* **2012**, *14*, 4986-89.
- (48) K. R. J. Thomas, J. T. Lin, Y.-T. Tao and C.-H. Chuen, New Carbazole–Oxadiazole Dyads for Electroluminescent Devices: Influence of Acceptor Substituents on Luminescent and Thermal Properties. *Chem. Mater.* **2004**, *16*, 5437-44.
- (49) M. Zhu, T. Ye, C.-G. Li, X. Cao, C. Zhong, D. Ma, J. Qin and C. Yang, Efficient Solution-Processed Nondoped Deep-Blue Organic Light-Emitting Diodes Based on Fluorene-Bridged Anthracene Derivatives Appended with Charge Transport Moieties. *J. Phys. Chem. C* **2011**,

115, 17965-72.

- (50) K. R. J. Thomas, J. T. Lin, Y.-T. Tao and C.-H. Chuen, Green and Yellow Electroluminescent Dipolar Carbazole Derivatives: Features and Benefits of Electron -Withdrawing Segments. *Chem. Mater.* **2002**, *14*, 3852-59.
- (51) W. Li, C. Du, F. Li, Y. Zhou, M. Fahlman, Z. Bo and F. Zhang, Benzothiadiazole-Based Linear and Star Molecules: Design, Synthesis, and Their Application in Bulk Heterojunction Organic Solar Cells. *Chem. Mater.* **2009**, *21*, 5327-34.
- (52) S. Kato, T. Matsumoto, M. Shigeiwa, H. Gorohmaru, S. Maeda, T. Ishi-i and S. Mataka, Novel 2,1,3-benzothiadiazole-based red-fluorescent dyes with enhanced two-photon absorption cross-sections. *Chem. Eur. J.* **2006**, *12*, 2303-17.
- (53) J. T. Bloking, X. Han, A. T. Higgs, J. P. Kastrop, L. Pandey, J. E. Norton, C. Risko, C. E. Chen, J.-L. Brédas, M. D. McGehee and A. Sellinger, Solution-Processed Organic Solar Cells with Power Conversion Efficiencies of 2.5% using Benzothiadiazole/Imide-Based Acceptors. *Chem. Mater.* **2011**, *23*, 5484-90.
- (54) D. Deng, Y. Yang, J. Zhang, C. He, M. Zhang, Z.-G. Zhang, Z. Zhang and Y. Li, Triphenylamine-containing linear D-A-D molecules with benzothiadiazole as acceptor unit for bulk-heterojunction organic solar cells. *Organic Electronics* **2011**, *12*, 614-22.
- (55) L. E. Polander, L. Pandey, S. Barlow, S. P. Tiwari, C. Risko, B. Kippelen, J.-L. Brédas and S. R. Marder, Benzothiadiazole-Dithienopyrrole Donor–Acceptor–Donor and Acceptor–Donor–Acceptor Triads: Synthesis and Optical, Electrochemical, and Charge-Transport Properties. *J. Phys. Chem. C* **2011**, *115*, 23149-63.
- (56) A. Luechai, J. Gasiowski, A. Petsom, H. Neugebauer, N. S. Sariciftci and P. Thamyongkit, Photosensitizing porphyrin–triazine compound for bulk heterojunction solar cells. *J. Mater. Chem.* **2012**, *22*, 23030-37.
- (57) R. Maragani, T. Jadhav, S. M. Mobin and R. Misra, C₃ symmetric ferrocenyl triazines: synthesis, structure, and properties. *RSC Advances* **2013**, *3*, 2889-92.
- (58) R. Maragani and R. Misra, Donor–acceptor ferrocenyl triazines: synthesis and properties. *Tetrahedron Lett.* **2013**, *54*, 5399-402.
- (59) W. Ying, F. Guo, J. Li, Q. Zhang, W. Wu, H. Tian and J. Hua, Series of new D-A-pi-A organic broadly absorbing sensitizers containing isoindigo unit for highly efficient dye-sensitized solar cells. *ACS Appl. Mater. Interfaces* **2012**, *4*, 4215-24.
- (60) D. Y. Chen, K. Y. Cheng, M. L. Ho, I. C. Wu, M. W. Chung, H. Fu and P. T. Chou, A new

Benzothiadiazole-phenothiazine conjugates

recognition concept using dye sensitized solar cell configuration. *Chem Commun* **2011**, 47, 985-87.

- (61) S. R. Li, C. P. Lee, H. T. Kuo, K. C. Ho and S. S. Sun, High-performance dipolar organic dyes with an electron-deficient diphenylquinoxaline moiety in the pi-conjugation framework for dye-sensitized solar cells. *Chem. Eur. J.* **2012**, 18, 12085-95.
- (62) C. Chen, X. Yang, M. Cheng, F. Zhang and L. Sun, Degradation of cyanoacrylic acid-based organic sensitizers in dye-sensitized solar cells. *ChemSusChem* **2013**, 6, 1270-75.
- (63) M. Alfonso, A. Tarraga and P. Molina, Ferrocenylbenzobisimidazoles for recognition of anions and cations. *Inorg. Chem.* **2013**, 52, 7487-96.
- (64) W.-Y. Hung, L.-C. Chi, W.-J. Chen, E. Mondal, S.-H. Chou, K.-T. Wong and Y. Chi, A carbazole-phenylbenzimidazole hybrid bipolar universal host for high efficiency RGB and white PhOLEDs with high chromatic stability. *J. Mater. Chem.* **2011**, 21, 19249-56.
- (65) D. Kumar, K. R. J. Thomas, C.-P. Lee and K.-C. Ho, Novel Pyrenoimidazole-Based Organic Dyes for Dye-Sensitized Solar Cells. *Org. Lett.* **2011**, 13, 2622-25.
- (66) B. A. D. Neto, A. A. M. Lapis, E. N. da Silva Júnior and J. Dupont, 2,1,3-Benzothiadiazole and Derivatives: Synthesis, Properties, Reactions, and Applications in Light Technology of Small Molecules. *Eur. J. Org. Chem.* **2013**, 2013, 228-55.
- (67) F. Pop, A. Amacher, N. Avarvari, J. Ding, L. M. Daku, A. Hauser, M. Koch, J. Hauser, S. X. Liu and S. Decurtins, Tetrathiafulvalene-benzothiadiazoles as redox-tunable donor-acceptor systems: synthesis and photophysical study. *Chem. Eur. J.* **2013**, 19, 2504-14.
- (68) G. Wu, G. Zhao, C. He, J. Zhang, Q. He, X. Chen and Y. Li, Synthesis and photovoltaic properties of a star-shaped molecule with triphenylamine as core and benzo[1,2,5]thiadiazol vinylene as arms. *Sol. Energy Mater. Sol. Cells* **2009**, 93, 108-13.
- (69) C. He, Q. He, Y. He, Y. Li, F. Bai, C. Yang, Y. Ding, L. Wang and J. Ye, Organic solar cells based on the spin-coated blend films of TPA-th-TPA and PCBM. *Sol. Energy Mater. Sol. Cells* **2006**, 90, 1815-27.
- (70) J. Zhang, J. Yu, C. He, D. Deng, Z.-G. Zhang, M. Zhang, Z. Li and Y. Li, Solution-processable star-shaped photovoltaic organic molecules based on triphenylamine and benzothiadiazole with longer pi-bridge. *Organic Electronics* **2012**, 13, 166-72.
- (71) Y. Hua, S. Chang, D. Huang, X. Zhou, X. Zhu, J. Zhao, T. Chen, W.-Y. Wong and W.-K. Wong, Significant Improvement of Dye-Sensitized Solar Cell Performance Using Simple Phenothiazine-Based Dyes. *Chem. Mater.* **2013**, 25, 2146-53.

- (72) T. Okamoto, M. Kuratsu, M. Kozaki, K. Hirotsu, A. Ichimura, T. Matsushita and K. Okada, Remarkable Structure Deformation in Phenothiazine Trimer Radical Cation. *Org. Lett.* **2004**, *6*, 3493-96.
- (73) J. Zhang, B. Xu, J. Chen, L. Wang and W. Tian, Oligo(phenothiazine)s: Twisted Intramolecular Charge Transfer and Aggregation-Induced Emission. *J. Phys. Chem. C* **2013**, *117*, 23117-25.
- (74) Y. Liu, H. Cao, J. Li, Z. Chen, S. Cao, L. Xiao, S. Xu and Q. Gong, Synthesis and electroluminescent properties of a phenothiazine-based polymer for nondoped polymer light-emitting diodes with a stable orange-red emission. *Journal of Polymer Science Part A: Polymer Chemistry* **2007**, *45*, 4867-78.
- (75) S. Chen, Y. Li, W. Yang, N. Chen, H. Liu and Y. Li, Synthesis and Tuning Optical Nonlinear Properties of Molecular Crystals of Benzothiadiazole. *J. Phys. Chem. C* **2010**, *114*, 15109-15.
- (76) Y. Li, L. Scudiero, T. Ren and W.-J. Dong, Synthesis and characterizations of benzothiadiazole-based fluorophores as potential wavelength-shifting materials. *Journal of Photochemistry and Photobiology A: Chemistry* **2012**, *231*, 51-9
- (77) B. Valeur, *Molecular Fluorescence: Principles and Applications*, WILEY-VCH Verlag GmbH, Weinheim, 2002.
- (78) M. Jozefowicz, J.R. Heldt, Dipole moments studies of fluorenone and 4-hydroxyfluorenone, *Spectrochim. Acta A* *67* (2007) 316–20.
- (79) G.V. Loukova, A.A. Milov, V.P. Vasiliev, V.A. Smirnov, Dipole moment of a metallocene precatalyst in the ground and excited states, *Russ. Chem. Bull. Int. Ed.* *57* (2008) 1166–1171.
- (80) C. Reichardt, Solvatochromic Dyes as Solvent Polarity Indicators. *Chem. Rev.* **1994**, *94*, 2319-58.
- (81) M. J. Kamlet, J. L. M. Abboud, M. H. Abraham and R. W. Taft, Linear solvation energy relationships. 23. A comprehensive collection of the solvatochromic parameters, π^* , α and β and some methods for simplifying the generalized solvatochromic equation. *J. Org. Chem.* **1983**, *48*, 2877-87.
- (82) J.-M. Lee, S. Ruckes and J. M. Prausnitz, Solvent Polarities and Kamlet-Taft Parameters for Ionic Liquids Containing a Pyridinium Cation. *J. Phys. Chem. B* **2008**, *112*, 1473-76.
- (83) V. Shrotriya, J. Ouyang, R. J. Tseng, G. Li and Y. Yang, Absorption spectra modification in poly(3-hexylthiophene):methanofullerene blend thin films. *Chem. Phys. Lett.* **2005**, *411*, 138-43.

Benzothiadiazole-phenothiazine conjugates

- (84) R. G. Parr and W. Yang, Density-Functional Theory of the Electronic Structure of Molecules. *Annu. Rev. Phys. Chem.* **1995**, *46*, 701-28.
- (85) A. D. Becke, A new mixing of Hartree–Fock and local densityfunctional theories. *The Journal of Chemical Physics* **1993**, *98*, 1372-77.
- (86) C. Lee, W. Yang and R. G. Parr, Development of the Colle-Salvetti correlation-energy formula into a functional of the electron density. *Physical Review B* **1988**, *37*, 785-49.
- (87) B. J. Lynch, P. L. Fast, M. Harris and D. G. Truhlar, Adiabatic Connection for Kinetics. *J. Phys. Chem. A* **2000**, *104*, 4811-15.
- (88) Y.-F. Liu, X.-F. Ren, L.-Y. Zou, A.-M. Ren, J.-K. Feng and C.-C. Sun, Theoretical study on photophysical properties of 2,1,3-benzothiadiazole-based star-shaped molecules. *Theor. Chem. Acc.* **2011**, *129*, 833-45.
- (89) K. R. J. Thomas, P. Singh, A. Baheti, Y.-C. Hsu, K.-C. Ho and J. T. Lin, Electro-optical properties of new anthracene based organic dyes for dye-sensitized solar cells. *Dyes Pigm.* **2011**, *91*, 33-43.

Chapter 7

Benzothiadiazole-Ferrocene π -Extended Conjugates with Vinyl Linkage: Synthesis, Structure, Electrochemical and Thermal Properties

7.1 Introduction

Organometallic complexes continue to attract wide attention owing to their applications in molecular devices based on photoinduced electron and energy transfer reactions like organic photovoltaics (OPVs), organic light-emitting diodes (OLEDs), dye-sensitized solar cells (DSSCs), organic field-effect transistors (OFETs), non-linear optics and lithium ion battery etc [1-8]. In the past two decades, organometallic complexes featuring platinum [9-10], ruthenium [11-16], iron [17-19], osmium [20-21] and iridium [22-24] compounds have been extensively explored in supramolecular chemistry and materials sciences. Especially platinum [25-28] and ruthenium [14] complexes integrated with benzothiadiazole (BTD) acceptor moiety exhibited broad absorption profiles due to intramolecular charge transfer (ICT), which is beneficial for the enhancement of photo current response in photovoltaic devices. In light of these considerations, incorporation of BTD into the integral part of the iron organometallic conjugated complex will be beneficial to improve the electronic properties of iron containing complexes.

Ferrocene can act as a strong donor, highly stable and show low sensitivity to di-oxygen and water [29]. Complexes with ferrocenyl groups as redox-active termini are extensively explored, due to their high thermal stability and the excellent electrochemical reversibility of the ferrocene's [Fe(II)/Fe(III)] redox couple [30-31]. Multi ferrocenyl compounds become a topic of interest in molecular electronics, quantum cellular automata, optoelectronic materials, and biochemistry due to their multiredox, magnetic coupling, and unpaired electron density migration properties [32-37]. In the literature it was found that, ferrocene in combination with hetero aromatic spacers and electron withdrawing moieties shows excellent metal-metal

Benzothiadiazole-Ferrocene Conjugates: Synthesis and Optical properties

interactions and large second-order nonlinear optical (NLO) properties [30, 38-42]. Since 1987, after the maiden report from Marder and co workers ferrocene has been exploited as an electron-donor moiety for several material science applications [29]. Especially ferrocene based push-pull systems have attracted considerable attention, owing to their efficient intramolecular charge transfer (ICT) from the donor to the acceptor and the molecule becomes polarized. The polarized molecule expected to show high first-order hyperpolarizability ($\chi^{(1)}$), in the presence of strong electromagnetic field of a laser beam [30]. The extent of intramolecular charge transfer (ICT) primarily is affected by the modification and exchange of the donor, π -spacer, and acceptor parts. So far, extensive research has been carried out on ferrocenyls linked with annulenes, arenes, porphyrins, five- and six-membered heterocycles, and electron deficient moieties etc [36, 43-48]. Many electron deficient heterocyclic moieties were integrated with ferrocene to form push-pull systems of various designs and arrangements [30, 38, 45, 49-55]. The optical and electrochemical properties in such complexes are mainly tuned by the electronic nature of the electron-deficient group attached to it. Heteroaromatic ring systems capped or joined by linear π -conjugation with ferrocenyl groups are numerous in the literature and identified as excellent candidates for studying intramolecular electron transfer, intervalence charge transfer (IVCT) [19, 31-32, 34, 43, 56].

Over the two decades, several research groups have focused on the design, synthesis, and application of ferrocene based push-pull systems. The heteroaromatic spacers which connect the push-pull can strengthen its thermal and chemical robustness. Recently Misra and co-workers reported a series of ferrocenyl substituted benzothiadiazoles [57-58] with acetylene linkage and the structures of the complexes are as shown in the Figure 7.1. The photophysical and electrochemical studies of these complexes reveals the existence of strong donor-acceptor interactions. These compounds are non-emissive in nature. Since the double bonds are found to be effective for the electronic communication in between the constituents of the molecular wire, we designed and synthesized a series of ferrocene-BTD conjugates possessing vinyl linkage. Within this series a systematic change from electron-donating to electron-withdrawing functionalities was realized, which also allowed elucidation of the structure-property relationships. Chromophores represent inorganic-organic hybrid systems in which heterocyclic acceptor 2,1,3-benzothiadiazole unit was connected to an electron-releasing ferrocenyl group as one of the terminal subunits through a π -conjugated system of double bond. Because of the

Benzothiadiazole-Ferrocene Conjugates: Synthesis and Optical properties

alleviated π -conjugation and planarization of the chromophore, we opted vinyl linkage rather than more electronegative (electron-deficient) ethynylene linkage.

Figure 7.1 Structures of the known ferrocene-benzothiadiazole dyes in the literature

It is expected that the integration of ferrocene and benzothiadiazole in a molecular structure with different chromophores on benzothiadiazole termini may impart favorable optical and charge transport properties desired for electronic applications. We wish to present here the synthesis, absorption, and redox behavior of the ferrocene with a low band gap chromophore. To the best of our knowledge, molecules containing ferrocene moiety attached to a low band chromophore like benzothiadiazole have been exploited barely and ferrocene attached to benzothiadiazole by vinyl linkage has not exploited. In this context, to establish the structure - property relationship between these donor-acceptor compounds, we systematically perturbed the tethering groups on the 7th position of BTD with different chromophores. The mutual electronic communication and impact of these tethering groups on new ferrocene-benzothiadiazole vinyl hybrids was explored by photophysical, electrochemical, DFT study and thermal properties. The new complexes possessed excellent light harvesting nature due to strong donor-acceptor interactions and may exhibit enhanced two photon absorption properties. The structures of the complexes synthesized and characterized in this study are presented in Figure 7.2.

Figure 7.2 Structures of the benzothiadiazole-ferrocene hybrid complexes

Molecules with π -conjugated systems bearing pyridyl substituents at the terminal positions are expected to be alligator clips for the synthesis of molecular devices. These terminal pyridyl containing molecules can form intermolecular interactions such as hydrogen and coordination bonds with metals to yield fascinating supramolecular building blocks [59-60]. So the derivative **30d** which contain pyridine at the termini can be useful for the synthesis of supramolecular building blocks and it can be applied as a sensitizer in dye-sensitized solar cells, since it can form strong coordinate bonding with the Lewis acid sites of TiO_2 by the lone pair of electrons on the nitrogen atom of the pyridine ring [61].

7.2 Results and Discussion

7.2.1 Synthesis of Ferrocene-Benzothiadiazole Conjugates

Figure 7.3 Ferrocene-benzothiadiazole vinyl hybrid complexes general representation

Benzothiadiazole-Ferrocene Conjugates: Synthesis and Optical properties

The general structural representation and numbering of the ferrocene-benzothiadiazole hybrids is shown Figure 7.3. The synthetic pathways leading to new ferrocene-benzothiadiazole conjugated complexes are shown in Scheme 7.1. The targeted molecules were extensively synthesized by utilizing palladium-catalyzed Heck coupling reaction with quantitative yields. The compounds vinyl ferrocene (**18c**) [62], 4,7-dibromobenzo[*c*][1,2,5]thiadiazole (**1**) [63], 4-bromo-7-(piperidin-1-yl)benzo[*c*][1,2,5]thiadiazole (**2a**) [64], and 4-bromo-7-(thiophen-2-yl)benzo[*c*][1,2,5]thiadiazole (**29**) [65], were prepared by adopting reported procedures. (*E*)-4-bromo-7-(2-(pyridin-4-yl)vinyl)benzo[*c*][1,2,5]thiadiazole (**16**) was prepared from 4,7-dibromobenzo[*c*][1,2,5]thiadiazole (**1**) by adopting Heck coupling protocol with one equivalent of vinyl pyridine. The bromo precursor (**2a-b**, **16**, **29**) were conveniently converted to the targeted complexes by treating with one equivalent of vinyl ferrocene (**18c**), and the complex **30d** was obtained by treating 4,7-dibromobenzo[*c*][1,2,5]thiadiazole (**1**) with two equivalents of vinyl ferrocene (**18c**) in the presence of Pd(OAc)₂, TBAB, and sodium acetate by Heck cross-coupling reaction. These ferrocene complexes has good solubility in common organic solvents such as tetrahydrofuran, dichloromethane and acetonitrile etc and are stable in the solid state as well as in solution towards air and moisture.

Scheme 7.1 Synthetic pathways leading to ferrocene-benzothiadiazole hybrid complexes

All these complexes were unambiguously characterized by IR, ¹H NMR, ¹³C NMR and HRMS. The data is consistent with the proposed structures, showing the expected features with correct integration ratios. From ¹H NMR, all the olefinic -CH=CH- units appeared as doublets with coupling constant of ca. 16 Hz, confirmed an (*E*) configuration in the double bond(s) introduced by Heck coupling reaction. The ferrocenyl group in all the complexes gave three

Benzothiadiazole-Ferrocene Conjugates: Synthesis and Optical properties

different signals, the unsubstituted cyclopentadienyl (C₅H₅) moiety of ferrocene exhibited a sharp singlet below 4.20 ppm and the mono substituted cyclopentadienyl (C₅H₄) ring exhibited two different broad unresolved multiplets above 4.30 ppm due to different chemical environment. These signals appear at low field of the unsubstituted cyclopentadienyl (C₅H₅) singlet, showing that the highly electron withdrawing low band gap benzothiadiazole considerably deshielded all the four ring protons. This deshielding is less pronounced in the dye **30a** and **30b** due to the electron rich amines piperidine, morpholine groups on the 7th position of the BTd. Except **30d**, all the derivatives show two doublets corresponding to the chemically non-equivalent benzothiadiazole. The symmetrical nature of the benzothiadiazole in **30d** was revealed by the presence of singlet. The impact of the different tethering groups on the 7th position of the benzothiadiazole was studied by ¹H and ¹³C NMR. The signals associated with the ferrocenyl, vinyl and benzothiadiazole fragments were presented in the Table 7.1 and 7.2. The complex **30a** was also characterized by single-crystal X-ray diffraction.

Table 7.1 ¹H Spectral data of the complexes recorded in CDCl₃^a

Complex	Cp	Cp'	Vinyl (H _a & H _b)	BT-H5	BT-H6
30a	4.16	4.32, 4.56	7.12, 7.61	6.76	7.48
30b	4.15	4.31, 4.55	7.11, 7.58	6.75	7.45
30c	4.18	4.38, 4.61	7.24, 7.80	7.60	7.8
19c	4.19	4.40, 4.62	7.22, 7.75	7.61	7.69
30d	4.17	4.37, 4.60	7.20, 7.77	7.55	7.55

^aChemical shifts in ppm

Table 7.2 ¹³C Spectral data the complexes recorded in CDCl₃^a

Dye	Cp	Cp'	Vinyl
30a	69.2	66.8, 69.0, 84.1	112.2, 122.2
30b	69.3	66.9, 69.1, 83.8	112.1, 121.9
30c	69.4	67.3, 69.4, 83.1	-
19c	69.5	67.5, 69.9, 83.0	-
30d	69.4	67.2, 69.6, 83.5	121.1, 125.9

^aChemical shifts in ppm

7.2.2 X-ray Crystallography of **30a**

The single crystal of ferrocene-benzothiadiazole conjugate **30a** was grown via the slow diffusion of acetonitrile into dichloromethane solution at room temperature, is as shown Figure 7.4. The complex **30a** crystallizes in the monoclinic space group *P2₁/n*. The single crystal X-ray structure determination confirmed the presence of newly introduced C-C bonding between benzothiadiazole unit and vinyl ferrocene unit by Heck coupling protocol.

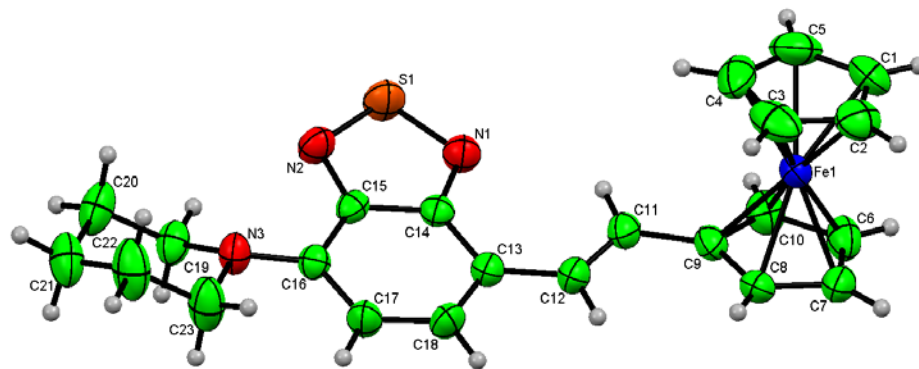


Figure 7.4 ORTEP plot of the complex **30a**

The benzothiadiazole ring is nearly coplanar with the neighboring vinyl entity. The BTD moiety and the ferrocenyl Cp are in mutual trans positions with respect to each other at the termini of the conjugated alkene, which is in agreement with the NMR assignment. The benzothiadiazole ring is slightly deviated from planarity with respect to vinylferrocene by 17.15°. Piperidine ring is non-planar with respect to benzothiadiazole ring by 28.90°. The bond lengths of C11=C12 (1.328 Å) longer than the C=C (1.34 Å) bond length. The C16-N3(1.386 Å) bond distances in between the piperidine nucleus and benzothiadiazole moiety is shorter than the aromatic C-N bond distance (C-N single bond 1.47 Å; double bond 1.34 Å; aromatic 1.43 Å), which indicates that the lone pair on the piperidine nitrogen is delocalized into the benzothiadiazole segment probably due to the electron-deficient nature of the thiadiazole nucleus.

7.2.3 Absorption spectra

To probe the charge transfer properties of the new ferrocene-benzothiadiazole complexes the electronic absorption spectra was recorded in dichloromethane and film at room temperature, is as shown in Figure 7.5(a), and the pertinent data are listed in Table 7.3. The dyes display broad absorption bands in the range of 300-700 nm. The absorption spectra of the all the dyes shows two major transitions. The higher energy transition around 300-380 nm is corresponding to the π - π^* transition and the lower energy transition from 390-650 nm is attributable to intramolecular charge transfer character with localized π - π^* transition. This assignment is further supported by the fact that extension of conjugation in **30c**, **19c** and **30d** on benzothiadiazole by different π -bridging chromophores, enhanced the molar extinction coefficient of the transition from 400-500 nm and by the inclusion of vinyl pyridine unit on the 7th position of benzothiadiazole in **19c**, enhanced the molar extinction coefficient and red shifted absorption in the range 500-650 nm

due to the more enhanced intramolecular charge transfer from ferrocene to benzothiadiazole unit.

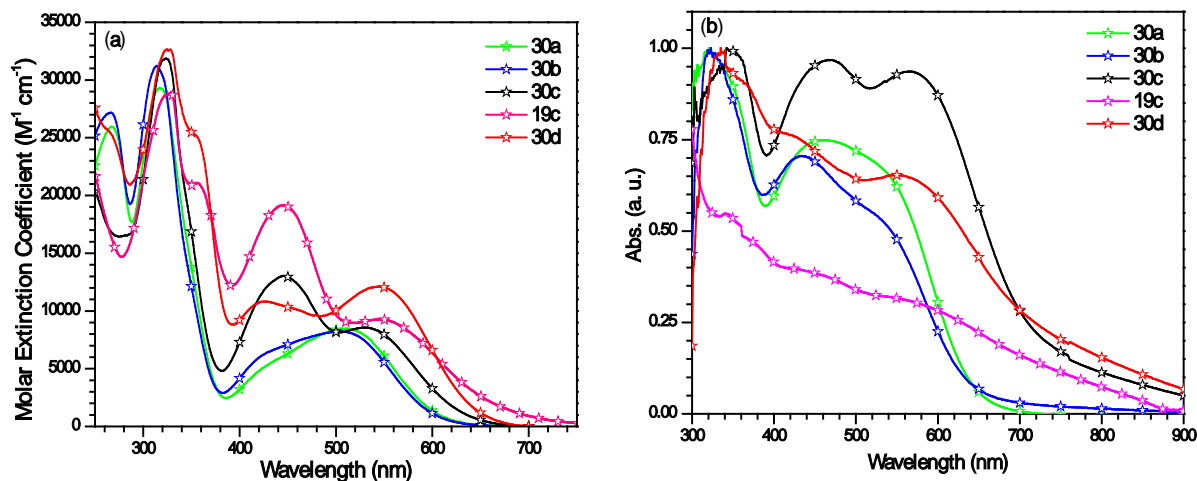


Figure 7.5 Absorption spectra of the complexes recorded in (a) dichloromethane (b) thin solid film

In general, the features of the lower energy transition are heavily controlled by the nature of the chromophore present on BTD. Thus, the peak positions of the lower-energy band in the dyes follow the order $19c > 30d > 30c > 30a > 30b$. The complex **30a** was red shifted by 9 nm than **30b**, due to more electron donating ability of the donor. Among all, **19c** showed red shifted absorption maximum in the series due to elongated conjugation and strong donor-acceptor interactions by the inclusion of vinyl pyridine unit. The absorption spectra of the dyes on the thin solid films (Figure 7.5(b)) were broadened and minor bathochromic shift was observed due to the existence of strong intermolecular interaction in the solid state.

To probe the effect of solvent environments on the ground state of the complexes, the solvatochromism was investigated by measuring the electronic absorption spectra in selected solvents such as cyclohexane (CH), toluene (TOL), tetrahydrofuran (THF), dichloromethane (DCM), acetonitrile (ACN), *N,N*-dimethylformamide (DMF) and methanol (MeOH) with different polarity indices. The absorption spectra of the complexes in different solvents are shown in Figures 7.6 and 7.7 (a). The absorption data in different solvents are rendered in Table 7.3. The absorption spectra of the complexes showed no significant difference by changing the solvent polarity. Thus the donor-acceptor interactions of the complexes were not affected by changing the solvent polarity resulting in unaffected absorption spectra. The donor-acceptor interactions and intramolecular charge transfer nature of these complexes were studied by recording absorption spectra in toluene by the addition of acid TFA and base TEA. The

Benzothiadiazole-Ferrocene Conjugates: Synthesis and Optical properties

absorption spectra of complexes before and after addition of TFA/TEA are shown in Figures 7.7 (b) and 7.8. The charge transfer transition of the complexes **30a**, **30b** and **19c** was red shifted by the addition of TFA and gained its original position by the addition of TEA. This observation was mainly due to the protonation of nitrogen at the alkyl amine piperidine/morpholine in **30a** and **30b**, where as in **19c** the protonation occurred at pyridine ring of nitrogen. Now this positive charge on the benzothiadiazole side makes it more deficient and enhanced the intramolecular charge transfer from ferrocene to benzothiadiazole, consequently the absorption maximum was red shifted. This enhanced intramolecular charge transfer was restored by addition of TEA. Interestingly due to lack of any protonating site in the complexes **30c** and **30d**, the absorption was unaltered by the addition of TFA/TEA. Indeed all the complexes absorption spectra were unaltered by the addition of the TEA due to deficiency of interacting site. The absorption data of the complexes recorded in toluene by the addition of TFA/TEA was collected in Table 7.4. It should be noted that ferrocene is an efficient excited state quencher and due to the fast non-radiative deactivation of the excited state with intramolecular charge transfer all these complexes were in non-emissive in nature.

Table 7.3 Absorption spectral data of the hybrid complexes recorded in different solvents

Complex	λ_{abs} , nm ($\epsilon \times 10^3 \text{ M}^{-1} \text{ cm}^{-1}$)						
	CH	TOL	THF	DCM	ACN	DMF	Film
30a	269,	319 (25.1),	316 (25.0),	268 (26.0),	267 (24.1),	318 (28.1),	321
	316,	512 (7.4)	506 (6.5)	317 (29.3),	315 (29.0),	514 (7.8)	
	507 ^a			512 (8.5)	503 (8.2)		
30b	268,	316 (26.0),	314 (21.7),	266 (27.2),	267 (19.4),	315 (25.5),	323,
	313,	508 (6.9)	503 (5.1)	314 (31.2),	312 (23.7),	508 (6.4)	434
	506 ^a			503 (8.2)	504 (6.2)		
30c	320,	323 (24.6),	321 (30.0),	324 (31.8),	319 (32.2),	323 (30.9),	342,
	449,	449 (9.9),	448 (11.7),	445 (13.0),	443 (12.9),	449 (11.9),	467,
	530 ^a	530 (6.9)	529 (7.5)	531 (8.6)	519 (8.3)	529 (7.9)	567
19c	317,	330 (33.4),	329 (33.3),	329 (22.2),	328, 437,	330 (38.0),	-
	355,	358 (26.0),	354 (25.4),	356 (18.1),	535 ^a	354 (28.1),	
	441,	442 (19.8),	442 (18.9),	437 (7.3),		443 (21.2),	
	543 ^a	549 (11.1)	546 (9.9)	548 (9.6)		540 (10.4)	
30d	265,	327 (26.0),	323 (26.0),	325 (32.6),	263, 322,	325 (24.8),	335,
	322,	426 (8.3),	423 (8.7),	427 (10.8),	416, 527 ^a	424 (7.9),	549
	423,	545 (10.2)	541 (8.9)	544 (12.1)		545 (8.5)	
	541 ^a						

^aMolar extinction coefficient is not obtained due to less solubility

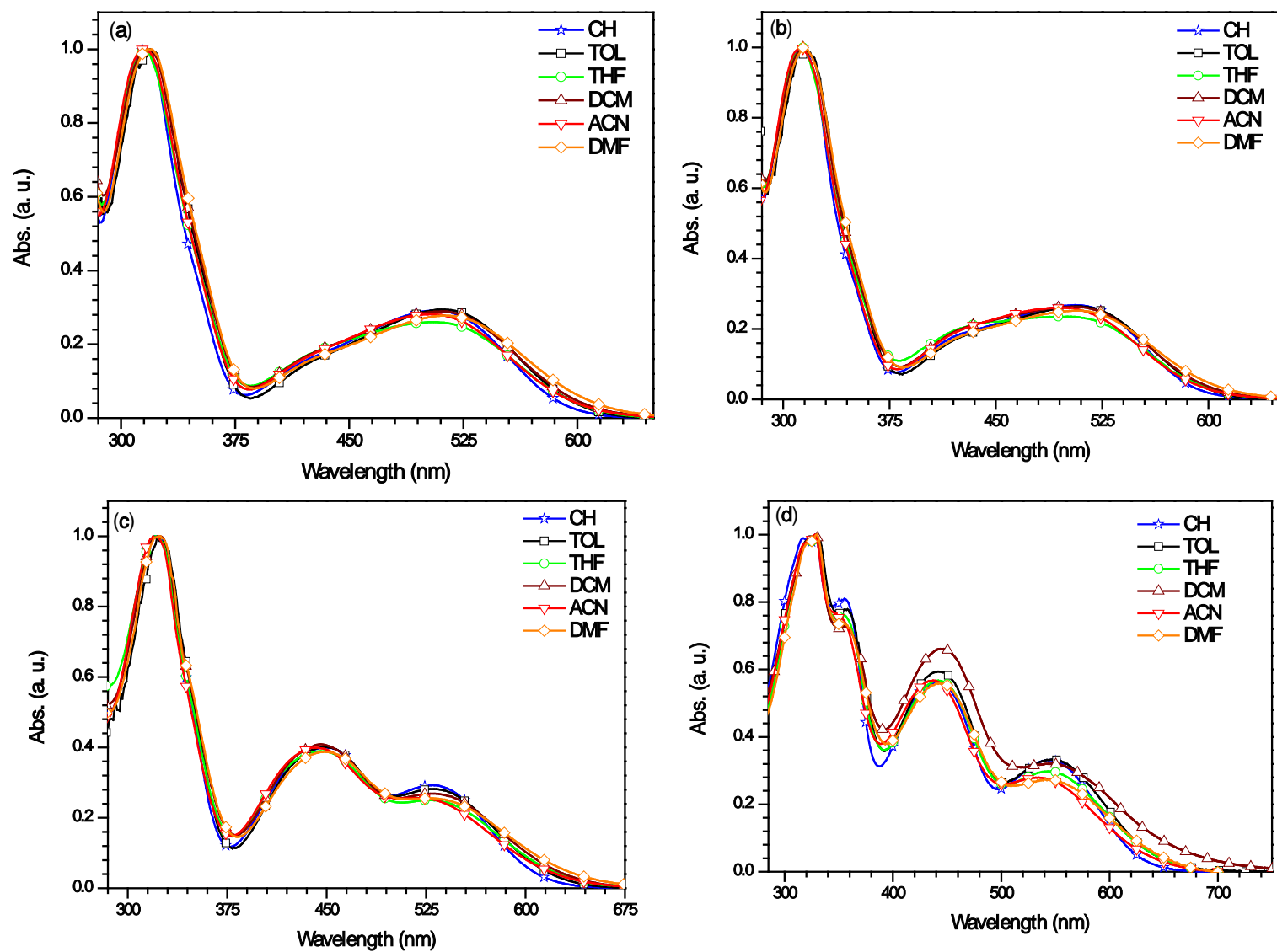


Figure 7.6 Absorption spectra of the complexes recorded in different solvents (a) 30a (b) 30b, (c) 30c and (d) 19c

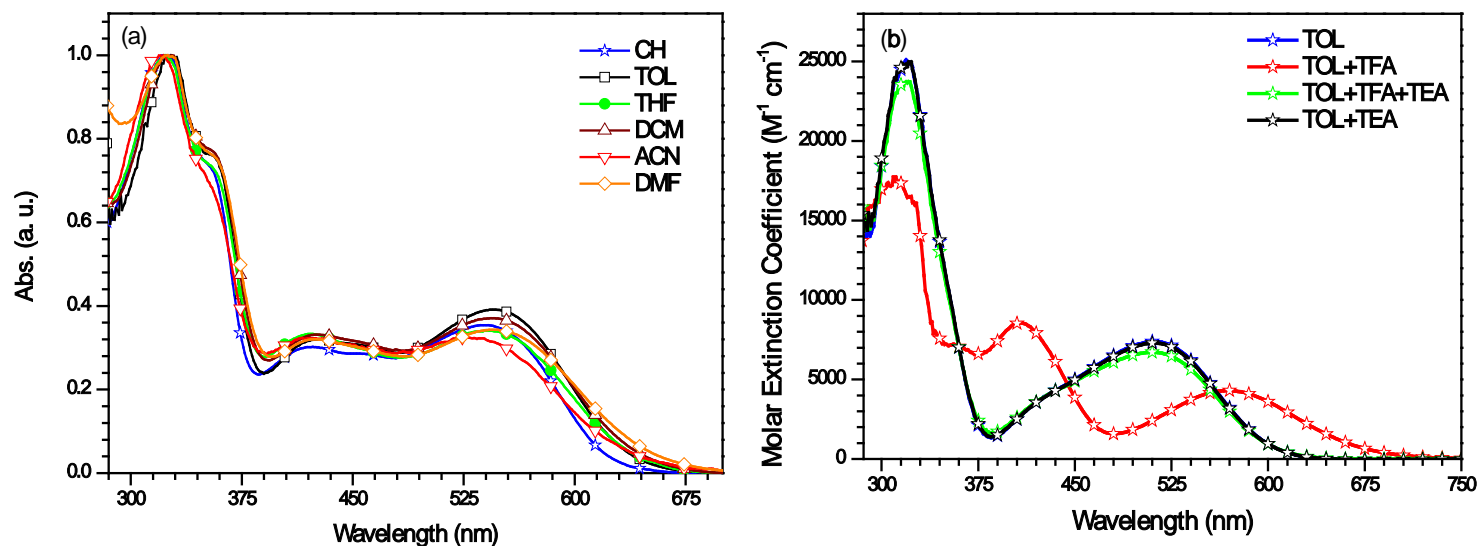


Figure 7.7 Absorption spectra of the complex (a) **30d** recorded in different solvents (b) **30a** in toluene before and after addition of TFA or TEA

Table 7.4 Absorption data of the complexes recorded in toluene before and after addition of TFA/TEA

Complex	λ_{abs} , nm ($\epsilon \times 10^3 \text{ M}^{-1} \text{ cm}^{-1}$)			
	TOL	TOL+TFA	TOL+TFA+TEA	TOL+TEA
30a	319 (25.1), 512 (7.4)	311 (17.7), 408 (8.6), 569 (4.3)	321 (23.7), 510 (6.7)	323 (25.0), 511 (7.3)
30b	316 (26.0), 508 (6.9)	310 (19.1), 409 (8.5), 566 (5.0)	316 (26.2), 507 (6.6)	315 (25.8), 508 (6.7)
30c	323 (24.6), 449 (9.9), 530 (6.9)	323 (23.6), 458 (10.8)	323 (23.6), 448 (9.6), 530 (6.3)	322 (24.4), 449 (9.7), 531 (6.8)
19c	330 (24.7), 356 (19.1), 442 (14.5), 546 (8.0)	331 (17.4), 449 (21.2), 624 (3.0)	331 (24.7), 355 (19.1), 441 (14.5), 547 (8.1)	331 (25.1), 357 (19.2), 441 (14.5), 547 (8.0)
30d	327(26.0), 352 (19.9), 429 (8.3), 545 (10.2)	323 (24.9), 355 (18.3), 435 (8.4), 550 (9.2)	327 (25.5), 355 (19.3), 426 (8.4), 544 (9.7)	328 (25.9), 353 (19.8), 426 (8.3), 544 (10.1)

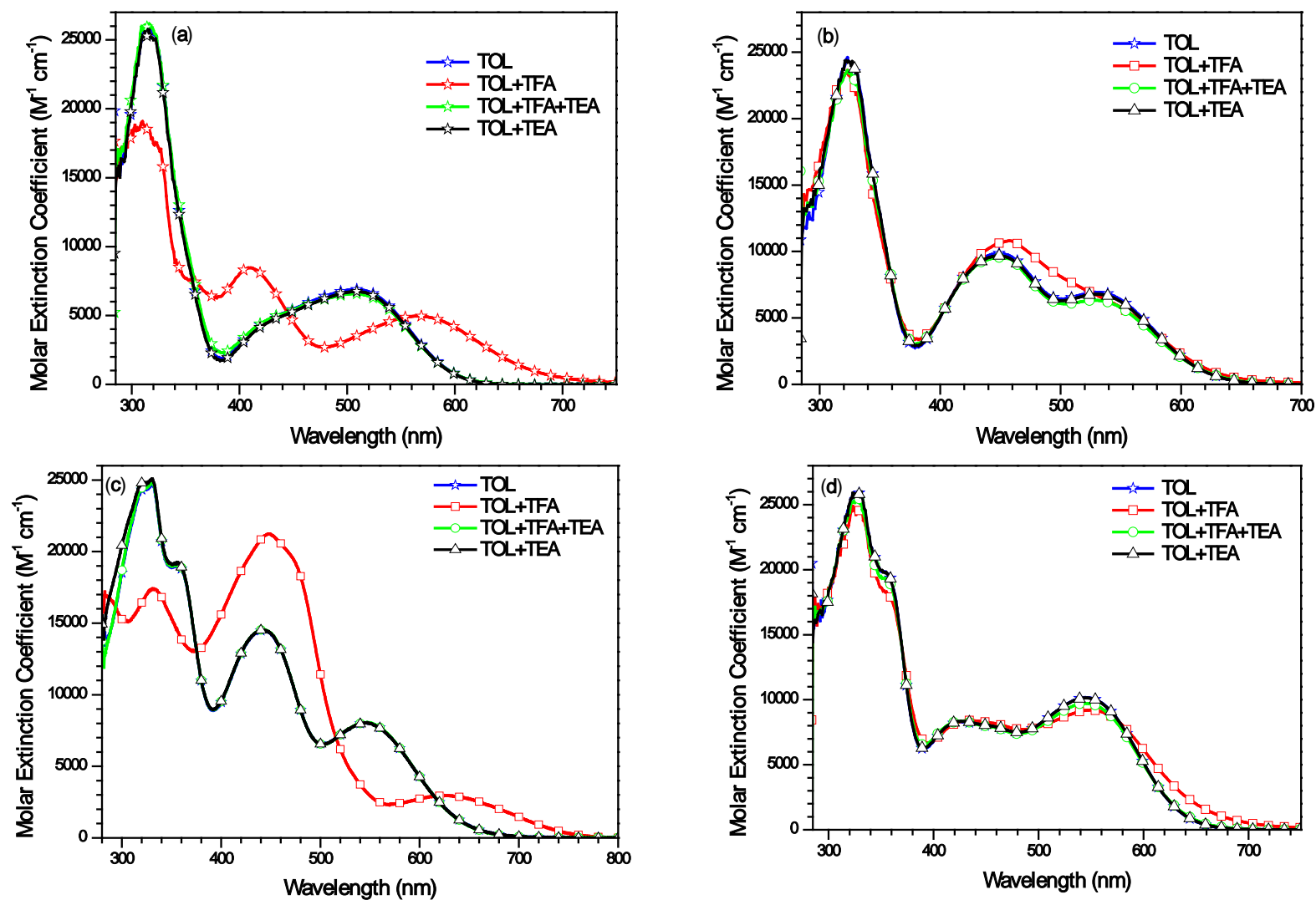


Figure 7.8 Absorption spectra of (a) **30b**, (b) **30c**, (c) **19c** and (d) **30d** in toluene before and after addition of TFA or TEA

7.2.4 Electrochemical Studies

To investigate the possibility of electronic interactions between ferrocene and benzothiadiazole units in the complexes cyclic voltammetry (CV) and differential pulse voltammetry (DPV) experiments were performed in dichloromethane solution (2×10^{-4} M) using tetrabutylammonium perchlorate as a supporting electrolyte. The cyclic voltammograms of the ferrocene-benzothiadiazole complexes **19c** are shown in Figure 7.9 and pertinent redox data are presented in Table 7.5.

Table 7.5 Electrochemical data of complexes recorded in dichloromethane

Complex	E_{ox}, V^a ($\Delta E_p, mV$)	E_{red}, V^a ($\Delta E_p, mV$)	HOMO, eV ^b	LUMO, eV ^b	E_{0-0}, eV	E_{ox}^*, V^c
30a	-0.053 (71), 0.145 (70)	2.065	4.747	2.735	2.012	-1.295
30b	-0.029 (71), 0.238 (70)	2.043	4.771	2.757	2.014	-1.273
30c	0.006 (74)	1.797 (74)	4.806	3.003	1.803	-1.027
19c	0.053(155)	-	4.853	3.082	1.771	-0.948
30d	0.015 (106)	1.869 (54)	4.815	2.931	1.884	-1.099

^a Measured for dichloromethane solutions using tetrabutylammonium perchlorate (TBAP) as the supporting electrolyte at a scan rate of 100 mV/s. ^b Deduced from the equations HOMO = $E_{ox} + 4.8$ and LUMO = $E_{red} + 4.8$

^c Excited-state oxidation potential versus NHE

All the complexes showed well-defined redox response in the CV measurements. The complexes exhibited a reversible oxidation of the ferrocene to ferrocenium ion and reduction wave due to the electron deficient benzo[*c*][1,2,5]thiadiazole. In addition, to the oxidation of the ferrocene moiety, the dyes **30a** and **30b** exhibited a second reversible oxidation wave at higher potential, attributed to the oxidation of the piperidine and morpholine amine donors, respectively. The first oxidation potentials of the dyes follow the order **30a** < **30b** < **30c** < **30d** < **19c**. The reduction potentials of the dyes follow the trend **30c** < **30d** < **30b** < **30a**. The first oxidation potential increases when the substituent functionality changes from electron-donating to electron withdrawing group. Therefore, we can conclude that the nature of the tethering group on benzothiadiazole strongly affects the electron density at the iron centre, as well as on benzothiadiazole moiety. The trends observed in the oxidation and reduction potentials mainly depend upon the nature of the tethered group at 7th position of benzothiadiazole. The HOMO and LUMO energies of these complexes were calculated by using the ferrocene/ferrocenium redox couple as a reference (4.8 eV) and were within the range 4.747-4.853 eV and 2.735-3.082 eV. The electro chemical band gaps (E_g) of the dyes are in the range of 1.771–2.014 eV. Compared with **30c**, **19c** and **30d** the HOMO energy levels of **30a**, **30b** are significantly raised, due to the introduction of stronger donating amine group in the complexes. These results clearly show that a modification in the electronic

Benzothiadiazole-Ferrocene Conjugates: Synthesis and Optical properties

structure of the tethering group attached to benzothiadiazole can dramatically change the interaction between the ferrocene and benzothiadiazole and the redox behaviour of the complex.

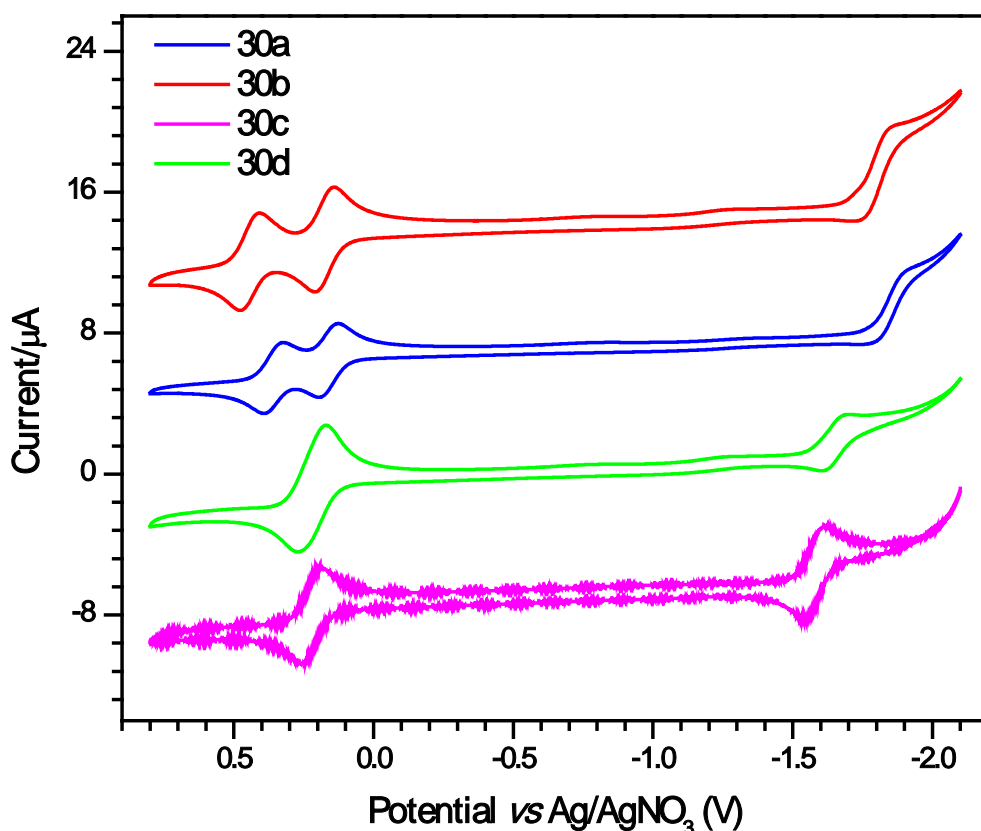


Figure 7.9 Cyclic voltammograms of the ferrocene benzothiadiazole conjugates recorded in dichloromethane at the scan rate 100 mV/sec

All the new ferrocene-benzothiadiazole complexes have strong absorption in the visible region and the enough electrochemical stability. So to evaluate the possibility of photo induced electron transfer process from these complexes to electron acceptors in BHJ solar cells, we have examined the HOMO and LUMO energy levels of the complexes as donor materials. To have an efficient charge separation in bulk-heterojunction (BHJ) solar cells, it was essential to have a minimum offset of approximately 0.3-0.4 eV between the LUMO of the donor and the LUMO of the acceptor. The LUMO of the complexes is determined from the reduction wave. Complexes have their LUMO level ranging ((-2.757)-(-3.003)) eV which is higher than the PC₇₀BM level (-4.3 eV), making the photoinduced ICT and charge separation possible at the interface between the donor and acceptor when applied in the BHJ solar cells. The band gap of the P3HT is 1.9-2.0 eV [66], which is used as an efficient donor in BHJ solar cells. The band gap of the new ferrocene-benzothiadiazole complexes is 1.771-2.014 eV. From this comparison, it is clear that these materials can serve as efficient donors. Both the HOMO and LUMO energy levels of complexes are proper for BHJ solar cells when

Benzothiadiazole-Ferrocene Conjugates: Synthesis and Optical properties

PCBM or its derivatives were used as the electron acceptor. The comparison of energy levels was shown in Figure 7.10.

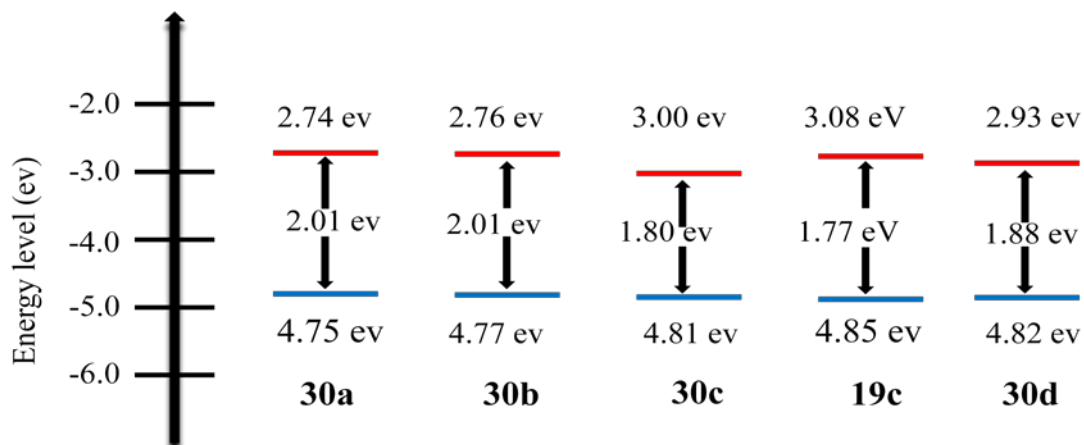


Figure 7.10 Energy-level diagram of the ferrocene-benzothiadiazole hybrid complexes

To establish the structure and property relationship in the new ferrocene-benzothiadiazole vinyl complexes, we compared the lower energy absorption maxima and first oxidation potentials (ferrocene oxidation) of the complexes. The in detail trends were shown schematically in the Figure 7.11.

Figure 7.11 Structures and trends in optical and electrochemical data of complexes studied in this chapter

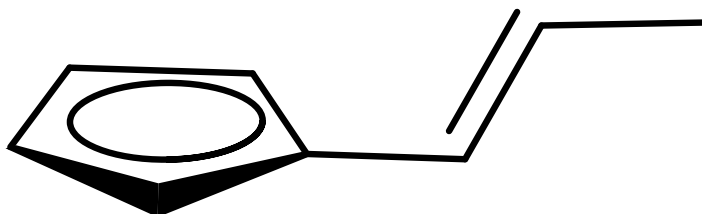


Figure 7.12 Trends in optical and electrochemical data for the ferrocene derivatives

It is interesting to compare the optical and the electrochemical properties of **30d** with the known π -conjugated ferrocene vinyl derivatives with phenyl, thiophene and furan derivatives to know the impact of the benzothiadiazole on the ferrocene. And also we compared with acetylene linked ferrocene-benzothiadiazole dye to evaluate the impact of vinyl linkage on the photophysical and electrochemical properties. The permutation of phenyl, thiophene and furan by the benzothiadiazole unit in **30d** greatly enhances the light-harvesting nature in the long wavelength region [33, 42] (bathochromically shifted). The phenyl analogue of **30d** was blue shifted by 85 nm. Interestingly the red shifting and broadening of the lower energy transition band, enhanced redox stability and minimised the HOMO-LUMO gap was caused by the inclusion of the BTD unit in the complexes. Indeed, the oxidation potential of the ferrocene anodically shifted by the inclusion of benzothiadiazole, which reveals the strong electron withdrawing nature of the BTD unit. The introduction of vinyl bridge by the replacement of acetylene linkage, red shifted the absorption maxima by 21 nm. This may be attributed to the fact that in the alkene bridged complex **30d**, all the carbon atoms are sp^2 hybridized to give a relatively longer conjugation. While in the case of alkyne bridged complex the carbon atoms are in both sp and sp^2 hybridized, which results poorer π -orbital overlap and mismatch in energy of the π -orbitals, leading to a blue shift in the absorption [67]. The in detail trends were presented in Figure 7.12.

7.2.5 Computational Chemistry

To scrutinize in more detail the electronic communication and interactions between the ferrocene and benzothiadiazole units with the appropriate tethering group, density functional theory (DFT) and time-dependent density functional theory (TDDFT) calculations were

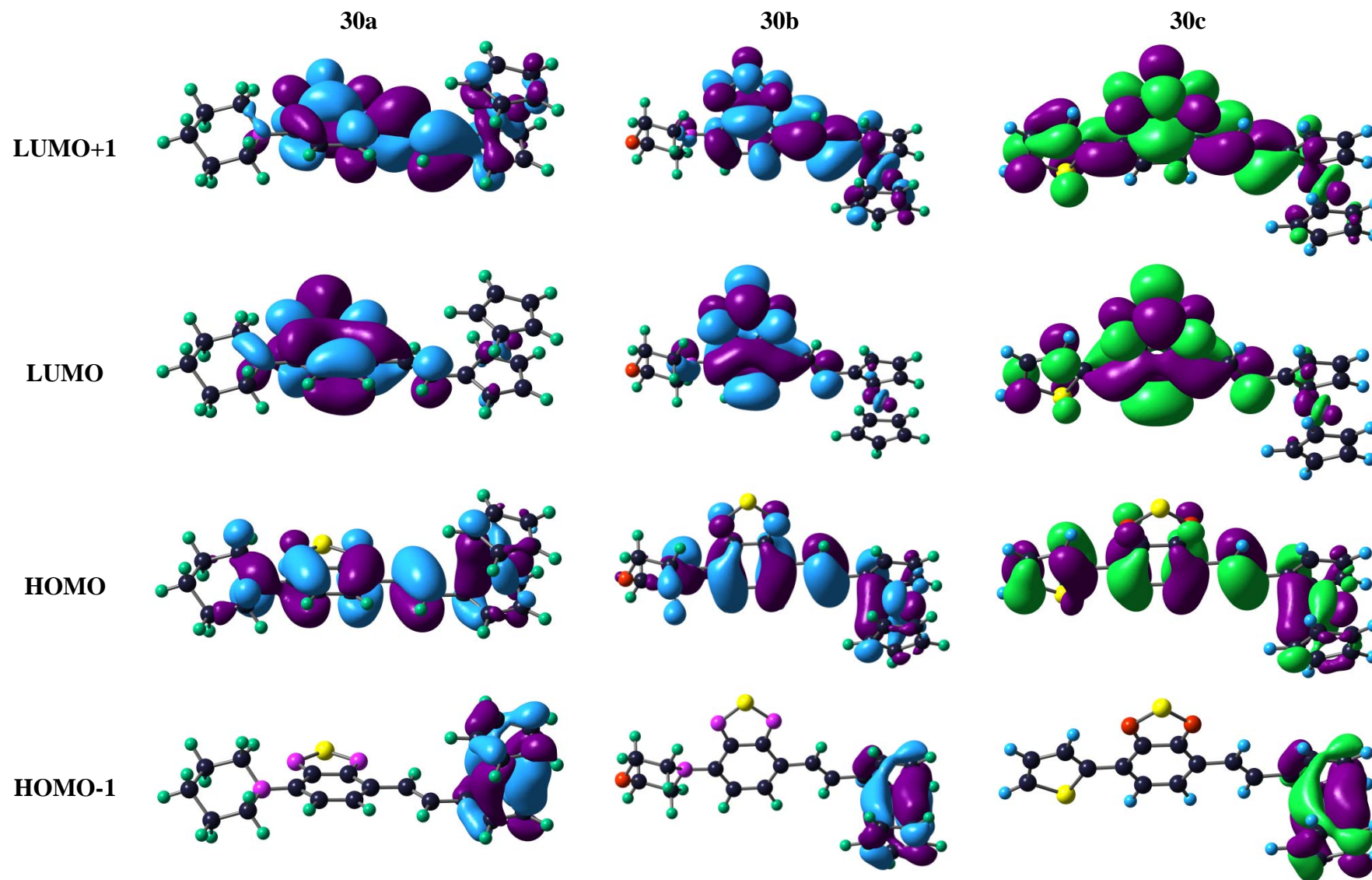
Benzothiadiazole-Ferrocene Conjugates: Synthesis and Optical properties

performed at the molecular level [68]. Figure 7.13 and 7.14 show the plots of the most representative molecular frontier orbitals in the ground states of the new benzothiadiazole and ferrocene complexes.

In all complexes, the HOMO is localized on the entire complex, while the HOMO-1 has a strongly weighted contribution of the iron center (ferrocene). The LUMO and LUMO+1 are almost predominately contributed by the benzothiadiazole and vinyl bridge. The ferrocene characteristic HOMO-1 and the BTD characteristic LUMO, LUMO+1 indicate that the HOMO→LUMO, LUMO+1 and HOMO-1→LUMO, LUMO+1 absorption transitions bears a significant intramolecular charge-transfer (ICT) character. The higher wavelength vertical transitions predicted by the theory for the complexes possess major contribution from the HOMO to LUMO electronic excitation and possess medium oscillator strength. As we can observe from the table, the maximum absorption wavelengths of complexes from experimental data largely blue shifted from maximum absorption wavelengths of complexes calculated by using B3LYP [69-70] functional.

In general the overestimation of absorption wavelengths for the complexes containing intramolecular charge transfer systems by B3LYP function is attributed to the incorrect asymptotic behaviour [71]. As we discussed earlier the complexes possess strong donor-acceptor interactions, we adopted the PBE1PBE [72-73] functional for more reliable prominent absorption spectra resulted from the electronic promotions. The prominent higher wavelength vertical transitions, dipole moments and their oscillator strength (f) predicted by the theory is collected in Table 7.6 and 7.7. According to the PBE1PBE computations, the longer wavelength vertical transitions in the complexes originate from the HOMO to LUMO electronic excitations with reasonable oscillator strengths. From this it is evident that the electronic excitation from HOMO to LUMO would result in the migration of charge from donor segments to the benzothiadiazole moiety. The higher energy transition occurring in the complexes ranging 315-330 nm with high molar extinction coefficient in THF solutions are well matched with absorption maxima and oscillator strength calculated for the complexes, this transition mainly composed of electronic excitation such as HOMO to LUMO+1. The energy transition occurring in the complexes **30c**, **19c** and **30d** ranging from 420-450 nm are composed of several electronic excitations. The oscillator strength of the complexes also echoes the experimental absorption coefficients. Among all complexes, the HOMO level of the complexes **30a** and **30b** raised by the presence of strong electron donating amines. Interestingly the complex **19c** which contains auxiliary acceptor (vinyl pyridine) have low lying LUMO level and high dipole moment.

Figure 7.13 Electronic distributions in the frontier molecular orbitals of the complexes 30a-c



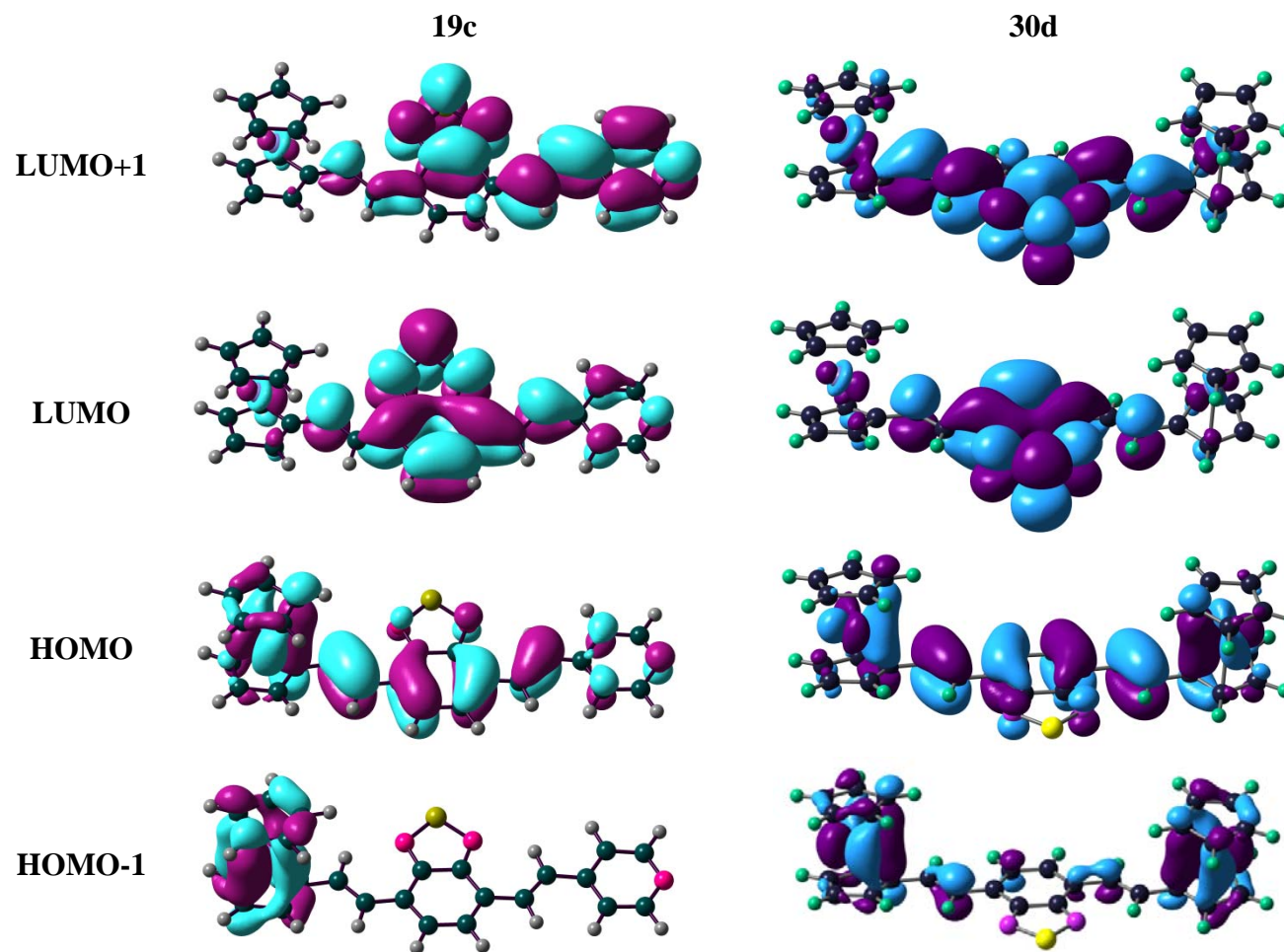


Figure 7.14 Electronic distributions in the frontier molecular orbitals of the complexes 30d-e

Benzothiadiazole-Ferrocene Conjugates: Synthesis and Optical properties

Table 7.6 Computed vertical transition energies, oscillator strengths (f), and their assignment for the complexes^[a] using B3LYP (gas)

Complex	λ_{\max}/nm	f	Configuration	μ_g [D]	HOMO (eV)	LUMO (eV)	E_g (eV)
30a	565.6	0.1528	HOMO→LUMO (68%)	2.54	4.81	2.13	2.69
30b	565.5	0.1382	HOMO→LUMO (66%)	1.54	4.92	2.22	2.69
30c	586.8	0.1864	HOMO→LUMO (61%)	1.50	5.09	2.51	2.58
	520.4	0.1797	HOMO→LUMO (35%), HOMO-2→LUMO (18%), HOMO-1→LUMO+3 (17%)				
19c	609.3	0.2162	HOMO→LUMO (72%)	4.80	5.21	2.72	2.49
	521.5	0.2244	HOMO-2→LUMO (28%), HOMO→LUMO (23%), HOMO-1→LUMO+4 (17%)				
	374.5	0.3028	HOMO-4→LUMO (52%), HOMO→LUMO+1 (42%)				
	361.6	0.3595	HOMO→LUMO+1 (45%), HOMO-4→LUMO (39%)				
	345.9	0.1280	HOMO-3→LUMO+6 (19%), HOMO-1→LUMO+4 (18%) HOMO-3→LUMO+2 (12%)				
	326.3	0.3249	HOMO-2→LUMO+1 (80%)				
30d	605.3	0.3489	HOMO→LUMO (77%)	1.63	4.91	2.43	2.48
	523.8	0.1095	HOMO-2→LUMO+4 (12%) HOMO-3→LUMO+3 (10%) HOMO-1→LUMO+2 (10%)				

[a] Contributions of less than 10% are omitted.

Benzothiadiazole-Ferrocene Conjugates: Synthesis and Optical properties

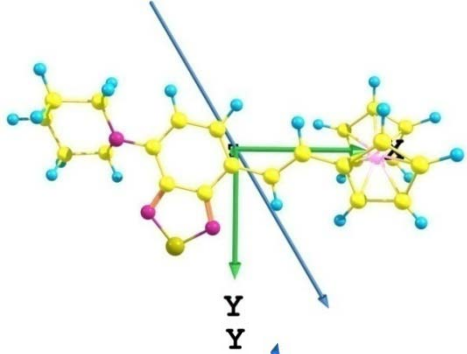
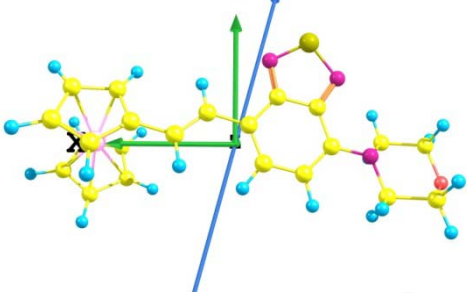
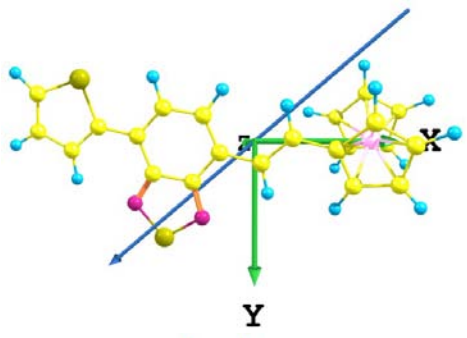
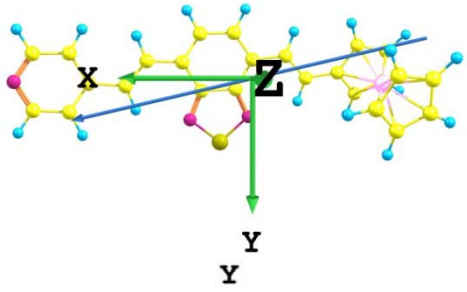
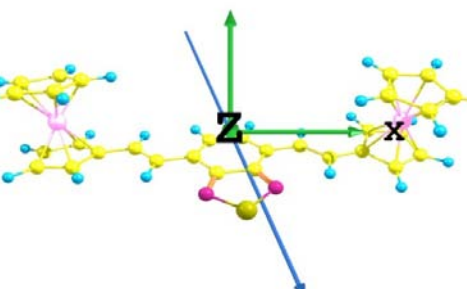
Table 7.7 Computed vertical transition energies, oscillator strengths (f), and their assignment for the complexes^[a] using PBE1PBE (THF)

Complex	λ_{\max}/nm	f	Configuration	μ_g [D]	HOMO (eV)	LUMO (eV)	E_g (eV)
30a	528.7	0.2690	HOMO→LUMO (84%)	3.35	5.20	2.15	3.05
	322.8	0.8680	HOMO→LUMO+1 (72%), HOMO-4→LUMO (12%)				
	276.2	0.1270	HOMO-6→LUMO (52%), HOMO-7→LUMO (17%) HOMO→LUMO+3 (16%)				
30b	523.1	0.2447	HOMO→LUMO (78%)	2.08	5.28	2.19	3.08
	318.2	0.9052	HOMO→LUMO+1 (82%)				
	275.4	0.1245	HOMO-7→LUMO (69%), HOMO→LUMO+2 (16%)				
30c	543.3	0.3673	HOMO→LUMO (71%)	1.95	5.47	2.52	2.95
	489.8	0.1847	HOMO→LUMO (26%), HOMO-2→LUMO (22%), HOMO-1→LUMO+3 (15%)				
	329.0	0.6912	HOMO→LUMO+1 (74%)				
	323.8	0.1131	HOMO-3→LUMO (31%), HOMO-3→LUMO+4 (15%), HOMO-3→LUMO+6 (10%)				
	290.9	0.1627	HOMO-8→LUMO (48%), HOMO→LUMO+2 (29%), HOMO-7→LUMO (11%)				
19c	554.6	0.4407	HOMO→LUMO (75%)	5.82	5.55	2.66	2.89
	488.6	0.2852	HOMO-2→LUMO (29%), HOMO→LUMO (21%), HOMO-1→LUMO+5 (14%), HOMO-2→LUMO+7 (12%)				
	355.0	0.6297	HOMO→LUMO+1 (74%), HOMO-4→LUMO (18%)				
30d	340.8	0.2332	HOMO-4→LUMO (76%), HOMO→LUMO+1 (16%)	2.17	5.32	2.45	2.86
	561.2	0.5549	HOMO→LUMO (83%)				
	356.9	0.1118	HOMO-6→LUMO (37%), HOMO→LUMO+1 (13%) HOMO-3→LUMO+3 (11%), HOMO-2→LUMO+4 (10%)				
	338.8	1.0016	HOMO→LUMO+1 (76%)				

[a] Contributions of less than 10% are omitted

Benzothiadiazole-Ferrocene Conjugates: Synthesis and Optical properties

Table 7.8 Direction and size of dipole moment of the complexes

Complex	B3LYP/6-31g(d,p)-vacuum	μ_g (D)
30a		2.54
30b		1.54
30c		1.50
19c		4.80
30d		1.63

It is also expected that the tethering groups on the benzothiadiazole unit, which have different electron densities over it, will affect the direction and size of the dipole moment of the complexes. Table 7.8 shows the direction and size of dipole moment of the ferrocene-benzothiadiazole complexes calculated by TD-DFT with the B3LYP functional. Generally

the dipole moments of all the complexes except **19c** directed from benzene ring (δ^+) to thiadiazole (δ^-). While in **19c**, by the introduction of auxiliary acceptor vinyl pyridine the dipole moment is directed towards electron deficient pyridine ring (δ^-) from ferrocene segment (δ^+) and the value significantly enhanced.

7.2.6 Thermal Properties

Thermal stability has a significant impact on the device performance and an essential requirement of the organic/ organometallic material to serve in optoelectronic devices. So the thermal stability of the ferrocene-benzothiadiazole hybrids was evaluated by the thermogravimetric analysis (TGA) at a heating rate of $10\text{ }^\circ\text{C min}^{-1}$ up to $900\text{ }^\circ\text{C}$ under a nitrogen atmosphere (Figure 7.15). A summary of the thermogravimetric analysis data of the complexes are compiled in Table 7.9. The results show that ferrocene-benzothiadiazole vinyl derivatives are relatively robust. The decomposition temperatures (T_d) for compounds in nitrogen atmosphere are above $343\text{ }^\circ\text{C}$. The onset decomposition temperatures of the compounds lie in the range from 292 to $358\text{ }^\circ\text{C}$. Among all, the dye **30d** possesses lower thermal decomposition temperature. The highest thermal stability is observed for derivative **30a** is $395\text{ }^\circ\text{C}$, indicative of excellent thermal stability. The higher decomposition temperatures observed for **30b** and **19c** are quite interesting. All the derivatives are thermally stable enough for the use in suitable optoelectronic device.

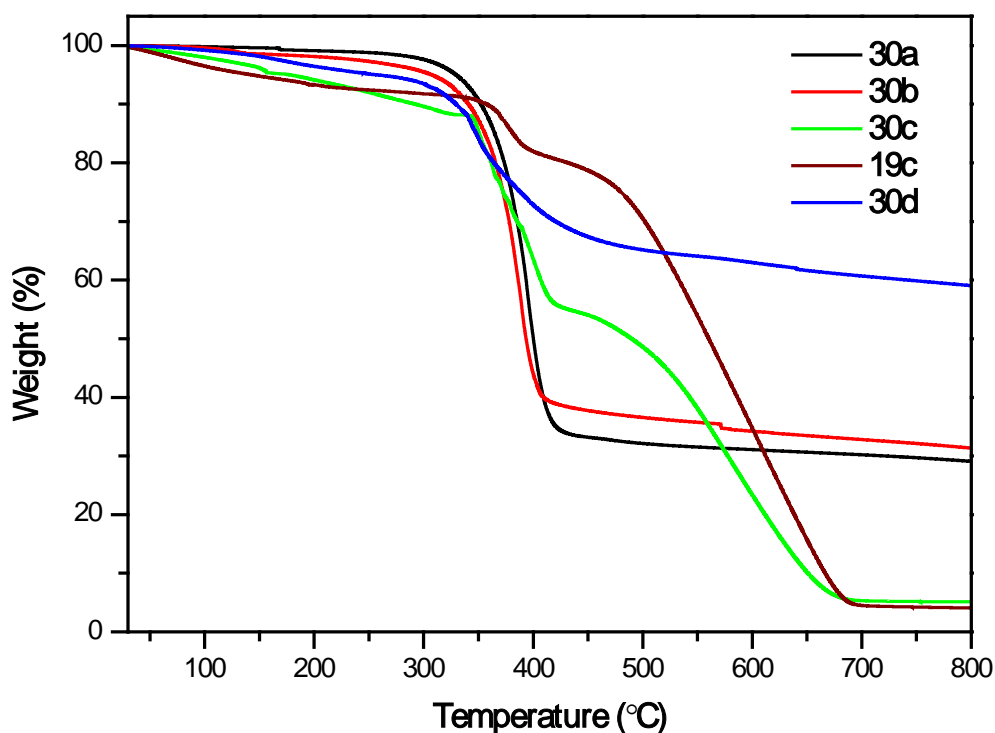


Figure 7.15 TGA plots for ferrocene-benzothiadiazole complexes

Table 7.9 Thermal properties of the benzothiadiazole-ferrocene complexes

Complex	$T_{\text{onset}}, ^\circ\text{C}^{\text{a}}$	$T_{\text{d}}, ^\circ\text{C}^{\text{b}}$
30a	352	395
30b	341	391
30c	292	364
19c	358	371
30d	330	343

^aTemperature corresponding to 10% weight loss ^bHeating rate 10 °C/min in nitrogen.

7.3 Conclusions

In summary, we have been successfully designed and synthesized five new ferrocene-benzothiadiazole based hybrid materials containing vinyl linkage with different tethering groups on benzothiadiazole. The ferrocene-benzothiadiazole complexes were synthesized by palladium-catalyzed Heck cross coupling reactions and characterized by NMR, UV-Vis spectroscopy, cyclic voltametry and thermo gravimetric analysis. NMR studies reveals that the substituents on benzothiadiazole have a significant effect on the electron density in the ferrocene termini, which could be monitored nicely by the ^1H and ^{13}C shifts. The structure of the **30a** was further evaluated by single crystal XRD. The dyes were showing excellent light absorbing properties and stable in the ground state. The red shift in the absorption maxima is in agreement with an increase in the effective conjugation length and nature of the terminal group on the benzothiadiazole segment. It was demonstrated that the optical and electrochemical properties of the complexes are tuned by attaching an appropriate electroactive group on the benzothiadiazole unit. The photophysical and electrochemical properties reveals the presence of considerable electronic interaction between the BTD core and ferrocenyl termini (strong donor-acceptor interactions) of the complexes. The choice of vinyl linkage between BTD chromophore and ferrocene, found to benefit the optical properties when compared to the complex in which BTD and ferrocene were integrated by acetylene linkage. On the other hand phenyl, thiophene and furan analogues of **30d** showed hypsochromic shift in the absorption and cathodically shifted oxidation potential of the ferrocene, which is attributed to the increased electron density on the ferrocene vicinity. The photophysical and energies of the frontier molecular orbitals were found to be in agreement with the theoretical hypothesis. The pyridine containing complex **19c** showed highest dipole moment in the series. The thermal decomposition temperatures of complexes in nitrogen atmosphere are above 343 °C. Nevertheless, these new materials are stable enough to apply in suitable opto-electronic device for material chemistry like BHJs and nonlinear optical applications and so on. These results have been demonstrated the important implications for

the design and synthesis of new small molecule based low band gap conjugated iron-complexes featured with benzothiadiazole for near IR absorption in the future.

7.4 Experimental Section

General methods are similar to those described in the earlier chapters

(E)-4-(2-ferrocenylvinyl)-7-(piperidin-1-yl)benzo[*c*][1,2,5]thiadiazole (30a):

In a 100 mL pressure tube mixture of 4-bromo-7-(piperidin-1-yl)benzo[*c*][1,2,5]thiadiazole (**2a**) (0.3 g, 1 mmol), vinyl ferrocene (**18c**) (0.212 g, 1 mmol), Pd(OAc)₂ (2.245 mg, 0.01 mmol), NaOAc (0.82 g, 10 mmol), and *n*-Bu₄NBr (0.065 g, 0.2 mmol) was dissolved in degassed *N,N*-dimethylformamide (5 mL). The solution was kept under a nitrogen atmosphere at 100 °C for 24 h with stirring. The mixture was poured into water. The precipitate was filtered, washed with water, dissolved in dichloromethane, and dried over anhydrous sodium sulfate. After evaporation of the solvent, the residue was purified by column chromatography on silica gel, using a hexane/dichloromethane mixture as eluant. A dark red solid weighing 0.245 g (57%, 0.57 mmol) was obtained. m.p. 148-150 °C; IR (KBr, cm⁻¹): 2943, 2913, 2851, 1623, 1545, 1493, 1387, 1281; ¹H NMR (CDCl₃, 500.13 MHz): δ 3.48 (t, *J* = 5.0 Hz, 4H), 4.15 (s, 5H), 4.31 (s, 2H), 4.55 (s, 2H), 6.75 (d, *J* = 8.0 Hz, 1H), 7.11 (d, *J* = 16.0 Hz, 1H), 7.45 (d, *J* = 8.0 Hz, 1H), 7.58 (d, *J* = 16.0 Hz, 1H); ¹³C NMR (CDCl₃, 125.75 MHz): δ 24.5, 25.9, 51.7, 66.8, 69.0, 69.2, 84.1, 112.2, 122.2, 123.2, 127.1, 128.8, 143.6, 150.4, 154.6. MALDI-TOF MS *m/z*: calculated for C₂₃H₂₃FeN₃S 429.0962[M]; found: 429.0775

(E)-4-(7-(2-ferrocenylvinyl)benzo[*c*][1,2,5]thiadiazol-4-yl)morpholine (30b):

Complex **30b** was prepared by following a procedure similar to that described above for **30a**, by taking one equivalent of 4-bromo-7-morpholinobenzo[*c*][1,2,5]thiadiazole (**2b**). Dark orange solid; Yield = 62%; m.p. 130-132 °C; IR (KBr, cm⁻¹): 2951, 2854, 1642, 1545, 1491, 1451, 1380, 1262; ¹H NMR (CDCl₃, 500.13 MHz): δ 3.54 (t, *J* = 4.5 Hz, 4H), 4.00 (t, *J* = 4.5 Hz, 4H), 4.16 (s, 4 H), 4.32 (s, 2H), 4.56 (s, 2H), 6.76 (d, *J* = 8 Hz, 1H), 7.12 (d, *J* = 16.0 Hz, 1H), 7.48 (d, *J* = 8.0 Hz, 1H), 7.61 (d, *J* = 16.0 Hz, 1H); ¹³C NMR (125.75 MHz, CDCl₃): δ 50.5, 66.86, 66.90, 69.1, 69.3, 112.1, 121.9, 124.1, 126.7, 129.6, 142.3, 150.0, 154.5; MALDI-TOF MS *m/z*: calculated for C₂₂H₂₁FeN₃OS 431.0755 [M]; found: 431.1331

(E)-4-(2-ferrocenylvinyl)-7-(thiophen-2-yl)benzo[*c*][1,2,5]thiadiazole (30c): Complex **30c** was prepared by following a procedure similar to that described above for **30a**, by taking one equivalent of 4-bromo-7-(thiophen-2-yl)benzo[*c*][1,2,5]thiadiazole (**29**). Black solid; Yield = 71%; m.p. 145-147 °C; IR (KBr, cm⁻¹): 2921, 2852, 1620, 1536, 1485, 1424, 1376, 1246; ¹H NMR (CDCl₃, 500.13 MHz): δ 4.82 (s, 10H), 4.38 (s, 2H), 4.61 (s, 2H), 7.20 (m, 2H), 7.44

Benzothiadiazole-Ferrocene Conjugates: Synthesis and Optical properties

(d, $J = 5.0$ Hz, 1H), 7.60 (d, $J = 8.0$ Hz, 1H), 7.80 (d, $J = 16.0$ Hz, 1H), 7.84 (d, $J = 8.0$ Hz, 1H), 8.1 (m, 1H); ^{13}C NMR (125.75 MHz, CDCl_3): δ 67.3, 69.4, 69.6, 121.6, 124.8, 125.4, 126.1, 126.3, 127.0, 127.9, 129.7, 132.9, 139.8, 152.8, 153.5; MALDI-TOF MS m/z : calculated for $\text{C}_{22}\text{H}_{16}\text{FeN}_2\text{S}_2$ 428.0104 [M]; found 428.0066.

4-((*E*)-2-ferrocenylvinyl)-7-((*E*)-2-(pyridin-4-yl)vinyl)benzo[*c*][1,2,5]thiadiazole (19c):

Complex **19c** was prepared by following a procedure similar to that described above for **30a**, by taking one equivalent of (*E*)-4-bromo-7-(2-(pyridin-4-yl)vinyl)benzo[*c*][1,2,5]thiadiazole (**16**). Dark black solid; Yield = 61%; m.p. 184-186 °C; IR (KBr, cm^{-1}): 2924, 2847, 1622, 1380, 1100, 965; ^1H NMR (CDCl_3 , 500.13 MHz): δ 4.19 (s, 5H), 4.40 (s, 2H), 4.62 (s, 2H), 7.22 (s, 1H), 7.50 (s, 2H), 7.61 (s, 2H), 7.69 (d, $J = 6.0$ Hz, 1H), 7.75 (d, $J = 16.0$ Hz, 1H), 7.84 (d, $J = 16.0$ Hz, 1H), 7.99 (d, $J = 16.0$ Hz, 1H), 8.60 (s, 2H); ^{13}C NMR (125.75 MHz, CDCl_3): δ 67.5, 69.5, 69.9, 83.0, 121.0, 121.5, 125.2, 126.8, 129.1, 129.2, 129.8, 131.2, 134.0, 145.0, 150.2, 153.7, 153.9. MALDI-TOF MS m/z : calculated for $\text{C}_{25}\text{H}_{19}\text{FeN}_3\text{S}$ 449.0649 [M]; found: 449.0623.

4,7-bis((*E*)-2-ferrocenylvinyl)benzo[*c*][1,2,5]thiadiazole (30d):

Complex **30d** was prepared by following a procedure similar to that described above for **30a**, by taking half equivalent of (*E*)-4-bromo-7-(2-(pyridin-4-yl)vinyl)benzo[*c*][1,2,5]thiadiazole (**1**). Red solid; Yield = 50%; m.p. > 300 °C; IR (KBr, cm^{-1}): 2921, 2848, 1620, 1487, 1405, 1242; ^1H NMR (CDCl_3 , 500.13 MHz): δ 4.17 (s, 10H), 4.37 (s, 4H), 4.60 (s, 4H), 7.20 (d, $J = 16.0$ Hz, 2H), 7.55 (s, 2H), 7.77 (d, $J = 16.0$ Hz, 2H); ^{13}C NMR (125.75 MHz, CDCl_3): δ 67.2, 69.4, 69.6, 83.5, 122.1, 125.9, 128.8, 132.0, 158.9. MALDI-TOF MS m/z : calculated for $\text{C}_{30}\text{H}_{24}\text{Fe}_2\text{N}_2\text{S}$ 556.0359 [M]; found: 556.0328.

7.5 References

- (1) Cheng, S.-H. Yang and C.-S. Hsu, Synthesis of Conjugated Polymers for Organic Solar Cell Applications. *Chem. Rev.* **2009**, *109*, 5868-923.
- (2) C. Wang, H. Dong, W. Hu, Y. Liu and D. Zhu, Semiconducting π -Conjugated Systems in Field-Effect Transistors: A Material Odyssey of Organic Electronics. *Chem. Rev.* **2011**, *112*, 2208-67.
- (3) K. R. J. Thomas, Y.-C. Hsu, J. T. Lin, K.-M. Lee, K.-C. Ho, C.-H. Lai, Y.-M. Cheng and P.-T. Chou, 2,3-Disubstituted Thiophene-Based Organic Dyes for Solar Cells. *Chem. Mater.* **2008**, *20*, 1830-40.
- (4) D. Kumar, K. R. J. Thomas, C.-P. Lee and K.-C. Ho, Novel Pyrenoimidazole-Based Organic Dyes for Dye-Sensitized Solar Cells. *Org. Lett.* **2011**, *13*, 2622-5.

Benzothiadiazole-Ferrocene Conjugates: Synthesis and Optical properties

- (5) A. Mishra, M. K. R. Fischer and P. Bäuerle, Metal-Free Organic Dyes for Dye-Sensitized Solar Cells: From Structure: Property Relationships to Design Rules. *Angew. Chem. Int. Ed.* **2009**, *48*, 2474-99.
- (6) C. Su, Y. Ye, L. Xu and C. Zhang, Synthesis and charge-discharge properties of a ferrocene-containing polytriphenylamine derivative as the cathode of a lithium ion battery. *J. Mater. Chem.* **2012**, *22*, 22658-62.
- (7) S. Scuppa, L. Orian, D. Dini, S. Santi and M. Meneghetti, Nonlinear Absorption Properties and Excited State Dynamics of Ferrocene. *J. Phys. Chem. A* **2009**, *113*, 9286-94.
- (8) C. Su, Y. Ye, L. Xu and C. Zhang, Synthesis and charge-discharge properties of a ferrocene-containing polytriphenylamine derivative as the cathode of a lithium ion battery. *J. Mater. Chem.* **2012**, *22*, 22658-62.
- (9) W. Wu, J. Zhang, H. Yang, B. Jin, Y. Hu, J. Hua, C. Jing, Y. Long and H. Tian, Narrowing band gap of platinum acetylide dye-sensitized solar cell sensitizers with thiophene π -bridges. *J. Mater. Chem.* **2012**, *22*, 5382-89.
- (10) J. Yang, F. Guo, J. Hua, X. Li, W. Wu, Y. Qu and H. Tian, Efficient and stable organic DSSC sensitizers bearing quinacridone and furan moieties as a planar π -spacer. *J. Mater. Chem.* **2012**, *22*, 24356-65.
- (11) A. Abbotto and N. Manfredi, Electron-rich heteroaromatic conjugated polypyridine ruthenium sensitizers for dye-sensitized solar cells. *Dalton Trans.* **2011**, *40*, 12421-38.
- (12) E. Wuttke, F. Pevny, Y. M. Hervault, L. Norel, M. Drescher, R. F. Winter and S. Rigaut, Fully delocalized (ethynyl)(vinyl)phenylene bridged triruthenium complexes in up to five different oxidation states. *Inorg. Chem.* **2012**, *51*, 1902-15.
- (13) J. Warnan, V.-M. Guerin, F. B. Anne, Y. Pellegrin, E. Blart, D. Jacquemin, T. Pauporté and F. Odobel, Ruthenium Sensitizer Functionalized by Acetylacetone Anchoring Groups for Dye-Sensitized Solar Cells. *J. Phys. Chem. C* **2013**, *117*, 8652-60.
- (14) A. Colombo, C. Dragonetti, D. Roberto, R. Ugo, L. Falcicola, S. Luzzati and D. Kotowski, A Novel Diruthenium Acetylide Donor Complex as an Unusual Active Material for Bulk Heterojunction Solar Cells. *Organometallics* **2011**, *30*, 1279-82.
- (15) F. Pevny, E. Di Piazza, L. Norel, M. Drescher, R. F. Winter and S. p. Rigaut, Fully Delocalized (Ethynyl)(vinyl)phenylene-Bridged Diruthenium Radical Complexes. *Organometallics* **2010**, *29*, 5912-18.

Benzothiadiazole-Ferrocene Conjugates: Synthesis and Optical properties

- (16) K. R. J. Thomas, J. T. Lin, H.-M. Lin, C.-P. Chang and C.-H. Chuen, Ruthenium and Rhenium Complexes of Fluorene-Based Bipyridine Ligands: Synthesis, Spectra, and Electrochemistry. *Organometallics* **2001**, *20*, 557-63.
- (17) S. Ferrere and B. A. Gregg, Photosensitization of TiO₂ by [FeII(2,2'-bipyridine-4,4'-dicarboxylic acid)₂(CN)₂]: Band Selective Electron Injection from Ultra-Short-Lived Excited States. *J. Am. Chem. Soc.* **1998**, *120*, 843-44.
- (18) F. Zapata, A. Caballero, A. Espinosa, A. Tarraga and P. Molina, A selective redox and chromogenic probe for Hg(II) in aqueous environment based on a ferrocene-azaquinoxaline dyad. *Inorg. Chem.* **2009**, *48*, 11566-75.
- (19) A. Hildebrandt, D. Schaarschmidt and H. Lang, Electronically Intercommunicating Iron Centers in Di- and Tetraferrocenyl Pyrroles. *Organometallics* **2011**, *30*, 556-63.
- (20) S.-H. Chang, C.-F. Chang, J.-L. Liao, Y. Chi, D.-Y. Zhou, L.-S. Liao, T.-Y. Jiang, T.-P. Chou, E. Y. Li, G.-H. Lee, T.-Y. Kuo and P.-T. Chou, Emissive Osmium(II) Complexes with Tetradentate Bis(pyridylpyrazolate) Chelates. *Inorg. Chem.* **2013**, *52*, 5867-75.
- (21) L. K. Filak, S. Göschl, P. Heffeter, K. Ghannadzadeh Samper, A. E. Egger, M. A. Jakupec, B. K. Keppler, W. Berger and V. B. Arion, Metal–Arene Complexes with Indolo[3,2-*c*]-quinolines: Effects of Ruthenium vs Osmium and Modifications of the Lactam Unit on Intermolecular Interactions, Anticancer Activity, Cell Cycle, and Cellular Accumulation. *Organometallics* **2013**, *32*, 903-14.
- (22) C.-H. Lin, C.-Y. Lin, J.-Y. Hung, Y.-Y. Chang, Y. Chi, M.-W. Chung, Y.-C. Chang, C. Liu, H.-A. Pan, G.-H. Lee and P.-T. Chou, Stepwise Formation of Iridium(III) Complexes with Monocyclometalating and Dicyclicmetalating Phosphorus Chelates. *Inorg. Chem.* **2012**, *51*, 1785-95.
- (23) C. Fan, L. Zhu, B. Jiang, Y. Li, F. Zhao, D. Ma, J. Qin and C. Yang, High Power Efficiency Yellow Phosphorescent OLEDs by Using New Iridium Complexes with Halogen-Substituted 2-Phenylbenzo[*d*]thiazole Ligands. *J. Phys. Chem. C* **2013**, *117*, 19134-41.
- (24) S. Lee, S.-O. Kim, H. Shin, H.-J. Yun, K. Yang, S.-K. Kwon, J.-J. Kim and Y.-H. Kim, Deep-Blue Phosphorescence from Perfluoro Carbonyl-Substituted Iridium Complexes. *J. Am. Chem. Soc.* **2013**, *135*, 14321-28.
- (25) J. Mei, K. Ogawa, Y. G. Kim, N. C. Heston, D. J. Arenas, Z. Nasrollahi, T. D. McCarley, D. B. Tanner, J. R. Reynolds and K. S. Schanze, Low-band-gap platinum acetylide polymers as active materials for organic solar cells. *ACS Appl. Mater.*

Benzothiadiazole-Ferrocene Conjugates: Synthesis and Optical properties

- Interfaces* **2009**, *1*, 150-61.
- (26) F. R. Dai, H. M. Zhan, Q. Liu, Y. Y. Fu, J. H. Li, Q. W. Wang, Z. Xie, L. Wang, F. Yan and W. Y. Wong, Platinum(II)-bis(aryleneethynylene) complexes for solution-processible molecular bulk heterojunction solar cells. *Chem. Eur. J.* **2012**, *18*, 1502-11.
- (27) X. Zhao, C. Piliego, B. Kim, D. A. Poulsen, B. Ma, D. A. Unruh and J. M. J. Fréchet, Solution-Processable Crystalline Platinum-Acetylide Oligomers with Broadband Absorption for Photovoltaic Cells. *Chem. Mater.* **2010**, *22*, 2325-32.
- (28) W.-Y. Wong, X. Wang, H.-L. Zhang, K.-Y. Cheung, M.-K. Fung, A. B. Djurišić and W.-K. Chan, Synthesis, characterization and photovoltaic properties of a low-bandgap platinum(II) polyyne functionalized with a 3,4-ethylenedioxythiophene-benzothiadiazole hybrid spacer. *J. Organomet. Chem.* **2008**, *693*, 3603-12.
- (29) M. L. H. Green, S. R. Marder, M. E. Thompson, J. A. Bandy, D. Bloor, P. V. Kolinsky and R. J. Jones, Synthesis and structure of (cis)-[1-ferrocenyl-2-(4-nitrophenyl)ethylene], an organotransition metal compound with a large second-order optical nonlinearity. *Nature* **1987**, *330*, 360-62.
- (30) J. Kulhanek, F. Bures, W. Kuznik, I. V. Kityk, T. Mikysek and A. Ruzicka, Ferrocene-donor and 4,5-dicyanoimidazole-acceptor moieties in charge-transfer chromophores with π linkers tailored for second-order nonlinear optics. *Chem. Asian J.* **2013**, *8*, 465-75.
- (31) U. Pfaff, A. Hildebrandt, D. Schaarschmidt, T. Hahn, S. Liebing, J. Kortus and H. Lang, Di- and Triferrocenyl (Hetero)Aromatics: Synthesis, Characterization, (Spectro-)Electrochemistry, and Calculations. *Organometallics* **2012**, *31*, 6761-71.
- (32) A. Hildebrandt, D. Schaarschmidt, R. Claus and H. Lang, Influence of electron delocalization in heterocyclic core systems on the electrochemical communication in 2,5-di- and 2,3,4,5-tetraferrocenyl thiophenes, furans, and pyrroles. *Inorg. Chem.* **2011**, *50*, 10623-32.
- (33) K. R. J. Thomas, J. T. Lin and Y. S. Wen, Biferrocenes with Heteroaromatic Spacers: Synthesis, Structure, and Electrochemistry. *Organometallics* **2000**, *19*, 1008-12.
- (34) A. Hildebrandt and H. Lang, Influencing the electronic interaction in diferrocenyl-1-phenyl-1H-pyrroles. *Dalton Trans.* **2011**, *40*, 11831-37.
- (35) . Rodriguez Gonzalez, M. C. Ruiz Delgado, R. Caballero, P. De la Cruz, F. Langa, J. T. Lopez Navarrete and J. Casado, Delocalization-to-localization charge transition in

Benzothiadiazole-Ferrocene Conjugates: Synthesis and Optical properties

diferrocenyl-oligothienylene-vinylene molecular wires as a function of the size by Raman spectroscopy. *J. Am. Chem. Soc.* **2012**, *134*, 5675-81.

- (36) D. Miesel, A. Hildebrandt, M. Korb, P. J. Low and H. Lang, Synthesis and (Spectro)electrochemical Behavior of 2,5-Diferrocenyl-1-phenyl-1H-phosphole. *Organometallics* **2013**, *32*, 2993-3002.
- (37) K. Kaleta, A. Hildebrandt, F. Strehler, P. Arndt, H. Jiao, A. Spannenberg, H. Lang and U. Rosenthal, Ferrocenyl-substituted metallacycles of titanocenes: oligocyclopentadienyl complexes with promising properties. *Angew. Chem. Int. Ed.* **2011**, *50*, 11248-52.
- (38) Q. Zheng, G. S. He, C. Lu and P. N. Prasad, Synthesis, two- and three-photon absorption, and optical limiting properties of fluorene-containing ferrocene derivatives. *J. Mater. Chem.* **2005**, *15*, 3488-93.
- (39) B. Dhokale, P. Gautam, S. M. Mobin and R. Misra, Donor-acceptor, ferrocenyl substituted BODIPYs with marvelous supramolecular interactions. *Dalton Trans.* **2013**, *42*, 1512-18.
- (40) N. Tsuboya, R. Hamasaki, M. Ito, M. Mitsuishi, T. Miyashita and Y. Yamamoto, Nonlinear optical properties of novel fullerene-ferrocene hybrid molecules *J. Mater. Chem.* **2003**, *13*, 511-13.
- (41) N. Tsuboya, M. Lamrani, R. Hamasaki, M. Ito, M. Mitsuishi, T. Miyashita and Y. Yamamoto, Nonlinear optical properties of novel carborane-ferrocene conjugated dyads. Electron-withdrawing characteristics of carboranes. *J. Mater. Chem.* **2002**, *12*, 2701-5.
- (42) J. A. Mata, E. Peris, I. Asselberghs, R. Van Boxel and A. Persoons, Large second-order NLO properties of new conjugated oligomers with a pendant ferrocenyl and an end-capped pyridine. *New J. Chem.* **2001**, *25*, 1043-6.
- (43) . M. Speck, R. Claus, A. Hildebrandt, T. Ruffer, E. Erasmus, L. van As, J. C. Swarts and H. Lang, Electron Transfer Studies on Ferrocenylthiophenes: Synthesis, Properties, and Electrochemistry. *Organometallics* **2012**, *31*, 6373-80.
- (44) D. J. Roberts, D. J. Gregg, C. M. Fitchett and S. M. Draper, Ferrocenyl-polyphenylenes: Toward Metallo-organic Polyaromatics. *Organometallics* **2010**, *29*, 6541-47.
- (45) P. Gautam, B. Dhokale, S. M. Mobin and R. Misra, Ferrocenyl BODIPYs: synthesis, structure and properties. *RSC Advances* **2012**, *2*, 12105-07.
- (46) C. J. McAdam, B. H. Robinson, J. Simpson and T. Tagg, Ferrocenyl+Naphthalimide

Benzothiadiazole-Ferrocene Conjugates: Synthesis and Optical properties

- Donor–Acceptor Dyads with Aromatic Spacer Groups. *Organometallics* **2010**, *29*, 2474-83.
- (47) M. Madalska, P. Lönnecke and E. Hey-Hawkins, 1,2-Disubstituted Aryl-Based Ferrocenyl Phosphines. *Organometallics* **2013**, *32*, 2019-25.
- (48) D. T. Gryko, F. Zhao, A. A. Yasserli, K. M. Roth, D. F. Bocian, W. G. Kuhr and J. S. Lindsey, Synthesis of Thiol-Derivatized FerrocenePorphyrins for Studies of Multibit Information Storage. *J. Org. Chem.* **2000**, *65*, 7356-62.
- (49) R. Chauhan, M. Trivedi, L. Bahadur and A. Kumar, Application of π -extended ferrocene with varied anchoring groups as photosensitizers in TiO₂-based dye-sensitized solar cells (DSSCs). *Chem. Asian J.* **2011**, *6*, 1525-32.
- (50) .-H. Gong, P. Audebert, F. Yang, F. Miomandre, X.-C. Lian and J. Tang, New pyridinium conjugated ferrocenes: Synthesis and electrochemical properties. *J. Electroanal. Chem.* **2007**, *606*, 8-16.
- (51) R. Maragani, T. Jadhav, S. M. Mobin and R. Misra, C₃ symmetric ferrocenyl triazines: synthesis, structure, and properties. *RSC Advances* **2013**, *3*, 2889-92.
- (52) R. Maragani, T. Jadhav, S. M. Mobin and R. Misra, Synthesis, structure, photophysical, and electrochemical properties of donor–acceptor ferrocenyl derivatives. *Tetrahedron* **2012**, *68*, 7302-8.
- (53) F. Yang, X.-L. Xu, Y.-H. Gong, W.-W. Qiu, Z.-R. Sun, J.-W. Zhou, P. Audebert and J. Tang, Synthesis and nonlinear optical absorption properties of two new conjugated ferrocene-bridge-pyridinium compounds. *Tetrahedron* **2007**, *63*, 9188-94.
- (54) B. Dhokale, P. Gautam and R. Misra, Donor–acceptor perylenediimide–ferrocene conjugates: synthesis, photophysical, and electrochemical properties. *Tetrahedron Lett.* **2012**, *53*, 2352-54.
- (55) Maragani and R. Misra, Donor–acceptor ferrocenyl triazines: synthesis and properties. *Tetrahedron Lett.* **2013**, *54*, 5399-402.
- (56) J. M. Speck, D. Schaarschmidt and H. Lang, Atropisomeric 1,5'-bis(ferrocenyl)-2,2'-bithiophene: Synthesis, Solid-State Structure, and Electrochemistry. *Organometallics* **2012**, *31*, 1975-82.
- (57) R. Misra, P. Gautam, R. Sharma and S. M. Mobin, Donor– π –acceptor– π –donor ferrocenyl benzothiadiazoles: synthesis, structure, and properties. *Tetrahedron Lett.* **2013**, *54*, 381-83.
- (58) R. Misra, P. Gautam, T. Jadhav and S. M. Mobin, Donor-acceptor ferrocenyl-substituted benzothiadiazoles: synthesis, structure, and properties. *J. Org. Chem.*

Benzothiadiazole-Ferrocene Conjugates: Synthesis and Optical properties

2013, 78, 4940-8.

- (59) M. Akhtaruzzaman, M. Tomura, M. B. Zaman, J.-i. Nishida and Y. Yamashita, Synthesis and Characterization of New Linear π -Conjugated Molecules Containing Bis(ethynylpyridine) Units with a Benzothiadiazole Spacer. *J. Org. Chem.* **2002**, *67*, 7813-18.
- (60) M. Akhtaruzzaman, M. Tomura, J.-i. Nishida and Y. Yamashita, Synthesis and Characterization of Novel Dipyritylbenzothiadiazole and Bisbenzothiadiazole Derivatives. *J. Org. Chem.* **2004**, *69*, 2953-58.
- (61) Y. Ooyama, S. Inoue, T. Nagano, K. Kushimoto, J. Ohshita, I. Imae, K. Komaguchi and Y. Harima, Dye-sensitized solar cells based on donor-acceptor π -conjugated fluorescent dyes with a pyridine ring as an electron-withdrawing anchoring group. *Angew. Chem. Int. Ed.* **2011**, *50*, 7429-33.
- (62) Y.-P. Wang, T.-S. Lin, R.-S. Shyu, J.-M. Hwu, Y. Wang and M.-C. Cheng, Syntheses, spectra and crystal structure of $(\text{CO})_2(\text{NO})\text{Cr}(\eta^5\text{-C}_5\text{H}_4)\text{CH}_2(\eta^5\text{-C}_5\text{H}_4)\text{Fe}[\text{vinyl}(\eta^5\text{-C}_5\text{H}_4)]$. *J. Organomet. Chem.* **1989**, *371*, 57-69.
- (63) K. Pilgram, M. Zupan and R. Skiles, Bromination of 2,1,3-benzothiadiazoles. *J. Heterocycl. Chem.* **1970**, *7*, 629-33.
- (64) S. Chen, Y. Li, W. Yang, N. Chen, H. Liu and Y. Li, Synthesis and Tuning Optical Nonlinear Properties of Molecular Crystals of Benzothiadiazole. *J. Phys. Chem. C* **2010**, *114*, 15109-15.
- (65) D. W. Chang, S.-J. Ko, G.-H. Kim, S.-Y. Bae, J. Y. Kim, L. Dai and J.-B. Baek, Molecular engineering of conjugated polymers for solar cells and field-effect transistors: Side-chain versus main-chain electron acceptors. *Journal of Polymer Science Part A: Polymer Chemistry* **2012**, *50*, 271-79.
- (66) V. Shrotriya, J. Ouyang, R. J. Tseng, G. Li and Y. Yang, Absorption spectra modification in poly(3-hexylthiophene):methanofullerene blend thin films. *Chem. Phys. Lett.* **2005**, *411*, 138-43.
- (67) D. H. Lee, M. J. Lee, H. M. Song, B. J. Song, K. D. Seo, M. Pastore, C. Anselmi, S. Fantacci, F. De Angelis, M. K. Nazeeruddin, M. Grätzel and H. K. Kim, Organic dyes incorporating low-band-gap chromophores based on π -extended benzothiadiazole for dye-sensitized solar cells. *Dyes Pigm.* **2011**, *91*, 192-98.
- (68) Gaussian 09, Revision A.02, M. J. Frisch, G. W. Trucks, H. B. Schlegel, G. E. Scuseria, M. A. Robb, J. R. Cheeseman, G. Scalmani, V. Barone, B. Mennucci, G. A. Petersson, H. Nakatsuji, M. Caricato, X. Li, H. P. Hratchian, A. F. Izmaylov, J.

Benzothiadiazole-Ferrocene Conjugates: Synthesis and Optical properties

- Bloino, G. Zheng, J. L. Sonnenberg, M. Hada, M. Ehara, K. Toyota, R. Fukuda, J. Hasegawa, M. Ishida, T. Nakajima, Y. Honda, O. Kitao, H. Nakai, T. Vreven, J. A., Jr., Montgomery, J. E. Peralta, F. Ogliaro, M. Bearpark, J. J. Heyd, E. Brothers, K. N. Kudin, V. N. Staroverov, R. Kobayashi, J. Normand, K. Raghavachari, A. Rendell, J. C. Burant, S. S. Iyengar, J. Tomasi, M. Cossi, N. Rega, N. J. Millam, M. Klene, J. E. Knox, J. B. Cross, V. Bakken, C. Adamo, J. Jaramillo, R. Gomperts, R. E. Stratmann, O. Yazyev, A. J. Austin, R. Cammi, C. Pomelli, J. W. Ochterski, R. L. Martin, K. Morokuma, V. G. Zakrzewski, G. A. Voth, P. Salvador, J. J. Dannenberg, S. Dapprich, A. D. Daniels, Ö. Farkas, J. B. Foresman, J. V. Ortiz, J. Cioslowski, D. J. Fox, Gaussian, Inc., Wallingford, CT, **2009**.
- (69) J. Lu, X. Xu, Z. Li, K. Cao, J. Cui, Y. Zhang, Y. Shen, Y. Li, J. Zhu, S. Dai, W. Chen, Y. Cheng and M. Wang, Zinc porphyrins with a pyridine-ring-anchoring group for dye-sensitized solar cells. *Chem. Asian J.* **2013**, *8*, 956-62.
- (70) J. Mao, F. Guo, W. Ying, W. Wu, J. Li and J. Hua, Benzotriazole-bridged sensitizers containing a furan moiety for dye-sensitized solar cells with high open-circuit voltage performance. *Chem. Asian J.* **2012**, *7*, 982-91.
- (71) Y.-F. Liu, X.-F. Ren, L.-Y. Zou, A.-M. Ren, J.-K. Feng and C.-C. Sun, Theoretical study on photophysical properties of 2,1,3-benzothiadiazole-based star-shaped molecules. *Theor. Chem. Acc.* **2011**, *129*, 833-45.
- (72) D. Y. Chen, K. Y. Cheng, M. L. Ho, I. C. Wu, M. W. Chung, H. Fu and P. T. Chou, A new recognition concept using dye sensitized solar cell configuration. *Chem Commun* **2011**, *47*, 985-87.
- (73) S. W. Chiu, L. Y. Lin, H. W. Lin, Y. H. Chen, Z. Y. Huang, Y. T. Lin, F. Lin, Y. H. Liu and K. T. Wong, A donor-acceptor-acceptor molecule for vacuum-processed organic solar cells with a power conversion efficiency of 6.4%. *Chem Commun* **2012**, *48*, 1857-59.

Chapter 8

Summary

In this thesis work, we aimed to design and synthesis the benzothiadiazole based functional materials and they were characterized by optical and electrochemical studies. We have developed several series of dipolar compounds for application in dye sensitized solar. We found that by modifying the molecular structure, both the photophysical and electrochemical properties of the molecules has been suitably altered. The success of the synthesis of the intermediates and target molecule is attributed to the judicious choice of the protocols such as Stille coupling, Vilsmeier-Haack reaction, Knoevenagel condensation, Wittig reaction and Heck coupling. The structural compositions of the compounds were thoroughly established by ^1H and ^{13}C NMR and mass spectral methods.

In Chapter 3, we have successfully designed and synthesized a series of dyes comprising piperidine/morpholine donor, benzothiadiazole and phenyl/thiophene/bithiophene units as a conjugated spacer. The compounds were successfully synthesized in good yields by the use of Stille-coupling and Knoevenagel condensation. It was observed that the optical and electrochemical properties of the compounds were highly dependent on the donor as well as the π -spacer. Extension of conjugation by coplanar structural arrangement led to red-shifted absorption and cathodic shift in the oxidation potential. A blue shift in the absorption profile of the compounds observed by the protonation of amine unit by addition of TFA and deprotonation of carboxylic acid moiety by addition of TEA. The best photovoltaic performance was achieved by the morpholine based compound **6b**, resulting in an efficiency of 3.07% with $J_{\text{SC}} = 12.40 \text{ mA cm}^{-2}$, $V_{\text{OC}} = 0.396 \text{ V}$, $ff = 0.63$.

In Chapter 4, we have synthesized four new phenothiazine donor based sensitizers, comprising benzothiadiazole/benzotriazole auxiliary acceptors and the cyanoacrylic acid unit as an electron acceptor. The effect of auxiliary acceptor and the π -linker on optical and electrochemical properties of the dyes was investigated. The absorption profile of the dyes was highly dependent on the nature of the auxiliary acceptor and π -bridge which connects the auxiliary acceptor and cyanoacrylic acid (acceptor) units. Incorporation of a phenothiazine donor group on the benzo(thiadiazole/triazole) conjugation segment bathochromically shifted the absorption wavelength. Due to the low LUMO energy levels benzothiadiazole sensitizers displayed lower band gap than benzotriazole sensitizers. Similar structures of auxiliary acceptors which differ only the hetero atom present on the 2-position

Benzothiadiazole-Ferrocene Conjugates: Synthesis and Optical properties

allowed, a systematic comparative investigations in choice of the auxiliary acceptors in D-A- π -A dyes for DSSCs. The HOMO and LUMO energy levels of the four sensitizers are ideal to be promising material for DSSC devices.

In chapter 5, by employing Heck-cross coupling reaction we synthesized pyridine terminal anchoring group sensitizers comprising different electron donating segments such as piperidine, morpholine, carbazole, phenothiazine and ferrocene on benzothiadiazole unit. The modulation of donor segment successfully led to structure-dependent optical, redox and photovoltaic properties. Using the benzothiadiazole group as exciton confinement center, we have extended the absorption onset into the long-wavelength range beyond 600 nm in the pyridine anchoring sensitizers. The absorption maxima for all the dyes remain fairly constant by increasing the solvent polarity. These materials exhibited good thermal stability and their thermal-decomposition temperatures fell within the range 355-407 °C. The π -extended arylamine dyes achieved higher efficiency than the alkylamine dyes, due to the red shifted absorption profiles and high molar extension coefficients. The DSSC device with the phenothiazine based sensitizer **19b** showed a power conversion efficiency of 1.97%, which is a promising efficiency with pyridine anchoring group under AM 1.5 G simulated solar light at a light intensity of 100 mW cm⁻². The promising performance of the dye **19b** is intriguing as it does not possess cyanoarylic acid anchoring/acceptor group.

In chapter 6, we have successfully designed, synthesized a series of donor-acceptor compounds containing phenothiazine donor, benzothiadiazole acceptor by palladium-catalyzed Heck cross coupling reactions. The compounds exhibited interesting photophysical, electrochemical properties which are highly dependent on the conjugation length and the donor attached to benzothiadiazole unit. All the dyes displayed one-electron quasi-reversible oxidation couple and an irreversible reduction wave in cyclic voltammetry, which are attributable to the oxidation of the sulphur atom in phenothiazine unit and reduction of benzothiadiazole unit. There is a reasonable correlation between the optical properties proposed by TDDFT and the experimental data. The decomposition temperatures of the dyes are quite good enough to apply in any opto-electronic device. Finally, in this work we established the structure-property relationships in the new phenothiazine-benzothiadiazole dyes extended through vinyl spacer.

In chapter 7, we have been successfully designed and synthesized five new ferrocene-benzothiadiazole based hybrid materials containing vinyl linkage with different tethering groups on benzothiadiazole. It was demonstrated that the optical and electro chemical properties of the complexes are tuned by attaching an appropriate electroactive group on the

Benzothiadiazole-Ferrocene Conjugates: Synthesis and Optical properties

benzothiadiazole unit. The choice of vinyl linkage between BTD chromophore and ferrocene, found to benefit the optical properties when compared to the complex in which BTD and ferrocene were integrated by acetylene linkage. The photophysical and energies of the frontier molecular orbitals were found to be in agreement with the theoretical hypothesis. The pyridine containing complex **25d** showed highest dipole moment in the series. The thermal decomposition temperatures of complexes in nitrogen atmosphere are above 343 °C. Nevertheless, these new materials are stable enough to apply in suitable opto-electronic device for material chemistry like BHJs and nonlinear optical applications and so on.

The phenothiazine donor based sensitizers are under process for DSSCs fabrication for photovoltaic applications. Phenothiazine-benzothiadiazole conjugates and ferrocene-benzothiadiazole conjugates under process for BHJs device fabrication, two photon absorption applications. In outlook, we believe that the excellent light absorbing properties of benzothiadiazole derivatives can be further utilized to develop promising electronic materials. Also, functionalization and utilization of 5,6-position of BTD systems are still unexplored and many opportunities and discoveries remain to be made to explore new possibilities.